University of Illinois at Urbana-Champaign

ACRC

Air Conditioning and Refrigeration Center A National Science Foundation/University Cooperative Research Center

Control-Oriented Modeling of Transcritical Vapor Compression Systems

B. P. Rasmussen, R. Shah, A. B. Musser, A. G. Alleyne,
C. W. Bullard, P. S. Hrnjak, and N. R. Miller

ACRC TR-204 October 2002

For additional information:

Air Conditioning and Refrigeration Center
University of Illinois
Mechanical & Industrial Engineering Dept.
1206 West Green Street
Urbana, IL 61801

(217) 333-3115

Prepared as part of ACRC Project #123
Strategies for Improving Operation and Reliability of Vapor Compression Systems
A. G. Alleyne, N. R. Miller, P. S. Hrnjak, and C. W. Bullard, Principal Investigators

The Air Conditioning and Refrigeration Center was founded in 1988 with a grant from the estate of Richard W. Kritzer, the founder of Peerless of America Inc. A State of Illinois Technology Challenge Grant helped build the laboratory facilities. The ACRC receives continuing support from the Richard W. Kritzer Endowment and the National Science Foundation. The following organizations have also become sponsors of the Center.

Alcan Aluminum Corporation
Amana Refrigeration, Inc.
Arçelik A. S.
Brazeway, Inc.
Carrier Corporation
Copeland Corporation
Dacor
Daikin Industries, Ltd.
Delphi Harrison Thermal Systems
General Motors Corporation
Hill PHOENIX
Honeywell, Inc.
Hydro Aluminum Adrian, Inc.
Ingersoll-Rand Company
Kelon Electrical Holdings Co., Ltd.
Lennox International, Inc.
LG Electronics, Inc.
Modine Manufacturing Co.
Parker Hannifin Corporation
Peerless of America, Inc.
Samsung Electronics Co., Ltd.
Tecumseh Products Company
The Trane Company
Valeo, Inc.
Visteon Automotive Systems
Wolverine Tube, Inc.
York International, Inc.

For additional information:

Air Conditioning & Refrigeration Center
Mechanical & Industrial Engineering Dept.
University of Illinois
1206 West Green Street
Urbana, IL 61801

217 333 3115

Abstract

This thesis details the efforts to develop a dynamic model of a transcritical vapor compression system suitable for multivariable control design purposes. The modeling approach is described and the developed models are validated with experimental data. The models are nonlinear, independent of fluid type, and based on first principles. Linearized versions of the nonlinear models are presented. Analysis of the linearized models and empirical models created using system identification techniques suggest that lower order models are adequate for the prediction of dominant system dynamics. Singular perturbation techniques are used to justify model reduction. Based on the reduced order models, the dominant dynamics of these systems are identified and described in terms of physical phenomena. Although all results presented are for a transcritical vapor compression cycle with carbon dioxide as the working fluid, the methodology and results can be extended to both subcritical and transcritical systems.

Table of Contents

List of Figures

Page

List of Tables

Page

Nomenclature

List of Abbreviations

AC&R – air conditioning and refrigeration
COP – coefficient of performance
MIMO – multi-input, multi-output
ODE – ordinary differential equation
PDE – partial differential equation
PRBS – pseudo-random binary sequence
R134a – refrigerant commonly used in automobile air conditioning systems
R22 – refrigerant commonly used in residential air conditioning systems
R404a – refrigerant commonly used in air conditioning systems
R744 – CO_2 – carbon dioxide as a working fluid
SISO – single-input, single-output

List of Symbols

Variable	Explanation
A	Area
A,B,C,D	State Space Matrices
a	Heat Transfer Coefficient
C_p	Specific Heat
E	Energy
h	Efficiency
f, g	Continuous Functions
g	Void Fraction
$\bar{g}$	Mean Void Fraction
H, h	Enthalpy, Specific Enthalpy
I	Identity Matrix
L	Length
l	Eigenvalue
$\dot{m}$	Mass Flow Rate
P	Pressure
p	Perimeter
Q	Heat
Re	Reynold's Number
r	Density
S	Slip Ratio; Scaling Matrix
s	Specific Entropy
s	Singular Value
T	Temperature
t	Time
U, u	Internal Energy, Specific Internal Energy; Controllable Inputs
UA	Lumped Heat Transfer Coefficient
V	Volume; Voltage
W	Work

x	Quality; Dynamic States
y	Outputs
z	Spatial Coordinate
Z	Matrix

Subscript	**Explanation**
1,2,3	1^{st}, 2^{nd}, 3^{rd} Region
a, air	Air
ave	Average
c	Cold; Gas Cooler
cs	Cross-Sectional
d	Diameter
f	Liquid
g	Vapor
h	Hot
hsv	Hankel Singular Value
hx	Internal Heat Exchanger
i	Inner
in	In
int	Intermediate
k	Compressor
o	Outer; Steady State
out	Out
r	Refrigerant; Reduced Order
sys	System
total	Total
v	Valve
w	Wall

Chapter 1. Introduction

1.1 Motivation

There is both strong industrial and academic interest in developing control-oriented models of vapor compression systems. The motivation for this work can be divided into four categories: efficiency, stability, performance, and understanding.

1.1.1 Efficiency

Each year billions of dollars are spent in the United States on energy for household, automotive and industrial air conditioning and refrigeration devices (10.2 billion dollars was spent for household AC&R devices alone in 1997 [1]). Clearly, an increase of efficiency in AC&R systems would have a notable effect on the nation's economy as well as the average individual's budget. Additionally, increasing the efficiency of these systems would have a much larger societal and environmental impact because of the reduction in fossil fuels required to provide this energy. Significant progress has been made in recent years to improve component efficiency in AC&R systems. With the increasing availability of inexpensive computing power, a veritable leap in increased efficiency is possible using complex control techniques.

Residential and industrial AC&R systems have extremely large start-up times. Automotive AC systems rarely operate at steady state conditions, and are constantly attempting to compensate for changing setpoints and external conditions. For each type of system, traditional control strategies have included single-input single-output (SISO) control or simple on/off ("bang-bang") control. On/off control schemes limit the system's overall efficiency and ability to maintain a desired setpoint with only small variations while detrimentally affecting efficiency by introducing start-up and shut-down transients. Furthermore, multiple SISO control techniques are less efficient because of the extensive cross-coupling of the system dynamics. Multivariable control strategies could improve efficiency while simultaneously benefiting from the coupled system dynamics.

1.1.2 Stability

The use of SISO control techniques with AC&R systems often results in a phenomenon known in the industry as "valve hunting." This condition is characterized by oscillations in the length of two-phase flow in the evaporator, and thus oscillations in the amount of superheated vapor at the evaporator exit. This condition was first qualitatively documented in 1963 by Zahn in [42]. In 1966 Wedekind and Stoecker published data demonstrating this phenomenon in [38]. Later Broersen and van der Jagt in [7] used a lumped parameter model to show that this phenomenon is caused by the interaction of the controller with the system dynamics. They made various suggestions how to avoid valve hunting, but all have noted disadvantages and require the system to function at less efficient conditions. This condition has been widely observed in industry and is usually solved by adjusting the controller parameters resulting in decreased performance. By using multivariable control schemes this phenomenon could be avoided while allowing the system to function at more efficient operating conditions.

1.1.3 Performance

While achieving multiple performance objectives with AC&R systems is desirable, it is generally impractical. Using multiple SISO control strategies for this purpose often leads to conflicting control actions because of the coupled nature of the system dynamics. Sophisticated control techniques traditionally have been used

only in large industrial systems, where the economy of scale made these techniques cost effective. These techniques required extensive tuning using empirical data and lumped parameters.

Part of the solution to the problem again lies in model-based multivariable control strategies. By developing a general lumped parameter model, a large number of AC&R systems could be included within the framework. Multivariable control schemes developed using a form of this model would allow the control scheme to be adapted based on physical parameters of the individual systems. Additionally, these control schemes could be designed to meet multiple performance objectives such as maximizing COP, exchanging efficiency for capacity when needed, controlling not only temperature, but also humidity, and so on.

1.1.4 Understanding

An additional motivation for developing control-oriented models of these systems is to increase understanding of the system dynamics. Because of the mathematical complexity of thermofluid dynamics, little physical insight is gained by evaluating the general form of the governing equations. In practice, however, many dynamic phenomena can be neglected. For these systems, a deceptively simple question has yet to be answered: What are the dominant dynamic phenomena of an air conditioning system?

1.2 Objectives

The principle objectives of this research are to provide a means to increase efficiency and performance of air conditioning systems. The plan for achieving this is to lay the groundwork for the design of advanced control strategies by: 1) developing a modeling approach for these systems, 2) identifying the dominant system dynamics, and 3) developing reduced order control-oriented dynamic models.

1.2.1 Dynamic Model of Vapor Compression Systems

The first objective of this research is to develop dynamic models for transcritical cycles using a moving boundary, lumped parameter approach. These nonlinear models are linearized about an operating condition, and reduced in order to include only the most important system dynamics. The full order, nonlinear models and the reduced order, linear models are validated using data taken on experimental systems available at the University of Illinois at Urbana-Champaign.

1.2.2 Identification of Dominant System Dynamics

In reality, an AC&R system is a highly nonlinear, infinite-dimensional system. However, to develop a control strategy only the dominant dynamics are of interest. These can be obtained empirically for individual systems. However, an explanation of these dominant dynamics in terms of physical parameters would allow controllers to be designed without extensive testing. Additionally, an understanding of what parameters influence the dynamics of the system could assist in the design of individual components.

1.2.3 Reduced Order Control-Oriented Model

Current industry practice for simple AC&R systems employs one or two SISO control strategies. The shortcomings of such an approach have already been mentioned. Not only would a model-based MIMO control strategy eliminate the problems associated with SISO control strategies, but it would also allow several simultaneous control objectives. The advanced control design techniques for high order models generally yield high order controllers. Some of the difficulties in developing low order controllers for high order systems are discussed by

Anderson in [2]. In practice a low order controller is developed by: 1) reducing the model order prior to controller design, or 2) designing a high order controller, and then numerically reducing the order of the controller. Although both approaches could be applied, the first approach is selected because of the added objective to identify the dominant system dynamics.

1.3 Vapor Compression Systems

Vapor compression systems are a type of thermodynamic machinery, which utilize a compressible fluid to transfer heat. While these devices can be used for heat generation, this project deals specifically with cooling applications. For ease of explanation, we categorize these systems into two groups: subcritical and transcritical cycles. These titles refer to fluid's condition throughout the cycle; whether the fluid is always below its critical point (subcritical) or whether the fluid operates both below and above the critical point (transcritical).

1.3.1 Subcritical Systems

Subcritical systems form the bulk of the systems used today, whether in homes, automobiles, or industry. The refrigerants commonly used are R134a, R22, and R404a. A diagram of the system is shown with the accompanying P-h diagram in Figure 1.1.

The simplest cycle operates with four components: compressor, condenser, expansion valve, and evaporator. The fluid enters the compressor as a superheated vapor at a low pressure. The fluid is compressed to a high pressure by the compressor and then enters the condenser. At this higher pressure, the fluid has a higher temperature than the ambient conditions, and as a fan blows air across the condenser, heat is transferred to the air, and the fluid condenses. The fluid exits the condenser as a subcooled liquid at a high pressure. The fluid then passes through an expansion device. At the exit of the expansion valve the fluid is generally two-phase, and at a low pressure. The fluid then enters the evaporator. At this lower pressure the fluid has a lower temperature than ambient conditions, and as a fan blows air across the evaporator, heat is transferred to the fluid, and the fluid evaporates. The fluid exits the evaporator as a superheated vapor and enters the compressor.

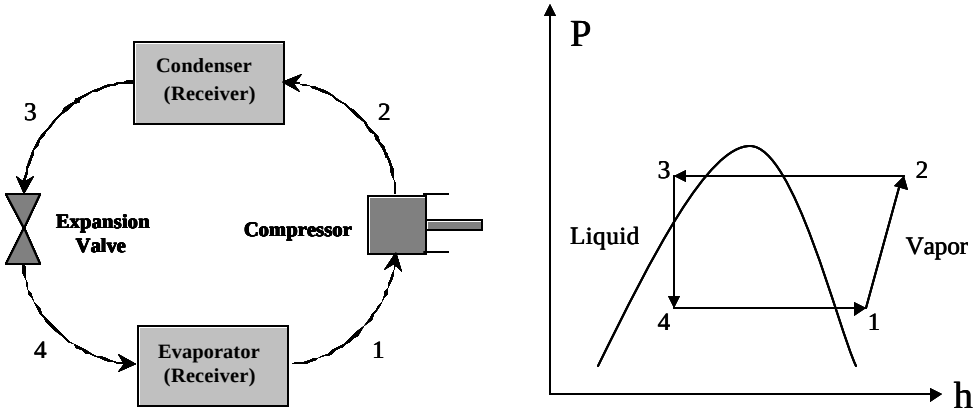

Figure 1.1 Diagram: Subcritical Cycle

A slight variation to this system is the addition of receivers. When a receiver is placed at the exit of the evaporator, the fluid enters and exits the evaporator as a two-phase fluid. The two-phase fluid enters the receiver, and the compressor draws fluid from the top of the receiver. In this manner the fluid entering the compressor is

always a saturated vapor. Similarly, when a receiver is placed at the exit of the condenser, the fluid does not exit as a subcooled liquid, but as a two-phase fluid. The entrance to the expansion device is from the bottom of the receiver. Thus the fluid entering the expansion device is always a saturated liquid.

To model this system a few standard assumptions are made. First, the compression of the fluid is assumed to be adiabatic with an isentropic efficiency. Second, isobaric conditions in the condenser and evaporator are assumed. Third, expansion through the valve is assumed to be isenthalpic.

To maximize efficiency of this system for a cooling application, the portion of the evaporator with two-phase flow needs to be maximized. Because the heat transfer coefficient between the liquid and the evaporator walls is much higher than the heat transfer coefficient between the vapor and the evaporator walls, the two-phase portion of the evaporator provides virtually all of the cooling capacity of the system. However, to ensure safe and reliable operation of the compressor, the fluid entering the compressor must be completely vapor. Systems with a receiver at the evaporator exit can ensure safe operation of the compressor, while maximizing the evaporator's performance. For systems without a receiver, a generally acceptable compromise is for the fluid to be 5° C above the saturation temperature. This is generally referred to as 5° C of superheat.

1.3.2 Transcritical Systems

The most common transcritical systems use carbon dioxide (CO_2 or R744) as the working fluid. The main disadvantage of this system is the high operating pressures necessary. Recently the lower environmental impact of this refrigerant has led to an increase in its appeal. A diagram of the system is shown with the accompanying P-h diagram in Figure 1.2.

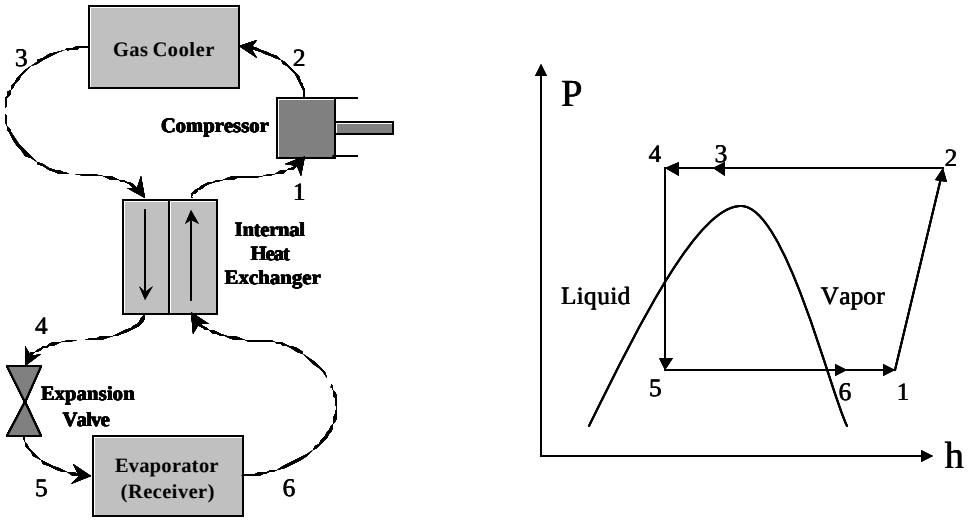

Figure 1.2 Diagram: Transcritical Cycle

This system resembles the subcritical system with a few alterations. As the fluid leaves the compressor, the fluid has an extremely high pressure and is above the critical point. This supercritical fluid behaves differently than both of the liquid and gas phases. At this state the fluid is compressible, which must be taken into account when modeling the heat exchanger. Because the fluid does not condense as it flows through the heat exchanger, the term "gas cooler" is used to describe the heat exchanger. Additionally, there is a third heat exchanger in the system. This is a counterflow heat exchanger and placed in between the gas cooler and expansion device, and between the

evaporator and compressor. This is generally referred to as the internal heat exchanger. In this manner the high temperature fluid leaving the gas cooler heats the fluid leaving the evaporator before it enters the compressor. This ensures that the fluid entering the compressor is superheated vapor, as well as providing some efficiency benefits that are more pronounced for CO_2 than for most subcritical refrigerants. The thermodynamic assumptions and performance considerations for this system are the same as those for the subcritical system.

1.3.3 Component Description

Compressors offer a small variety as to the means of controlling the mass flow. Simple compressors have a fixed displacement, and the mass flow rate is dictated by the inlet and outlet pressures, and the rotational speed. In automotive applications, the rotational speed is dictated by the engine speed, and can be engaged/disengaged by means of a clutch. In other applications the speed is altered in an on/off manner, or varied continuously by using a variable speed motor. More advanced compressors offer more variety in means to control the mass flow. For example, variable displacement compressors use a swashplate to vary the displacement of the compressor.

Expansion devices can be a fixed orifice, manual control valve, electronically controlled valve (EEV), thermostatic expansion valve, or high-side pressure-maintaining valve. The titles are self explanatory, except for the thermostatic expansion valve. This valve senses the amount of superheat at the exit of the evaporator and adjusts the valve opening to maintain a fixed amount of superheat.

Heat exchangers come in various types. In general there are three classes: microchannel, plate, and tube-and-fin. These terms refer to the geometric style of the exchanger.

1.4 Literature Review

1.4.1 Modeling of Vapor Compression Systems

The literature is replete with attempts to model the dynamics of vapor compression systems. Lebrun [22] and Bendapudi [5] both provide literature reviews of notable research in this area. Much of this section is drawn from these literature reviews. Bendapudi notes that there is considerable interest in deriving models that are simple mathematically but without losing relevant detail. Bendapudi also reports that the "largest task in modeling a refrigeration system was, usually, the modeling of the heat exchangers." He continues to note that the heat exchanger models can be classified into three groups: phase-dependent moving boundary method, the phase-independent finite difference methods, and a moving boundary with finite difference method (resulting from the combination of the first two methods).

Several authors make notable contributions to this field of research. Wedekind was among the first to study the transient behavior. In 1966 he and W. Stoecker published research regarding the transient response of the effective dry out point in evaporating flows [38]. In 1978 he proposed using a mean void fraction to develop a transient model for the evaporating and condensing flows of a vapor compression system [4,37]. Wedekind's research plays a critical role in the moving boundary method of modeling vapor compression cycles. The mean void fraction assumption is applied almost universally by other researchers developing moving boundary models, allowing the two-phase region to be modeled in lumped form.

Dhar and Soedel developed a dynamic model of an entire air conditioning system using a lumped parameter, moving boundary approach [11]. The two fluid phases are assumed to exchange mass internally and heat

externally. Chi and Didion also present a dynamic model of a complete vapor compression cycle using a moving boundary, lumped parameter formulation [10].

MacArthur used a distributed formulation for modeling these systems and presented simulation results in [24]. Later these models were compared to experimental data [25]. In 1992 Grald and MacArthur presented a moving boundary approach model [13].

Many other authors developed models similar to the moving boundary models or discretized models discussed. However, the references listed are sufficient for introducing the different modeling approaches and establishing their validity. All references given thus far have focused on subcritical cycles or components. Little research has been published on dynamic modeling of transcritical vapor compression cycles. Admittedly, the existing modeling approaches developed for subcritical cycles are applicable and appropriate for transcritical cycles. The few known publications regarding dynamic modeling of transcritical cycles, generally use a discretized modeling approach [30]. This thesis makes a unique contribution simply by applying some of the existing methodology to develop a control-oriented model of this unique cycle.

1.4.2 Void Fraction

As mentioned previously, the moving boundary, lumped parameter approach uses the concept of mean void fraction. Void fraction is defined as the ratio of vapor volume to total volume, and has long been used to describe certain characteristics of two-phase flows. Many experimental correlations have been proposed for predicting void fraction for various conditions and fluids. Excellent reviews of well known correlations can be found in [32] and [41]. These can be categorized into four divisions, listed in order of increasing complexity: Homogeneous, Slip Ratio, Lockhart-Martinelli, and Mass Flux Dependent. The latter two types are notably complex, whereas the first two are remarkably simple. Slip ratio is defined as the ratio of vapor velocity to liquid velocity. The slip ratio correlation defines void fraction as Equation 1.1, where x is the fluid quality. Fluid quality is defined as the ratio of vapor mass to total mass, and is therefore only meaningful for two-phase mixtures [8]. Assuming that the slip ratio is independent of fluid quality, this equation can be integrated to derive an expression for mean void fraction (Equations 1.2 and 1.3 where $b = 1 - a$ and $a = \left(\frac{r_g}{r_f} \right) S$). The homogenous correlation is simply a special case with the slip ratio equal to unity.

$$g = \frac{1}{1 + \left(\frac{1-x}{x} \right) \left(\frac{r_g}{r_f} \right) S} \tag{1.1}$$

$$\bar{g} = \frac{1}{x_2 - x_1} \int_{x_1}^{x_2} g(x) dx \tag{1.2}$$

$$\bar{g} = \frac{1}{b} + \frac{1}{x_2 - x_1} \left[\frac{a}{b} \ln \left(\frac{b x_1 + a}{b x_2 + a} \right) \right] \tag{1.3}$$

As mentioned, Wedekind developed the idea of using the concept of a mean void fraction when attempting to predict the transient behavior of two-phase flows. This idea has been subsequently used by many authors attempting to model evaporating or condensing flows. In many cases the authors assume that the value of mean void fraction is time-invariant for small transients. While this is an acceptable approximation, and simplifies the modeling of heat exchangers with complete evaporation or condensation, it cannot be used for conditions when the exiting fluid is two-phase. For this condition, the dynamic variable of interest is the quality or enthalpy of the exiting fluid. This information is explicitly contained in the formulation of mean void fraction. Therefore if the change of exit quality with respect to time is desired, mean void fraction must be allowed to be time-varying.

1.4.3 Control of Vapor Compression Systems

Much of the original research regarding control of vapor compression cycles focused on the performance of the thermostatic expansion valve (TEV). The TEV is used as an expansion device with a mechanical control device. All variations of the TEV use some measure of evaporator superheat to control the expansion valve opening. The marginally stable behavior of this type of control is well documented. The observed sinusoidal fluctuations in superheat temperature are generally termed "valve hunting". In 1966 W. Stoecker presented a simplified dynamical analysis of valve hunting [35,38], and in 1973 Najork attempted to give optimal parameter settings to minimize hunting [27]. In 1980 Broersen and van der Jagt used a mean void fraction model of the evaporator to show that valve hunting is caused by the interaction between the TEV and evaporator dynamics [7]. Gruhle and Isermann used a discretized model of the evaporator to show similar results and contrasted the TEV with the proportional-integral (PI) controlled valve in 1985 [14].

To the author's knowledge, the first research to be concerned with control-oriented modeling of vapor compression cycles for the use of designing advanced control strategies was the work of Xiang-Dong He. Together with Harry Asada, Sheng Liu, and Hiroyuki Itoh a number of articles were published that used the moving boundary, lumped parameter approach to model an entire subcritical vapor compression cycle. The model was then used for designing MIMO control strategies. Of particular relevance to this research were X.D. He's dissertation [15] and two journal articles [16] and [17]. In [16], a reduced order model is proposed, analyzed, and used for controller design. Unfortunately no simulation or validation results for the reduced order model were presented, and no conclusion can be made regarding the simplifying assumptions made.

Beginning with X.D. He's research, an increasing amount of research has focused on developing control-oriented models of vapor compression systems. Some of these are documented in [19] and in the two part article [40] and [29] (these articles only present models of the evaporator, not an entire system). The same approach has also been used on other types of systems for control-oriented modeling (see Aström's work on drum boiler dynamics [3]). There has also been considerable work on intelligent control, as well as empirical model-based control of complex HVAC systems, but because this is not the focus of this research, a review of the literature is not presented here.

1.5 Notation

This section attempts to clarify the notational conventions used in this thesis, specifically with regard to the derivations in Chapters 2 and 6. As much as possible, standard thermodynamic notation is used. Because

thermodynamic properties are evaluated at equilibrium conditions, combining thermodynamic properties with dynamic modeling can result in conflicts in commonly accepted notational conventions.

For example, saturated liquid density is known to be a function of only one thermodynamic variable, such as pressure, $r_f = f(P)$. The gradient of this property with respect to pressure would commonly be denoted as in Equation 1.4. Thus the time derivative of saturated liquid density would be denoted as in Equation 1.5.

$$\left(\frac{dr_f}{dP}\right) \tag{1.4}$$

$$\dot{r}_f = \left(\frac{dr_f}{dt}\right) = \left(\frac{dr_f}{dP}\right)\left(\frac{dP}{dt}\right) = \left(\frac{dr_f}{dP}\right)\dot{P} \tag{1.5}$$

However, when pressure is considered to be a function of time, mathematical conventions would require different notation. Consider the general case in Equation 1.6. Then the correct mathematical notation for the partial derivative of x with respect to z is given in Equation 1.7. To be mathematically precise the above partial derivative of saturated liquid density should be written as in Equation 1.8. However, writing the gradient of saturated liquid density with respect to pressure as a partial derivative is unsettling to the thermodynamic community. Therefore, in this thesis, the thermodynamic conventions are followed at the sacrifice of mathematical precision (Equation 1.5).

$$\begin{aligned} x &= f(y) \\ y &= f(z) \end{aligned} \tag{1.6}$$

$$\frac{dx}{dz} = \left(\frac{\partial x}{\partial y}\right)\left(\frac{\partial y}{\partial z}\right) \tag{1.7}$$

$$\dot{r}_f = \left(\frac{dr_f}{dt}\right) = \left(\frac{\partial r_f}{\partial P}\right)\left(\frac{\partial P}{\partial t}\right) = \left(\frac{\partial r_f}{\partial P}\right)\dot{P} \tag{1.8}$$

For those properties that are functions of more than one variable, the partial derivative symbol is used. Because thermodynamic properties can generally be calculated as a function of more than one variable, it is necessary to specify which variables are being considered. For example, temperature can be calculated from pressure and enthalpy, $T = f(P,h)$, or pressure and entropy, $T = f(P,s)$. The partial derivative of temperature with respect to pressure will be different if the secondary variable is considered to be enthalpy or entropy (Equation 1.9).

Additionally, often in a single derivation the same gradient is used multiple times, but evaluated at different conditions. To clearly indicate the point at which the gradient should be evaluated, the appropriate subscripts will be used. For example, assuming the outlet temperature is calculated from the outlet enthalpy and outlet pressure, the partial derivative of temperature with respect to enthalpy at a constant pressure is denoted as in Equation 1.10. Finally, if a partial derivative is derived in terms of other quantities, it is distinguished by intentionally not including the "pipe" symbol. An example is given in Equations 1.11 and 1.12.

$$\left(\left.\frac{\partial T}{\partial P}\right|_{h}\right) \neq \left(\left.\frac{\partial T}{\partial P}\right|_{s}\right) \tag{1.9}$$

$$\left(\left.\frac{\partial T_{out}}{\partial h_{out}}\right|_{P_{out}}\right) \tag{1.10}$$

$$f(x, y) = x^2 y \tag{1.11}$$

$$\left(\frac{\partial f}{\partial x}\right) = 2xy \tag{1.12}$$

1.6 Organization of Thesi s

The remainder of this thesis is organized as follows. Chapter 2 describes the modeling procedure for each of the components and presents the resulting model. Chapter 3 presents the simulation environment developed for simulation, model validation, and controller design. Chapter 4 details the experimental setup, explains the experiments conducted, and also presents the methodology and results for the empirical models developed using this data. Model validation results are given in Chapter 5. The approach for deriving a linearized version of the nonlinear models is presented in Chapter 6. This chapter also details some dynamic analysis based on the resulting models. Chapter 7 presents the general approach used to derive reduced order models for the models, the resulting reduced order models, and identifies the dominant system dynamics. Conclusions and suggestions for future work are given in Chapter 8.

Chapter 2. Dynamic Modeling

"I would not recommend this as a Ph.D. project. The ratio of [perspiration] to inspiration is very high."
[Dr. Karl Aström discussing dynamic modeling of two-phase flows during a visit to the University of Illinois at Urbana-Champaign]

2.1 Introduction

This chapter discusses the vapor compression system being modeled, and presents a detailed explanation of the methods used to model each component of the system. For each component a qualitative description, modeling assumptions, derivation, and resulting model are given. This thesis is concerned with a low order model of the dominant dynamic behavior of a transcritical vapor compression system. The system being modeled is depicted in Figure 2.1. The dynamics of this system is assumed to be dominated by the dynamics of the heat exchangers. The dynamics of the actuating components (compressor, valve, etc.) are considered to be fast relative to the dynamics of the heat exchangers. Thus the actuating components are modeled with static (algebraic) relationships. The modeling of the other components is significantly more complex. Fluid flow through the gas cooler is supercritical (above the critical point). Fluid flow through the evaporator involves one or more transitions between different fluid phases. Detailed modeling of dynamic two-phase fluid flow is difficult and mathematically complex, generally requiring the use of computational fluid dynamics. Past efforts to create simple models for computational reasons now become useful in creating simple models for control. The approach most applicable to the objectives of this research is known as the lumped parameter, moving boundary approach. This approach assumes a time-varying boundary between regions of different fluid state (i.e. subcooled liquid, two-phase, or superheated vapor). Separate control volumes are considered for each of the fluid regions, and the necessary distributed parameters are "lumped" for each of these regions.

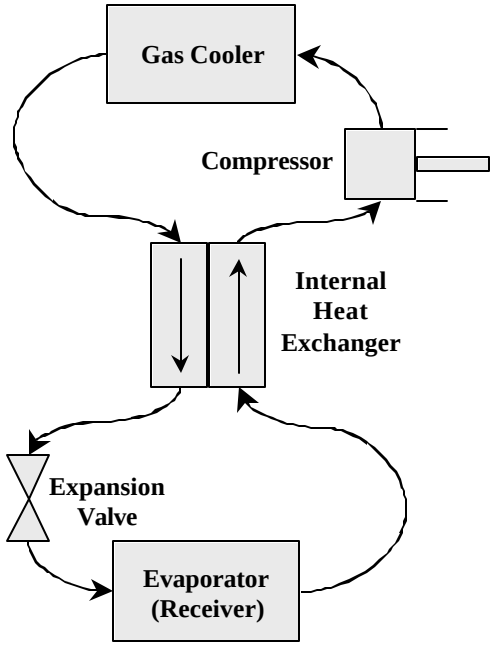

Figure 2.1 Transcritical Air Conditioning System

To derive governing differential equations suitable for simulation or analysis, the most common method [13,17,19,40] is to begin with the governing partial differential equations (PDEs) for fluid flow in a tube. After applying a few simplifying assumptions, these PDEs can be integrated along the length of the heat exchanger to remove the spatial dependence and yield several ordinary differential equations (ODEs). The number of ODEs depends on the number of fluid regions assumed. From a controls perspective, this approach yields a dynamic model with the state variables predetermined in the derivation. The resulting model is well suited for simulation, but ill suited for model reduction. This will be referred to as the PDE method. An alternative method uses the unsteady state form of the conservation of mass and energy equations. By assuming control volumes associated with each of the fluid regions, these equations can be expanded into several forms. This method will be shown to be completely equivalent to the PDE method. However, this method has some distinct advantages including derivation simplicity, conceptual simplicity, decoupled dynamics, and most importantly, freedom in choosing the dynamic states. This will be referred to as the energy method. The following sections will outline the modeling approach for each static and dynamic component necessary for modeling a transcritical vapor compression cycle. The sections regarding the gas cooler and the evaporator include the modeling assumptions for both the PDE and energy methods and the resulting models.

2.2 Variable Speed Compressor

The compressor is assumed to be a variable speed compressor (i.e. mass flow rate is modulated by changing the rotational speed of the compressor). Two algebraic relationships are used to model this component. Mass flow rate is calculated in Equation 2.1 where $r_k = r\left(P_{k,in}, h_{k,in}\right)$, and a volumetric efficiency, h_{vol}, is assumed. Additionally, compression is assumed to be an adiabatic process with an isentropic efficiency, and therefore the relationship between the entrance and exit enthalpies is given in Equation 2.2, where $h_{out,isentropic} = h\left(P_{out}, s_k\right)$ and $s_k = s\left(P_{in}, h_{in}\right)$. For implementation, this is rearranged to give Equation 2.3. Because the isentropic efficiency changes with operating condition, it is assumed to be a linear function of pressure ratio (Equation 2.4). For simulation purposes, the change of compressor speed is rate limited to reflect the limitations of a real compressor.

$$\dot{m}_k = w_k V_k r_k \underbrace{\left(1 + C_k - D_k\left(\frac{P_{out}}{P_{in}}\right)^{\frac{1}{n}}\right)}_{h_{vol}} \tag{2.1}$$

$$\frac{h_{out,isentropic} - h_{in}}{h_{out} - h_{in}} = h_k \tag{2.2}$$

$$h_{out} = \frac{1}{h_k}\left[h_{out,isentropic} + h_{in}\left(h_k - 1\right)\right] \tag{2.3}$$

$$h_k = A_k\left(\frac{P_{out}}{P_{in}}\right) + B_k \tag{2.4}$$

2.3 Expansion Valve

The expansion device is assumed to be an electronic expansion valve (i.e. mass flow rate is modulated by changing the valve area with an electronic input). Two algebraic relationships are used to model this component. Mass flow rate is calculated in Equation 2.5 where $r_v = r\left(P_{v,in}, h_{v,in}\right)$, and assuming an effective valve area, A_v, and discharge coefficient, C_v. Since the expansion valve is electronically controlled, the area of the valve is assumed to be a linear function of some control input (Equation 2.6). The discharge coefficient is assumed to be a function of Reynold's number, or approximately mass flow rate (Equation 2.7). Thus the mass flow rate equation is a function of three empirical coefficients (Equation 2.8). Additionally, compression is assumed to be an isenthalpic process (Equation 2.9). For simulation purposes, the change in electronic input is rate limited to reflect the limitations of a real expansion valve.

$$\dot{m}_v = A_v C_v \left[r_v \left(P_{in} - P_{out} \right) \right]^n \tag{2.5}$$

$$A_v = b_1 + b_2 u_v \tag{2.6}$$

$$\begin{aligned} C_v &= b_3 \left(1 + \frac{b_4}{\mathrm{Re}_d} \right) \\ &\approx b_3 \left(1 + \frac{b_5}{\dot{m}_v} \right) \end{aligned} \tag{2.7}$$

$$\dot{m}_v = k_1 \left(1 + k_2 u_v\right) \left(1 + \frac{k_3}{\dot{m}_v} \right) \left[r_v \left(P_{in} - P_{out} \right) \right]^n \tag{2.8}$$

$$h_{v,in} = h_{v,out} \tag{2.9}$$

2.4 Gas Cooler

For transcritical cycles, a gas cooler replaces the condenser (the traditional component in subcritical cycles). This component is arguably the simplest possible case for heat exchanger modeling. The fluid is assumed to be neither gas nor liquid, but a supercritical fluid, which behaves differently than both of the subcritical phases. For this component a single fluid region is assumed (Figure 2.2).

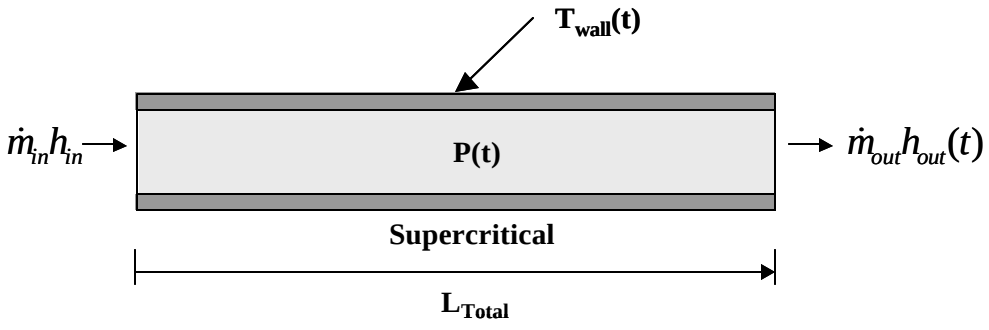

Figure 2.2 Diagram: Gas Cooler

2.4.1 Modeling Assumptions

The modeling methods to be presented require several assumptions about the fluid flow in the heat exchangers. These assumptions were commonly used in past modeling efforts and are as follows:

- The heat exchanger is a long, thin, horizontal tube.
- The refrigerant flowing through the heat exchanger tube can be modeled as a one-dimensional fluid flow.
- Axial conduction of refrigerant is negligible.
- Pressure drop along the heat exchanger tube due to momentum change in refrigerant and viscous friction is negligible (refrigerant pressure along the entire heat exchanger tube can be assumed to be uniform). Thus the equation for conservation of momentum is not needed.

2.4.2 PDE Method

As mentioned in the introduction, the most common method for deriving ordinary differential equations using the lumped parameter, moving boundary approach is to integrate the governing partial differential equations along the length of the heat exchanger tube to remove spatial dependence. An explanation of the partial differential equations for conservation of refrigerant mass and energy can be found in [13], and are replicated in Equations 2.10 - 2.11 respectively, where $\vec{u}$ is the fluid velocity vector, $\vec{f}$ is the body force vector and s is the stress tensor. (The conservation of momentum is neglected and not included here.) By applying the assumptions outlined in the previous section, it is possible to simplify these equations to one-dimensional PDEs. A detailed explanation of these steps can be found in [13]. (The derivation presented in this thesis differs from that presented in the cited source only by not neglecting the rate change of pressure with respect to time in the conservation of energy equation.) The resulting equations for conservation of refrigerant mass and energy in the heat exchanger tube are given in Equations 2.12 - 2.13. Additionally an equation for the conservation of heat exchanger wall energy is given in Equation 2.14. The necessary notation is described in Table 2.1.

$$\frac{\partial r}{\partial t} + \nabla \cdot (r\vec{u}) = 0 \tag{2.10}$$

$$\frac{\partial (r\vec{u})}{\partial t} + \nabla \cdot (r\vec{u}\vec{u}) = r\vec{f} + \nabla \cdot s \tag{2.11}$$

$$\frac{\partial (rA_{cs})}{\partial t} + \frac{\partial (\dot{m})}{\partial z} = 0 \tag{2.12}$$

$$\frac{\partial (rA_{cs}h - A_{cs}P)}{\partial t} + \frac{\partial (\dot{m}h)}{\partial z} = p_i a_i (T_w - T_r) \tag{2.13}$$

$$\left(C_p rA\right)_w \frac{\partial (T_w)}{\partial t} = p_i a_i (T_r - T_w) + p_o a_o (T_a - T_w) \tag{2.14}$$

Table 2.1 Notation for Governing Partial Differential Equations

r	density of refrigerant
P	pressure of refrigerant
h	enthalpy of refrigerant
p_i	inner perimeter (interior surface area per unit length)
p_o	outer perimeter (exterior surface area per unit length)
T_r	temperature of refrigerant
T_w	tube wall temperature
a_i	heat transfer coefficient between tube wall and internal fluid
a_o	heat transfer coefficient between tube wall and external fluid
A_{cs}	cross-sectional area of the inside of tube
$\dot{m}$	mass flow rate of refrigerant flowing along the tubes
$(C_p r A)_w$	thermal capacitance of tube wall per unit length

2.4.3 Simplification of the PDEs

The governing PDEs presented are used to derive lumped parameter ODEs to model the dynamics of two-phase flow heat exchangers. These equations are integrated along the length of the tube for each section of tube. To perform the necessary integrations, an integration rule commonly known as Leibniz's equation will be used (Equation 2.15), with z being the spatial coordinate. Thus the limits of integration depend on the how the regions are defined for each heat exchanger. For the gas cooler the limits of integration are simply $z_1 = 0$ and $z_2 = L_{total}$.

$$\int_{z_1(t)}^{z_2(t)} \frac{\partial f(z,t)}{\partial t} dz = \frac{d}{dt}\left[\int_{z_1(t)}^{z_2(t)} f(z,t)dz\right] - f(z_2(t),t)\frac{d(z_2(t))}{dt} + f(z_1(t),t)\frac{d(z_1(t))}{dt} \qquad (2.15)$$

The resulting ordinary differential equations can be combined, simplified, and organized into matrix form. This form is generally referred to in controls applications as "state space form." The general form for a linear, time-invariant system is given in Equation 2.16. In this form, u is the vector of inputs, y the vector of outputs, and x the vector of states. $\{A, B, C, D\}$ are constant matrices. Because the systems resulting from the outlined modeling approach are nonlinear models, an alternate state space form is used (Equation 2.17). The resulting set of equations can be solved numerically given appropriate initial conditions. The dynamic order, or number of state variables for each component, reflects the relative complexity of the component dynamics.

$$\begin{aligned} \dot{x} &= Ax + Bu \\ y &= Cx + Du \end{aligned} \qquad (2.16)$$

$$\begin{aligned} \dot{x} &= f(x,u) \\ y &= g(x,u) \end{aligned} \qquad (2.17)$$

2.4.3.1 Conservation of Refrigerant Mass

The PDE for conservation of refrigerant mass is given in Equation 2.18. Each term of this equation is integrated from $z = 0$ to $z = L_{total}$. Integrating the first term and assuming a constant cross-sectional area results in Equation 2.19. Applying Leibniz's equation results in Equation 2.20. Assuming an average density in the gas cooler, r_c, and performing the integration results in Equation 2.21. Taking the time derivative results in Equation 2.22. Selecting pressure and enthalpy as the independent variables for calculating thermodynamic properties, and assuming an average enthalpy, h_c, Equation 2.22 can be rewritten as Equation 2.23. Integrating the second term of the PDE results in Equation 2.24. Combining the results of the integration results in Equation 2.25 for the conservation of refrigerant mass.

$$\frac{\partial(rA_{cs})}{\partial t} + \frac{\partial(\dot{m})}{\partial z} = 0 \tag{2.18}$$

$$\int_0^{L_{total}} \frac{\partial(rA_{cs})}{\partial t} dz = A_{cs}\left[\int_0^{L_{total}} \frac{\partial(r)}{\partial t} dz\right] \tag{2.19}$$

$$\int_0^{L_{total}} \frac{\partial(rA_{cs})}{\partial t} dz = A_{cs}\left[\frac{d}{dt}\int_0^{L_{total}} r\,dz\right] \tag{2.20}$$

$$\int_0^{L_{total}} \frac{\partial(rA_{cs})}{\partial t} dz = A_{cs}\left[\frac{d}{dt}(r_c L_{total})\right] \tag{2.21}$$

$$\int_0^{L_{total}} \frac{\partial(rA_{cs})}{\partial t} dz = A_{cs} L_{total}[\dot{r}_c] \tag{2.22}$$

$$\int_0^{L_{total}} \frac{\partial(rA_{cs})}{\partial t} dz = A_{cs} L_{total}\left[\left(\frac{\partial r}{\partial P_c}\bigg|_{h_c}\right)\dot{P}_c + \left(\frac{\partial r}{\partial h_c}\bigg|_{P_c}\right)\dot{h}_c\right] \tag{2.23}$$

$$\int_0^{L_{total}} \frac{\partial(\dot{m})}{\partial z} dz = \dot{m}_{out} - \dot{m}_{in} \tag{2.24}$$

$$\left[\left(\frac{\partial r}{\partial P_c}\bigg|_{h_c}\right)A_{cs} L_{total}\right]\dot{P}_c + \left[\left(\frac{\partial r}{\partial h_c}\bigg|_{P_c}\right)A_{cs} L_{total}\right]\dot{h}_c + \dot{m}_{out} - \dot{m}_{in} = 0 \tag{2.25}$$

2.4.3.2 Conservation of Refrigerant Energy

The PDE for conservation of refrigerant energy is given in Equation 2.26. Each term of this equation is integrated from $z = 0$ to $z = L_{total}$. Integrating the first term and assuming a constant cross-sectional area results in Equation 2.27. Applying Leibniz's equation results in Equation 2.28. Assuming an average density in the gas cooler, r_c, and an average enthalpy, h_c, results in Equation 2.29. Taking the time derivative results in Equation 2.30. Selecting pressure and enthalpy as the independent variables for calculating thermodynamic properties Equation 2.30 can be rewritten as Equation 2.31, and then rearranged into Equation 2.32. Integrating the second term of the PDE results in Equation 2.33. Taking the time derivative and performing the integration results in

Equations 2.34 and 2.35 respectively. Integrating the third term of the PDE results in Equation 2.36. Integrating the right side of the equation and rearranging results in Equations 2.37 and 2.38 respectively. Combining the results of the integration results in Equation 2.39 for the conservation of refrigerant energy.

$$\frac{\partial(rA_{cs}h - A_{cs}P)}{\partial t} + \frac{\partial(\dot{m}h)}{\partial z} = p_i a_i (T_w - T_r) \tag{2.26}$$

$$\int_0^{L_{total}} \frac{\partial(rA_{cs}h)}{\partial t} dz = A_{cs}\left[\int_0^{L_{total}} \frac{\partial(rh)}{\partial t} dz\right] \tag{2.27}$$

$$\int_0^{L_{total}} \frac{\partial(rA_{cs}h)}{\partial t} dz = A_{cs}\left[\frac{d}{dt}\int_0^{L_{total}} rh dz\right] \tag{2.28}$$

$$\int_0^{L_{total}} \frac{\partial(rA_{cs}h)}{\partial t} dz = A_{cs}\left[\frac{d}{dt}(r_c h_c L_{total})\right] \tag{2.29}$$

$$\int_0^{L_{total}} \frac{\partial(rA_{cs}h)}{\partial t} dz = A_{cs} L_{total}\left[\dot{r}_c h_c + r_c \dot{h}_c\right] \tag{2.30}$$

$$\int_0^{L_{total}} \frac{\partial(rA_{cs}h)}{\partial t} dz = A_{cs} L_{total}\left[\left[\left(\frac{\partial r}{\partial P_c}\bigg|_{h_c}\right)\dot{P}_c + \left(\frac{\partial r}{\partial h_c}\bigg|_{P_c}\right)\dot{h}_c\right]h_c + r_c \dot{h}_c\right] \tag{2.31}$$

$$\int_0^{L_{total}} \frac{\partial(rA_{cs}h)}{\partial t} dz = \left[\left(\frac{\partial r}{\partial P_c}\bigg|_{h_c}\right)h_c\right]A_{cs}L_{total}\dot{P}_c + \left[\left(\frac{\partial r}{\partial h_c}\bigg|_{P_c}\right)h_c + r_c\right]A_{cs}L_{total}\dot{h}_c \tag{2.32}$$

$$\int_0^{L_{total}} \frac{\partial(A_{cs}P)}{\partial t} dz = A_{cs}\int_0^{L_{total}} \frac{\partial(P)}{\partial t} dz \tag{2.33}$$

$$\int_0^{L_{total}} \frac{\partial(A_{cs}P)}{\partial t} dz = A_{cs}\int_0^{L_{total}} \dot{P}_c dz \tag{2.34}$$

$$\int_0^{L_{total}} \frac{\partial(A_{cs}P)}{\partial t} dz = A_{cs} L_{total}\dot{P}_c \tag{2.35}$$

$$\int_0^{L_{total}} \frac{\partial(\dot{m}h)}{\partial z} dz = \dot{m}_{out}h_{out} - \dot{m}_{in}h_{in} \tag{2.36}$$

$$\int_0^{L_{total}} p_i a_i (T_w - T_r) dz = p_i L_{total} a_i (T_w - T_r) \tag{2.37}$$

$$\int_0^{L_{total}} p_i a_i (T_w - T_r) dz = a_i A_i (T_w - T_r) \tag{2.38}$$

$$\left[\left(\left.\frac{\partial r}{\partial P_c}\right|_{h_c}\right)h_c+1\right]A_{cs}L_{total}\dot{P}_c+\left[\left(\left.\frac{\partial r}{\partial h_c}\right|_{P_c}\right)h_c+r_c\right]A_{cs}L_{total}\dot{h}_c \\ +\dot{m}_{out}h_{out}-\dot{m}_{in}h_{in}=\alpha_i A_i(T_w-T_r) \tag{2.39}$$

2.4.3.3 Conservation of Tube Wall Energy

The PDE for the conservation of tube wall energy is given in Equation 2.40. Integrating each side of this equation from $z=0$ to $z=L_{total}$ results in Equation 2.41, and can be simplified to Equation 2.42.

$$(C_p rA)_w\frac{\partial(T_w)}{\partial t}=p_i\alpha_i(T_r-T_w)+p_o\alpha_o(T_a-T_w) \tag{2.40}$$

$$(C_p rA)_w L_{total}\frac{\partial(T_w)}{\partial t}=p_i L_{total}\alpha_i(T_r-T_w)+p_o L_{total}\alpha_o(T_a-T_w) \tag{2.41}$$

$$(C_p rV)_w\frac{\partial(T_w)}{\partial t}=\alpha_i A_i(T_r-T_w)+\alpha_o A_o(T_a-T_w) \tag{2.42}$$

2.4.3.4 Governing Ordinary Differential Equations

Combining the final results of the integrated PDEs into a matrix form results in Equation 2.43, which is of the $Z(x,u)\cdot\dot{x}=f(x,u)$ form, with states $x=\begin{bmatrix}P & h_c & T_w\end{bmatrix}^T$, and where the elements of the $Z(x,u)$ matrix are given in Table 2.2.

$$\begin{bmatrix}z_{11} & z_{12} & 0\\ z_{21} & z_{22} & 0\\ 0 & 0 & z_{33}\end{bmatrix}\begin{bmatrix}\dot{P}_c\\ \dot{h}_c\\ \dot{T}_w\end{bmatrix}=\begin{bmatrix}\dot{m}_{in}h_{in}-\dot{m}_{out}h_{out}-\alpha_i A_i(T_r-T_w)\\ \dot{m}_{in}-\dot{m}_{out}\\ \alpha_i A_i(T_r-T_w)-\alpha_o A_o(T_w-T_a)\end{bmatrix} \tag{2.43}$$

Table 2.2 Matrix Elements of $Z(x,u)$ for the Gas Cooler

z_{11}	$\left[\left(\left.\frac{\partial r_c}{\partial P_c}\right\|_{h_c}\right)h_c-1\right]A_{cs}L_{total}$
z_{12}	$\left[\left(\left.\frac{\partial r_c}{\partial h_c}\right\|_{P_c}\right)h_c+r_c\right]A_{cs}L_{total}$
z_{21}	$\left(\left.\frac{\partial r_c}{\partial P_c}\right\|_{h_c}\right)A_{cs}L_{total}$
z_{22}	$\left(\left.\frac{\partial r_c}{\partial h_c}\right\|_{P_c}\right)A_{cs}L_{total}$
z_{33}	$(C_p rV)_w$

2.4.4 Energy Method

The conservation of refrigerant energy for each region is given in Equation 2.44 where $\dot{U}$ is the rate of change of the total internal energy of the refrigerant in the region considered, $\dot{H}_{in}$ is the rate of energy entering the region by means of refrigerant mass, $\dot{H}_{out}$ is the rate of energy leaving the region by means of refrigerant mass, $\dot{Q}_w$ is the rate of energy leaving the region through heat transfer to the heat exchanger wall, and $\dot{W}$ is the rate of moving boundary work being performed because of a change in the boundary between the regions. Special care regarding the proper sign convention of this term is essential. In general $\dot{W} = \frac{d}{dt}(PV) = +\dot{P}V - P\dot{V}$ where the sign of each of these two terms depends on the definition of work. For this thesis, the work added by an increase in pressure is positive, $+\dot{P}V$, and the work done by an increasing the volume by a change in the moving boundary is negative, $-P\dot{V}$.

$$\dot{U} = \dot{H}_{in} - \dot{H}_{out} - \dot{Q}_w - \dot{W} \tag{2.44}$$

The conservation of wall energy for each region is given in Equation 2.45 where $\dot{E}_w$ is the rate of change of the total energy of the heat exchanger wall in the region considered, $\dot{Q}_a$ is the rate of energy leaving the heat exchanger wall through heat transfer to the external fluid, and $\dot{E}_{\text{int}}$ is the rate of energy being transferred to another region of the heat exchanger wall by a change in the boundary between the regions.

$$\dot{E}_w = \dot{Q}_w - \dot{Q}_a - \dot{E}_{\text{int}} \tag{2.45}$$

The conservation of mass for the entire heat exchanger is given in Equation 2.46 where the rate of change of the total refrigerant mass in the heat exchanger is equal to the difference between mass entering and leaving the gas cooler.

$$\dot{m} = \dot{m}_{in} - \dot{m}_{out} \tag{2.46}$$

Applying the unsteady state form of the conservation of mass, refrigerant energy, and wall energy to the single region of the gas cooler, and arranging in matrix form results in Equation 2.47.

$$\begin{bmatrix} \dot{U}_c \\ \dot{m}_c \\ \dot{E}_w \end{bmatrix} = \begin{bmatrix} \dot{m}_{in}h_{in} - \dot{m}_{out}h_{out} - a_i A_i (T_r - T_w) \\ \dot{m}_{in} - \dot{m}_{out} \\ a_i A_i (T_r - T_w) - a_o A_o (T_w - T_a) \end{bmatrix} \tag{2.47}$$

2.4.5 Equivalence

By applying the assumptions regarding operating condition, the time derivative terms in the above equations can be expanded in terms of other variables. This allows some freedom in choosing the dynamic state variables. The results of this approach can be shown to be equivalent to the results of the PDE approach by selecting the same state variables for the energy approach as those given by the PDE approach.

Defining the total internal energy in terms of the total refrigerant mass and an average specific internal energy $U_c = m_c u_c$, the time derivative of this term can be expanded as in Equation 2.48. Defining the refrigerant mass in terms of an average density, r_c, and the internal volume, $V_c = A_{cs} L_{total}$, yields Equation 2.49. Since density and internal energy can be given as functions of pressure, P_c, and enthalpy, h_c, the time derivative of these variables can be written in terms of the desired state (Equation 2.50). Simplifying this expression and substituting the formal definition of enthalpy $h = u + Pv$ or $h = u + P/r$, and its partial derivatives of $\left.\frac{\partial u}{\partial P}\right|_h = -\frac{1}{r}$ and $\left.\frac{\partial u}{\partial h}\right|_P = 1 + \frac{P}{r^2}\left(\left.\frac{\partial r}{\partial h}\right|_P\right)$ results in Equations 2.51 and 2.52 respectively. Likewise expanding the time derivative of total mass inventory results in Equations 2.53 and 2.54. Finally, defining the total wall energy as the product of thermal capacitance and temperature $E_w = \left(C_p r V\right)_w T_w$, the time derivative of this term can be written as in Equation 2.55. Comparing Equations 2.52, 2.54, and 2.55 to Equation 2.43 reveals that they are equivalent.

$$\dot{U}_c = \dot{m}_c u_c + m_c \dot{u}_c \tag{2.48}$$

$$\dot{U}_c = (\dot{r}_c u_c + r_c \dot{u}_c) A_{cs} L_{total} \tag{2.49}$$

$$\dot{U}_c = \left[\left(\left.\frac{\partial r_c}{\partial P_c}\right|_{h_c}\right)\dot{P}_c + \left(\left.\frac{\partial r_c}{\partial h_c}\right|_{P_c}\right)\dot{h}_c\right] u_c + \left[\left(\left.\frac{\partial u_c}{\partial P_c}\right|_{h_c}\right)\dot{P}_c + \left(\left.\frac{\partial u_c}{\partial h_c}\right|_{P_c}\right)\dot{h}_c\right] r_c \Bigg] A_{cs} L_{total} \tag{2.50}$$

$$\dot{U}_c = \left[\left(\left.\frac{\partial r_c}{\partial P_c}\right|_{h_c}\right) u_c + \left(\left.\frac{\partial u_c}{\partial P_c}\right|_{h_c}\right) r_c\right] A_{cs} L_{total} \dot{P}_c + \left[\left(\left.\frac{\partial r_c}{\partial h_c}\right|_{P_c}\right) u_c + \left(\left.\frac{\partial u_c}{\partial h_c}\right|_{P_c}\right) r_c\right] A_{cs} L_{total} \dot{h}_c \tag{2.51}$$

$$\dot{U}_c = \left[\left(\left.\frac{\partial r_c}{\partial P_c}\right|_{h_c}\right) h_c - 1\right] A_{cs} L_{total} \dot{P}_c + \left[\left(\left.\frac{\partial r_c}{\partial h_c}\right|_{P_c}\right) h_c + r_c\right] A_{cs} L_{total} \dot{h}_c \tag{2.52}$$

$$\dot{m}_c = \dot{r}_c A_{cs} L_{total} \tag{2.53}$$

$$\dot{m}_c = \left[\left(\left.\frac{\partial r_c}{\partial P_c}\right|_{h_c}\right)\dot{P}_c + \left(\left.\frac{\partial r_c}{\partial h_c}\right|_{P_c}\right)\dot{h}_c\right] A_{cs} L_{total} \tag{2.54}$$

$$\dot{E}_w = \left(C_p r V\right)_w \dot{T}_w \tag{2.55}$$

2.4.6 Second Representation

A second representation can be derived by simply expanding the time derivative of $U_c = m_c u_c$ in terms of pressure, P_c, and density, r_c (Equations 2.56 - 2.59). This results in what will be referred to as the second representation, and will be denoted with the prime notation (i.e. $Z'(x', u') \cdot \dot{x}' = f'(x', u')$). When the resulting equations are arranged in matrix form, the resulting model is of the same form as Equation 2.43, but with alternative

state variables of $x' = [P \quad m_c \quad T_w]^T$. The resulting model is given in Equation 2.60 where the elements of the $Z'(x',u')$ matrix are given in Table 2.3.

$$\dot{U}_c = \dot{m}_c u_c + m_c \dot{u}_c \tag{2.56}$$

$$\dot{U}_c = \dot{m}_c u_c + m_c \left(\left(\left. \frac{\partial u_c}{\partial P_c} \right|_{r_c} \right) \dot{P}_c + \left(\left. \frac{\partial u_c}{\partial r_c} \right|_{P_c} \right) \dot{r}_c \right) \tag{2.57}$$

$$\dot{U}_c = \dot{m}_c u_c + m_c \left(\left(\left. \frac{\partial u_c}{\partial P_c} \right|_{r_c} \right) \dot{P}_c + \left(\left. \frac{\partial u_c}{\partial r_c} \right|_{P_c} \right) \frac{\dot{m}_c}{V_c} \right) \tag{2.58}$$

$$\dot{U}_c = \left[u_c + \left(\left. \frac{\partial u_c}{\partial r_c} \right|_{P_c} \right) \frac{m_c}{V_c} \right] \dot{m}_c + \left[m_c \left(\left. \frac{\partial u_c}{\partial P_c} \right|_{r_c} \right) \right] \dot{P}_c \tag{2.59}$$

$$\begin{bmatrix} z'_{11} & z'_{12} & 0 \\ 0 & 1 & 0 \\ 0 & 0 & z'_{33} \end{bmatrix} \begin{bmatrix} \dot{P}_c \\ \dot{m}_c \\ \dot{T}_w \end{bmatrix} = \begin{bmatrix} \dot{m}_{in} h_{in} - \dot{m}_{out} h_{out} - a_i A_i (T_r - T_w) \\ \dot{m}_{in} - \dot{m}_{out} \\ a_i A_i (T_r - T_w) - a_o A_o (T_w - T_a) \end{bmatrix} \tag{2.60}$$

Table 2.3 Matrix Elements of $Z'(x',u')$ for the Gas Cooler

z'_{11}	$m_c \left(\left. \frac{\partial u_c}{\partial P_c} \right|_{r_c} \right)$
z'_{12}	$u_c + \left(\left. \frac{\partial u_c}{\partial r_c} \right|_{P_c} \right) r_c$
z'_{33}	$(C_p r V)_w$

A useful result that stems from the equivalence of the various representations is that the matrix $Z'(x',u')$ can be calculated directly from the elements of $Z(x,u)$. By observing that $f(x,u) = f'(x',u')$, and thus $Z(x,u) \cdot \dot{x} = Z'(x',u') \cdot \dot{x}'$, algebraic manipulation results in the relationships in Equations 2.61 - 2.63 for defining the elements of $Z'(x',u')$. Evaluation of these elements in terms of their thermodynamic functions confirms these relationships.

$$z'_{11} = \frac{z_{11} z_{22} - z_{12} z_{21}}{z_{22}} \tag{2.61}$$

$$z'_{12} = \frac{z_{12}}{z_{22}} \tag{2.62}$$

$$z'_{33} = z_{33} \tag{2.63}$$

2.4.7 Third Representation

Finally, the original derivation result of the energy approach is defined as the third representation, and denoted with the double prime notation (i.e. $Z''(x'',u'')\cdot\dot{x}'' = f''(x'',u'')$). This model is also of the same form as Equation 2.43, but with alternative state variables of $x'' = \begin{bmatrix} U_c & m_c & E_w \end{bmatrix}^T$. The resulting model is given in Equation 2.64 where the $Z''(x'',u'')$ matrix is defined simply as $Z''(x'',u'') = I^{3x3}$.

$$\begin{bmatrix} \dot{U}_c \\ \dot{m}_c \\ \dot{E}_w \end{bmatrix} = \begin{bmatrix} \dot{m}_{in}h_{in} - \dot{m}_{out}h_{out} - a_i A_i (T_r - T_w) \\ \dot{m}_{in} - \dot{m}_{out} \\ a_i A_i (T_r - T_w) - a_o A_o (T_w - T_a) \end{bmatrix} \tag{2.64}$$

2.4.8 Summary

The gas cooler is the simplest case for all the possible heat exchangers. However, the general methods presented here can be extended to each of the other types of heat exchangers. More importantly, the equivalence of model representations independent of modeling approach or choice of dynamic state variables extends to all other heat exchangers as well. Furthermore, the advantages of the energy approach become more apparent and more important when applied to the heat exchangers with phase changes. Specifically, the simplicity of the approach and the ability to choose the state variables becomes of great interest when evaluating possibilities for model reduction. Note that for all three modeling representations $f(x,u) = f'(x',u') = f''(x'',u'')$ and $u = u' = u''$. Also note that many other model representations and choices for state variables are possible.

2.5 Evaporator

The evaporator is assumed to operate in one of three different conditions: with one, two, or three fluid regions. Note that the same assumptions apply to a condenser in a subcritical cycle, but with the order of the regions reversed.

Condition 1: If the fluid entering and exiting the evaporator is two-phase it is modeled with only one region. For this condition the quality of the fluid at the evaporator outlet becomes the dynamic variable of interest. This condition generally occurs when the evaporator operates with a receiver at its outlet. The development of an appropriate model for this condition will be the subject of future research.

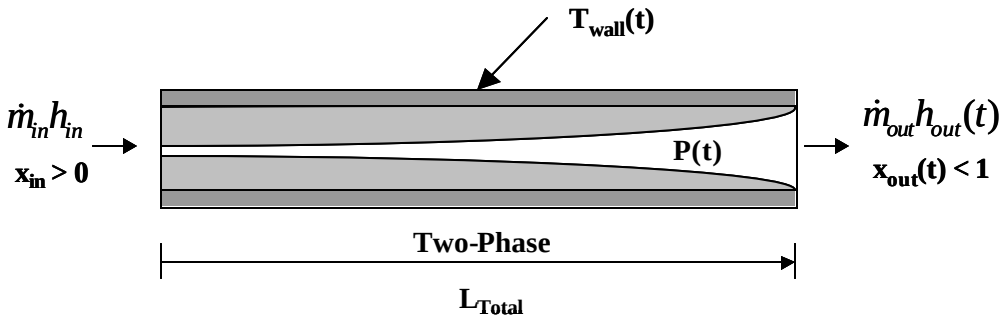

Figure 2.3 Diagram: Evaporator Operating in Condition 1

Condition 2: If the fluid entering the evaporator is two-phase and the fluid exiting the evaporator is superheated vapor, the evaporator is modeled with two regions: a two-phase region, and a superheat region. The

boundary between these regions is a moving interface and although extremely difficult to measure physically, it is the variable of greatest interest.

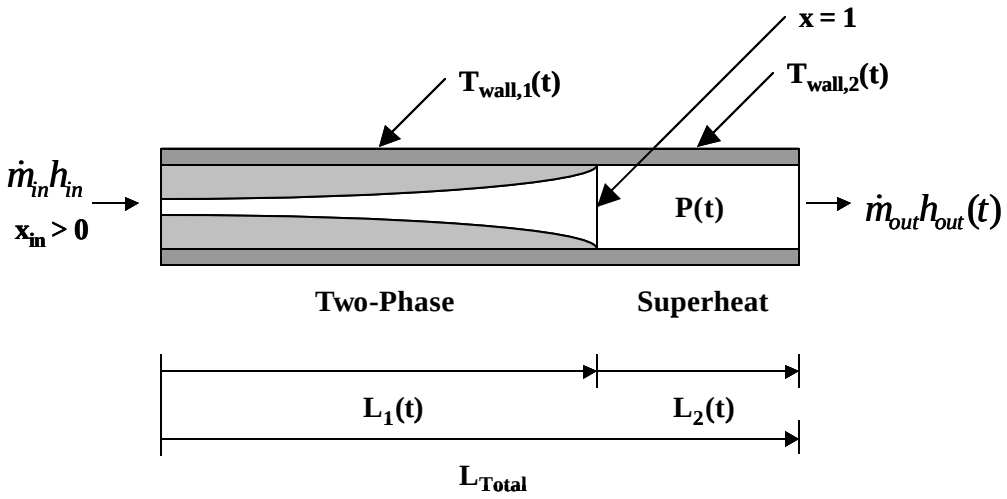

Figure 2.4 Diagram: Evaporator Operating in Condition 2

Condition 3: If the fluid enters the evaporator as subcooled liquid and exits as a superheated vapor the evaporator is modeled with three regions: a subcool region, two-phase region, and a superheat region. This operating condition is not developed in this thesis. However, a moving boundary model for an evaporator in this condition can be found in [19].

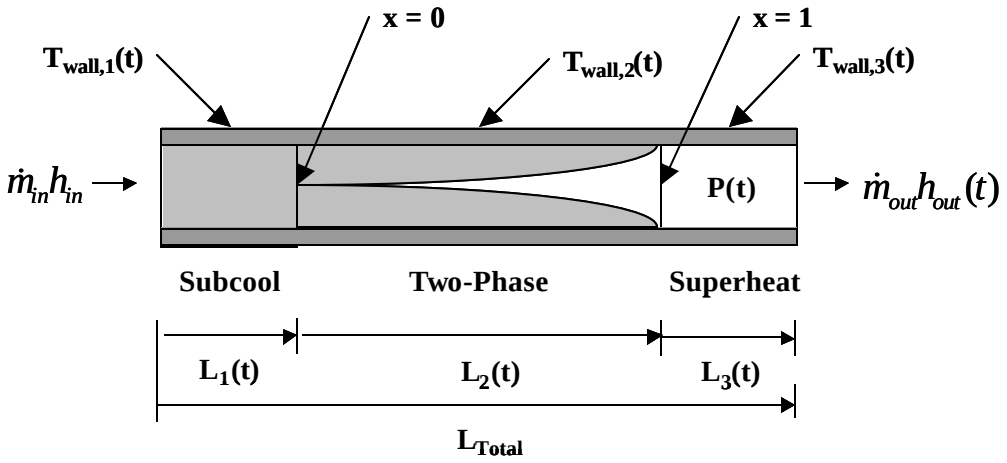

Figure 2.5 Diagram: Evaporator Operating in Condition 3

2.5.1 Modeling Assumptions

The same modeling assumptions about the fluid flow used for the gas cooler derivation are applied here. Additionally the assumption of mean void fraction is used. As discussed in Chapter 1, void fraction is defined as the ratio of vapor volume to total volume, and has long been used to describe certain characteristics of two-phase flows. In many cases the authors assume that the value of mean void fraction is time-invariant for small transients. While this is an acceptable approximation and simplifies the modeling of heat exchangers with complete evaporation or condensation, it cannot be used for conditions when the exiting fluid is two-phase. As mentioned earlier, for this condition, the dynamic variable of interest is the quality or enthalpy of the exiting fluid. This information is

explicitly contained in the formulation of mean void fraction. Therefore if the change of exit quality with respect to time is desired, mean void fraction must be allowed to be time-varying. For this reason, the derivations for the evaporator are initially presented without assuming that mean void fraction is time-invariant. However, because the models developed are for an evaporator in the second operating condition, the assumption of time-invariant mean void fraction is applied as the final step.

2.5.2 PDE Method

The same governing PDEs for fluid flow used for the gas cooler are used for the evaporator. However, Leibniz's equation is applied with different limits of integration. For the evaporator the limits of integration are $z_1 = 0$ and $z_2 = L_1$ for the two-phase region, and $z_1 = L_1$ and $z_2 = L_{total}$ for the superheated region.

2.5.2.1 Conservation of Refrigerant Mass: Two-Phase Region

The PDE for conservation of refrigerant mass is given in Equation 2.65. Each term of this equation is integrated from $z_1 = 0$ to $z_2 = L_1$. Integrating the first term and assuming a constant cross-sectional area results in Equation 2.66. Applying Leibniz's equation results in Equation 2.67. Applying the assumption of void fraction results in Equation 2.68. Integrating results in Equation 2.69. Taking the time derivative results in Equation 2.70, and can be reordered to yield Equation 2.71. Because saturated densities are only a function of pressure, Equation 2.71 can be rewritten as Equation 2.72. Integrating the second term of the PDE results in Equation 2.73. Combining the results of the integration results in Equation 2.74 for the conservation of refrigerant mass in the two-phase region.

$$\frac{\partial(rA_{cs})}{\partial t} + \frac{\partial(\dot{m})}{\partial z} = 0 \tag{2.65}$$

$$\int_0^{L_1} \frac{\partial(rA_{cs})}{\partial t} dz = A_{cs}\left[\int_0^{L_1} \frac{\partial(r)}{\partial t} dz\right] \tag{2.66}$$

$$\int_0^{L_1} \frac{\partial(rA_{cs})}{\partial t} dz = A_{cs}\left[\frac{d}{dt}\left(\int_0^{L_1} (r) dz\right) - r_g \dot{L}_1\right] \tag{2.67}$$

$$\int_0^{L_1} \frac{\partial(rA_{cs})}{\partial t} dz = A_{cs}\left[\frac{d}{dt}\left(\int_0^{L_1} \left(r_f(1-g) + r_g(g)\right) dz\right) - r_g \dot{L}_1\right] \tag{2.68}$$

$$\int_0^{L_1} \frac{\partial(rA_{cs})}{\partial t} dz = A_{cs}\left[\frac{d}{dt}\left(\left(r_f(1-\bar{g}) + r_g(\bar{g})\right)L_1\right) - r_g \dot{L}_1\right] \tag{2.69}$$

$$\int_0^{L_1} \frac{\partial(rA_{cs})}{\partial t} dz = A_{cs}\left[\begin{array}{l}\left(r_f(1-\bar{g}) + r_g(\bar{g})\right)\dot{L}_1 + \left(\dot{r}_f(1-\bar{g}) + \dot{r}_g(\bar{g})\right)L_1 \\ + \left(r_g - r_f\right)L_1\dot{\bar{g}} - r_g\dot{L}_1\end{array}\right] \tag{2.70}$$

$$\begin{aligned}\int_0^{L_1} \frac{\partial(rA_{cs})}{\partial t} dz = &\left(\dot{r}_f(1-\bar{g}) + \dot{r}_g(\bar{g})\right)A_{cs}L_1 + \left(r_g - r_f\right)A_{cs}L_1\dot{\bar{g}} \\ &+ \left(r_f - r_g\right)(1-\bar{g})A_{cs}\dot{L}_1\end{aligned} \tag{2.71}$$

$$\int_0^{L_1} \frac{\partial(rA_{cs})}{\partial t} dz = \left(\frac{dr_f}{dP_e}(1-\bar{g}) + \frac{dr_g}{dP_e}(\bar{g}) \right) A_{cs} L_1 \dot{P}_e + (r_f - r_g)(1-\bar{g}) A_{cs} \dot{L}_1 + (r_g - r_f) A_{cs} L_1 \dot{\bar{g}} \tag{2.72}$$

$$\int_0^{L_1} \frac{\partial(\dot{m})}{\partial z} dz = \dot{m}_{\text{int}} - \dot{m}_{in} \tag{2.73}$$

$$\left(\frac{dr_f}{dP_e}(1-\bar{g}) + \frac{dr_g}{dP_e}(\bar{g}) \right) A_{cs} L_1 \dot{P}_e + (r_f - r_g)(1-\bar{g}) A_{cs} \dot{L}_1 + (r_g - r_f) A_{cs} L_1 \dot{\bar{g}} + \dot{m}_{\text{int}} - \dot{m}_{in} = 0 \tag{2.74}$$

2.5.2.2 Conservation of Refrigerant Mass: Superheat Region

The PDE for conservation of refrigerant mass is given in Equation 2.75. Each term of this equation is integrated from $z_1 = L_1$ to $z_2 = L_{total}$. Integrating the first term and assuming a constant cross-sectional area results in Equation 2.76. Applying Leibniz's equation results in Equation 2.77. Assuming an average density in the superheat region of the evaporator, r_2, results in Equation 2.78. Taking the time derivative results in Equation 2.79. Since $\dot{L}_2 = -\dot{L}_1$ Equation 2.79 can be rewritten as Equation 2.80. Selecting pressure and enthalpy as the independent variables for calculating thermodynamic properties, and assuming an average enthalpy in the superheat region, h_2, Equation 2.80 can be rewritten as Equation 2.81. Since $h_2 = \frac{h_g + h_{out}}{2}$, then $\dot{h}_2 = \frac{\dot{h}_g + \dot{h}_{out}}{2}$, resulting in Equation 2.82. Since saturated enthalpies are only a function of pressure, then Equation 2.82 can be rewritten as Equation 2.83. Integrating the second term of the PDE results in Equation 2.84. Combining the results of the integration results in Equation 2.85 for the conservation of refrigerant mass in the superheat region.

$$\frac{\partial(rA_{cs})}{\partial t} + \frac{\partial(\dot{m})}{\partial z} = 0 \tag{2.75}$$

$$\int_{L_1}^{L_{Total}} \frac{\partial(rA_{cs})}{\partial t} dz = A_{cs} \left[\int_{L_1}^{L_{Total}} \frac{\partial(r)}{\partial t} dz \right] \tag{2.76}$$

$$\int_{L_1}^{L_{Total}} \frac{\partial(rA_{cs})}{\partial t} dz = A_{cs} \left[\frac{d}{dt} \left(\int_{L_1}^{L_{Total}} (r) dz \right) + r_g \dot{L}_1 \right] \tag{2.77}$$

$$\int_{L_1}^{L_{Total}} \frac{\partial(rA_{cs})}{\partial t} dz = A_{cs} \left[\frac{d}{dt}(r_2 L_2) + r_g \dot{L}_1 \right] \tag{2.78}$$

$$\int_{L_1}^{L_{Total}} \frac{\partial(rA_{cs})}{\partial t} dz = A_{cs} \left[\dot{r}_2 L_2 + r_2 \dot{L}_2 + r_g \dot{L}_1 \right] \tag{2.79}$$

$$\int_{L_1}^{L_{Total}} \frac{\partial(rA_{cs})}{\partial t} dz = A_{cs} \left[\dot{r}_2 L_2 - r_2 \dot{L}_1 + r_g \dot{L}_1 \right] \tag{2.80}$$

$$\int_{L_1}^{L_{Total}} \frac{\partial(rA_{cs})}{\partial t} dz = A_{cs}\left[\left[\left(\left.\frac{\partial r_2}{\partial P_e}\right|_{h_2}\right)\dot{P}_e + \left(\left.\frac{\partial r_2}{\partial h_2}\right|_{P_e}\right)\dot{h}_2\right]L_2 + (r_g - r_2)\dot{L}_1\right] \tag{2.81}$$

$$\int_{L_1}^{L_{Total}} \frac{\partial(rA_{cs})}{\partial t} dz = A_{cs}\left[\left[\left(\left.\frac{\partial r_2}{\partial P_e}\right|_{h_2}\right)\dot{P}_e + \left(\left.\frac{\partial r_2}{\partial h_2}\right|_{P_e}\right)\left(\frac{\dot{h}_g + \dot{h}_{out}}{2}\right)\right]L_2 + (r_g - r_2)\dot{L}_1\right] \tag{2.82}$$

$$\begin{aligned}\int_{L_1}^{L_{Total}} \frac{\partial(rA_{cs})}{\partial t} dz = &\left[\left(\left.\frac{\partial r_2}{\partial P_e}\right|_{h_2}\right) + \frac{1}{2}\left(\left.\frac{\partial r_2}{\partial h_2}\right|_{P_e}\right)\left(\frac{dh_g}{dP_e}\right)\right]A_{cs}L_2\dot{P}_e \\ &+ \frac{1}{2}\left(\left.\frac{\partial r_2}{\partial h_2}\right|_{P_e}\right)A_{cs}L_2\dot{h}_{out} + (r_g - r_2)A_{cs}\dot{L}_1\end{aligned} \tag{2.83}$$

$$\int_{L_1}^{L_{Total}} \frac{\partial(\dot{m})}{\partial z} dz = \dot{m}_{out} - \dot{m}_{\text{int}} \tag{2.84}$$

$$\begin{aligned}&\left[\left(\left.\frac{\partial r_2}{\partial P_e}\right|_{h_2}\right) + \frac{1}{2}\left(\left.\frac{\partial r_2}{\partial h_2}\right|_{P_e}\right)\left(\frac{dh_g}{dP_e}\right)\right]AL_2\dot{P}_e + \frac{1}{2}\left(\left.\frac{\partial r_2}{\partial h_2}\right|_{P_e}\right)AL_2\dot{h}_{out} \\ &+ (r_g - r_2)A\dot{L}_1 + \dot{m}_{out} - \dot{m}_{\text{int}} = 0\end{aligned} \tag{2.85}$$

2.5.2.3 Conservation of Refrigerant Energy: Two-Phase Region

The PDE for conservation of refrigerant energy is given in Equation 2.86. Each term of this equation is integrated from $z_1 = 0$ to $z_2 = L_1$. Integrating the first term and assuming a constant cross-sectional area results in Equation 2.87. Applying Leibniz's equation results in Equation 2.88. Applying the assumption of void fraction results in Equation 2.89. Integrating results in Equation 2.90. Taking the time derivative results in Equation 2.91. Since saturated properties are only a function of pressure, Equation 2.91 can be rewritten as Equation 2.92, and then rearranged into Equation 2.93. Integrating the second term of the PDE results in Equation 2.94. Applying Leibniz's equation results in Equation 2.95. Performing the integration and taking the time derivative results in Equations 2.96 and 2.97 respectively. Simplifying results in Equation 2.98. Integrating the third term of the PDE results in Equation 2.99. Integrating the right side of the equation and manipulating results in Equations 2.100, 2.101, and 2.102. Combining the results of the integration results in Equation 2.103 for the conservation of refrigerant energy in the two-phase region.

$$\frac{\partial(rA_{cs}h - A_{cs}P)}{\partial t} + \frac{\partial(\dot{m}h)}{\partial z} = p_i a_i (T_w - T_r) \tag{2.86}$$

$$\int_0^{L_1} \frac{\partial(rA_{cs}h)}{\partial t} dz = A_{cs}\left[\int_0^{L_1} \frac{\partial(rh)}{\partial t} dz\right] \tag{2.87}$$

$$\int_0^{L_1} \frac{\partial(rA_{cs}h)}{\partial t} dz = A_{cs}\left[\frac{d}{dt}\left(\int_0^{L_1} (rh) dz\right) - r_g h_g \dot{L}_1\right] \tag{2.88}$$

$$\int_0^{L_1}\frac{\partial(rA_{cs}h)}{\partial t}dz = A_{cs}\left[\frac{d}{dt}\left(\int_0^{L_1}\left(r_f h_f(1-g)+r_g h_g(g)\right)dz\right)-r_g h_g \dot{L}_1\right] \tag{2.89}$$

$$\int_0^{L_1}\frac{\partial(rA_{cs}h)}{\partial t}dz = A_{cs}\left[\frac{d}{dt}\left[\left(r_f h_f(1-\bar{g})+r_g h_g(\bar{g})\right)L_1\right]-r_g h_g \dot{L}_1\right] \tag{2.90}$$

$$\int_0^{L_1}\frac{\partial(rA_{cs}h)}{\partial t}dz = A_{cs}\begin{bmatrix}\left(r_f h_f(1-\bar{g})+r_g h_g(\bar{g})\right)\dot{L}_1\\ +\left(\dfrac{d\left(r_f h_f\right)}{dt}(1-\bar{g})+\dfrac{d\left(r_g h_g\right)}{dt}(\bar{g})\right)L_1\\ +\left(r_g h_g - r_f h_f\right)L_1\dot{\bar{g}} - r_g h_g \dot{L}_1\end{bmatrix} \tag{2.91}$$

$$\int_0^{L_1}\frac{\partial(rA_{cs}h)}{\partial t}dz = A_{cs}\begin{bmatrix}\left(r_f h_f(1-\bar{g})+r_g h_g(\bar{g})\right)\dot{L}_1+\left(r_g h_g - r_f h_f\right)L_1\dot{\bar{g}}\\ - r_g h_g \dot{L}_1+\left(\dfrac{d\left(r_f h_f\right)}{dP_e}(1-\bar{g})+\dfrac{d\left(r_g h_g\right)}{dP_e}(\bar{g})\right)L_1\dot{P}_e\end{bmatrix} \tag{2.92}$$

$$\begin{aligned}\int_0^{L_1}\frac{\partial(rA_{cs}h)}{\partial t}dz = &\left(\frac{d\left(r_f h_f\right)}{dP_e}(1-\bar{g})+\frac{d\left(r_g h_g\right)}{dP_e}(\bar{g})\right)A_{cs}L_1\dot{P}_e\\ &+\left(r_f h_f - r_g h_g\right)(1-\bar{g})A_{cs}\dot{L}_1+\left(r_g h_g - r_f h_f\right)A_{cs}L_1\dot{\bar{g}}\end{aligned} \tag{2.93}$$

$$\int_0^{L_1}\frac{\partial(A_{cs}P)}{\partial t}dz = A_{cs}\left[\int_0^{L_1}\frac{\partial(P)}{\partial t}dz\right] \tag{2.94}$$

$$\int_0^{L_1}\frac{\partial(A_{cs}P)}{\partial t}dz = A_{cs}\left[\frac{d}{dt}\left(\int_0^{L_1}(P)dz\right)-P_e\dot{L}_1\right] \tag{2.95}$$

$$\int_0^{L_1}\frac{\partial(A_{cs}P)}{\partial t}dz = A_{cs}\left[\frac{d}{dt}(P_e L_1)-P_e\dot{L}_1\right] \tag{2.96}$$

$$\int_0^{L_1}\frac{\partial(A_{cs}P)}{\partial t}dz = A_{cs}\left[\dot{P}_e L_1+P_e\dot{L}_1-P_e\dot{L}_1\right] \tag{2.97}$$

$$\int_0^{L_1}\frac{\partial(A_{cs}P)}{\partial t}dz = A_{cs}L_1\dot{P}_e \tag{2.98}$$

$$\int_0^{L_1}\frac{\partial(\dot{m}h)}{\partial z} = \dot{m}_{\text{int}}h_{\text{int}}-\dot{m}_{in}h_{in} \tag{2.99}$$

$$\int_0^{L_1}p_i a_i(T_w-T_r) = p_i a_i L_1(T_{w1}-T_{r1}) \tag{2.100}$$

$$\int_0^{L_1}p_i a_i(T_w-T_r) = a_i p_i L_{Total}\left(\frac{L_1}{L_{Total}}\right)(T_{w1}-T_{r1}) \tag{2.101}$$

$$\int_0^{L_1} p_i a_i (T_w - T_r) = a_i A_i \left(\frac{L_1}{L_{Total}} \right) (T_{w1} - T_{r1}) \tag{2.102}$$

$$\left(\frac{d(r_f h_f)}{dP_e}(1-\bar{g}) + \frac{d(r_g h_g)}{dP_e}(\bar{g}) - 1 \right) A_{cs} L_1 \dot{P}_e + (r_f h_f - r_g h_g)(1-\bar{g}) A_{cs} \dot{L}_1 + (r_g h_g - r_f h_f) A_{cs} L_1 \dot{\bar{g}} + \dot{m}_{int} h_{int} - \dot{m}_{in} h_{in} = a_i A_i \left(\frac{L_1}{L_{Total}} \right) (T_{w1} - T_{r1}) \tag{2.103}$$

2.5.2.4 Conservation of Refrigerant Energy: Superheat Region

The PDE for conservation of refrigerant energy is given in Equation 2.104. Each term of this equation is integrated from $z_1 = L_1$ to $z_2 = L_{total}$. Integrating the first term and assuming a constant cross-sectional area results in Equation 2.105. Applying Leibniz's equation results in Equation 2.106. Assuming average properties in the superheat region of the evaporator, r_2 and h_2, and performing the integration results in Equation 2.107. Taking the time derivative results in Equation 2.108. Since $\dot{L}_2 = -\dot{L}_1$ Equation 2.108 can be rewritten as Equation 2.109. Selecting pressure and enthalpy as the independent variables for calculating thermodynamic properties, Equation 2.109 can be rewritten as Equation 2.110 and then Equation 2.111. Since $h_2 = \frac{h_g + h_{out}}{2}$, then $\dot{h}_2 = \frac{\dot{h}_g + \dot{h}_{out}}{2}$, resulting in Equation 2.112 and then 2.113. Since saturated enthalpies are only a function of pressure, then Equation 2.113 can be rewritten as Equation 2.114 and then Equation 2.115. Integrating the second term of the PDE results in Equation 2.116. Applying Leibniz's equation results in Equation 2.117. Performing the integration and taking the time derivative results in Equations 2.118 and 2.119 respectively. Since $\dot{L}_2 = -\dot{L}_1$ Equation 2.119 can be rewritten as Equation 2.120. Simplifying yields 2.121. Integrating the third term of the PDE results in Equation 2.122. Integrating the right side of the equation and manipulating results in Equations 2.123, 2.124, and 2.125. Combining the results of the integration results in Equation 2.126 for the conservation of refrigerant energy in the superheat region.

$$\frac{\partial(rA_{cs}h - A_{cs}P)}{\partial t} + \frac{\partial(\dot{m}h)}{\partial z} = p_i a_i (T_w - T_r) \tag{2.104}$$

$$\int_{L_1}^{L_{Total}} \frac{\partial(rA_{cs}h)}{\partial t} dz = A_{cs} \left[\int_{L_1}^{L_{Total}} \frac{\partial(rh)}{\partial t} dz \right] \tag{2.105}$$

$$\int_{L_1}^{L_{Total}} \frac{\partial(rA_{cs}h)}{\partial t} dz = A_{cs} \left[\frac{d}{dt} \left(\int_{L_1}^{L_{Total}} (rh) dz \right) + r_g h_g \dot{L}_1 \right] \tag{2.106}$$

$$\int_{L_1}^{L_{Total}} \frac{\partial(rA_{cs}h)}{\partial t} dz = A_{cs} \left[\frac{d}{dt} (r_2 h_2 L_2) + r_g h_g \dot{L}_1 \right] \tag{2.107}$$

$$\int_{L_1}^{L_{Total}} \frac{\partial(rA_{cs}h)}{\partial t}dz = A_{cs}\left[\dot{r}_2 h_2 L_2 + r_2 \dot{h}_2 L_2 + r_2 h_2 \dot{L}_2 + r_g h_g \dot{L}_1\right] \tag{2.108}$$

$$\int_{L_1}^{L_{Total}} \frac{\partial(rA_{cs}h)}{\partial t}dz = A_{cs}\left[\dot{r}_2 h_2 L_2 + r_2 \dot{h}_2 L_2 - r_2 h_2 \dot{L}_1 + r_g h_g \dot{L}_1\right] \tag{2.109}$$

$$\int_{L_1}^{L_{Total}} \frac{\partial(rA_{cs}h)}{\partial t}dz = A_{cs}\begin{bmatrix}\left[\left(\left.\frac{\partial r_2}{\partial P_e}\right|_{h_2}\right)\dot{P}_e + \left(\left.\frac{\partial r_2}{\partial h_2}\right|_{P_e}\right)\dot{h}_2\right]h_2 L_2 \\ + r_2 \dot{h}_2 L_2 - r_2 h_2 \dot{L}_1 + r_g h_g \dot{L}_1\end{bmatrix} \tag{2.110}$$

$$\begin{aligned}\int_{L_1}^{L_{Total}} \frac{\partial(rA_{cs}h)}{\partial t}dz = &\left[\left(\left.\frac{\partial r_2}{\partial P_e}\right|_{h_2}\right)h_2\right]A_{cs}L_2\dot{P}_e + \left[\left(\left.\frac{\partial r_2}{\partial h_2}\right|_{P_e}\right)h_2 + r_2\right]A_{cs}L_2\dot{h}_2 \\ &+ \left(r_g h_g - r_2 h_2\right)A_{cs}\dot{L}_1\end{aligned} \tag{2.111}$$

$$\begin{aligned}\int_{L_1}^{L_{Total}} \frac{\partial(rA_{cs}h)}{\partial t}dz = &\left[\left(\left.\frac{\partial r_2}{\partial P_e}\right|_{h_2}\right)h_2\right]A_{cs}L_2\dot{P}_e + \left(r_g h_g - r_2 h_2\right)A_{cs}\dot{L}_1 \\ &+ \left[\left(\left.\frac{\partial r_2}{\partial h_2}\right|_{P_e}\right)h_2 + r_2\right]A_{cs}L_2\left(\frac{\dot{h}_g + \dot{h}_{out}}{2}\right)\end{aligned} \tag{2.112}$$

$$\begin{aligned}\int_{L_1}^{L_{Total}} \frac{\partial(rA_{cs}h)}{\partial t}dz = &\left[\left(\left.\frac{\partial r_2}{\partial P_e}\right|_{h_2}\right)h_2\right]A_{cs}L_2\dot{P}_e + \left[\left(\left.\frac{\partial r_2}{\partial h_2}\right|_{P_e}\right)h_2 + r_2\right]\left(\frac{1}{2}\right)A_{cs}L_2\dot{h}_g \\ &+ \left[\left(\left.\frac{\partial r_2}{\partial h_2}\right|_{P_e}\right)h_2 + r_2\right]\left(\frac{1}{2}\right)A_{cs}L_2\dot{h}_{out} + \left(r_g h_g - r_2 h_2\right)A_{cs}\dot{L}_1\end{aligned} \tag{2.113}$$

$$\begin{aligned}\int_{L_1}^{L_{Total}} \frac{\partial(rA_{cs}h)}{\partial t}dz = &\left[\left(\left.\frac{\partial r_2}{\partial P_e}\right|_{h_2}\right)h_2 + \left(\left(\left.\frac{\partial r_2}{\partial h_2}\right|_{P_e}\right)h_2 + r_2\right)\left(\frac{1}{2}\right)\left(\frac{dh_g}{dP_e}\right)\right]A_{cs}L_2\dot{P}_e \\ &+ \left[\left(\left.\frac{\partial r_2}{\partial h_2}\right|_{P_e}\right)h_2 + r_2\right]\left(\frac{1}{2}\right)A_{cs}L_2\dot{h}_{out} + \left(r_g h_g - r_2 h_2\right)A_{cs}\dot{L}_1\end{aligned} \tag{2.114}$$

$$\begin{aligned}\int_{L_1}^{L_{Total}} \frac{\partial(rA_{cs}h)}{\partial t}dz = &\begin{bmatrix}\left(\left(\left.\frac{\partial r_2}{\partial P_e}\right|_{h_2}\right) + \left(\frac{1}{2}\right)\left(\frac{dh_g}{dP_e}\right)\left(\left.\frac{\partial r_2}{\partial h_2}\right|_{P_e}\right)\right)h_2 \\ + \left(\frac{1}{2}\right)\left(\frac{dh_g}{dP_e}\right)r_2\end{bmatrix}A_{cs}L_2\dot{P}_e \\ &+ \left[\left(\left.\frac{\partial r_2}{\partial h_2}\right|_{P_e}\right)h_2 + r_2\right]\left(\frac{1}{2}\right)A_{cs}L_2\dot{h}_{out} + \left(r_g h_g - r_2 h_2\right)A_{cs}\dot{L}_1\end{aligned} \tag{2.115}$$

$$\int_{L_1}^{L_{Total}} \frac{\partial(A_{cs}P)}{\partial t}dz = A_{cs}\left[\int_{L_1}^{L_{Total}} \frac{\partial(P)}{\partial t}dz\right] \tag{2.116}$$

$$\int_{L_1}^{L_{Total}} \frac{\partial (A_{cs} P)}{\partial t} dz = A_{cs} \left[\frac{d}{dt} \left(\int_{L_1}^{L_{Total}} (P) dz \right) + P_e \dot{L}_1 \right] \tag{2.117}$$

$$\int_{L_1}^{L_{Total}} \frac{\partial (A_{cs} P)}{\partial t} dz = A_{cs} \left[\frac{d}{dt} (P_e L_2) + P_e \dot{L}_1 \right] \tag{2.118}$$

$$\int_{L_1}^{L_{Total}} \frac{\partial (A_{cs} P)}{\partial t} dz = A_{cs} \left[\dot{P}_e L_2 + P_e \dot{L}_2 + P_e \dot{L}_1 \right] \tag{2.119}$$

$$\int_{L_1}^{L_{Total}} \frac{\partial (A_{cs} P)}{\partial t} dz = A_{cs} \left[\dot{P}_e L_2 - P_e \dot{L}_1 + P_e \dot{L}_1 \right] \tag{2.120}$$

$$\int_{L_1}^{L_{Total}} \frac{\partial (A_{cs} P)}{\partial t} dz = A_{cs} L_2 \dot{P}_e \tag{2.121}$$

$$\int_{L_1}^{L_{Total}} \frac{\partial (\dot{m} h)}{\partial z} = \dot{m}_{out} h_{out} - \dot{m}_{int} h_{int} \tag{2.122}$$

$$\int_{L_1}^{L_{Total}} p_i a_i (T_w - T_r) = p_i a_i L_2 (T_{w2} - T_{r2}) \tag{2.123}$$

$$\int_{L_1}^{L_{Total}} p_i a_i (T_w - T_r) = a_i p_i L_{Total} \left(\frac{L_2}{L_{Total}} \right) (T_{w2} - T_{r2}) \tag{2.124}$$

$$\int_{L_1}^{L_{Total}} p_i a_i (T_w - T_r) = a_i A_i \left(\frac{L_2}{L_{Total}} \right) (T_{w2} - T_{r2}) \tag{2.125}$$

$$\left[\left(\left(\frac{\partial r_2}{\partial P_e} \bigg|_{h_2} \right) + \left(\frac{1}{2} \right) \left(\frac{dh_g}{dP_e} \right) \left(\frac{\partial r_2}{\partial h_2} \bigg|_{P_e} \right) \right) h_2 + \left(\frac{1}{2} \right) \left(\frac{dh_g}{dP_e} \right) r_2 - 1 \right] A_{cs} L_2 \dot{P}_e$$
$$+ \left[\left(\frac{\partial r_2}{\partial h_2} \bigg|_{P_e} \right) h_2 + r_2 \right] \left(\frac{1}{2} \right) A_{cs} L_2 \dot{h}_{out} + \left(r_g h_g - r_2 h_2 \right) A_{cs} \dot{L}_1 \tag{2.126}$$
$$+ \dot{m}_{out} h_{out} - \dot{m}_{int} h_{int} = a_i A_i \left(\frac{L_2}{L_{Total}} \right) (T_{w2} - T_{r2})$$

2.5.2.5 Conservation of Tube Wall Energy: Two-Phase Region

The PDE for the conservation of tube wall energy is given in Equation 2.127. Multiplying both sides by L_{Total} results in Equation 2.128. For arbitrary limits of integration z_1 and z_2, this equation integrates as Equations 2.129 and 2.130. Applying Leibniz's equation results in Equation 2.131. Performing the integration results in Equation 2.132. Differentiating results in Equation 2.133. For the two-phase region Equation 2.133 becomes Equation 2.134. Because of our assumption of uniform temperature for each region, the wall temperature evaluated at the moving boundary is a discontinuous function. However, by assuming that this wall temperature is equal to the wall temperature in the two-phase region, this simplifies to Equation 2.135. Because the temperature at the

boundary between the two-phase and superheat regions is actually closer to the lumped two-phase wall temperature than the lumped superheat region temperature this assumption is the most logical choice.

$$\left(C_p rA\right)_w \frac{\partial(T_w)}{\partial t} = p_i a_i (T_r - T_w) + p_o a_o (T_a - T_w) \tag{2.127}$$

$$\left(C_p rV\right)_w \frac{\partial(T_w)}{\partial t} = a_i A_i (T_r - T_w) + a_o A_o (T_a - T_w) \tag{2.128}$$

$$\int_{z_1}^{z_2}\left[\left(C_p rV\right)_w \frac{\partial(T_w)}{\partial t}\right]dz = \int_{z_1}^{z_2}[a_i A_i (T_r - T_w) + a_o A_o (T_a - T_w)]dz \tag{2.129}$$

$$\left(C_p rV\right)_w \left[\int_{z_1}^{z_2}\left(\frac{\partial(T_w)}{\partial t}\right)dz\right] = [a_i A_i (T_r - T_w) + a_o A_o (T_a - T_w)][z_2 - z_1] \tag{2.130}$$

$$\left(C_p rV\right)_w \left[\frac{d}{dt}\left(\int_{z_1}^{z_2} T_w dz\right) + \left(T_w|_{z_1}\right)\left(\frac{dz_1}{dt}\right) - \left(T_w|_{z_2}\right)\left(\frac{dz_2}{dt}\right)\right] \tag{2.131}$$
$$= [a_i A_i (T_r - T_w) + a_o A_o (T_a - T_w)][z_2 - z_1]$$

$$\left(C_p rV\right)_w \left[\frac{d}{dt}\left[\left(T_w|_{z_2 - z_1}\right)(z_2 - z_1)\right] + \left(T_w|_{z_1}\right)\left(\frac{dz_1}{dt}\right) - \left(T_w|_{z_2}\right)\left(\frac{dz_2}{dt}\right)\right] \tag{2.132}$$
$$= [a_i A_i (T_r - T_w) + a_o A_o (T_a - T_w)][z_2 - z_1]$$

$$\left(C_p rV\right)_w \left[\begin{array}{l} \dfrac{d\left(T_w|_{z_2 - z_1}\right)}{dt}(z_2 - z_1) + \dfrac{d(z_2 - z_1)}{dt}\left(T_w|_{z_2 - z_1}\right) \\ + \left(T_w|_{z_1}\right)\left(\dfrac{dz_1}{dt}\right) - \left(T_w|_{z_2}\right)\left(\dfrac{dz_2}{dt}\right) \end{array}\right] \tag{2.133}$$
$$= [a_i A_i (T_r - T_w) + a_o A_o (T_a - T_w)][z_2 - z_1]$$

$$\left(C_p rV\right)_w \left[\dot{T}_{w1} L_1 + \left(T_{w1} - T_w|_{L_1}\right)\dot{L}_1\right] = [a_i A_i (T_r - T_w) + a_o A_o (T_a - T_w)]L_1 \tag{2.134}$$

$$\left(C_p rV\right)_w \dot{T}_{w1} = a_i A_i (T_r - T_w) + a_o A_o (T_a - T_w) \tag{2.135}$$

2.5.2.6 Conservation of Tube Wall Energy: Superheat Region

Using the results from the conservation of wall energy for the two-phase region, the equation for arbitrary limits of integration (Equation 2.133) can be evaluated for the superheat region with $z_1 = L_1$ to $z_2 = L_{total}$ (Equation 2.136). Again assuming that the wall temperature at the moving boundary is equal to the wall temperature in the two-phase region, this simplifies to Equation 2.137, and then Equation 2.138.

$$\left(C_p rV\right)_w \left[\dot{T}_{w2} L_2 + \left(T_{w2} - T_w|_{L_1}\right)\dot{L}_2\right] = [a_i A_i (T_r - T_w) + a_o A_o (T_a - T_w)]L_2 \tag{2.136}$$

$$\left(C_p rV\right)_w \left[\dot{T}_{w2} + \left(\frac{T_{w2} - T_{w1}}{L_2}\right)\dot{L}_2\right] = a_i A_i (T_r - T_w) + a_o A_o (T_a - T_w) \tag{2.137}$$

$$\left(C_p rV\right)_w \left[\dot{T}_{w2} - \left(\frac{T_{w2} - T_{w1}}{L_2}\right)\dot{L}_1\right] = a_i A_i (T_r - T_w) + a_o A_o (T_a - T_w) \tag{2.138}$$

2.5.2.7 Governing Ordinary Differential Equations

The resulting six differential equations for conservation of refrigerant mass, refrigerant energy, and wall energy for the two-phase and superheat regions only contain five explicit time derivatives: $\dot{L}_1$, $\dot{P}_e$, $\dot{h}_{out}$, $\dot{T}_{w1}$, and $\dot{T}_{w2}$. One of the equations can be used to eliminate the variable $\dot{m}_{\text{int}}$. The two equations for conservation of mass can be solved for $\dot{m}_{\text{int}}$, and are given in Equations 2.139 and 2.140. Substituting Equation 2.139 into the conservation of refrigerant energy for the two-phase region yields Equation 2.141. Substituting Equation 2.140 into the conservation of refrigerant energy for the superheat region yields Equation 2.142. Combining Equations 2.139 and 2.140 yields Equation 2.143.

$$-\dot{m}_{\text{int}} = \left(\frac{dr_f}{dP_e}(1-\bar{g}) + \frac{dr_g}{dP_e}(\bar{g})\right) A_{cs} L_1 \dot{P}_e + \left(r_f - r_g\right)(1-\bar{g}) A_{cs} \dot{L}_1 + \left(r_g - r_f\right) A_{cs} L_1 \dot{\bar{g}} - \dot{m}_{in} \tag{2.139}$$

$$\dot{m}_{\text{int}} = \left[\left(\left.\frac{\partial r_2}{\partial P_e}\right|_{h_2}\right) + \frac{1}{2}\left(\left.\frac{\partial r_2}{\partial h_2}\right|_{P_e}\right)\left(\frac{dh_g}{dP_e}\right)\right] A_{cs} L_2 \dot{P}_e + \frac{1}{2}\left(\left.\frac{\partial r_2}{\partial h_2}\right|_{P_e}\right) A_{cs} L_2 \dot{h}_{out} + \left(r_g - r_2\right) A_{cs} \dot{L}_1 + \dot{m}_{out} \tag{2.140}$$

$$\left[\left(\frac{d\left(r_f h_f\right)}{dP_e} - \frac{dr_f}{dP_e} h_g\right)(1-\bar{g}) + \left(\frac{d\left(r_g h_g\right)}{dP_e} - \frac{dr_g}{dP_e} h_g\right)(\bar{g}) - 1\right] A_{cs} L_1 \dot{P}_e + \left[r_f\left(h_f - h_g\right)\right](1-\bar{g}) A_{cs} \dot{L}_1 + \left[r_f\left(h_g - h_f\right)\right] A_{cs} L_1 \dot{\bar{g}} = \dot{m}_{in} h_{in} - \dot{m}_{in} h_g + a_i A_i \left(\frac{L_1}{L_{Total}}\right)\left(T_{w1} - T_{r1}\right) \tag{2.141}$$

$$\left[\left(\left(\left.\frac{\partial r_2}{\partial P_e}\right|_{h_2}\right) + \left(\frac{1}{2}\right)\left(\left.\frac{\partial r_2}{\partial h_2}\right|_{P_e}\right)\left(\frac{dh_g}{dP_e}\right)\right)\left(h_2 - h_g\right) + \left(\frac{r_2}{2}\right)\left(\frac{dh_g}{dP_e}\right) - 1\right] A_{cs} L_2 \dot{P}_e + r_2\left(h_g - h_2\right) A_{cs} \dot{L}_1 + \left[\left(\frac{1}{2}\right)\left(\left.\frac{\partial r_2}{\partial h_2}\right|_{P_e}\right)\left(h_2 - h_g\right) + \left(\frac{r_2}{2}\right)\right] A_{cs} L_2 \dot{h}_{out} = \dot{m}_{out} h_g - \dot{m}_{out} h_{out} + a_i A_i \left(\frac{L_2}{L_{Total}}\right)\left(T_{w2} - T_{r2}\right) \tag{2.142}$$

$$\left[\left[\left(\left.\frac{\partial r_2}{\partial P_e}\right|_{h_2}\right) + \frac{1}{2}\left(\left.\frac{\partial r_2}{\partial h_2}\right|_{P_e}\right)\left(\frac{dh_g}{dP_e}\right)\right] L_2 + \left[\left(\frac{dr_f}{dP_e}\right)(1-\bar{g}) + \left(\frac{dr_g}{dP_e}\right)(\bar{g})\right] L_1\right] A_{cs} \dot{P}_e + \frac{1}{2}\left(\left.\frac{\partial r_2}{\partial h_2}\right|_{P_e}\right) A_{cs} L_2 \dot{h}_{out} + \left[\left(r_g - r_2\right) + \left(r_f - r_g\right)(1-\bar{g})\right] A_{cs} \dot{L}_1 + \left(r_g - r_f\right) A_{cs} L_1 \dot{\bar{g}} = \dot{m}_{in} - \dot{m}_{out} \tag{2.143}$$

Combining the final five governing equations (Equations 2.141, 2.142, 2.143, 2.135, and 2.138) into a matrix form and assuming time-invariant mean void fraction results in Equation 2.144, which is of the

$Z(x,u)\cdot\dot{x} = f(x,u)$ form, with states $x = [L_1 \quad P_e \quad h_{out} \quad T_{w1} \quad T_{w2}]^T$, and where the elements of the $Z(x,u)$ matrix are given in Table 2.4.

$$\begin{bmatrix} z_{11} & z_{12} & 0 & 0 & 0 \\ z_{21} & z_{22} & z_{23} & 0 & 0 \\ z_{31} & z_{32} & z_{33} & 0 & 0 \\ 0 & 0 & 0 & z_{44} & 0 \\ z_{51} & 0 & 0 & 0 & z_{55} \end{bmatrix} \begin{bmatrix} \dot{L}_1 \\ \dot{P}_e \\ \dot{h}_{out} \\ \dot{T}_{w1} \\ \dot{T}_{w2} \end{bmatrix} = \begin{bmatrix} \dot{m}_{in}(h_{in} - h_g) + a_{i1}A_i\left(\frac{L_1}{L_{Total}}\right)(T_{w1} - T_{r1}) \\ \dot{m}_{out}(h_g - h_{out}) + a_{i2}A_i\left(\frac{L_2}{L_{Total}}\right)(T_{w2} - T_{r2}) \\ \dot{m}_{in} - \dot{m}_{out} \\ a_o A_o(T_a - T_{w1}) - a_{i1}A_i(T_{w1} - T_{r1}) \\ a_o A_o(T_a - T_{w2}) - a_{i2}A_i(T_{w2} - T_{r2}) \end{bmatrix} \tag{2.144}$$

Table 2.4 Matrix Elements of $Z(x,u)$ for the Evaporator

z_{11}	$[r_f(h_f - h_g)](1-\bar{g})A_{cs}$
z_{12}	$\left[\left(\frac{d(r_f h_f)}{dP_e} - \frac{dr_f}{dP_e}h_g\right)(1-\bar{g}) + \left(\frac{d(r_g h_g)}{dP_e} - \frac{dr_g}{dP_e}h_g\right)(\bar{g}) - 1\right]A_{cs}L_1$
z_{21}	$r_2(h_g - h_2)A_{cs}$
z_{22}	$\left[\left(\left(\frac{\partial r_2}{\partial P_e}\Big\|_{h_2}\right) + \left(\frac{1}{2}\right)\left(\frac{\partial r_2}{\partial h_2}\Big\|_{P_e}\right)\left(\frac{dh_g}{dP_e}\right)\right)(h_2 - h_g) + \left(\frac{r_2}{2}\right)\left(\frac{dh_g}{dP_e}\right) - 1\right]A_{cs}L_2$
z_{23}	$\left[\left(\frac{1}{2}\right)\left(\frac{\partial r_2}{\partial h_2}\Big\|_{P_e}\right)(h_2 - h_g) + \left(\frac{r_2}{2}\right)\right]A_{cs}L_2$
z_{31}	$[(r_g - r_2) + (r_f - r_g)(1-\bar{g})]A_{cs}$
z_{32}	$\left[\left[\left(\left(\frac{\partial r_2}{\partial P_e}\Big\|_{h_2}\right) + \frac{1}{2}\left(\frac{\partial r_2}{\partial h_2}\Big\|_{P_e}\right)\left(\frac{dh_g}{dP_e}\right)\right]L_2 + \left[\left(\frac{dr_f}{dP_e}\right)(1-\bar{g}) + \left(\frac{dr_g}{dP_e}\right)(\bar{g})\right]L_1\right]A_{cs}$
z_{33}	$\frac{1}{2}\left(\frac{\partial r_2}{\partial h_2}\Big\|_{P_e}\right)A_{cs}L_2$
z_{44}	$(C_p r V)_w$
z_{51}	$(C_p r V)_w\left(\frac{T_{w1} - T_{w2}}{L_2}\right)$
z_{55}	$(C_p r V)_w$

2.5.3 Energy Method

The same conservation equations used for the gas cooler are used for the evaporator (Equations 2.145 - 2.147). However, separate equations for the conservation of refrigerant and wall energy are used for two -phase region and the superheat region. The resulting five equations are arranged in matrix form (Equation 2.148).

$$\dot{U} = \dot{H}_{in} - \dot{H}_{out} - \dot{Q}_w - \dot{W} \tag{2.145}$$

$$\dot{E}_w = \dot{Q}_w - \dot{Q}_a - \dot{E}_{\text{int}} \tag{2.146}$$

$$\dot{m} = \dot{m}_{in} - \dot{m}_{out} \tag{2.147}$$

$$\begin{bmatrix} \dot{U}_1 \\ \dot{U}_2 \\ \dot{m}_e \\ \dot{E}_{w1} \\ \dot{E}_{w2} \end{bmatrix} = \begin{bmatrix} \dot{H}_{in} - \dot{H}_{\text{int}} + \dot{Q}_{w1} + \dot{P}V_1 - P\dot{V}_1 \\ \dot{H}_{\text{int}} - \dot{H}_{out} + \dot{Q}_{w2} + \dot{P}V_2 - P\dot{V}_2 \\ \dot{m}_{in} - \dot{m}_{out} \\ \dot{Q}_{a1} - \dot{Q}_{w1} + \dot{E}_{\text{int}} \\ \dot{Q}_{a2} - \dot{Q}_{w2} - \dot{E}_{\text{int}} \end{bmatrix} \tag{2.148}$$

The terms on the right hand side of Equation 2.148 can be expanded into more explicit terms. Assuming a constant cross-sectional area, the volumes can be defined as $V_1 = A_{cs} L_1$ and $V_2 = A_{cs} L_2$, where $\dot{L}_2 = -\dot{L}_1$. The fluid flow energy terms are defined as $\dot{H}_{in} = \dot{m}_{in} h_{in}$, $\dot{H}_{\text{int}} = \dot{m}_{\text{int}} h_{\text{int}}$, and $\dot{H}_{out} = \dot{m}_{out} h_{out}$. The wall heat transfer terms are defined as $\dot{Q}_{w1} = \alpha_{i1} A_i \left(\frac{L_1}{L_{Total}} \right) (T_{w1} - T_{r1})$ and $\dot{Q}_{w2} = \alpha_{i2} A_i \left(\frac{L_2}{L_{Total}} \right) (T_{w2} - T_{r2})$. The air heat transfer terms are defined as $\dot{Q}_{a1} = \alpha_o A_o \left(\frac{L_1}{L_{Total}} \right) (T_a - T_{w1})$ and $\dot{Q}_{a2} = \alpha_o A_o \left(\frac{L_2}{L_{Total}} \right) (T_a - T_{w2})$. Finally, the wall boundary heat transfer term is defined as $\dot{E}_{\text{int}} = (C_p \rho V)_w \left(\frac{\dot{L}_1}{L_{Total}} \right) (T_{w1})$. Making these substitutions, Equation 2.148 becomes Equation 2.149.

$$\begin{bmatrix} \dot{U}_1 \\ \dot{U}_2 \\ \dot{m}_e \\ \dot{E}_{w1} \\ \dot{E}_{w2} \end{bmatrix} = \begin{bmatrix} \dot{m}_{in} h_{in} - \dot{m}_{\text{int}} h_{\text{int}} + \alpha_{i1} A_i \left(\frac{L_1}{L_{Total}} \right) (T_{w1} - T_{r1}) + \dot{P}_e A_{cs} L_1 - P_e A_{cs} \dot{L}_1 \\ \dot{m}_{\text{int}} h_{\text{int}} - \dot{m}_{out} h_{out} + \alpha_{i2} A_i \left(\frac{L_2}{L_{Total}} \right) (T_{w2} - T_{r2}) + \dot{P}_e A_{cs} L_2 + P_e A_{cs} \dot{L}_1 \\ \dot{m}_{in} - \dot{m}_{out} \\ \alpha_o A_o \left(\frac{L_1}{L_{Total}} \right) (T_a - T_{w1}) - \alpha_{i1} A_i \left(\frac{L_1}{L_{Total}} \right) (T_{w1} - T_{r1}) + (C_p \rho V)_w \left(\frac{\dot{L}_1}{L_{Total}} \right) (T_{w1}) \\ \alpha_o A_o \left(\frac{L_2}{L_{Total}} \right) (T_a - T_{w2}) - \alpha_{i2} A_i \left(\frac{L_2}{L_{Total}} \right) (T_{w2} - T_{r2}) - (C_p \rho V)_w \left(\frac{\dot{L}_1}{L_{Total}} \right) (T_{w1}) \end{bmatrix} \tag{2.149}$$

2.5.4 Equivalence

By applying the assumptions regarding operating condition, the time derivative terms in the above equations can be expanded in terms of other variables. This allows some freedom in choosing the dynamic state variables. The results of this approach can be shown to be equivalent to the results of the PDE approach by selecting the same state variables for the energy approach as those given by the PDE approach.

To clearly define the state variables, the following relationships are defined. The total volume is defined as the sum of the volumes of the two regions, $V = V_1 + V_2$, where the volume of the first region is the sum of the volumes of the vapor and liquid phases:$V_1 = V_f + V_g$. The volumes of the associated liquid and vapor phases are defined using the mean void fraction: $V_f = V_1(1-\bar{g})$ and $V_g = V_1(\bar{g})$. The total refrigerant mass is the sum of the masses in the two regions, $m_e = m_1 + m_2$, where the mass in the first region is the sum of the liquid and vapor mass, $m_1 = m_f + m_g$. These can also be defined in terms of densities and volumes: $m_f = r_f V_f$, $m_g = r_g V_g$, and $m_2 = r_2 V_2$. By substitution: $m_1 = \left[r_f(1-\bar{g}) + r_g(\bar{g})\right]A_{cs} L_1$ and $m_2 = r_2 A_{cs} L_2$. Likewise the total internal energy of the two regions is defined by $U_1 = m_f u_f + m_g u_g$ and $U_2 = m_2 u_2$. The wall energy terms are defined as the product of thermal capacitance per unit length, wall temperature, and the length of the respective region. By substitution, the state variables are defined in Equations 2.150 - 2.154.

$$U_1 = \left[r_f u_f (1-\bar{g}) + r_g u_g (\bar{g})\right]A_{cs} L_1 \tag{2.150}$$

$$U_2 = \left[r_2 u_2\right]A_{cs} L_2 \tag{2.151}$$

$$m_e = \left[r_f (1-\bar{g}) + r_g (\bar{g})\right]A_{cs} L_1 + r_2 A_{cs} L_2 \tag{2.152}$$

$$E_{w1} = \left(C_p r V\right)_w \left(\frac{L_1}{L_{Total}}\right) T_{w1} \tag{2.153}$$

$$E_{w2} = \left(C_p r V\right)_w \left(\frac{L_2}{L_{Total}}\right) T_{w2} \tag{2.154}$$

To place Equation 2.149 into a more familiar form, several substitutions are made. Employing conservation of refrigerant mass for each of the regions yields $\dot{m}_1 = \dot{m}_{in} - \dot{m}_{\text{int}}$ and $\dot{m}_2 = \dot{m}_{\text{int}} + \dot{m}_{out}$. Using the substitutions $\dot{m}_{\text{int}} = \dot{m}_{in} - \dot{m}_1$ and $\dot{m}_{\text{int}} = \dot{m}_2 + \dot{m}_{out}$, and rearranging the equations, Equation 2.149 becomes Equation 2.155. The right hand side of this equation is identical to Equation 2.144. The elements of the left hand side of Equation 2.155 are defined as pseudo-states (Equation 2.156).

$$\begin{bmatrix} \tilde{\dot{U}}_1 \\ \tilde{\dot{U}}_2 \\ \tilde{\dot{m}}_e \\ \tilde{\dot{E}}_{w1} \\ \tilde{\dot{E}}_{w2} \end{bmatrix} = \begin{bmatrix} \dot{m}_{in}(h_{in} - h_{\text{int}}) + a_{i1} A_i \left(\frac{L_1}{L_{Total}}\right)(T_{w1} - T_{r1}) \\ \dot{m}_{out}(h_{\text{int}} - h_{out}) + a_{i2} A_i \left(\frac{L_2}{L_{Total}}\right)(T_{w2} - T_{r2}) \\ \dot{m}_{in} - \dot{m}_{out} \\ a_o A_o (T_a - T_{w1}) - a_{i1} A_i (T_{w1} - T_{r1}) \\ a_o A_o (T_a - T_{w2}) - a_{i2} A_i (T_{w2} - T_{r2}) \end{bmatrix} \tag{2.155}$$

$$\begin{bmatrix} \dot{\tilde{U}}_1 \\ \dot{\tilde{U}}_2 \\ \dot{\tilde{m}}_e \\ \dot{\tilde{E}}_{w1} \\ \dot{\tilde{E}}_{w2} \end{bmatrix} = \begin{bmatrix} \dot{U}_1 - \dot{m}_1 h_{\text{int}} - \dot{P}_e A_{cs} L_1 + P_e A_{cs} \dot{L}_1 \\ \dot{U}_2 - (\dot{m}_e - \dot{m}_1) h_{\text{int}} - \dot{P}_e A_{cs} L_2 - P_e A_{cs} \dot{L}_1 \\ \dot{m}_e \\ \left(\dot{E}_{w1} - \dot{E}_{\text{int}}\right)\left(\frac{L_{Total}}{L_1}\right) \\ \left(\dot{E}_{w2} + \dot{E}_{\text{int}}\right)\left(\frac{L_{Total}}{L_2}\right) \end{bmatrix} \tag{2.156}$$

To demonstrate that this representation is equivalent to the model derived by the PDE approach, the elements of Equation 2.156 are expanded in terms of the state variables $x = [L_1 \quad P_e \quad h_{out} \quad T_{w1} \quad T_{w2}]^T$. Time derivatives of U_1, U_2, m_1, m_2, E_{w1}, and E_{w2} are given in Equations 2.157 - 2.162. Substituting these results and using the formal definition of enthalpy and its partial derivatives, $h = u + P/r$, $\left.\frac{\partial u}{\partial P}\right|_h = -\frac{1}{r}$, and $\left.\frac{\partial u}{\partial h}\right|_P = 1 + \frac{P}{r^2}\left(\left.\frac{\partial r}{\partial h}\right|_P\right)$, the elements of Equation 2.156 can be written as Equations 2.163 - 2.167. Upon evaluation, these equations are identical to the left hand side of Equation 2.144.

$$\begin{aligned} \dot{U}_1 = &\left[\frac{d(r_f u_f)}{dP_e}(1-\bar{g}) + \frac{d(r_g u_g)}{dP_e}(\bar{g})\right] A_{cs} L_1 \dot{P}_e \\ &+ \left[r_f u_f (1-\bar{g}) + r_g u_g (\bar{g})\right] A_{cs} \dot{L}_1 + \left[r_g u_g - r_f u_f\right] A_{cs} L_1 \dot{\bar{g}} \end{aligned} \tag{2.157}$$

$$\begin{aligned} \dot{U}_2 = &\left[\left(\left.\frac{\partial (r_2 u_2)}{\partial P_e}\right|_{h_2}\right) + \frac{1}{2}\left(\left.\frac{\partial (r_2 u_2)}{\partial h_2}\right|_{P_e}\right)\left(\frac{dh_g}{dP_e}\right)\right] A_{cs} L_2 \dot{P}_e \\ &+ \frac{1}{2}\left(\left.\frac{\partial (r_2 u_2)}{\partial h_2}\right|_{P_e}\right) A_{cs} L_2 \dot{h}_{out} + r_2 u_2 A_{cs} \dot{L}_2 \end{aligned} \tag{2.158}$$

$$\begin{aligned} \dot{m}_1 = &\left[\frac{dr_f}{dP_e}(1-\bar{g}) + \frac{dr_g}{dP_e}(\bar{g})\right] A_{cs} L_1 \dot{P}_e \\ &+ \left[r_f (1-\bar{g}) + r_g (\bar{g})\right] A_{cs} \dot{L}_1 + \left[r_g - r_f\right] A_{cs} L_1 \dot{\bar{g}} \end{aligned} \tag{2.159}$$

$$\begin{aligned} \dot{m}_2 = &\left[\left(\left.\frac{\partial r_2}{\partial P_e}\right|_{h_2}\right) + \left(\frac{1}{2}\left(\left.\frac{\partial r_2}{\partial h_2}\right|_{P_e}\right)\left(\frac{dh_g}{dP_e}\right)\right)\right] A_{cs} L_2 \dot{P}_e \\ &+ \left[\left(\frac{1}{2}\left(\left.\frac{\partial r_2}{\partial h_2}\right|_{P_e}\right)\right)\right] A_{cs} L_2 \dot{h}_{out} + r_2 A_{cs} \dot{L}_2 \end{aligned} \tag{2.160}$$

$$\dot{E}_{w1} = \left(C_p r V\right)_w \left(\frac{L_1}{L_{Total}}\right) \dot{T}_{w1} + \left(C_p r V\right)_w \left(\frac{\dot{L}_1}{L_{Total}}\right) T_{w1} \tag{2.161}$$

$$\dot{E}_{w2} = \left(C_p r A\right)_w \left(\frac{L_2}{L_{Total}}\right)\dot{T}_{w2} + \left(C_p r A\right)_w \left(\frac{\dot{L}_2}{L_{Total}}\right) T_{w2} \tag{2.162}$$

$$\begin{aligned}\dot{\tilde{U}}_1 = &\left[\left(\frac{d\left(r_f h_f\right)}{dP_e} - \frac{dr_f}{dP_e}h_g\right)\left(1-\bar{g}\right) + \left(\frac{d\left(r_g h_g\right)}{dP_e} - \frac{dr_g}{dP_e}h_g\right)\left(\bar{g}\right) - 1\right] A_{cs} L_1 \dot{P}_e \\ &+ \left[r_f\left(h_f - h_g\right)\right]\left(1-\bar{g}\right) A\dot{L}_1 + \left[r_f\left(h_g - h_f\right)\right] A L_1 \dot{\bar{g}}\end{aligned} \tag{2.163}$$

$$\begin{aligned}\dot{\tilde{U}}_2 = &\left[\left(\left(\left.\frac{\partial r_2}{\partial P_e}\right|_{h_2}\right) + \left(\frac{1}{2}\left(\left.\frac{\partial r_2}{\partial h_2}\right|_{P_e}\right)\left(\frac{dh_g}{dP_e}\right)\right)\left(h_2 - h_g\right) + \left(\frac{r_2}{2}\right)\left(\frac{dh_g}{dP_e}\right) - 1\right] A L_2 \dot{P}_e \\ &+ \left[\left(\frac{1}{2}\left(\left.\frac{\partial r_2}{\partial h_2}\right|_{P_e}\right)\left(h_2 - h_g\right) + \left(\frac{1}{2}\right) r_2\right] A L_2 \dot{h}_{out} + r_2\left(h_g - h_2\right) A\dot{L}_1\end{aligned} \tag{2.164}$$

$$\begin{aligned}\dot{\tilde{m}}_e = &\left[\begin{array}{l}\left[\frac{dr_f}{dP_e}\left(1-\bar{g}\right) + \frac{dr_g}{dP_e}\left(\bar{g}\right)\right] L_1 \\ + \left[\left(\left.\frac{\partial r_2}{\partial P_e}\right|_{h_2}\right) + \left(\frac{1}{2}\left(\left.\frac{\partial r_2}{\partial h_2}\right|_{P_e}\right)\left(\frac{dh_g}{dP_e}\right)\right)\right] L_2\end{array}\right] A_{cs}\dot{P}_e \\ &+ \left[r_f\left(1-\bar{g}\right) + r_g\left(\bar{g}\right) - r_2\right] A_{cs}\dot{L}_1 \\ &+ \left[\left(\frac{1}{2}\left(\left.\frac{\partial r_2}{\partial h_2}\right|_{P_e}\right)\right)\right] A_{cs} L_2 \dot{h}_{out} + \left[r_g - r_f\right] A_{cs} L_1 \dot{\bar{g}}\end{aligned} \tag{2.165}$$

$$\dot{\tilde{E}}_{w1} = \left(C_p r V\right)_w \dot{T}_{w1} \tag{2.166}$$

$$\dot{\tilde{E}}_{w2} = \left(C_p r V\right)_w \dot{T}_{w2} - \left(C_p r V\right)_w \left(\frac{T_{w2} - T_{w1}}{L_2}\right)\dot{L}_1 \tag{2.167}$$

2.5.5 Second Representation

The elements of Equation 2.156 can also be expanded in terms of an alternative set of state variables $x' = \left[L_1 \quad P_e \quad m_e \quad T_{w1} \quad T_{w2}\right]^T$. For this the thermodynamic functions are defined in terms of pressure and density. Using the time derivatives given in Equations 2.157, 2.159, 2.160, and 2.168, the internal energy states of Equation 2.156 can be derived as in Equations 2.169 - 2.170. Combining these results with previously derived expressions in Equations 2.166 and 2.167 and arranging in matrix form results in Equation 2.171. This results in what will be referred to as the second representation, and will be denoted with the prime notation (i.e. $Z'(x',u')\cdot\dot{x}' = f'(x',u')$). When the resulting equations are arranged in matrix form, the resulting model is of the same form as Equation 2.144, but with alternative state variables of $x' = \left[L_1 \quad P_e \quad m_e \quad T_{w1} \quad T_{w2}\right]^T$. The elements of the $Z'(x',u')$ matrix are given in Table 2.5.

$$\dot{U}_2 = \left[u_2 + \left(\left.\frac{\partial u_2}{\partial r_2}\right|_{P_e}\right) r_2\right](\dot{m}_e - \dot{m}_1) + \left[m_2\left(\left.\frac{\partial u_2}{\partial P_e}\right|_{r_2}\right)\right]\dot{P} + \left[\left(\left.\frac{\partial u_2}{\partial r_2}\right|_{P_e}\right)(r_2)^2\right]A_{cs}\dot{L}_1 \tag{2.168}$$

$$\dot{\bar{U}}_1 = \left[\left(\frac{d(r_f u_f)}{dP_e} - \frac{dr_f}{dP_e}h_g\right)(1-\bar{g}) + \left(\frac{d(r_g u_g)}{dP_e} - \frac{dr_g}{dP_e}h_{gt}\right)(\bar{g}) - 1\right]A_{cs}L_1\dot{P}_e + \left[(r_f u_f - r_f h_g)(1-\bar{g}) + (r_g u_g - r_g h_g)(\bar{g}) + P_e\right]A_{cs}\dot{L}_1 + \left[r_g(u_g - h_g) - r_f(u_f - h_g)\right]A_{cs}L_1\dot{\bar{g}} \tag{2.169}$$

$$\dot{\bar{U}}_2 = \left[\left(\left.\frac{\partial u_2}{\partial r_2}\right|_{P_e}\right)(r_2)^2 - \left(u_2 + \left(\left.\frac{\partial u_2}{\partial r_2}\right|_{P_e}\right)r_2 - h_g\right)\left(r_f(1-\bar{g}) + r_g(\bar{g})\right) - P_e\right]A_{cs}\dot{L}_1 + \begin{bmatrix} m_2\left(\left.\frac{\partial u_2}{\partial P_e}\right|_{r_2}\right) - A_{cs}L_2 \\ -\left(u_2 + \left(\left.\frac{\partial u_2}{\partial r_2}\right|_{P_e}\right)r_2 - h_g\right)\left(\frac{dr_f}{dP_e}(1-\bar{g}) + \frac{dr_g}{dP_e}(\bar{g})\right)A_{cs}L_1 \end{bmatrix}\dot{P}_e + \left[u_2 + \left(\left.\frac{\partial u_2}{\partial r_2}\right|_{P_e}\right)r_2 - h_g\right]\dot{m}_e - \left[\left(u_2 + \left(\left.\frac{\partial u_2}{\partial r_2}\right|_{P_e}\right)r_2 - h_g\right)(r_g - r_f)\right]A_{cs}L_1\dot{\bar{g}} \tag{2.170}$$

$$\begin{bmatrix} z'_{11} & z'_{12} & 0 & 0 & 0 \\ z'_{21} & z'_{22} & z'_{23} & 0 & 0 \\ 0 & 0 & 1 & 0 & 0 \\ 0 & 0 & 0 & z'_{44} & 0 \\ z'_{51} & 0 & 0 & 0 & z'_{55} \end{bmatrix}\begin{bmatrix} \dot{L}_1 \\ \dot{P} \\ \dot{m}_e \\ \dot{T}_{w1} \\ \dot{T}_{w2} \end{bmatrix} = \begin{bmatrix} \dot{m}_{in}(h_{in} - h_g) + a_{i1}A_i\left(\frac{L_1}{L_{Total}}\right)(T_{w1} - T_{r1}) \\ \dot{m}_{out}(h_g - h_{out}) + a_{i2}A_i\left(\frac{L_2}{L_{Total}}\right)(T_{w2} - T_{r2}) \\ \dot{m}_{in} - \dot{m}_{out} \\ a_o A_o(T_a - T_{w1}) - a_{i1}A_i(T_{w1} - T_{r1}) \\ a_o A_o(T_a - T_{w2}) - a_{i2}A_i(T_{w2} - T_{r2}) \end{bmatrix} \tag{2.171}$$

Table 2.5 Matrix Elements of $Z'(x',u')$ for the Evaporator

z'_{11}	$\left[(r_f u_f - r_f h_g)(1-\bar{g}) + (r_g u_g - r_g h_g)(\bar{g}) + P_e\right] A_{cs}$
z'_{12}	$\left[\left(\frac{d(r_f u_f)}{dP_e} - \frac{dr_f}{dP_e} h_g\right)(1-\bar{g}) + \left(\frac{d(r_g u_g)}{dP_e} - \frac{dr_g}{dP_e} h_g\right)(\bar{g})\right] A_{cs} L_1$
z'_{21}	$\begin{bmatrix} \left(\left.\frac{\partial u_2}{\partial r_2}\right\|_{P_e}\right)(r_2)^2 - P_e \\ -\left(u_2 + \left(\left.\frac{\partial u_2}{\partial r_2}\right\|_{P_e}\right) r_2 - h_g\right)\left(r_f(1-\bar{g}) + r_g(\bar{g})\right) \end{bmatrix} A_{cs}$
z'_{22}	$m_2\left(\left.\frac{\partial u_2}{\partial P_e}\right\|_{r_2}\right) - A_{cs} L_2$ $-\left(u_2 + \left(\left.\frac{\partial u_2}{\partial r_2}\right\|_{P_e}\right) r_2 - h_g\right)\left(\frac{dr_f}{dP_e}(1-\bar{g}) + \frac{dr_g}{dP_e}(\bar{g})\right) A_{cs} L_1$
z'_{23}	$u_2 + \left(\left.\frac{\partial u_2}{\partial r_2}\right\|_{P_e}\right) r_2 - h_g$
z'_{44}	$(C_p r V)_w$
z'_{51}	$(C_p r V)_w \left(\frac{T_{w1} - T_{w2}}{L_2}\right)$
z'_{55}	$(C_p r V)_w$

As with the gas cooler, a useful result that stems from the equivalence of the various representations is that the matrix $Z'(x',u')$ can be calculated directly from the elements of $Z(x,u)$. Note that $f(x,u) = f'(x',u')$, and thus $Z(x,u)\cdot\dot{x} = Z'(x',u')\cdot\dot{x}'$. Algebraic manipulation of these equations results in the relationships in Equations 2.172 - 2.179 for defining the elements of $Z'(x',u')$. Evaluation of these elements in terms of their thermodynamic functions confirms these relationships.

$$z'_{11} = z_{11} \tag{2.172}$$

$$z'_{12} = z_{12} \tag{2.173}$$

$$z'_{21} = \frac{z_{21} z_{33} - z_{23} z_{31}}{z_{33}} \tag{2.174}$$

$$z'_{22} = \frac{z_{22} z_{33} - z_{23} z_{32}}{z_{33}} \tag{2.175}$$

$$z'_{23} = \frac{z_{23}}{z_{33}} \tag{2.176}$$

$$z'_{44} = z_{44} \tag{2.177}$$

$$z'_{51} = z_{51} \tag{2.178}$$

$$z'_{55} = z_{55} \tag{2.179}$$

2.5.6 Third Representation

Finally, the original derivation result of the energy approach is defined as the third representation, and denoted with the double prime notation (i.e. $Z''(x'',u'')\cdot\dot{x}'' = f''(x'',u'')$). This model is also of the same form as Equation 2.144, but with alternative state variables of $x'' = \left[\tilde{U}_1 \quad \tilde{U}_2 \quad \tilde{\dot{m}}_e \quad \tilde{E}_{w1} \quad \tilde{E}_{w2}\right]^T$. The resulting model is given in Equation 2.180 where the $Z''(x'',u'')$ matrix is defined simply as $Z''(x'',u'') = I^{5x5}$.

$$\begin{bmatrix} \dot{\tilde{U}}_1 \\ \dot{\tilde{U}}_2 \\ \dot{\tilde{m}}_e \\ \dot{\tilde{E}}_{w1} \\ \dot{\tilde{E}}_{w2} \end{bmatrix} = \begin{bmatrix} \dot{m}_{in}(h_{in} - h_{\text{int}}) + a_{i1}A_i\left(\frac{L_1}{L_{Total}}\right)(T_{w1} - T_{r1}) \\ \dot{m}_{out}(h_{\text{int}} - h_{out}) + a_{i2}A_i\left(\frac{L_2}{L_{Total}}\right)(T_{w2} - T_{r2}) \\ \dot{m}_{in} - \dot{m}_{out} \\ a_o A_o(T_a - T_{w1}) - a_{i1}A_i(T_{w1} - T_{r1}) \\ a_o A_o(T_a - T_{w2}) - a_{i2}A_i(T_{w2} - T_{r2}) \end{bmatrix} \tag{2.180}$$

2.5.7 Summary

The PDE approach was demonstrated to be somewhat tedious, and required the significant algebraic manipulation. The simpler energy approach resulted in a model shown to be equivalent to the PDE approach, but with obvious freedom in choosing the state variables. The simplicity of the approach and the ability to choose the state variables becomes of great interest when evaluating possibilities for model reduction. Note that for all three modeling representations $f(x,u) = f'(x',u') = f''(x'',u'')$ and $u = u' = u''$.

2.6 Internal Heat Exchanger

The internal heat exchanger is assumed to be a single-phase, counterflow heat exchanger (Figure 2.6). This component is also modeled using a lumped parameter approach. However, because the mode of heat transfer is significantly simpler, this component uses lumped capacitance assumptions to simplify the derivation. This results in a 3rd order model.

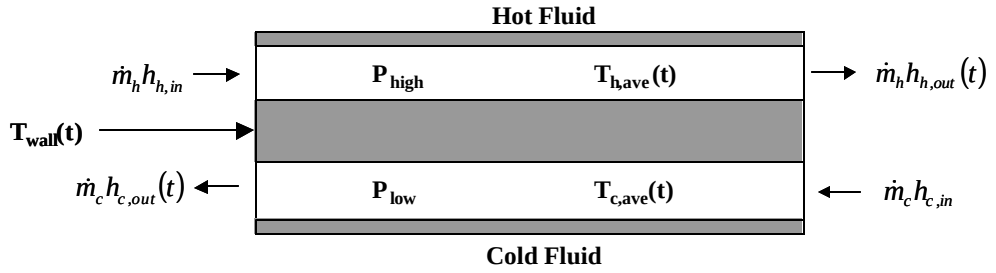

Figure 2.6 Diagram: Internal Heat Exchanger

The three differential equations are formed by using the unsteady state form of the conservation of energy equation for the hot fluid (Equation 2.181), the cold fluid (Equation 2.182), and the heat exchanger wall (Equation 2.183). Average fluid temperatures are assumed and defined as $T_{h,ave} = \frac{T_{h,in} + T_{h,out}}{2}$ and $T_{c,ave} = \frac{T_{c,in} + T_{c,out}}{2}$. Uniform refrigerant pressure is assumed for each side of the heat exchanger, and the inlet and outlet temperatures and enthalpies are then related in terms of the thermodynamic equation of state: $T_{h,in} = T(P_h, h_{h,in})$, $T_{c,in} = T(P_c, h_{c,in})$, $h_{h,out} = h(P_h, T_{h,out})$, and $h_{c,out} = h(P_c, T_{c,out})$.

$$\dot{m}_h (h_{h,in} - h_{h,out}) - a_h A_h (T_{h,ave} - T_{wall}) = (rVC_p)_h \dot{T}_{h,ave} \quad (2.181)$$

$$\dot{m}_c (h_{c,in} - h_{c,out}) - a_c A_c (T_{c,ave} - T_{wall}) = (rVC_p)_c \dot{T}_{c,ave} \quad (2.182)$$

$$a_c A_c (T_{c,ave} - T_{wall}) + a_h A_h (T_{h,ave} - T_{wall}) = (rVC_p)_{wall} \dot{T}_{wall} \quad (2.183)$$

Chapter 3. System Simulation

This chapter describes a set of simulation tools developed for the purposes of model validation, analysis, and controller design. This library was developed for use with MATLAB and its associated simulation program Simulink®. At the time of publication of this thesis, this software was entitled "Thermosys Toolbox" and available to the companies sponsoring this research effort (member companies of the Air Conditioning and Refrigeration Center at the University of Illinois at Urbana-Champaign).

3.1 Software Introduction

The primary purpose for the development of the Thermosys Toolbox was to facilitate this research by providing a means for model validation, dynamic analysis, and controller design. Much of the information included in this chapter can be found in greater detail in the Thermosys User's Manual [31].

The Thermosys Toolbox was developed for use in MATLAB. This software platform offers several distinct advantages. First, the widespread use of this program among industrial and academic institutions as a simulation and control design tool increases the applicability of the Thermosys Toolbox. Second, the open architecture style of programming allows users to customize, extend, and otherwise modify the tools provided. Third, the availability of additional toolboxes such as system identification, GUI creation, dynamic analysis, etc. that are available for use with MATLAB can also be used in conjunction with the Thermosys Toolbox.

3.2 Library Structure

Thermosys is a library of models and tools for simulating vapor compression systems. These models are created using the visual programming package Simulink®, while making extensive use of the commands and capabilities of MATLAB. These simulation tools can be easily accessed from the Simulink® Library Browser. The tools are organized into three directories: auxiliary tools, components, and fluid properties.

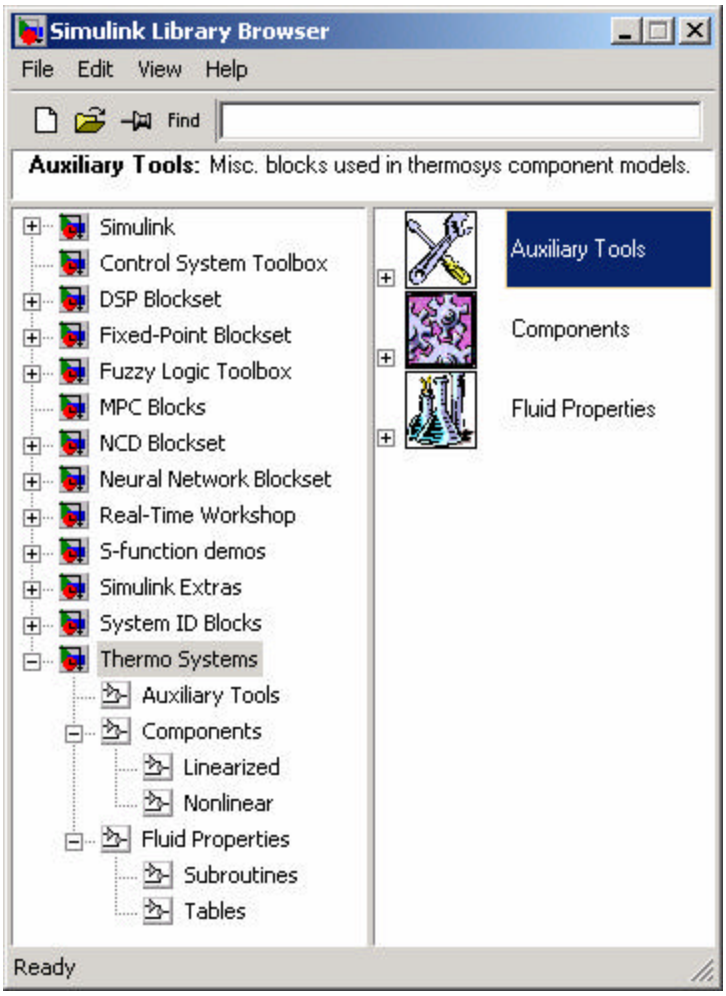

Figure 3.1 Overview of Thermosys Library from the Simulink® Browser

3.2.1 Auxiliary Tools

These blocks are miscellaneous subroutines used repeatedly by the component models. Blocks are included for calculating fluid quality, scaling of heat transfer coefficients with Reynold's number, and calculating mean void fraction based on a slip ratio correlation. A modified memory block (see Simulink® manual) that permits the initial condition to be set externally is also included.

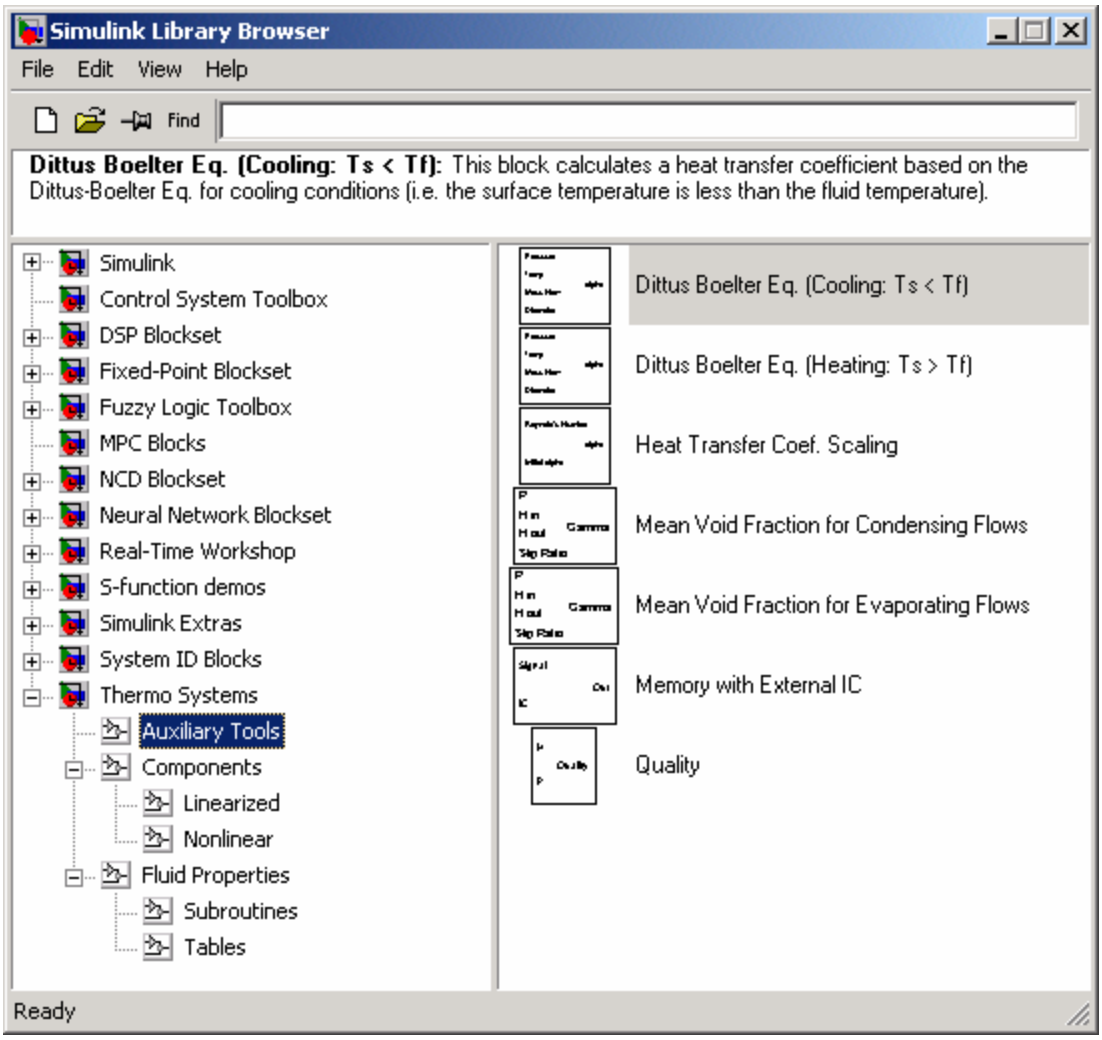

Figure 3.2 Overview of the Auxiliary Tools in the Thermosys Toolbox

3.2.2 Components

These blocks include the component models developed in this thesis. This includes the evaporator, condenser, gas cooler, internal heat exchanger, compressor and expansion valve. Preliminary models for an evaporator with receiver and a condenser with receiver are also included. Both nonlinear, linearized, and reduced order versions of these components are available. The nonlinear models are based on the nonlinear governing equations (Chapter 2), and generally require more computational time to simulate. The linear models use the equations resulting from a local linearization of the governing equations (Chapter 6). These models require less computational time while approximating closely the nonlinear models. The reduced order models are linear models that require fewer dynamic states and are developed in Chapter 7. These models require the least computational time and yield results indistinguishable from the full order linear models.

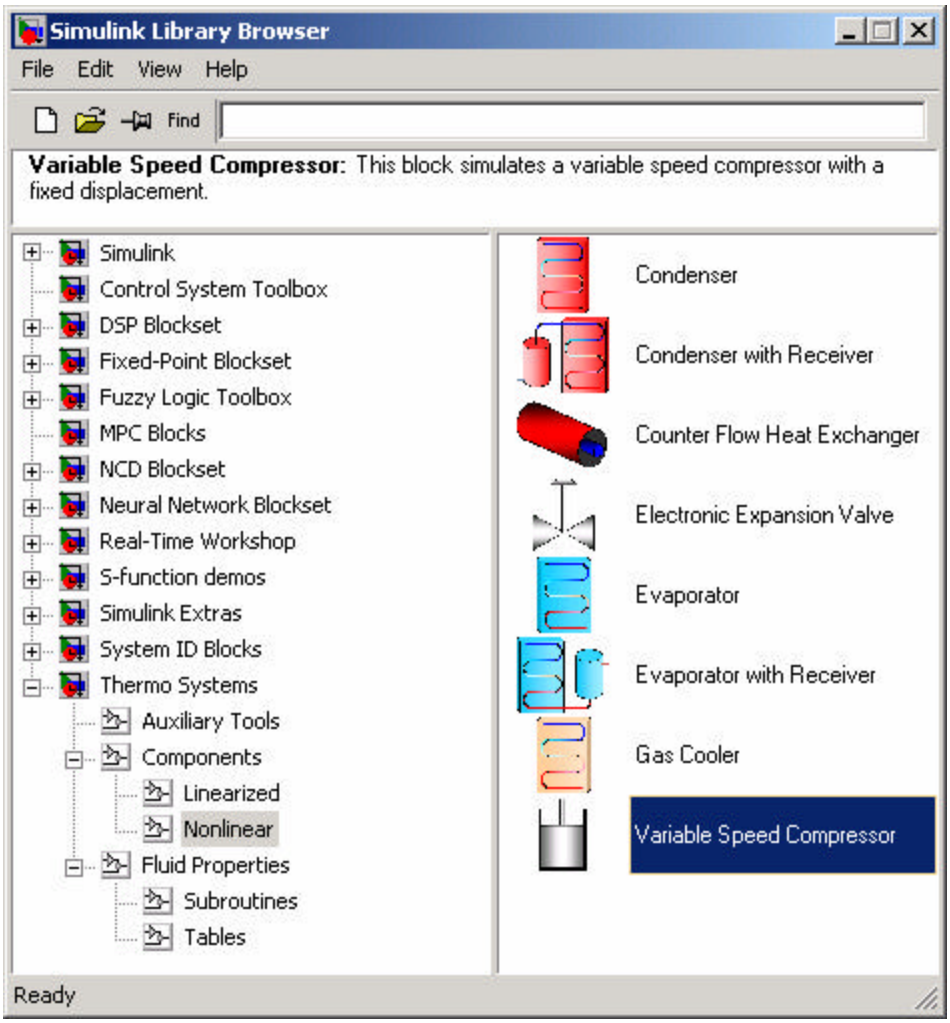

Figure 3.3 Overview of the Components in the Thermosys Toolbox

3.2.3 Fluid Properties

Fluid properties are calculated using tables or subroutines. The tables use interpolation based on predefined tables, whereas the subroutines iteratively solve empirical equations of state for the selected fluid. These are discussed in detail in Section 3.1.6.

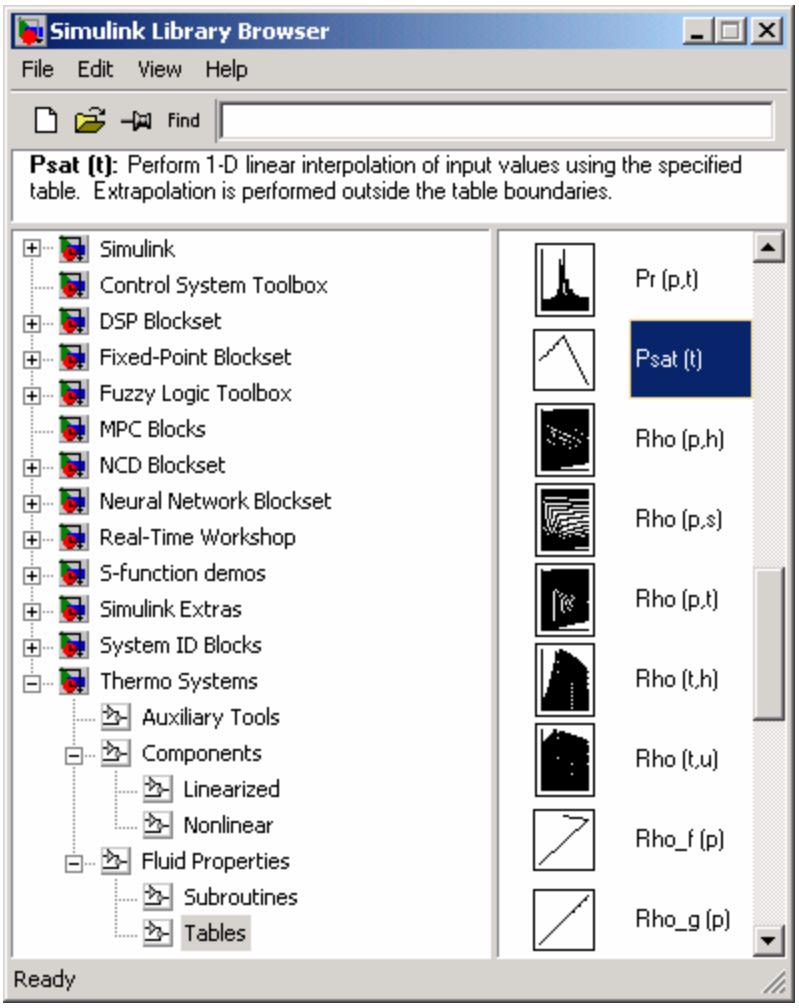

Figure 3.4 Overview of Fluid Properties in the Thermosys Toolbox

3.3 Component Models

Each component model consists of three essential parts: the graphical user interface, the Simulink® block diagram, and a component S-function.

3.3.1 Component GUIs

By double clicking on any component, an interactive graphical user interface (GUI) is activated which allows the user to specify the component's physical parameters, operating condition, and other necessary information. The author developed the initial versions of these GUIs; Joel Jeddolah developed the most recent versions. As an example, Figure 3.5 shows the graphical user interface for the evaporator model. The different parts of these GUIs generally consist of the component name, physical parameters, operating condition, heat transfer coefficients, recorded outputs, pressure and enthalpy drop, and save/load profile.

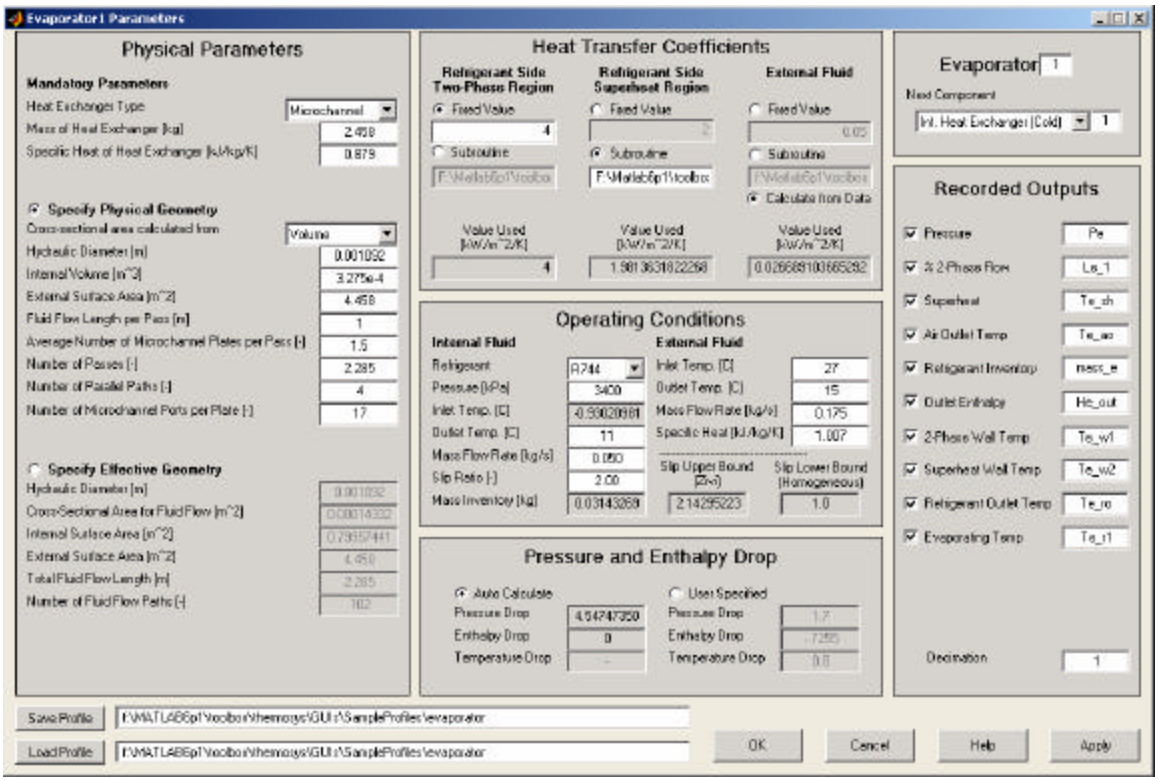

Figure 3.5 Evaporator GUI

3.3.1.1 Component Name

This allows the user to specify the "name" of the component by assigning it a number. This becomes critical for simulation of multi-component systems when several identical component blocks are used in the same system model. The user also specifies the next component. This allows the underlying code to automatically calculate the necessary pressure and temperature drops to ensure that the user-entered boundary conditions are met (see Section 3.3.1.6).

Figure 3.6 GUI: Component Name Section

3.3.1.2 Physical Parameters

Where applicable, the user is allowed to enter either measured physical geometry or the effective parameters required by the component model. If physical geometry are specified, the effective parameters are calculated and displayed.

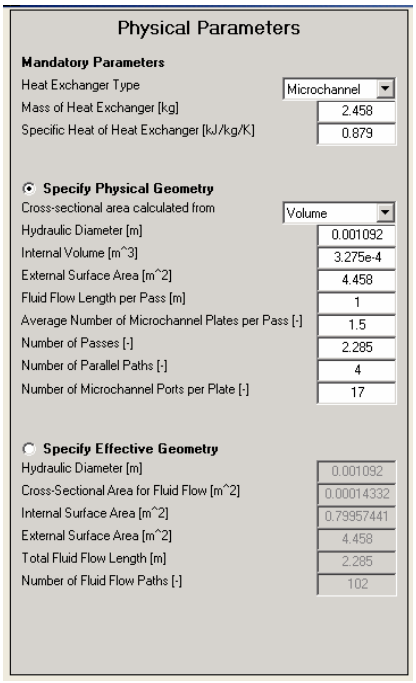

Figure 3.7 GUI: Physical Parameters Section

3.3.1.3 Operating Condition

The component models require appropriate initial conditions to begin the simulation. Unfortunately, many of the dynamic variables are not measurable, such as the effective length of two-phase flow. Therefore the user is asked for commonly measured variables that define the operating condition, such as pressures and temperatures. The GUI then uses this information to calculate the necessary initial conditions of the dynamic variables to match the user-specified operating condition. Also calculated and displayed for the heat exchanger models are the refrigerant mass inventory and the suggested upper and lower bounds for the slip ratio used in the mean void fraction correlation.

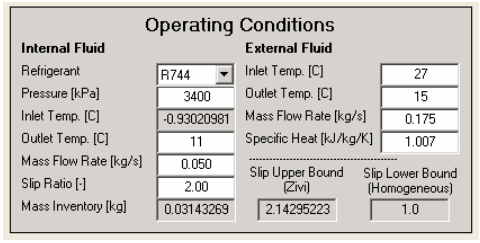

Figure 3.8 GUI: Operating Condition Section

3.3.1.4 Heat Transfer Coefficients

The heat exchanger components use correlations to calculate the necessary heat transfer coefficients. However, because of the unlimited number and variety of such correlations, it is impossible to include even a fraction of those desired. Therefore options are included to specify a constant value, a user-defined correlation, or to calculate the value from entered data. Note that these values are only used as initial values. During simulation all heat transfer coefficients are assumed to scale with Reynold's number.

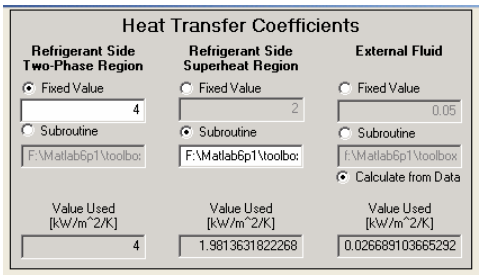

Figure 3.9 GUI: Heat Transfer Coefficients Section

3.3.1.5 Recorded Outputs

This section provides a simple interface for specifying which outputs are to be recorded during the simulation as well as the option to decimate this data. This provides a simple means for the user to select only the desired variables to be stored.

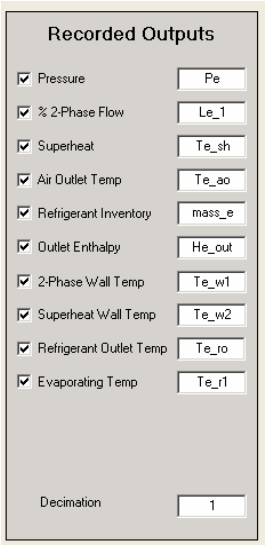

Figure 3.10 GUI: Recorded Outputs Section

3.3.1.6 Pressure and Enthalpy Drop

When specifying the operating condition for each of the component models, the user determines the boundary conditions for the fluid entering and exiting each component. Generally the operating conditions would be taken from an experimental system with energy losses between components. To resolve the discrepancy between the user-specified boundary conditions, the GUI automatically calculates the necessary static pressure drop and temperature (enthalpy) drop between the current and next component to ensure that the boundary conditions are met. Alternatively the user can disable this property by specifying the losses directly. Pipe loss models are also being developed by Rajat Shah based on turbulent flow friction factor correlations. These models will be included with future versions of the Thermosys Toolbox.

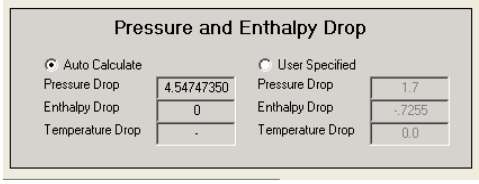

Figure 3.11 GUI: Pressure and Enthalpy Drop Section

3.3.1.7 Save/Load Profile

Perhaps the most important feature of the GUIs is the ability to save the current profile to a file or load a previously stored profile. This enables the user to quickly switch between commonly used component types or operating conditions. The "OK" button applies the changes made and closes the GUI without displaying the new calculated values. The "Cancel" button closes the GUI without applying the changes, and the "Apply" button applies the changes and displays the new calculated values without closing the GUI.

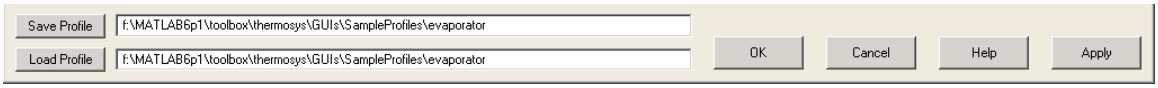

Figure 3.12 GUI: Save/Load Profile Section

3.3.2 Simulink® Block Diagram

Each of the component models in organized as a masked subsystem. The component "mask" simply displays an image of the component type. Underneath the mask, a Simulink® block diagram arranges and passes the component inputs, physical parameters, and calculated thermodynamic properties to the component S-function (Figure 3.13). The outputs of the S-function are then converted into the desired component outputs. Generally the outputs of the component S-function are state derivatives, which are integrated at each time step (Figure 3.14).

3.3.3 S-function

The component S-function is sequential code that performs operations more easily understood as text code rather than visual-based programming like block diagrams (Figure 3.14). This generally consists of matrix calculations and inversions. This code is compiled for faster execution.

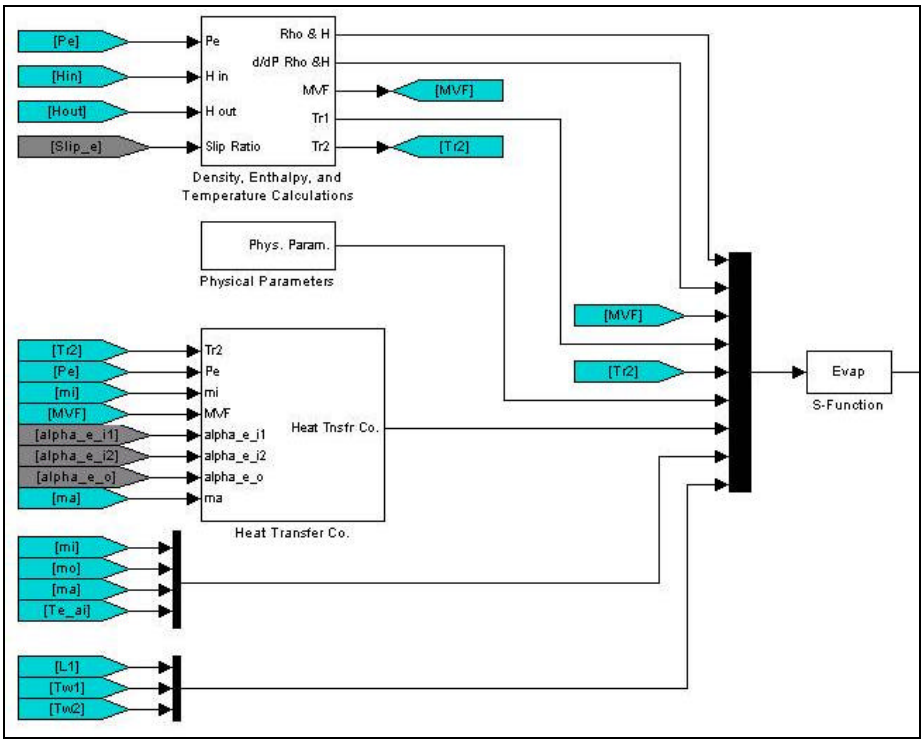

Figure 3.13 Sample Simulink® Block Diagram

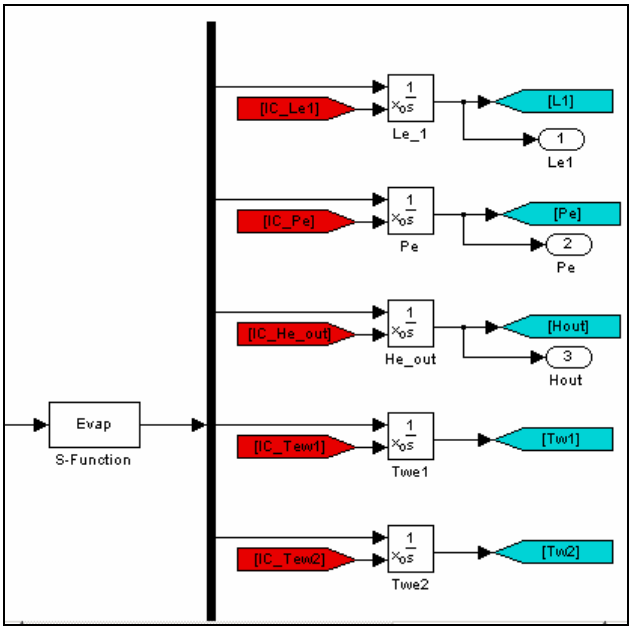

Figure 3.14 Integration of S-function Outputs

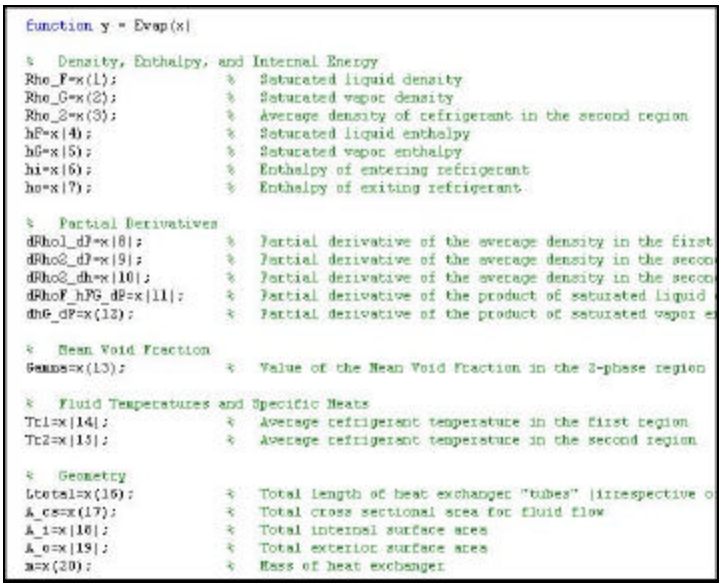

```
function y = Evap(x)

%   Density, Enthalpy, and Internal Energy
Rho_F=x(1);             %   Saturated liquid density
Rho_G=x(2);             %   Saturated vapor density
Rho_2=x(3);             %   Average density of refrigerant in the second region
hF=x(4);                %   Saturated liquid enthalpy
hG=x(5);                %   Saturated vapor enthalpy
hi=x(6);                %   Enthalpy of entering refrigerant
ho=x(7);                %   Enthalpy of exiting refrigerant

%   Partial Derivatives
dRho1_dP=x(8);          %   Partial derivative of the average density in the first
dRho2_dP=x(9);          %   Partial derivative of the average density in the secon
dRho2_dh=x(10);         %   Partial derivative of the average density in the secon
dRhoF_hFG_dP=x(11);     %   Partial derivative of the product of saturated liquid
dhG_dP=x(12);           %   Partial derivative of the product of saturated vapor e

%   Mean Void Fraction
Gamma=x(13);            %   Value of the Mean Void Fraction in the 2-phase region

%   Fluid Temperatures and Specific Heats
Tc1=x(14);              %   Average refrigerant temperature in the first region
Tc2=x(15);              %   Average refrigerant temperature in the second region

%   Geometry
Ltotal=x(16);           %   Total length of heat exchanger "tubes" (irrespective o
A_cs=x(17);             %   Total cross sectional area for fluid flow
A_i=x(18);              %   Total internal surface area
A_o=x(19);              %   Total exterior surface area
m=x(20);                %   Mass of heat exchanger
```

Figure 3.15 Sample S-function Code

3.4 System Models

To build a system simulation, the inputs and outputs of each component can be connected in a logical manner with a basic understanding of vapor comp ression systems. Color-coded “From” and “Go To” tags can be used to avoid confusing wire diagrams. The following figure demonstrates how the components of a subcritical vapor compression system can be connected together (Figure 3.16). Pressure, enthalpy, and mass flow rate are used to define the inputs and outputs of each component. Proper connection between all the components is required for correct simulation outcome. Sample models for subcritical and transcritical vapor compression systems with R134a and CO_2 as refrigerants, respectively, are included in the library. Various external inputs can be applied to the system. These include:

- Compressor speed
- Expansion valve opening
- Mass flow rate of inlet air to the evaporator
- Temperature of inlet air to the evaporator
- Mass flow rate of inlet air to the condenser/gas cooler
- Temperature of inlet air to the condenser/gas cooler

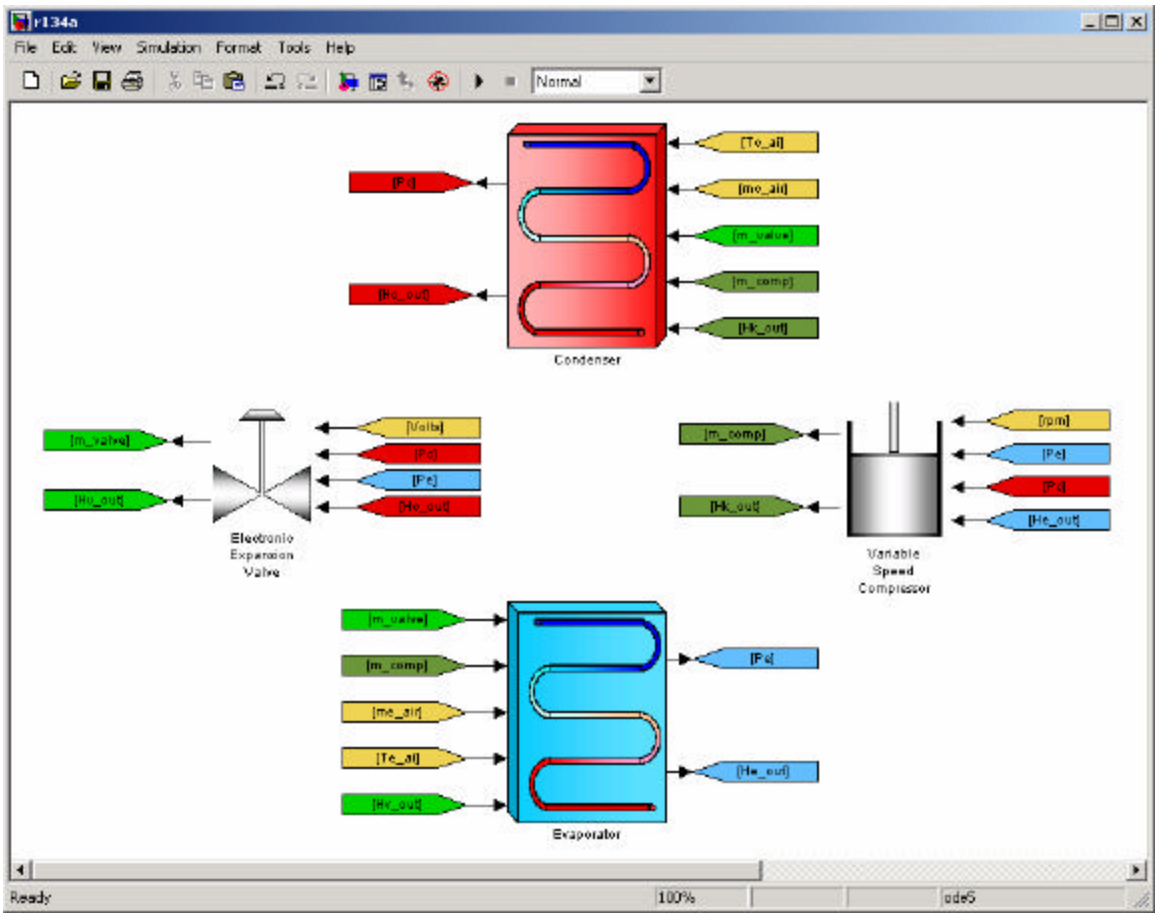

Figure 3.16 Sample System Simulation Model

3.5 Fluid Properties

The Thermosys Toolbox currently contains thermo-physical properties and data for four different refrigerants:

- R134a
- R744 (CO_2)
- R22
- R404a

3.5.1 Calculation

1-D and 2-D look-up tables were generated in EES (Engineering Equation Solver) and saved as comma-delimited files (csv). A MATLAB m-file loads the comma-delimited files and stores the data in matrix form. Partial derivatives of thermodynamic functions are also evaluated and stored as matrices. The tables can be used to calculate thermodynamic properties by using the interpolation routines included with MATLAB/Simulink®. The Thermosys Toolbox contains pre-programmed Simulink® 1-D and 2-D interpolation blocks for fluid property calculation (Figure 3.17). These are independent of the type of fluid. Whichever fluid properties are currently loaded in the MATLAB workspace are used.

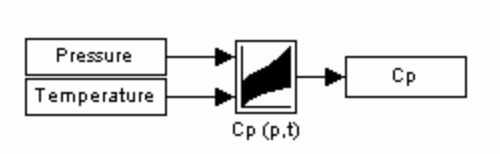

Figure 3.17 Sample Simulink® 2-D Interpolation Table

Because interpolation routines are problematic near the critical point (see Section 3.6), iterative subroutines for calculating fluid properties are also included. Because this problem is generally encountered only in transcritical cycles, these subroutines are only provided for carbon dioxide. These routines are based on FORTRAN subroutines that use the equation of state [34]. The FORTRAN subroutines were provided by the authors of [34], and adapted for use in Simulink® by the author of this thesis.

3.6 Library Limitations

The toolbox has a few notable limitations. The most important of these is that the simulation results are only valid when the assumptions applied in the modeling approach are valid. An obvious example: If the system being simulated has a 2-region evaporator model (a two-phase region and a superheat region) and the length of the superheat region goes to zero, the simulation will fail. For this purpose the component models have programming which halts the simulation if the model violates any of these constraints. Also, if the steady state conditions supplied to the system result in a solution that is physically impossible (e.g. negative lengths or pressures), the simulation will likewise stop.

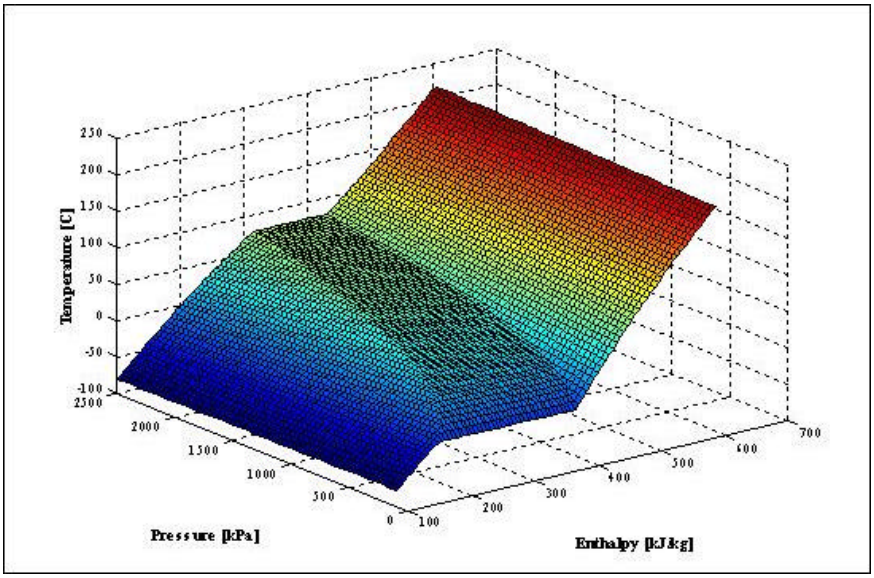

Figure 3.18 Sample Interpolation Table: Temperature as a Function of Pressure and Enthalpy for Carbon Dioxide

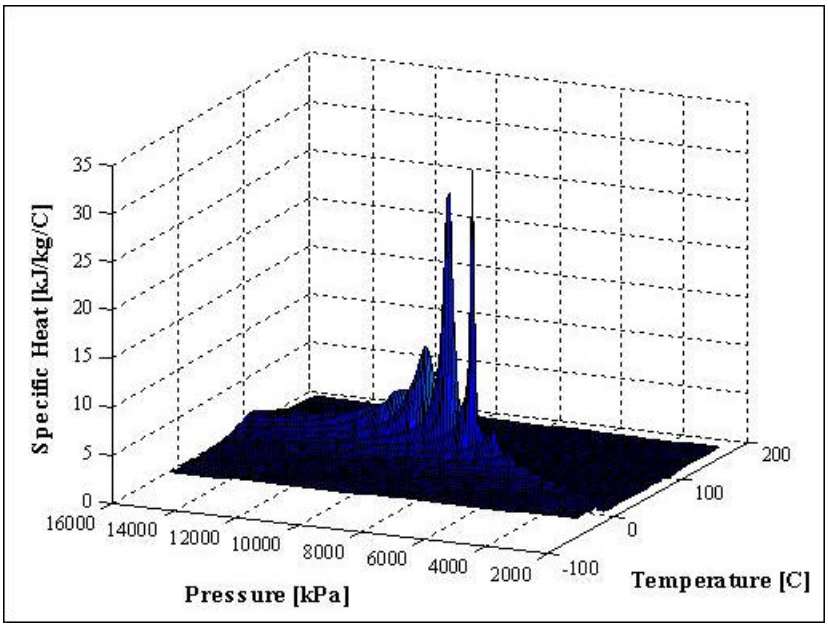

Figure 3.19 Sample Interpolation Table: Specific Heat as a Function of Pressure and Temperature for Carbon Dioxide

The primary method for fluid property calculation also has limitations. First, the calculated result is only as accurate as the mesh used to create the interpolation table (Figure 3.18). Second, when evaluating properties near the critical point, incorrect results are more likely. A good example of this can be seen when plotting specific heat near the critical point (Figure 3.19). Because specific heat approaches infinity at the critical point by definition, using interpolation tables near this point can be problematic. Because this is generally only a common problem for transcritical cycles, iterative subroutines for calculating the exact fluid properties based on the equation of state for carbon dioxide (CO_2) are included in the toolbox. These routines are extremely slow and only are recommended when reliable results are not possible using the look-up tables.

3.7 Future Additions

Efforts to improve the library are continuous. Planned additions to the library include refining of some of the preliminary models, such as the heat exchangers with receivers, as well as a greater variety of component models. Specifically, the necessary components to simulate multi-component systems are being developed by Rajat Shah. These will be used to simulate multi-evaporator systems, such as those found in automobile air conditioning and semi-trailer refrigeration units, and multi-evaporator/multi-compressor systems, such as complex residential air conditioning systems.

Chapter 4. Experimentation and System Identification

This chapter discusses the experimental testing equipment, the testing procedure, and the resulting data. This data is used for model validation (Chapter 5) and for the creation of empirical dynamic models using system identification techniques. The resulting empirical models are evaluated for possibilities of a low order dynamic model.

4.1 Test Facility

4.1.1 System Description

The test facility was located on the campus of the University of Illinois at Urbana-Champaign, where a variety of residential and mobile air conditioning systems were available in the Air Conditioning Research Center (ACRC). The principal facility was a prototype R744 mobile air conditioning system (MAC2R744). This system was used for several research projects. A detailed description of this system is given in [12]. Relevant information from this publication is replicated with permission in this section for convenience.

A diagram of the experimental system is shown in Figure 4.2. Beginning at the compressor, the fluid flows through an external oil separator. This component separates oil from the refrigerant and allows the oil to be returned to the compressor to guarantee lubrication. The mass flow rate of oil is measured by a mass flow meter and is a small percentage of the total mass flow. A valve controls the amount of fluid flow. The refrigerant flows from the oil separator to a microchannel gas cooler. From the gas cooler the refrigerant flows to one side (the "hot" side) of a microchannel counterflow heat exchanger. This internal heat exchanger uses the hot refrigerant from the gas cooler to heat the cold fluid leaving the evaporator. After the internal heat exchanger the refrigerant flows through a mass flow meter and to a manual expansion valve. For the transient tests an additional electronic expansion valve was placed in parallel with the manual valve. Because the size of the electronic expansion valve was insufficient to use without the manual valve, the opening of the manual valve was fixed during transient tests, and the opening of the electronic valve was varied as desired. Through these valves the fluid expands and transitions from a supercritical fluid to a two-phase flow mixture. The refrigerant then enters a distributor followed by the evaporator. The design of the microchannel evaporator used four similar fluid flow paths, and a distributor was necessary to divide the flow into the four paths. Unfortunately, this specific evaporator had notable problems with maldistribution (the unequal distribution of refrigerant to the four fluid flow paths). From the evaporator the refrigerant flows into an accumulator. Generally the refrigerant leaving the evaporator is two-phase and the accumulator collects the two-phase fluid and allows only refrigerant vapor to leave, leaving the remaining liquid to evaporate. If the fluid leaving the evaporator is a superheated vapor for a substantial period of time, any liquid in the accumulator will evaporate, and the accumulator will contain only refrigerant vapor. A valve is placed so that a small amount of refrigerant liquid can be allowed to leave the accumulator as desired. This is to ensure that oil does not amass in the accumulator. From the accumulator the refrigerant enters the cold side of the internal heat exchanger where the hot fluid from the gas cooler heats the cold fluid before entering the compressor. This ensures that the fluid entering the compressor is never damaged by liquid refrigerant.

A schematic of the system is given in Figure 4.1. The experimental system has two insulated chambers that are controlled to simulate arbitrary indoor and outdoor conditions. A heater and glycol chiller are used to heat and

cool the air flow after leaving the evaporator and gas cooler respectively. A motor and clutch system is used to drive the variable dis placement compressor. Extensive steady state calibration of the sensors is conducted to ensure the validity of all measurements [12].

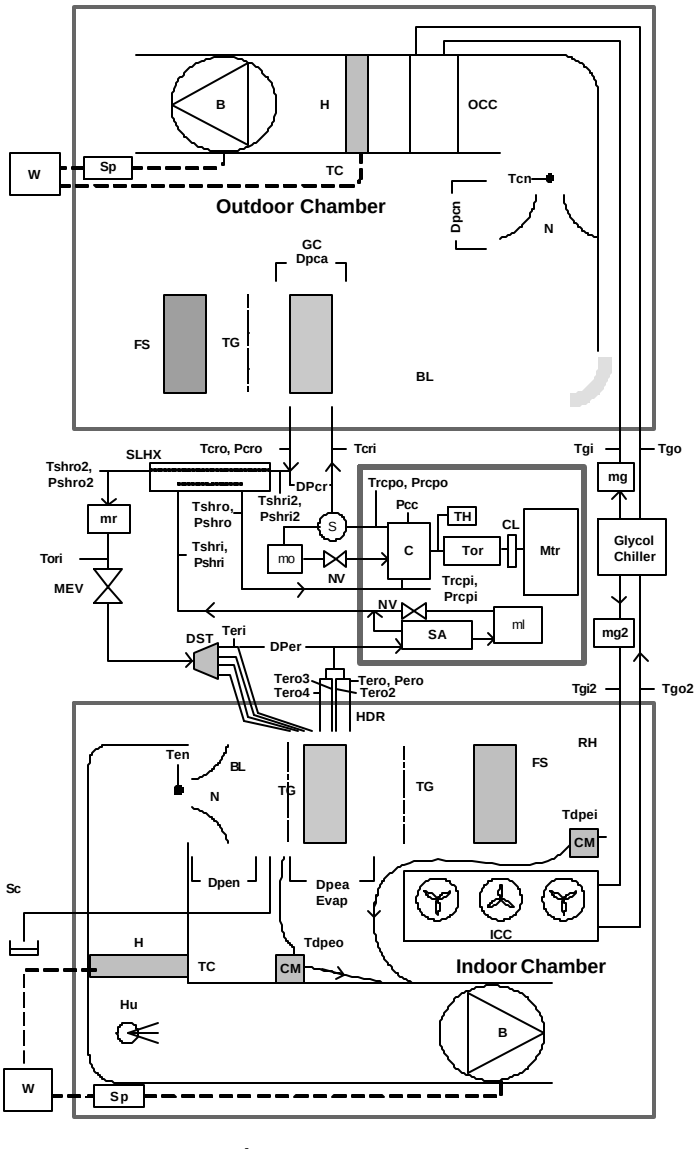

Figure 4.1 Schematic of Experimental System

[Symbols] **B** : Blower, **BL** : Air Blender, **BPV** : Back Pressure Valve, **C** : Compressor , **CL** : Compressor Clutch, **CM** : Chilled Mirror Dew Point Sensor, **Dp** : Differential Pressure Transducer, **DST** : Distributor, **Evap** : Evaporator, **FS** : Flow Straightener, **GC** : Gas Cooler, **H** : Heater, **HDR** : Pipe Header, **Hu** : Humidifier, **ICC** : Indoor Cooling Coil, **MEV** : Manual Expansion Valve, **mg** : Glycol Mass Flow Meter, **ml** : Liquid Mass Flow Meter, **mo** : Oil Mass Flow Meter, **mr** : Refrigerant Mass Flow Meter, **Mtr** : Motor, **N** : Nozzle, **NV** : Needle Valve, **OCC** : Outdoor Cooling Coil, **Or** : Orifice Tube, **P** : Pressure Transducer, **RH** : Relative Humidity Probe, **S** : Oil Separator, **SA** : Suction Accumulator, **SLHX** : Suction Line Heat Exchanger, **Sc** : Condensate Scale, **SG** : Sightglass, **Sp** : Speed Controller, **T** : Thermocouple, **TC** : Temperature Controller, **TG** : Thermocouple Grid, **TH** : Tachometer, **Tor** : Torque Transducer, **W** : Watt Transducer

[Indices] **a** : air, **c** : outdoor coil, **cc** : crankcase, **cp** : compressor, **dp** : dew point, **e** : indoor coil, **g** : glycol, **i** : inlet, **l** : liquid, **n** : nozzle, **o** : outlet, **r** : refrigerant, **sh** : suction line heat exchanger

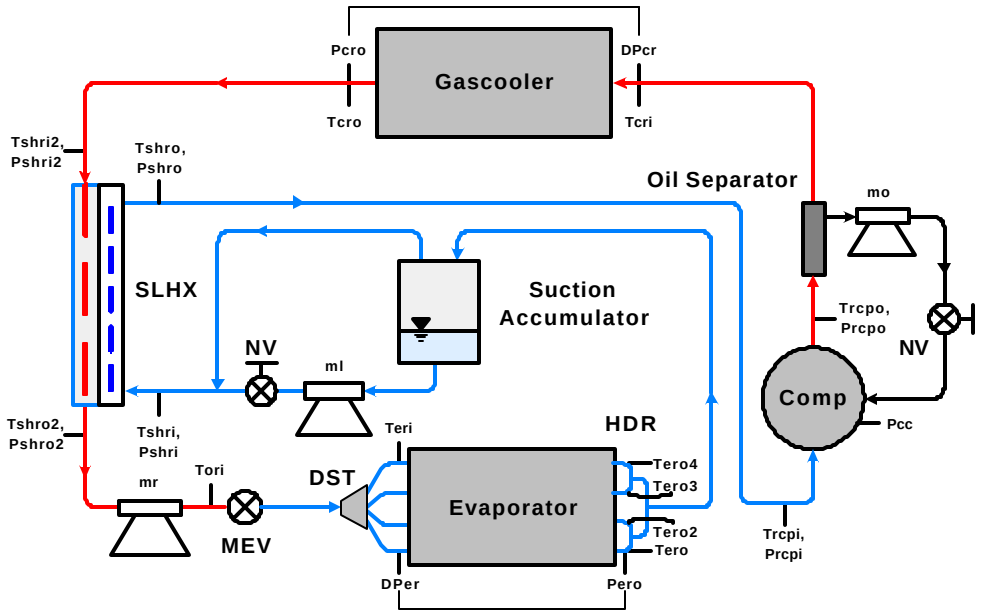

Figure 4.2 Diagram of Experimental System

The physical parameters of the system components are given in Table 4.2. Detailed information regarding the evaporator and gas cooler is given in Table 4.1. Photographs of the system components are shown in Figures 4.3 - 4.9.

Table 4.1 Heat Exchanger Parameters

System	MAC2R744	MAC2R744
Heat Exchanger	**Evaporator**	**Gas Cooler**
Face Area [cm^2]	430	2122
Core Depth [cm]	8.5	2.03
Core Volume [cm^3]	3655	4307
Air-Side Surface Area [m^2]	4.4	7.1
Free Flow Cross-Sectional Area [m^2]	0.0315	0.1617
Refrigerant-Side Surface Area [m^2]	0.92	0.53
Number of Ports	17	4
Port Diameter [mm]	1.092	0.635
Fin Pitch [mm]	1.49	1.16
Fin Thickness [mm]	0.1	0.1
Fin Density [fins/inch]	17	22
Louver angle [^{o}]	27	27
Louver pitch [mm]	1.40	1.06

*Approximate mass without header connections.

Table 4.2 Experimental System Parameters

System	Refrigerant	*R744*
	Type	Prototype
	Name	MAC2R744
Compressor:	Type	Reciprocating
	Displacement [cm^3]	Variable (33 @max)
Expansion device		Manual expansion valve
Outdoor heat exchanger	Description	Microchannel brazed Al tubes, 1 pass, 3 slabs, counter flow
	Mass [kg]	3.28 (3.14*)
	Face area (width x height) [cm^2]	60.8 x 34.9 = 2122
	Core depth [cm]	2.03
	Core volume [cm^3]	4307
	Air side surface area [m^2]	7.1
	Free Flow cross-sectional area [m^2]	0.1617
	Refrigerant side surface area [m^2]	0.53
Indoor heat exchanger	Description	Microchannel brazed Al tubes, 24 pass, 2 slabs, parallel flow
	Mass [kg]	2.51 (2.33*)
	Face area (width x height) [cm^2]	24.4 x 17.6 = 430
	Core depth [cm]	8.5
	Core volume [cm^3]	3655
	Air side surface area [m^2]	4.4
	Free Flow cross-sectional area [m^2]	0.0315
	Refrigerant side surface area [m^2]	0.92
Internal HX	Description	Brazed microchannel tubes, counterflow arrangement
	Mass [kg]	0.67
	Length [m]	0.44

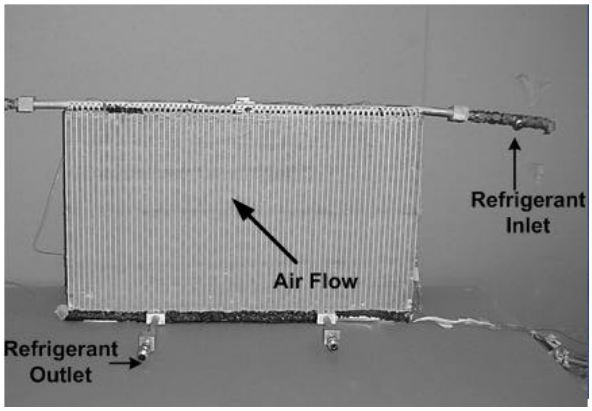

Figure 4.3 Photograph of the Gas Cooler

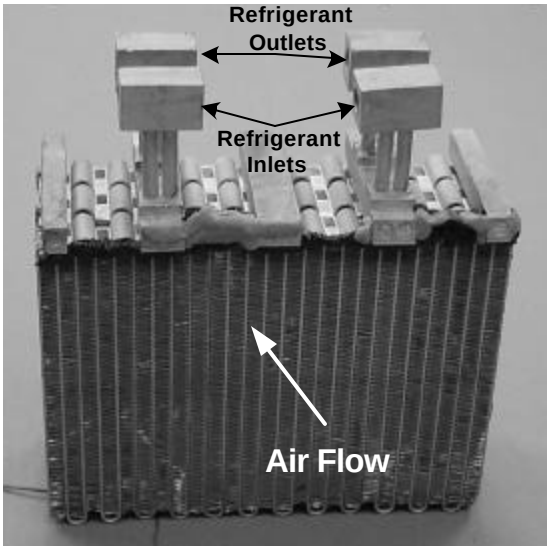

Figure 4.4 Photograph of the Evaporator

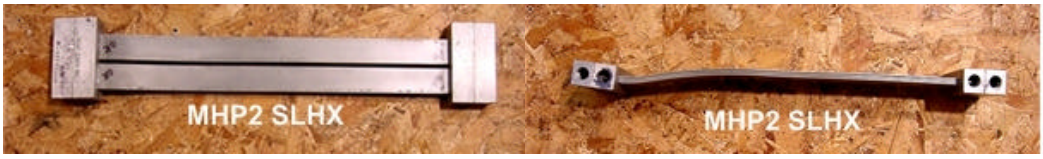

Figure 4.5 Photograph of the Internal Heat Exchanger

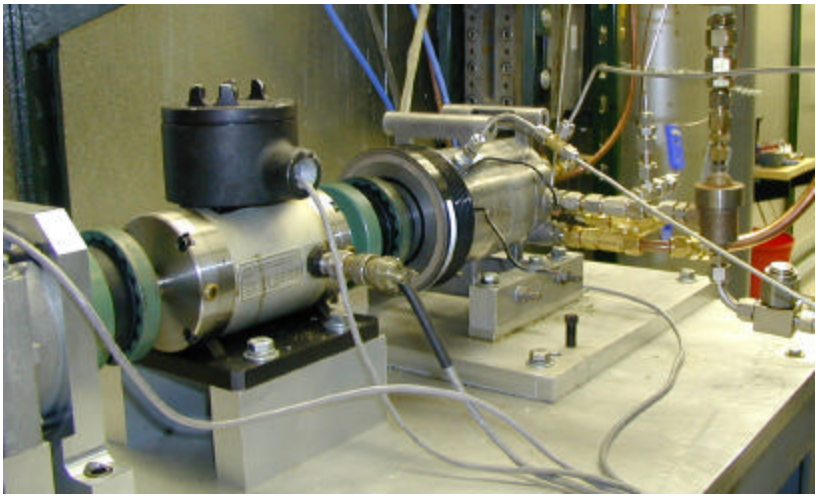

Figure 4.6 Photograph of the Variable Displacement Compressor

Figure 4.7 Photograph of the Electronic Expansion Valve

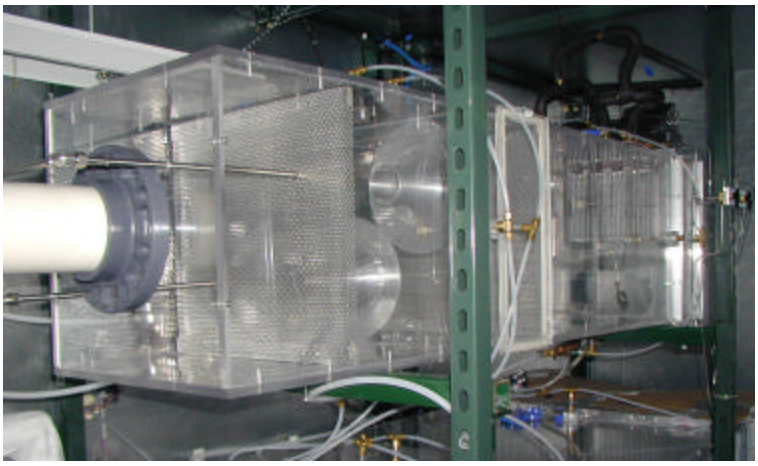

Figure 4.8 Photograph of Inside the Indoor Chamber

Figure 4.9 Photograph of the Outdoor Chamber and Data Acquisition System

4.1.2 Sensors

Information regarding the calibration of sensors is contained in [12]. This section includes supplemental information regarding the transient performance of the sensors used.

The thermocouples used for refrigerant temperature measurements were type T immersion thermocouples purchased from Omega Engineering, Inc. (part TMQSS). These thermocouples had a 304 stainless steel sheath 1/16" in diameter. Both ungrounded and grounded thermocouple types were used in this system. For air temperature measurements, bare thermocouple wire with welded tips was used. Generally a mesh of these thermocouples was used, and the resulting temperatures were averaged. Of principal concern to this research is the transient response of these thermocouples. The effective time constant of the thermocouple wire is expected to be extremely small. However, the time constant for the grounded and ungrounded immersion thermocouples may be significant (the time constant of the ungrounded thermocouple is approximately 1.5 times that of the grounded thermocouples). Unfortunately, no acceptable method for estimating the transient response of the thermocouples was found.

The pressure transducers used for refrigerant measurements were manufactured by Sensotec, Inc. Model TJE transducers (1000 and 3000 psia versions) were used for absolute pressure measurements, as well as model HLZ (50 psid version) for differential pressure measurements. Although the transient performance of these transducers is unpublished, the manufacturer reported that the time constants of these sensors were 6.67e-6, 25.0e-6, and 500.0e-6 seconds respectively. The transient response of these transducers is assumed to be negligible relative to the overall system dynamics.

The mass flow meters used for sensing refrigerant and oil mass flow rates were coriolis-type mass flow meters, purchased from MicroMotion. These sensors provide an analog signal that is discretely sampled, digitally filtered using a moving window average, and then sent to the data acquisition system to be discretely sampled. Although this sensor is accurate for steady state conditions, the filtering mechanism is undesirable for collecting transient data. A venturi meter was implemented later on the system and was used to verify that the signal given by the coriolis mass flow meter is a filtered version of the actual transient mass flow signal. In future tests, both sensors will be used to obtain both transient and steady state mass flow rates.

For steady state tests the sampling frequency is much lower than for the transient tests. For a given sampling frequency, the data acquisition system can only record a limited number of sensors. For steady state tests, the sampling frequency was sufficiently low to be able to record all desired temperatures, pressures, and mass flow rates. For transient tests, the sampling frequency was approximately 1 Hz. At this frequency only a portion of the sensors could be recorded. Specifically, temperature measurements at the inlets and outlets of the internal heat exchanger were not recorded. These temperatures were assumed to be the same as those measured at the inlet/outlet of the next component. For a small number of tests, transient data was recorded at 10 Hz. However, at this sampling frequency, the "dwell" time on each sensor was small, and the relative signal to noise ratio decreased significantly. Because of memory limitations of the data acquisition system, transient tests were limited to approximately 20 minutes at a sampling frequency of 1 Hz.

4.1.3 Actuators

The standard system actuators were altered temporarily for these experiments. An electronic expansion valve was installed in parallel with the existing manual expansion valve. During the experiments the opening of the manual expansion valve was fixed, and the electronic expansion valve was varied as desired.

A variable displacement compressor was used. This compressor used a pressure feedback to regulate the angular position of a swashplate, and thus the displacement of the compressor. During the experiments the compressor was fixed at full displacement and thus behaved like a variable speed compressor.

The experimental system also had the ability to vary the air flow rates. The ability to slowly vary the inlet air temperature and humidity was available but not used. For all experiments dry air was used to avoid complicated phenomenon such as condensation and frosting.

4.2 Experimental Procedure

4.2.1 Operating Conditions

Testing conditions were initially chosen to represent a variety of conditions and to be similar to previous test matrices (see [12]). However, the conditions were modified to ensure the refrigerant leaving the evaporator was

superheated. This ensured that the accumulator (low-side receiver) was completely filled with vapor and therefore did not affect the transient response of the system differently than a large section of pipe. Therefore the data could be compared to a simulation with a two-region evaporator without receiver. Future tests and simulations will include more common operating conditions that utilize the low-side receiver.

Testing was performed using a Visteon GRB variable displacement compressor. However, to approximate the response of a fixed-displacement, variable-speed compressor, full displacement was maintained throughout the tests. This eliminated the need to simulate the swashplate dynamics of a variable displacement compressor. These dynamics will be included in future tests and simulations.

Table 4.3 presents the matrix of operating conditions used for transient tests. The three operating conditions were chosen to represent as closely as possible the conditions encountered by an automotive air conditioning system during idle, city, and highway driving (the necessary variations were made to ensure superheated vapor at the evaporator exit).

Table 4.3 Operating Conditions for Experimental Tests

Condition	1 "Idle"	2 "City"	3 "Highway"
Indoor Air Flow Rate [cfm]	300	300	300
Outdoor Air Flow Rate [cfm]	950	950	2010
Compressor Speed [rpm]	850	1800	1800
Indoor Chamber Temperature [C]	32.1	27	32
Outdoor Chamber Temperature [C]	43.5	43.5	49.1
High Side Pressure [kPa]	8400	7845	10000
Low Side Pressure [kPa]	3600	3160	3300

4.2.2 Input Signals

The signals applied to the inputs of the system were a pseudo-random binary sequence (PRBS). The response time of the "fast" components (i.e. compressor, expansion valve) were identified, and the time for the system to arrive at a pseudo-steady state after a step change was identified. The PRBS was generated using these time measurements as the lower and upper limits respectively. This sequence was then used as an input signal for step changes for each of the system inputs. The deviation from the steady state input values was approximately 10%. Only small deviations were applied to ensure that the underlying modeling assumptions (two-region evaporator) were not violated during the transient response. Furthermore, assuming that the nonlinear systems dynamics can be approximated with locally linear dynamic models, small deviations were applied to limit the nonlinear effects that would be more notable with large transients. This type of signal was applied separately to each of the system inputs (compressor speed, electronic expansion valve voltage, evaporator fan speed, condenser fan speed). Tests were also conducted where all inputs were varied simultaneously.

4.2.3 Outputs

For each condition steady state data was taken first. Following this, the transient data was taken. Data was recorded at a sampling rate of approximately 1 Hz. For all of the conditions, step changes were performed on

compressor speed, expansion valve opening, indoor air flow rate, and outdoor flow rate individually. Additional tests were performed at a faster sampling rate of 10 Hz to verify that sampling at 1Hz lost no important dynamics.

4.2.4 Known Imperfections

For one testing condition, problems with the data acquisition buffer led to quantization of the data (Figure 4.10). This effect is clearly evident in some of the temperature measurements. Fortunately, this only slightly hinders the model validation procedure.

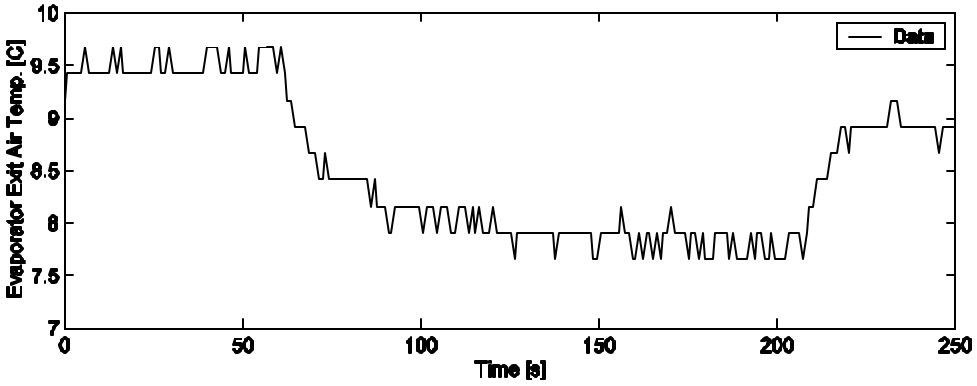

Figure 4.10 Sample Plot of Data Quantization

By coincidence, the fluid entering or exiting the internal heat exchanger for the 2nd operating condition (city driving) is very near the critical point of the fluid. This creates difficulties with the simulation, due to the increase in inaccuracy of the fluid property look-up tables near the critical point. Future work will include refining the model of the internal heat exchanger to handle this difficulty.

Due to realistic constraints on the variable speed drives and motors, the step changes in compressor speed, air flow rates, etc. are not instantaneous. This limitation is implemented in the simulations by rate limiting the input signals. Additionally, the compressor speed signal fluctuated 10-20 rpm due to noise (Figure 4.11). This fluctuation is assumed to not represent the true speed of the compressor.

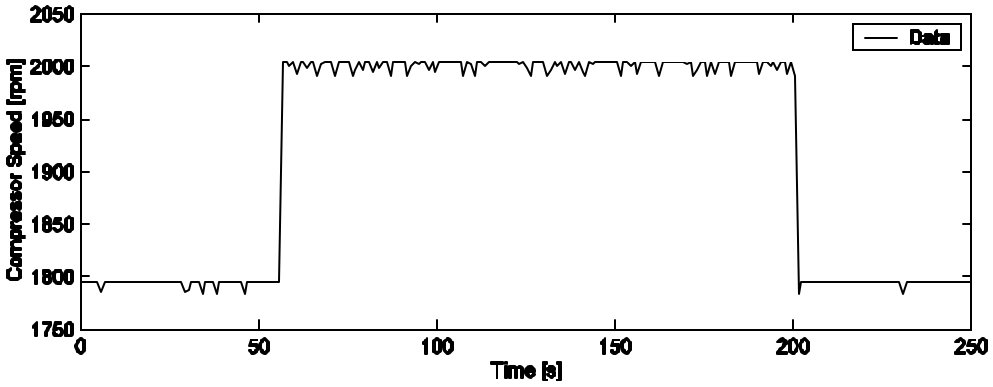

Figure 4.11 Sample Plot of Compressor Speed Signal with Noise

The recorded compressor inlet temperature is higher than the low-side internal heat exchanger exit temperature due to external bypass flow of hot oil from the crankcase to the suction line. This problem will be eliminated with future compressor models with internal oil recirculation.

The step changes in the expansion valve were implemented by hand using a variable voltage source, and thus have some variability in magnitude. However, this does not adversely affect the system identification or the model validation.

The chamber temperatures do not stay constant due to the relatively slow response of the temperature controllers and the thermal mass of chambers. Additionally, because the air is artificially heated or cooled, quick changes in the mass flow rate of air can also result in quick changes in inlet air temperature (see Chapter 5).

4.3 System Identification Procedure

4.3.1 Input/Output Selection

Before experimentation, several variables were selected as the variables of interest. These variables included possible measures of comfort or efficiency, and were defined to be the outputs of the system and included:

- Evaporator Superheat Temperature
- Evaporator Pressure
- Gas Cooler Pressure
- Evaporator Exit Air Temperature
- Gas Cooler Exit Air Temperature

The controllable inputs to the system were defined as:

- Compressor Speed
- Expansion Valve Opening
- Evaporator Air Flow Rate
- Gas Cooler Air Flow Rate

4.3.2 SISO Model Order/Structure Selection

The model structure selected was an ARMAX model. This is of the form: $A(q)y(t) = B(q)u(t) + C(q)e(t)$. This model structure is discussed in detail in [23]. For each of the possible input-output pairs, ARMAX models of orders 1 to 10 were computed. The minimum order necessary to adequately model the dynamics, while ensuring whiteness and independence of the model residuals, was selected. The specific criteria required that: 1) the assumption of independence (correlation between the model residuals and the inputs) was within a 99% confidence interval, and 2) the assumption of whiteness (cross-correlation between the residuals) is also within a 99% confidence interval. When determining the necessary model order, the data was divided. Part of the data was used for model estimation and part of the data was used for model validation. This procedure of cross-validation ensured that the models were not "over-fitted" to a specific data set. After the necessary model order was determined, the entire data set was used to estimate the final model. This process was repeated for each of the three operating conditions. Because SISO model identification is concerned only with individual input-output behavior, the models were estimated using the data sets where the controllable inputs were varied separately.

4.3.3 MIMO Model Order/Structure Selection

Two methods were used to create MIMO empirical models. The indirect method combined the aforementioned SISO models into a MIMO structure. Assuming complete independence of poles/zeros this resulted

in a 42nd order model. Because of the physical nature of the system, it is unlikely that all poles and zeros are independent. The Hankel Singular Values for the combined MIMO structure were evaluated and indicated a good choice for the minimal necessary model order. Balanced truncation model reduction techniques were used to remove redundant and unnecessary dynamic modes.

The direct method used subspace identification methods to estimate a MIMO model directly. Appropriate data to apply such an algorithm required simultaneous excitation of all inputs. Because a sufficient amount of this type of data was not taken with the original system, these tests were conducted later with a slightly modified system. All the major system components were the same, but the pipe lengths between components had been optimized and the indoor and outdoor chambers were improved. Although the resulting models may not be strictly comparable in exact detail, the data should be sufficient for achieving the primary objective of estimating the minimal model order to adequately model the system dynamics. Using this new data, empirical models were created. By evaluating the estimated model fit and the correlation errors, a minimal necessary model order was determined.

4.4 Experimental Data and System Identification Results

4.4.1 SISO System Identification Results

The minimum necessary order for each of the input-output pairs is given in Table 4.4. Identical results were obtained for each of the three operating conditions. Note that for some input-output pairs no dynamic relationship could be identified. The individual transfer functions for each of the input-output pairs for all three conditions are included in Table 4.6. Comparison between the SISO models and data is included with the comparisons of the MIMO models and is presented in Section 4.4.2.

4.4.2 Indirect MIMO System Identification Results

As mentioned earlier, two methods were used to create MIMO empirical models. The first method combined the individual SISO models into a MIMO structure. The Hankel Singular Values were then evaluated and plotted. To select the final model order, only the most significant Hankel Singular Values were considered, and low order models were chosen when the difference between sequential Hankel Singular Values was largest. When plotted on a semilog plot, a distinct difference in the values is observed to occur consistently for all three operating conditions after orders 5 and approximately 32. Because a low order model is suspected, a 5^{th} order model is selected. A Schur balanced truncation approach is then used to reduce the combined 42^{nd} order model to a 5^{th} order model. Figures 4.12 - 4.14 show all Hankel Singular Values for each of the operating conditions, as well as a closer view of only the first ten Hankel Singular Values. The resulting system eigenvalues for each of the operating conditions are given in Table 4.5.

Table 4.4 Minimum Necessary Order for Identified Input-Output Pairs

	Compressor Speed	Expansion Valve Opening	Evaporator Air Flow Rate	Gas Cooler Air Flow Rate
Evaporator Superheat	3	3	2	0
Evaporator Pressure	3	3	2	0
Gas Cooler Pressure	3	3	2	2
Evaporator Exit Air Temp.	3	3	2	0
Gas Cooler Exit Air Temp.	3	3	0	2

Table 4.5 Eigenvalues of 5th Order MIMO Models

Condition		
Idle	City	Highway
-3.392	-2.972	-1.968
-0.876	-1.023 +0.119i	-1.446
-0.504	-1.023 -0.119i	-0.502
-0.322	-0.598	-0.345
-0.019	-0.048	-0.032

Only a selection of model/data comparisons can be included here. The included results are for the highway driving condition, and can be assumed to be representative of all conditions (Figures 4.15 - 4.18). For convenience, the model predictions and experimental data are plotted with zero mean. As expected, the individual SISO models generally match well with data. The low order MIMO model, however, does show obvious discrepancies. Equation 4.1 is used as a measure of model fit, where the model variation, V_N, is calculated as the ratio of signal norms (Equation 4.2, and where $\hat{y}$ is the predicted output, y is the measured output, and $\bar{y}$ is the mean value of the measured output.

$$\%Fit = 100(1 - V_N) \tag{4.1}$$

$$V_N = \frac{\|\hat{y} - y\|_2}{\|y - \bar{y}\|_2} \tag{4.2}$$

Table 4.6 Identified SISO Transfer Functions

Input	Output	Condition 1			Condition 2			Condition 3		
		Gain	Zeros	Poles	Gain	Zeros	Poles	Gain	Zeros	Poles
Expansion Valve	Evaporator Superheat	-0.0777	2.0475	-1.2948	-0.0521	2.4932	-1.6629	-0.0373	2.4163	-0.7269
			1.8684	-0.2415		2.0469	-0.4673		2.0471	-0.2719
			-0.019	-0.0784		0.0047	-0.0875		-0.0263	-0.0896
	Evaporator Pressure	7.2037	2.1504	-0.8785	5.5413	2.18	-1.0242 + 0.1438i	1.0218	-14.1124	-1.6829 + 0.3148i
			2.0475	-0.4994		2.0469	-1.0242 - 0.1438i		2.0471	-1.6829 – 0.3148i
			-0.0238	-0.0209		-0.0478	-0.0499		2.0283	-0.3853
	Gas Cooler Pressure	-7.8117	8.5387	-3.3931	2.156	-21.258	-2.9707	-2.1558	23.1865	-1.998
			2.0475	-0.3196		2.0469	-0.5998		2.0471	-0.5095
			-0.0181	-0.017		-0.0427	-0.0474		-0.0285	-0.0326
	Evaporator Exit Air Temp.	-0.011	2.0475	-0.1119 + 0.2056i	0.0037	2.0469	-0.1160 + 0.2520i	-0.0098	2.0471	-0.1506 + 0.3067i
			0.4132	-0.1119 – 0.2056i		-0.8457	-0.1160 – 0.2520i		1.3199	-0.1506 – 0.3067i
			0.0997	-0.0565		0.11	-0.0728		0.0425	-0.0848
	Gas Cooler Exit Air Temp.	0.0536	6.1896	-234.8608	0.0063	2.0469	-0.5935	0.0084	2.0471	-0.4619
			2.0475	-0.7823		-0.0013 + 0.1094i	-0.098		0.0491 + 0.0800i	-0.1153
			-0.1265	-0.0115		-0.0013 – 0.1094i	-0.0249		0.0491 – 0.0800i	-0.0355
Compressor	Evaporator Superheat	0.0011	3.5228	-1.997	0.001	2.6024	-1.9642	0.0008	3.3082	-2.2542
			2.0456	-0.259		2.0513	-0.4632		2.0463	-0.2888
			0.003	-0.0681		0.0371	-0.0974		0.0127	-0.0514
	Evaporator Pressure	-0.0806	5.4033	-2.1626	-0.0744	3.4357	-1.5354	-0.0474	4.7698	-1.9981
			2.0456	-0.3504		2.0513	-0.834		2.0463	-0.3786
			-0.0171	-0.0191		-0.0486	-0.0524		-0.0858	-0.1077
	Gas Cooler Pressure	-0.2378	-3.6997	-3.0084	-0.0704	-10.7362	-3.1347	-0.1135	-5.3887	-2.8401
			2.0456	-0.3294		2.0513	-0.5557		2.0463	-0.4695
			-0.0241	-0.0254		-0.0661	-0.0671		-0.0712	-0.0912
	Evaporator Exit Air Temp.	0.0014	11.906	-179.54	-0.0001	2.0513	-0.0920 + 0.1889i	0.0001	106.6265	-72.0801
			2.0456	-0.08 + 0.06i		0.7191	-0.0920 – 0.1889i		2.0463	-0.2257
			0.5183	-0.08 – 0.06i		-0.168	-0.0573		0.5581	-0.1056
	Gas Cooler Exit Air Temp.	0.0002	2.0456	-0.2746 + 0.2314i	0.0001	2.0513	-0.2351 + 0.3279i	0.0002	2.0463	-0.5566 + 0.3936i
			0.979	-0.2746 – 0.2314i		1.1243	-0.2351 – 0.3279i		1.747	-0.5566 – 0.3936i
			-0.0333	-0.0134		-0.095	-0.0227		-0.0356	-0.014
Evaporator Air Flow Rate	Evaporator Superheat	0.0002	2.0429	-0.3914	0.0001	2.1938	-0.3163	0.0002	2.0509	-0.1676 + 0.0647i
			1.1092	-0.0939		2.0513	-0.1241		1.631	-0.1676 – 0.0647i
	Evaporator Pressure	-0.009	2.0429	-0.4172	-0.0044	2.0513	-0.457	-0.0303	2.0509	-0.4166
			-0.0718	-0.0254		-0.2655	-0.043		-0.0251	-0.0108
	Gas Cooler Pressure	-0.0008	2.0429	-0.5383	-0.0006	-9.1196	-0.9867	-0.0141	2.0509	-0.9152
			-1.9569	-0.0194		2.0513	-0.0357		-0.6529	-0.026
	Evaporator Exit Air Temp.	0.0003	2.0429	-0.3721	0.0003	2.0513	-0.4136	0.0002	2.6844	-0.477
			0.5927	-0.0999		0.801	-0.1155		2.0509	-0.1395
	Gas Cooler Exit Air Temp.	0	-	-	0	-	-	0	-	-
			-	-		-	-		-	-
Gas Cooler Air Flow Rate	Evaporator Superheat	0	-	-	0	-	-	0	-	-
			-	-		-	-		-	-
	Evaporator Pressure	0	-	-	0	-	-	0	-	-
			-	-		-	-		-	-
	Gas Cooler Pressure	0.0193	2.0437	-0.4565	0.0295	2.0513	-0.9774	0.0063	3.0753	-1.4937
			0.1055	-0.0145		0.0782	-0.0406		0.7601	-0.0671
	Evaporator Exit Air Temp.	0	-	-	0	-	-	0	-	-
			-	-		-	-		-	-
	Gas Cooler Exit Air Temp.	-0.0003	4.1651	-0.9881	-0.0014	2.0513	-0.7914	0.0006	3.0753	-0.589
			2.0437	-0.1648		1.9236	-0.3092		0.0032	-0.0016

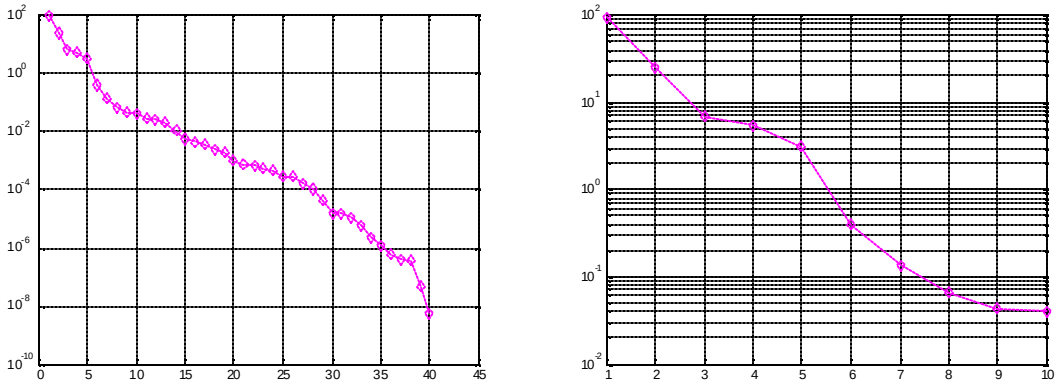

Figure 4.12 Hankel Singular Values of the Indirect MIMO Model: Idle Condition

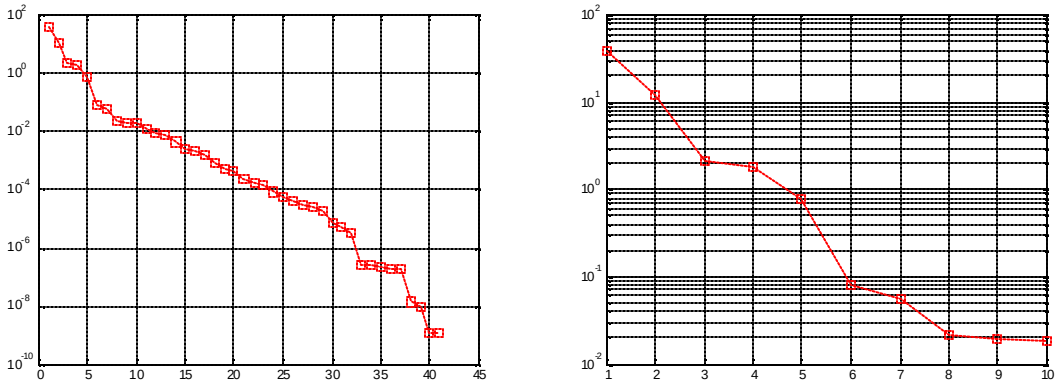

Figure 4.13 Hankel Singular Values of the Indirect MIMO Model: City Condition

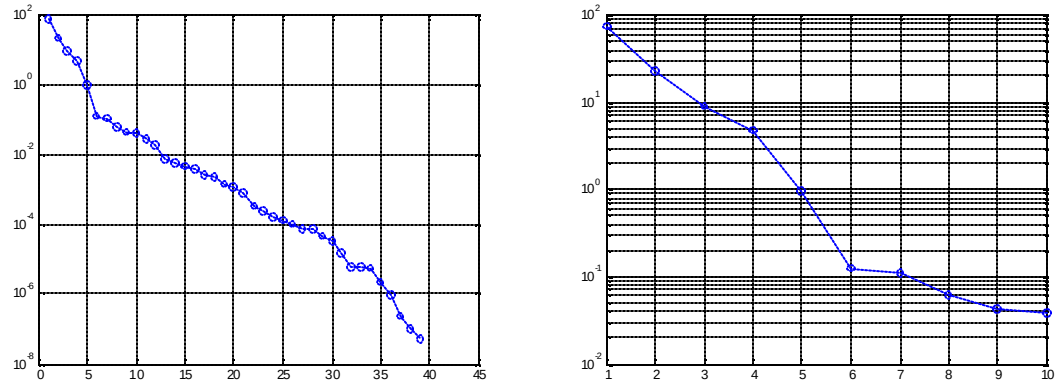

Figure 4.14 Hankel Singular Values of the Indirect MIMO Model: Highway Condition

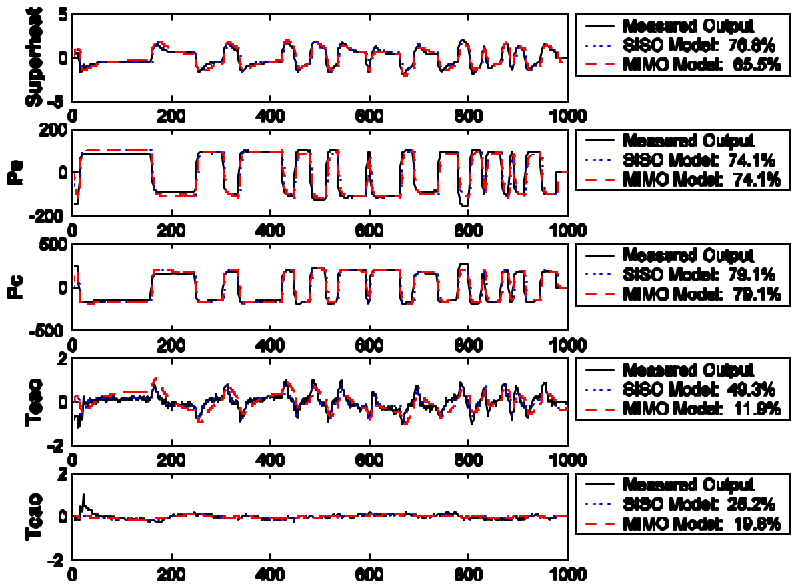

Figure 4.15 ARMAX SISO and Indirect MIMO System ID Results: Step Changes in Valve Opening

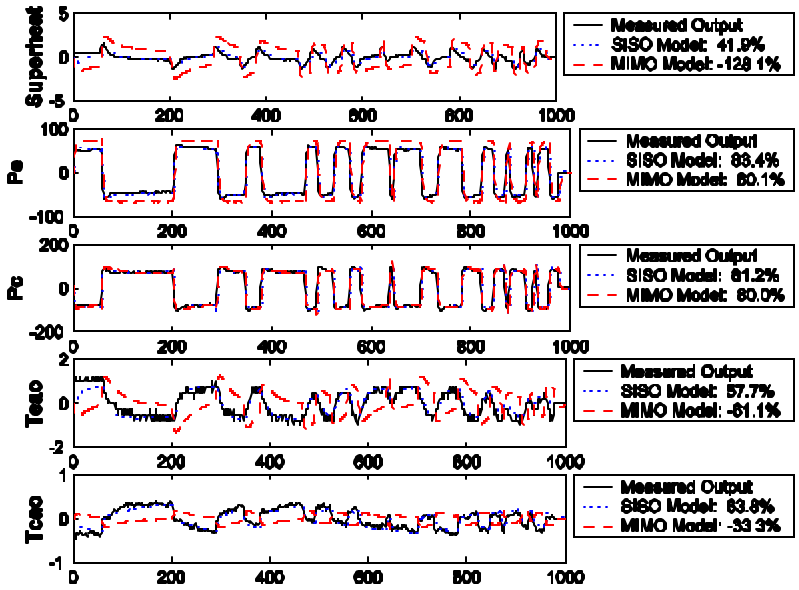

Figure 4.16 ARMAX SISO and Indirect MIMO System ID Results: Step Changes in Compressor Speed

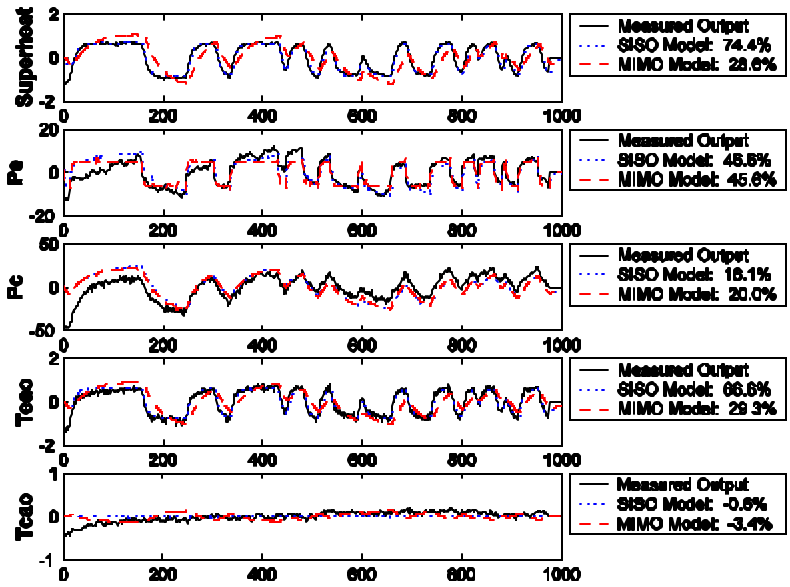

Figure 4.17 ARMAX SISO and Indirect MIMO System ID Results: Step Changes in Evaporator Air Flow Rate

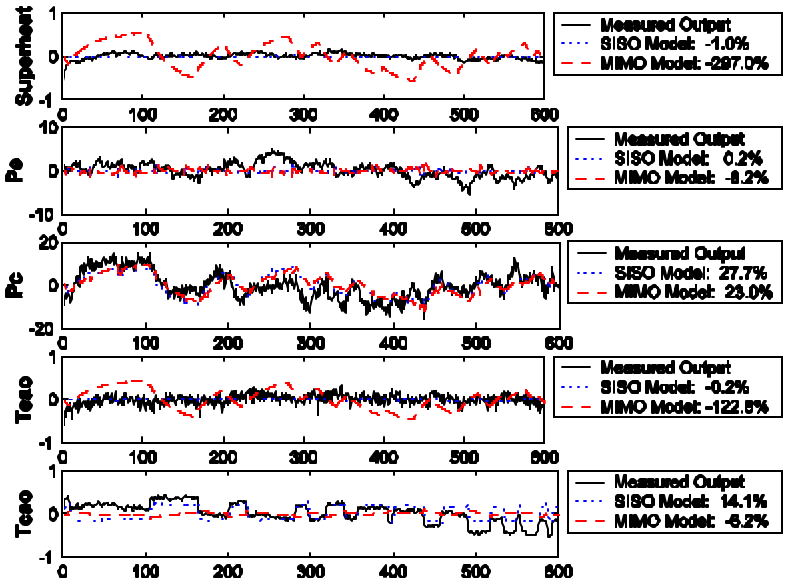

Figure 4.18 ARMAX SISO and Indirect MIMO System ID Results: Step Changes in Gas Cooler Air Flow Rate

4.4.3 Direct MIMO System Identification Results

Applying the subspace system identification methods yields improved results. Models of order 1 through 10 were estimated. As mentioned, models were estimated using this method with data where all four inputs were varied randomly and simultaneously. Again the data sets were divided into estimation and validation sets and the models were cross-validated. In the process of identification, the additional experimental tests for the highway condition were observed to include a condition where the compressor temporarily reduced displacement, and thus

changed the mass flow independently of compressor speed or valve opening. This unmodeled behavior created difficulties when estimating models for this condition. This condition will be avoided in future tests, but for this thesis only results from the idle and city driving conditions are included.

In general, models of order 1 or 2 were obviously insufficient for predicting the model outputs. Models of order 3 or 4 adequately predicted some output behavior, but the correlation errors were high (did not meet criteria for whiteness and independence of the assumed noise). Models of order 7-10 compared well against the estimated data set, but poorly against the validation set. This was viewed as an indication of overfitting the data to the estimation data set. Models of order 5 and 6 adequately predicted all outputs and had the lowest correlation errors of any of the models generated. For the idle driving condition, 5^{th} and 6^{th} order models matched equally well, and using the principle of parsimony, the 5^{th} order model was selected (Figure 4.19). For the city condition the 6^{th} order model matched the data better (Figure 4.20). This does not necessarily imply that the system order changed between conditions, but that the true minimal order of the system is probably 5^{th} or 6^{th} order.

The discrete-time identified models were converted to continuous time representations and the eigenvalues of the resulting A matrix were evaluated. The eigenvalues for the 5^{th} order model for the idle condition are given in Equation 4.3, and the eigenvalues of the 6^{th} order model for the city condition are given in Equation 4.4.

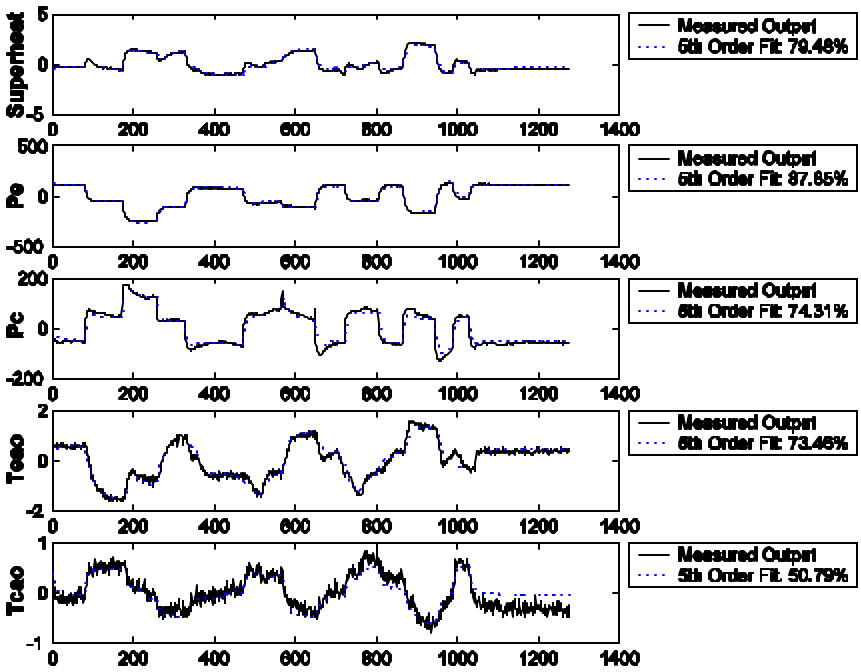

Figure 4.19 Direct MIMO System ID Results for Random Step Changes in All Inputs: Idle Condition

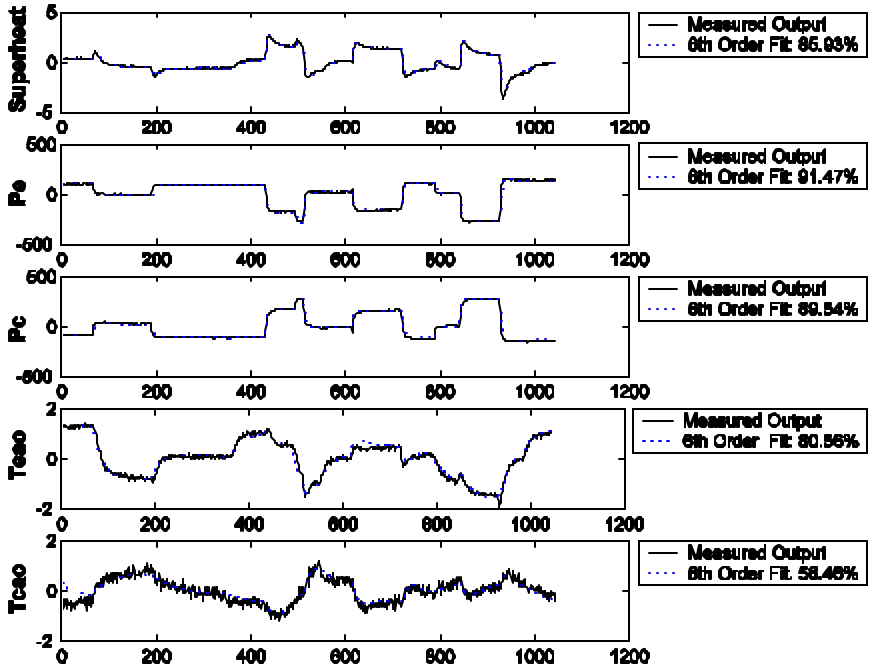

Figure 4.20 MIMO System ID Results for Random Step Changes in All Inputs: City Condition

$$l(A_{idle}) = \begin{bmatrix} -0.2386 \\ -0.1073 + 0.0693i \\ -0.1073 - 0.0693i \\ -0.0469 + 0.0038i \\ -0.0469 - 0.0038i \end{bmatrix} \tag{4.3}$$

$$l(A_{city}) = \begin{bmatrix} -1.8055 \\ -0.4067 \\ -0.1371 \\ -0.0447 + 0.0159i \\ -0.0447 - 0.0159i \\ -0.0130 \end{bmatrix} \tag{4.4}$$

4.5 Summary

The individual SISO models developed match well with data, and the resulting model residuals have been verified to be independent white noise. These models are low order. Analysis of the MIMO model created from combining the SISO models indicates a 5^{th} order model, but is less effective for developing a prediction model. Using subspace methods for creating a MIMO model also indicates a 5^{th} or 6^{th} order model, and is adequate for predicting the system dynamics.

Chapter 5. Model Validation

To ensure that the modeling approach outlined in this thesis appropriately predicts the dynamic behavior of vapor compression cycles, simulation results were compared to experimental data obtained as outlined in Chapter 4. Although the modeling approach presented in Chapter 2 is appropriate for both subcritical and transcritical cycles, the comparisons shown here are for an automotive transcritical vapor compression cycle.

The implicit assumption is made that the comparisons between simulated and experimental results for the given operating conditions are indicative of the model's predictive capability at all operating conditions allowed by the modeling assumptions. This reflects the observation that it is impossible to fully validate a model; it is merely possible to demonstrate that the model is not invalid for a given set of data.

The first section outlines the general validation procedure, and includes a description of the various parameters used in the simulation. The second section gives observations regarding the choice of parameters, and presents the initial model validation results. The final section discusses additions made to the model-based on the initial results, and presents the results of the improved model validation.

5.6 Validation Procedure

The parameters for each of the individual components are grouped in three categories: measurable, empirical, and tunable. The measurable parameters are physical characteristics of the component such as lengths, masses, diameters, etc. These were measured for each of the components and are assumed to be correct within measurement accuracy. The empirical parameters are efficiencies or other empirically determined relationships. The tunable parameters generally cannot be measured easily, but are known to be within a certain range of values and are assumed to follow commonly accepted parameter correlations.

Thus the general procedure for validating the model consists of fixing the measured and empirical parameters, and adjusting the tunable parameters within acceptable bounds so that the simulated dynamics approximate the experimentally recorded dynamics.

5.6.1 Physical Parameters

5.6.1.1 Evaporator and Gas Cooler

Hydraulic Diameter – For different types of heat exchangers (plate, tube, microchannel, etc.) this value will be calculated differently. Suggestions for calculating this value for the different types of heat exchangers are available in the literature, and are heat exchanger dependent. For the microchannel heat exchangers used in the experimental system, the microchannel port diameter was obtained from the manufacturer and verified with measurements.

Fluid Flow Length – This value is defined as the length that the fluid travels from the entrance to the exit of the heat exchanger. All possible fluid flow paths are assumed to have the same length. Many heat exchangers use a series of tubes or plates arranged in a serpentine manner for fluid flow. Often these tubes or plates will join at a "header" and the fluid is redistributed before entering the next "pass" or series of or tubes or plates.

Cross-sectional Area – This value can be calculated using the hydraulic diameter. For most heat exchangers the cross-sectional area is not constant. The number of tubes or plates per pass generally increases as the fluid evaporates or decreases as the fluid condensates, thus changing the cross-sectional area. For the purposes of

modeling a constant cross-sectional area is assumed. If the cross-sectional area is calculated from the hydraulic diameter, then it does not take into account headers, distributors, etc.

Internal Volume – This value can either be calculated as the product of cross-sectional area and fluid flow length or be measured experimentally. The former does not account for headers, entrance pipes, etc. and is considered to be the lower bound. The latter includes all these "extra" volumes and is considered to be the upper bound. Thus this parameter can be tuned within these bounds.

Internal Surface Area – This parameter is calculated from the hydraulic diameter.

External Surface Area – This parameter is either calculated from the known fin geometry, or obtained from the manufacturer.

Mass – This parameter is easily obtained from the manufacturer or measured. Because the header pipes do not play a critical role in heat transfer, the mass of these may be included or neglected.

Specific Heat – The value of this parameter is easily obtained from a standard heat transfer textbook with knowledge of the heat exchanger material.

5.6.1.2 Compressor

Displacement – The displacement of the compressor is generally available from the manufacturer.

5.6.1.3 Expansion Valve

Area of Opening – This value is generally available from the manufacturer.

5.6.1.4 Internal Heat Exchanger

Internal Volume of Hot/Cold Side – This value is generally available from the manufacturer.

Mass – This parameter is easily obtained from the manufacturer or measured. Because the header pipes do not play a critical role in heat transfer, the mass of these may be included or neglected.

Specific Heat – The value of this parameter is easily obtained from a standard heat transfer textbook with knowledge of the heat exchanger material.

5.6.2 Empirical Parameters

5.6.2.1 Evaporator and Gas Cooler

Mean Void Fraction – Many correlations are available as outlined in Chapter 1. For these simulations, a general slip ratio correlation is assumed.

Single-Phase Flow Heat Transfer Coefficient – This value can be estimated using an empirical correlation chosen by the user. For these simulations, the Dittus-Boelter correlation [18] was used.

5.6.2.2 Compressor

Isentropic Efficiency – This value can be estimated using experimental steady state data, or obtained from the manufacturer.

Volumetric Efficiency – This value can be estimated using experimental steady state data, or obtained from the manufacturer.

Rate Limit – Actual compressors are rate-limited in their ability to change speed. This value can be measured from data.

5.6.2.3 Expansion Valve

Control Input Relationship – The control input is related to the valve opening assuming a linear relationship. The empirical parameters for this equation can be determined using experimental data.

Discharge Coefficient – This value can be estimated using experimental steady state data, or obtained from the manufacturer.

Rate Limit – Actual expansion valves are rate-limited in their ability to change the valve opening. This value can be measured from data.

5.6.2.4 Internal Heat Exchanger

Lumped Heat Transfer Coefficient – This value can be estimated using experimental steady state data.

5.6.2.5 Pipe Losses

Between components there are both momentum losses associated with friction, as well as thermal losses/gains due to heat transfer to the environment. Both of these types of losses change during a transient response. From the Darcy-Weisbech equation [39] assuming horizontal pipe lengths, the momentum losses are given as $\frac{\Delta P}{rg} = f\frac{L}{d}\frac{V^2}{2g}$.

Using this equation a semi-empirical relationship can be obtained for modeling the pressure losses between components. However, a simple alternative is available. The use of pressure loss equations is to ensure the correct prediction of pressure at the inlet and outlet of the compressor and expansion valve, so that the calculated mass flow rates will be accurate. Instead of using the measured values of pressure at the compressor and expansion valve inlets and outlets to determine the empirical parameters used in the mass flow rate equations, the measured pressures of the gas cooler and evaporator are used. Thus the mass flow rate equations are adjusted to predict the correct mass flow rate using the pressures before they are adjusted with pressure drop correlations. The pressure drop correlations are effectively lumped into the empirical parameters for the mass flow rate equations.

The thermal losses/gains due to heat transfer to the environment are considered constant for the initial model validation. These dynamics will be included as part of the improved model validation.

5.6.3 Tunable Parameters

5.6.3.1 Evaporator

Void Fraction Slip Ratio – Slip ratio is defined as the ratio of the velocities of the vapor and liquid phases in a two-phase flow. The generally accepted bounds on this parameter are given by the homogeneous correlation and the Zivi correlation. The homogeneous correlation assumes a slip ratio of unity, $S = 1$, and the Zivi correlation gives the slip ratio as $S = \left(r_f / r_g\right)^{1/3}$. At the time of writing of this thesis, there was no known published data on measured void fraction for transcritical fluids. Therefore, they are assumed to behave similarly to the more commonly studied fluids. Because these correlations are not verifiable for carbon dioxide, the upper bound is not a hard bound, but a guideline to be considered when tuning this parameter.

Two-Phase Flow Heat Transfer Coefficient – For transcritical cycles, this parameter has been measured in [28] to be from 3 to 22 kW/(m^{2}K) depending on the quality of the fluid and the operating condition. Therefore the average heat transfer coefficient in the two-phase region could justifiably be chosen within this range.

5.7 Initial Model Validation

The final choice of most parameters is straightforward. The values used in the simulation are shown in Table 5.7. The effective cross-sectional area was originally calculated using the hydraulic diameter. However, the transient response of pressure was observed to be too fast, indicating that the volume was underestimated. Measured values for volume confirmed this conclusion. While the entrance/exit pipe length could have been included, this was found to be unnecessary. The selected value for cross-sectional area was calculated using the measured internal volume of the heat exchanger divided by the length of fluid flow. The value for the lumped two-phase flow heat transfer coefficient was selected as 4 $kW/(m^2K)$. This choice is consistent with experimental studies [28] and results in the appropriate transient behavior. The value for slip ratio was chosen by the Zivi correlation. Although higher values of slip ratio resulted in a better response for evaporator superheat, the lack of justifying research in the area of void fraction for carbon dioxide prevents the use of values higher than commonly accepted norms. The empirical relationships for mass flow through the compressor and expansion valve were developed using steady state data. However, since the transient response of pressure is largely a function of the time integral of net mass flow entering the heat exchanger, some tuning of these equations was required after including them in the simulation.

Recall from Chapter 4 that the experimental data consisted of a PRBS applied to the available inputs of compressor speed, expansion valve opening, evaporator air flow rate, and gas cooler air flow rate. For model validation the outputs of evaporator pressure, gas cooler pressure, evaporator superheat, evaporator exit air temperature, and gas cooler exit air temperature are compared. Mass flow rate is not compared because the mass flow rate sensor has significant dynamic filtering built into the measurement. For each transient response, the mass flow rate was verified to match at the steady state, but is not included because the sensor dynamics result in a transient response that is misleading. The model was compared to the experimental data taken and each of the three operating conditions. Only the results for the 3^{rd} operating condition (highway condition) are included here. For all results, the scale of the output variable is important when making comparisons and evaluating the validity of the model. Some of the resulting transients do not appear to agree, unless they are viewed in the proper context.

Table 5.7 Parameter Values for Model Validation

Component	Parameter	Units	Value	Comment
Evaporator	Mass	[kg]	2.458	Measured
	Specific Heat	[kJ/kg/K]	0.879	Aluminum
	Hydraulic Diameter	[m]	1.092E-03	From Manufacturer
	Internal Volume	[m^3]	3.275E-04	Measured
	Cross-Sectional Area	[m^2]	1.433E-04	Calculated from Internal Volume
	Internal Surface Area	[m^2]	0.800	Calculated from Hydraulic Diameter
	External Surface Area	[m^2]	4.458	From Manufacturer
	Fluid Flow Length per Pass	[m]	1.000	Measured
	Average Number of Micrchannel Plates per Pass	[-]	1.500	Measured
	Average Number of Passes	[-]	2.285	Measured
	Number of Parallel Paths	[-]	4	Measured
	Number of Micrchannel Ports per Plate	[-]	17	From Manufacturer
	Total Fluid Flow Length	[m]	2.285	Calculated
	Total Number of Fluid Flow Paths	[-]	102	Calculated
	Two-phase Flow Heat Transfer Coefficient	[kW/m^2/K]	4	Tuned Parameter
	Superheat Flow Heat Transfer Coefficient	[kW/m^2/K]	1.933	Calculated from Dittus-Boelter Equation
	Exterior Fluid Heat Transfer Coefficient	[kW/m^2/K]	0.0464	Calculated from data
	Exterior Fluid Specific Heat	[kJ/kg/K]	1.007	Air
	Slip Ratio	[-]	2.13	Zivi Correlation
Gas Cooler	Mass	[kg]	3.280	Measured
	Specific Heat	[kJ/kg/K]	0.879	Aluminum
	Hydraulic Diameter	[m]	6.350E-04	From Manufacturer
	Internal Volume	[m^3]	1.800E-04	Measured
	Cross-Sectional Area	[m^2]	1.651E-04	Calculated from Internal Volume
	Internal Surface Area	[m^2]	0.565	Calculated from Hydraulic Diameter
	External Surface Area	[m^2]	7.090	From Manufacturer
	Fluid Flow Length per Pass	[m]	1.090	Measured
	Average Number of Micrchannel Plates per Pass	[-]	65	Measured
	Average Number of Passes	[-]	1	Measured
	Number of Parallel Paths	[-]	1	Measured
	Number of Micrchannel Ports per Plate	[-]	4	From Manufacturer
	Total Fluid Flow Length	[m]	1.090	Calculated
	Total Number of Fluid Flow Paths	[-]	260	Calculated
	Supercritical Flow Heat Transfer Coefficient	[kW/m^2/K]	2.592	Calculated from Dittus-Boelter Equation
	Exterior Fluid Heat Transfer Coefficient	[kW/m^2/K]	0.042	Calculated from data
	Exterior Fluid Specific Heat	[kJ/kg/K]	1.007	Air
Internal Heat Exchanger	Mass	[kg]	0.865	Measured
	Specific Heat	[kJ/kg/K]	0.879	Aluminum
	Internal Volume (Hot Side)	[m^3]	1.260E-05	Measured
	Internal Volume (Cold Side)	[m^3]	2.202E-05	Measured
	Lumped Heat Transfer Coefficient	[kW/K]	0.0935	Calculated from data
Compressor	Compressor Displacement	[m^3]	5.000E-07	From Manufacturer
	Empirical Parameter: Ck	[-]	-0.0254	Calculated from data
	Empirical Parameter: Dk	[-]	0.117	Calculated from data
	Empirical Parameter: n	[-]	1.25	Calculated from data
	Empirical Parameter: Ak	[-]	-0.0357	Calculated from data
	Empirical Parameter: Bk	[-]	0.9227	Calculated from data
	Rate Limit	[rpm/s]	50	Calculated from data
Expansion Valve	Empirical Parameter: Kv #1	[-]	2.112E-05	Calculated from data
	Empirical Parameter: Kv #2	[-]	5.550E-02	Calculated from data
	Empirical Parameter: Kv #3	[-]	-6.906E-07	Calculated from data
	Empirical Parameter: n	[-]	0.5	Calculated from data
	Rate Limit	[V/s]	1	Calculated from data

Figures 5.21 - 5.26 show the model outputs for changes in compressor speed. For all the model outputs there is general agreement, but also notable discrepancies. For evaporator pressure the model agrees in the speed of the response and the steady state gain. However, a 2nd order effect is visible in the data, but absent in the model. For gas cooler pressure the speed of the response and the steady state gain also match within acceptable tolerances. There is an obvious discrepancy as the peak response of the model is larger and more pronounced than the data. For evaporator superheat, the general shape of the transient is correct, but the peak and steady state magnitudes are incorrect, as well as the speed of the response. The evaporator exit air temperature appears to match well. The exit air temperature for the gas cooler matches well, except for a constant steady state offset. This offset is due to a small

inaccuracy in calculating the initial conditions of the gas cooler. The total heat transfer from the gas cooler can be calculated from 1) the measured mass flow rate of air, and the inlet and exit air temperatures, or 2) the mass flow rate of refrigerant, and the inlet and exit fluid enthalpies (calculated from measured pressures and temperatures). Both of these methods are approximately equal at the steady state. In calculating the initial conditions, the system is forced to match the measured refrigerant conditions rather than the air conditions. However, the assumption of uniform pressure in the gas cooler skews the enthalpy calculations slightly, and thus the energy calculations. Thus the calculation of the gas cooler exit temperature is slightly higher than measured for all simulations.

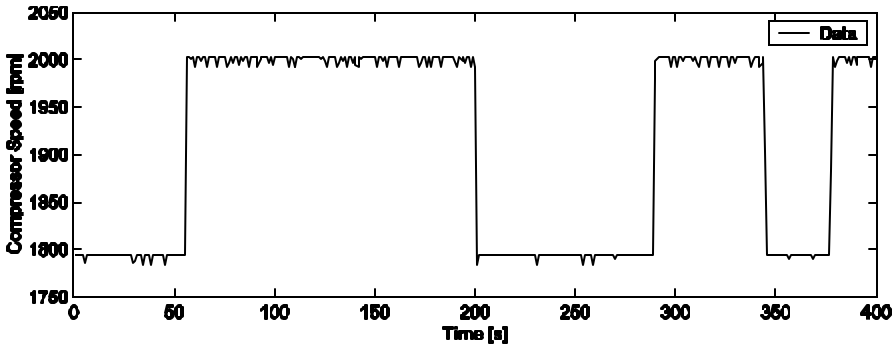

Figure 5.21 Model Validation: Compressor Speed Step Changes

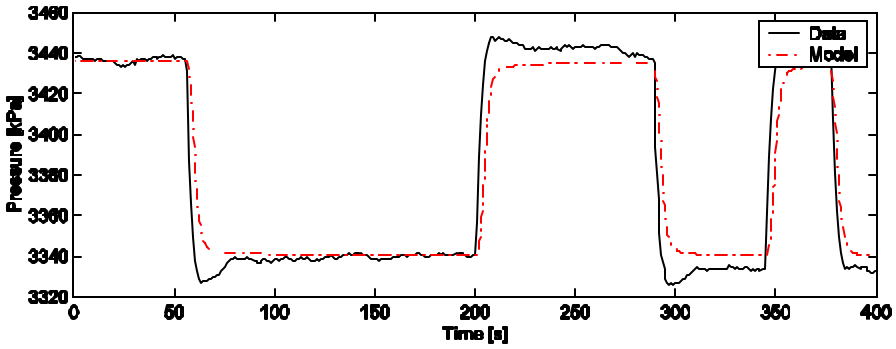

Figure 5.22 Model Validation: Evaporator Pressure for Step Changes in Compressor Speed

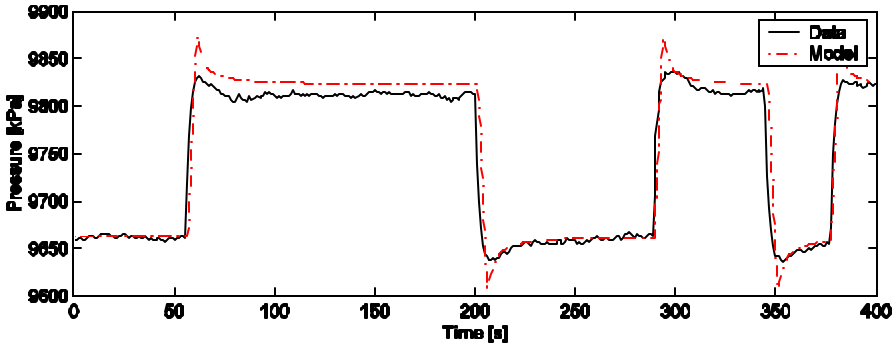

Figure 5.23 Model Validation: Gas Cooler Pressure for Step Changes in Compressor Speed

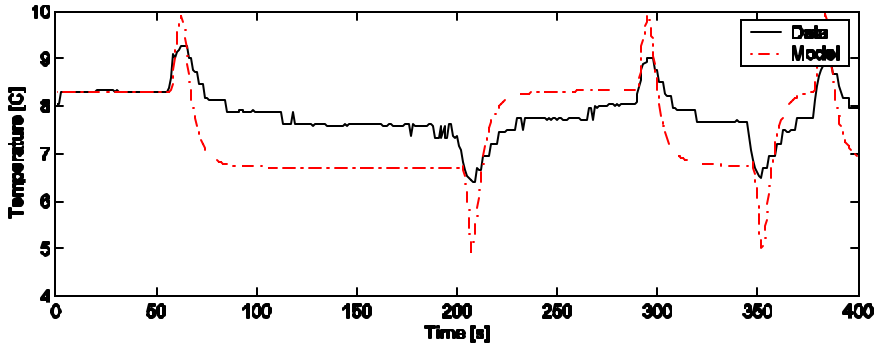

Figure 5.24 Model Validation: Evaporator Superheat for Step Changes in Compressor Speed

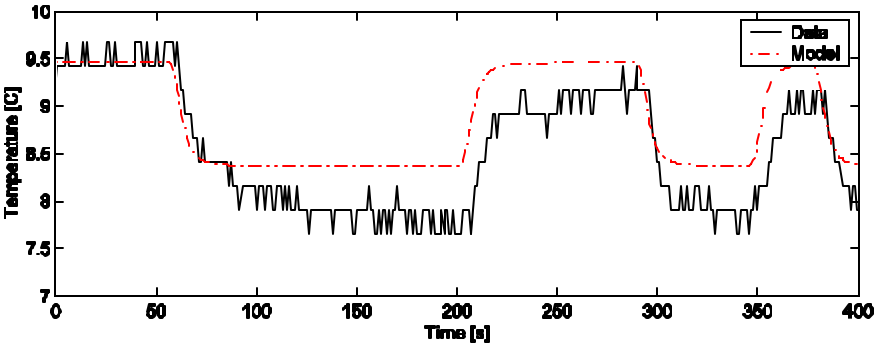

Figure 5.25 Model Validation: Evaporator Exit Air Temperature for Step Changes in Compressor Speed

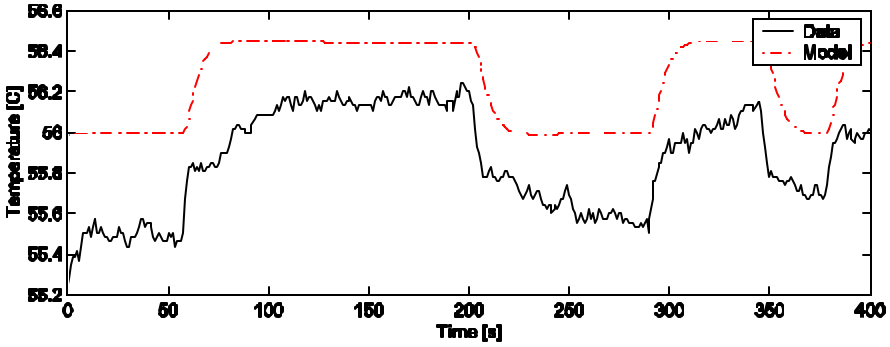

Figure 5.26 Model Validation: Gas Cooler Exit Air Temperature for Step Changes in Compressor Speed

Figures 5.29 - 5.34 show the model outputs for changes in expansion valve opening. Evaporator pressure matches well except for a small error in the gain. Gas cooler pressure also matches well except for a small offset and an initial peak response that is not present in the data. Evaporator superheat, evaporator exit air temperature, and gas cooler exit air temperature all predict poorly. The reason for this is evident upon closer evaluation of the experimental data. As the valve is opened, a surge of refrigerant enters the evaporator. This has two effects: first, the increase in net mass flow into the evaporator builds pressure, and second, the surge of mass flow increases the length of two-phase flow. As the pressure builds, the saturation temperature rises, and the difference in temperatures between the refrigerant and the heat exchanger wall (and air) decreases. This decrease contributes to less heat transfer. However, because the two-phase flow refrigerant has a higher heat transfer coefficient than the superheated refrigerant, the increase in two-phase flow length results in more heat transfer. Whether the bulk

temperature of the heat exchanger wall (and air) initially increases or decreases depends on which of these two effects dominates. In the experimental data, the exit air temperature from the evaporator initially decreases sharply and then increases. However, in simulation the rise in pressure, and thus refrigerant temperature, appears to dominate, and thus the exit air temperature simply increases. Experience has shown that by changing the simulation parameters the initial decrease can be captured, but not to the extent exhibited by the data.

The reason for the drastic initial decrease in exit air temperature is evident upon closer evaluation of the refrigerant and wall temperatures recorded in data. In Figure 5.27 these temperatures are shown. Note that the exit air temperature would appear to follow the exit refrigerant temperature. Upon closer examination (Figure 5.28), the data clearly shows that the exit air temperature actually decreases before the exit refrigerant temperature. This is an indication of the problem of maldistribution in the evaporator. Because the evaporator has four parallel paths, a distributor is used to allocate equal amounts of fluid flow to each of the four paths. However, if the distribution of fluid between the four paths is unequal, the evaporator will perform poorly. The evaporator used was known to have problems with maldistribution.

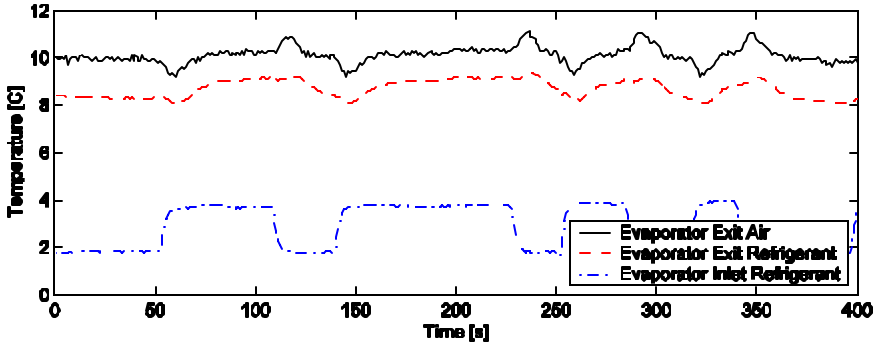

Figure 5.27 Evaporator Temperatures for Step Changes in Expansion Valve Opening

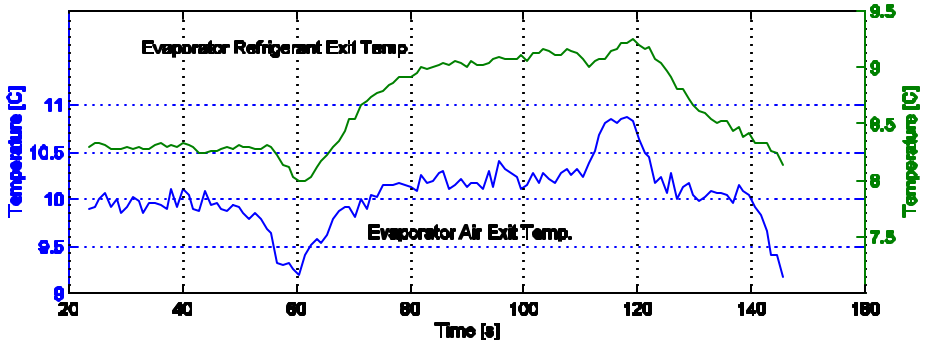

Figure 5.28 Evaporator Temperatures for Step Changes in Expansion Valve Opening (Close View)

During the transient tests, the number of temperature measurements was limited, the evaporator refrigerant outlet temperature is only measured at one of the four parallel paths. The decrease in exit air temperature before the decrease in refrigerant outlet temperature is evidence that when the valve was opened, the surge of mass flow almost instantaneously changed the distribution of fluid flow. Evaporator paths that previously were receiving very little liquid fluid flow suddenly received much more, rapidly cooling the heat exchanger walls and the exit air. Note that the data and simulation are similar excepting the initial drop in temperature.

This sudden decrease also explains the discrepancy in evaporator superheat temperature. Both data and model have the same transient shape, except that for data the steady state gain for an increase in superheat is negative, while the steady state gain for the model is positive. For this to happen in simulation requires that the heat transfer coefficient for the air side be greater than that for the refrigerant side. Since this is not physically feasible, the logical conclusion is that this is caused by an increase in heat transfer due to a suddenly improved refrigerant distribution.

The seeming discrepancy between the model and data for gas cooler exit air temperature can also be simply explained. Note that the magnitude of the change in temperature for data is a tenth of a degree and the relative signal to noise ratio is small. Although the predicted transient response is clear for the noise-free simulation, the magnitude of this change is also small, and no conclusion can be made whether data and model do or do not agree.

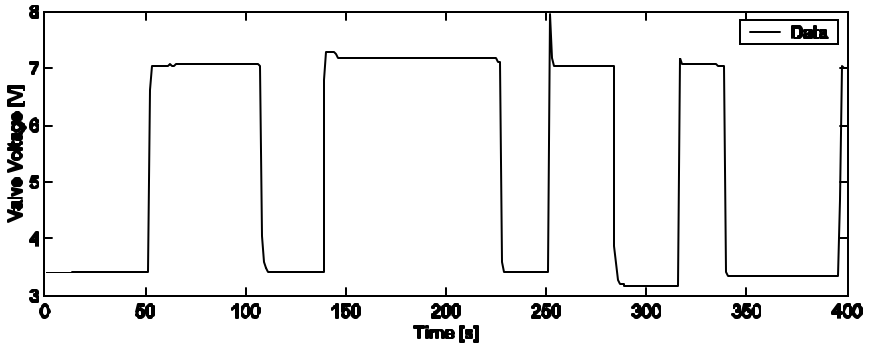

Figure 5.29 Model Validation: Expansion Valve Opening Step Changes

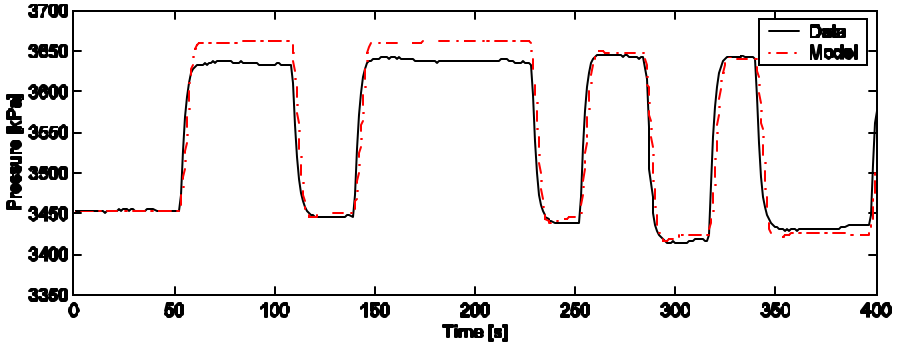

Figure 5.30 Model Validation: Evaporator Pressure for Step Changes in Expansion Valve Opening

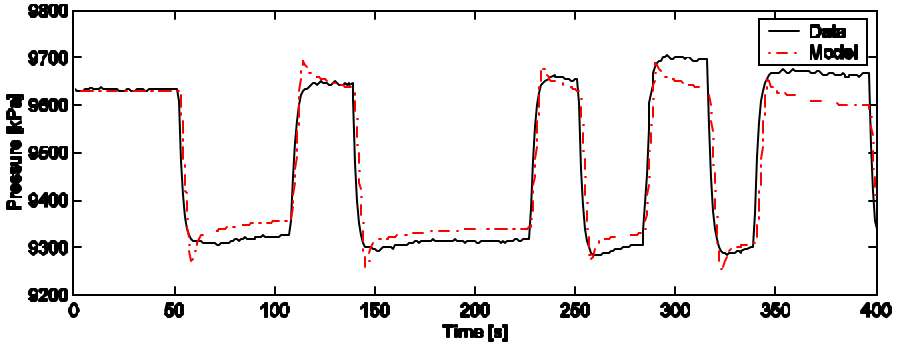

Figure 5.31 Model Validation: Gas Cooler Pressure for Step Changes in Expansion Valve Opening

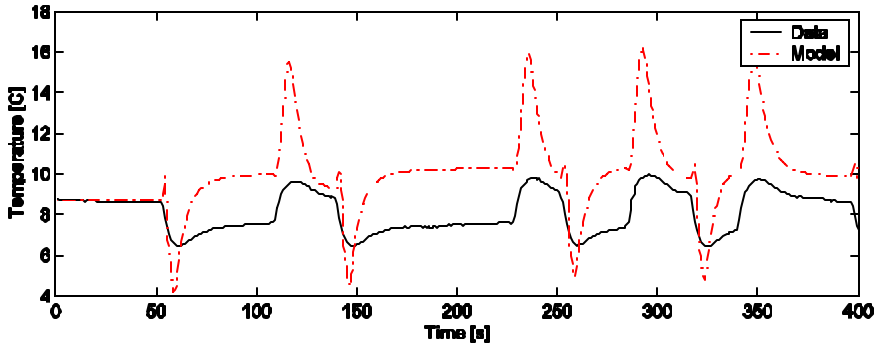

Figure 5.32 Model Validation: Evaporator Superheat for Step Changes in Expansion Valve Opening

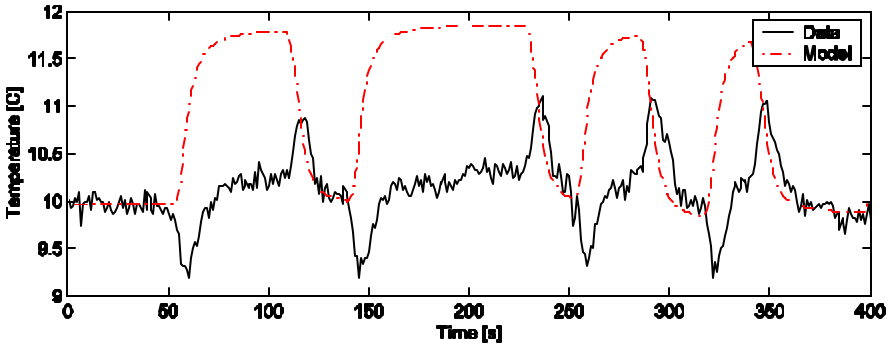

Figure 5.33 Model Validation: Evaporator Exit Air Temperature for Step Changes in Expansion Valve Opening

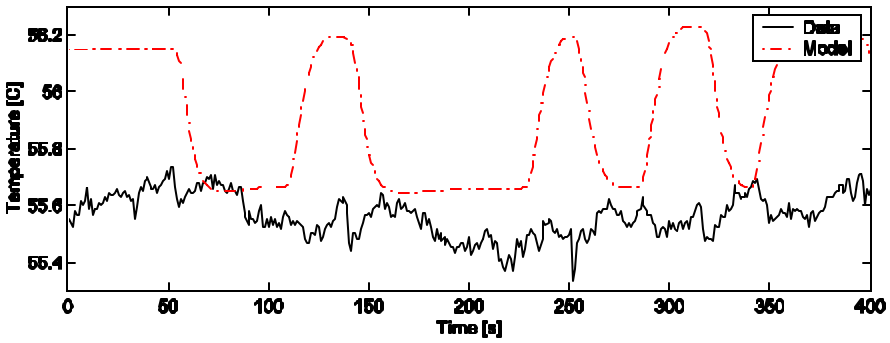

Figure 5.34 Model Validation: Gas Cooler Exit Air Temperature for Step Changes in Expansion Valve Opening

Figures 5.35 - 5.40 show the model outputs for changes in evaporator air flow rate. Model prediction and data match well for evaporator and gas cooler pressure in shape and response time, but with incorrect gain for the gas cooler pressure. Evaporator superheat matches extremely well. The model prediction for evaporator exit air temperature responds too quickly, but matches the steady state gain. Again, the responses for gas cooler exit air temperature are too small to make a definite conclusion.

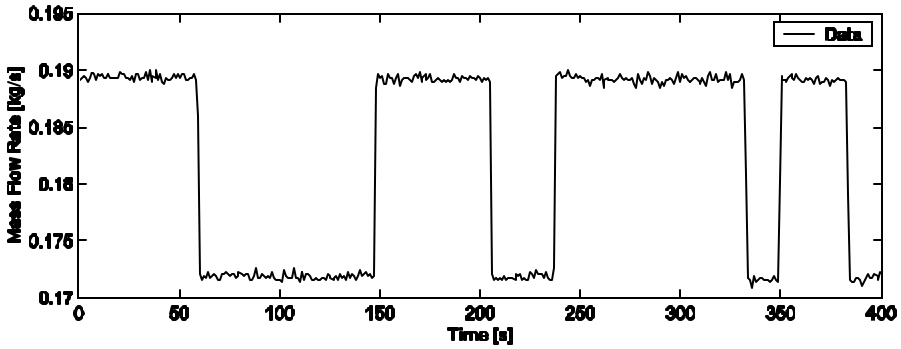

Figure 5.35 Model Validation: Evaporator Air Mass Flow Rate Step Changes

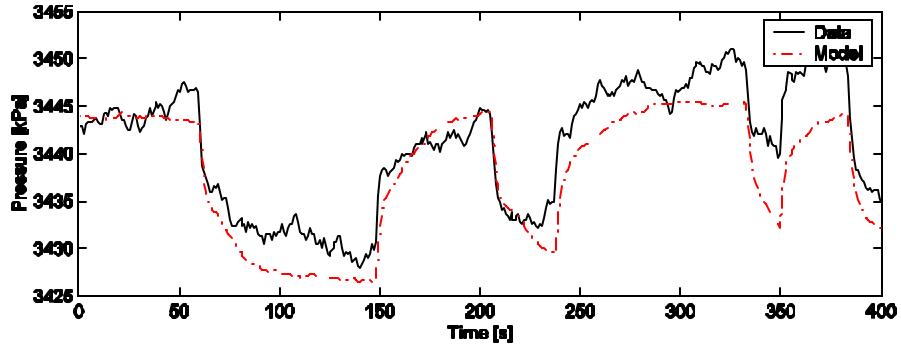

Figure 5.36 Model Validation: Evaporator Pressure for Step Changes in Evaporator Air Mass Flow Rate

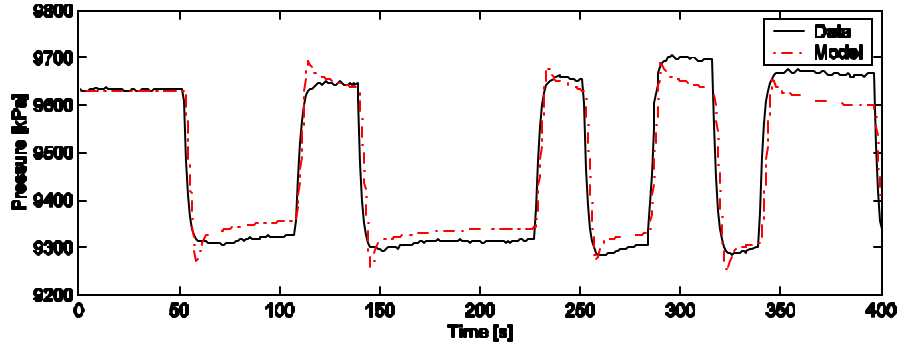

Figure 5.37 Model Validation: Gas Cooler Pressure for Step Changes in Evaporator Air Mass Flow Rate

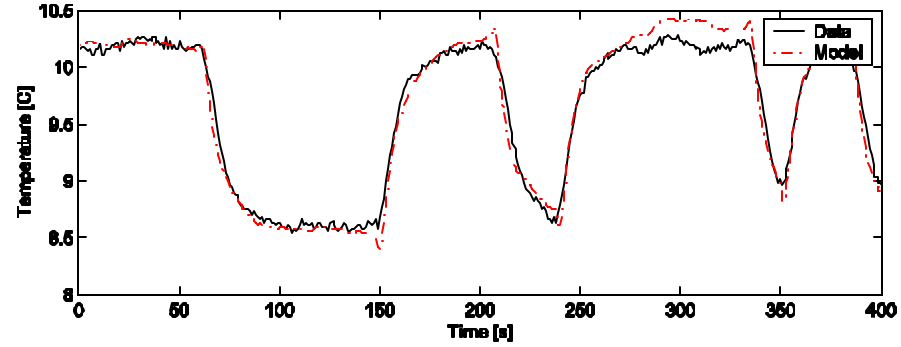

Figure 5.38 Model Validation: Evaporator Superheat for Step Changes in Evaporator Air Mass Flow Rate

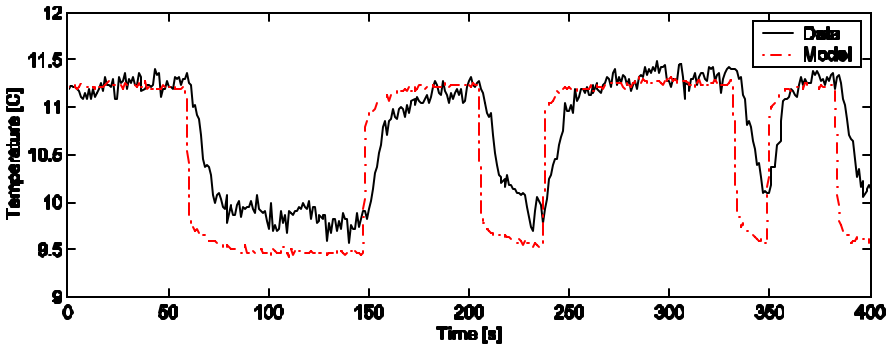

Figure 5.39 Model Validation: Evaporator Exit Air Temperature for Step Changes in Evaporator Air Mass Flow Rate

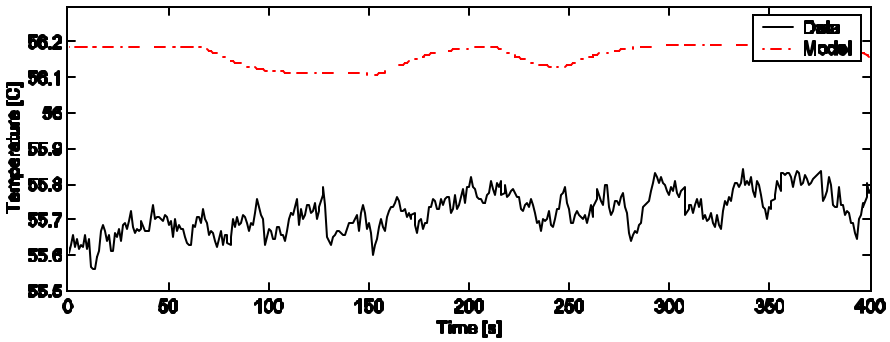

Figure 5.40 Model Validation: Gas Cooler Exit Air Temperature for Step Changes in Evaporator Air Mass Flow Rate

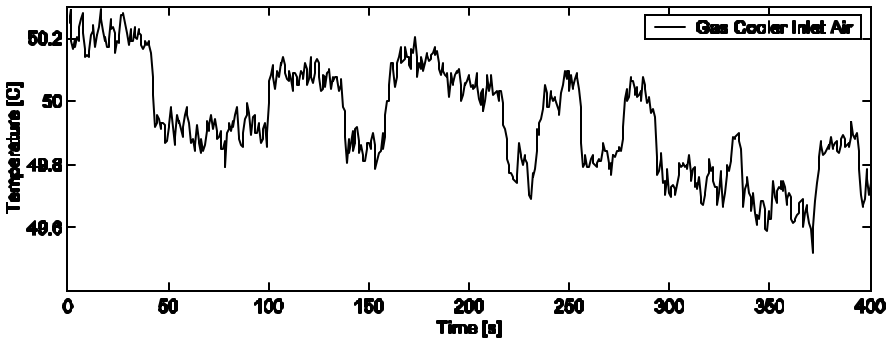

Figure 5.41 Gas Cooler Inlet Air Temperature for Step Changes in Gas Cooler Air Mass Flow Rate

Figures 5.42 - 5.47 show the model outputs for changes in gas cooler air mass flow rate. The transient responses for evaporator pressure, superheat and exit air temperature are without discernable dynamics and too small in magnitude to draw a conclusion. The responses for gas cooler exit air temperature match well excepting the constant offset. The model prediction for gas cooler pressure has small but discernable dynamics. The model predictions, however, are too small to compare. This can be explained by the experimental setup. The air that exits the gas cooler is recirculated through a glycol chiller before passing over the gas cooler again. When the mass flow rate of air is decreased suddenly, both the gas cooler and chiller are operating with the same capacity for heat transfer. Thus the exit air from the gas cooler becomes hotter, but the air entering the gas cooler becomes colder (Figure 5.41), and the net change in heat transfer is very small.

In the data the total heat being transferred from the gas cooler decreases slightly, explaining the small decrease in gas cooler pressure. However, in simulation the combined change of decreased mass flow rate of air and decreased inlet air temperature balance such that the pressure remains virtually constant.

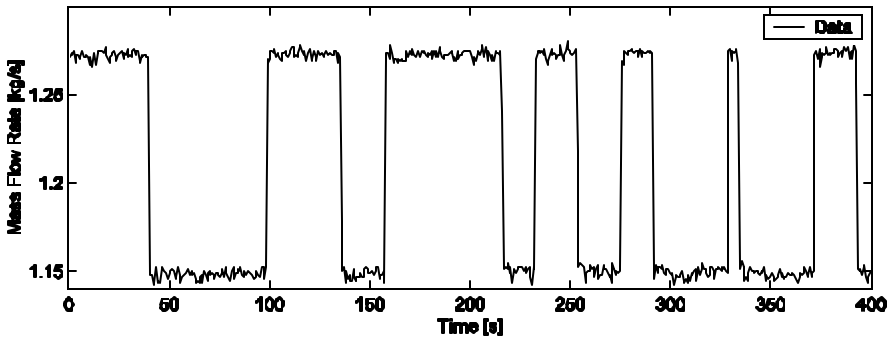

Figure 5.42 Model Validation: Gas Cooler Air Mass Flow Rate Step Changes

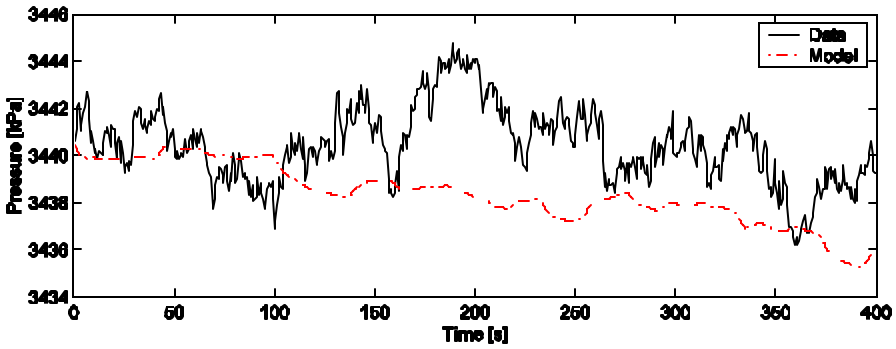

Figure 5.43 Model Validation: Evaporator Pressure for Step Changes in Gas Cooler Air Mass Flow Rate

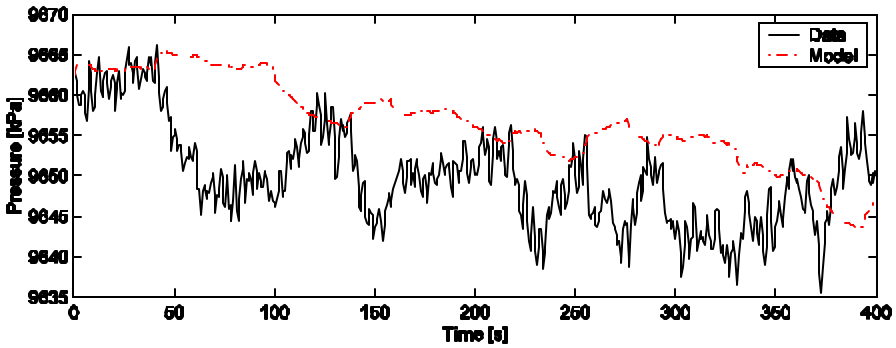

Figure 5.44 Model Validation: Gas Cooler Pressure for Step Changes in Gas Cooler Air Mass Flow Rate

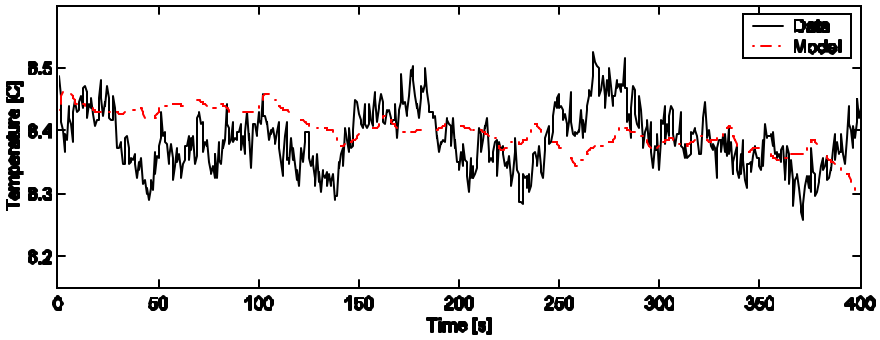

Figure 5.45 Model Validation: Evaporator Superheat for Step Changes in Gas Cooler Air Mass Flow Rate

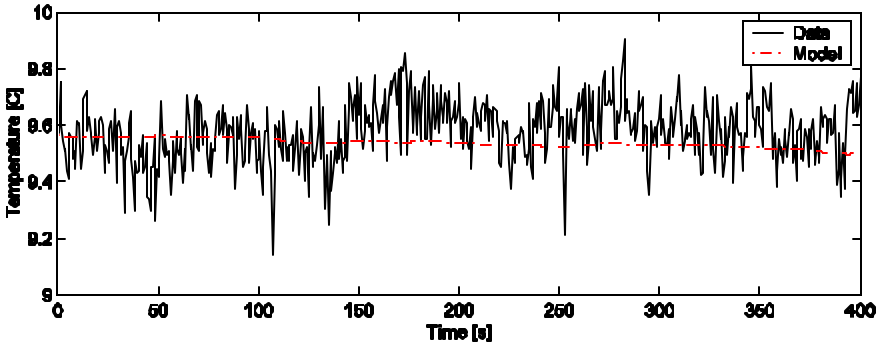

Figure 5.46 Model Validation: Evaporator Exit Air Temperature for Step Changes in Gas Cooler Air Mass Flow Rate

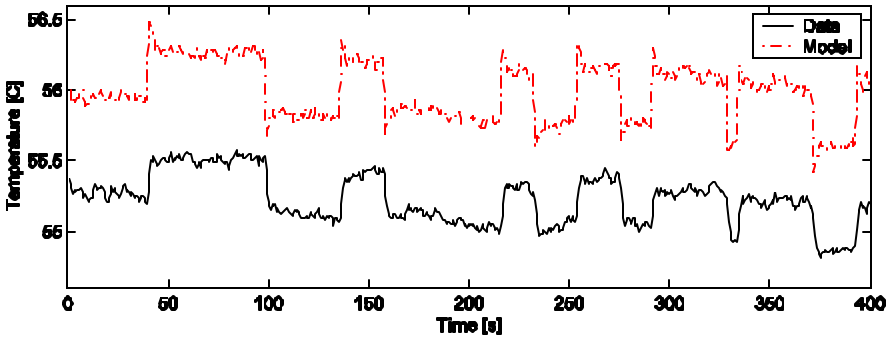

Figure 5.47 Model Validation: Gas Cooler Exit Air Temperature for Step Changes in Gas Cooler Air Mass Flow Rate

5.7.1 Observations

Some general observations need to be made regarding the model validation process. Most of the parameters required by the model are known values. Experience has shown that the transient response of the system was relatively insensitive to changes in most parameters. In general, a change of a factor of two or more in the value of any of the physical parameters was necessary to produce a noticeable difference in the transient response. For the control engineer this property of being robust to parameter changes is a desirable quality.

Moderate changes in other parameters, however, did result in different transient responses. Specifically, the choice of the two-phase flow heat transfer coefficient in the evaporator changed the shape and magnitude of the output responses. This effect is due, in part, to how the choice of this parameter affects the calculated initial

conditions of the system. Having calculated the amount of heat being transferred from the evaporator, and given the refrigerant side heat transfer coefficients, four equations are solved simultaneously for the external fluid heat transfer coefficient, length of two-phase flow, and the lumped wall temperatures of the two-phase and superheat regions. Different values for the two-phase flow heat transfer coefficient will result in a different initial value for the length of two-phase flow, which affects the dynamic response considerably. The choice of slip ratio also affects the transient response notably. The value for slip ratio determines the value of the void fraction, and thus the amount of liquid and vapor refrigerant. A larger slip ratio results in a smaller void fraction and more liquid mass in the evaporator. The amount of refrigerant mass inventory in the evaporator appears to affect the transient response much more than the values of the physical geometry of the heat exchanger.

The model is also extremely sensitive to the algebraic relationships for mass flow as given for the compressor and expansion valve. The principle dynamics of the system appear to be caused by the redistribution of mass inventory, and the unsteady state differences between inlet and outlet mass flow rate into the heat exchangers. The simplified dynamic model does not include some of the small, fast transient behavior that would dampen and stabilize the system. Like many nonlinear dynamic systems, a vapor compression cycle seems to have both slow and fast dynamic manifolds. The slow dynamic manifolds are determined by the dominant system dynamics. The fast dynamic manifolds that force the dynamic system to remain on the slow dynamic manifold in the physical system are neglected in the model for simplicity. This simplicity comes at the price of being sensitive to small changes in mass flow.

5.8 Improved Model Validation

5.8.1 Model Additions

5.8.1.1 Inter-Component Dynamics

The initial model assumed that the fluid exiting a component immediately enters the next component, and that transport delays, pipe chamber dynamics, etc. were negligible. However, the experimental data shows that dynamics are present in the pipe connections between components.

Figure 5.48 shows that the fluid entering the gas cooler has a constant offset demonstrating heat transfer losses from the pipe, as well as a 1^{st} order filtering effect. Using identification techniques, assuming that the compressor exit temperature is the driving signal, and that the gas cooler entrance temperature is the output signal, a clear 1^{st} order dynamic can be identified (the constant offset is removed for the identification). For the three operating conditions, the gains were identified to be 0.97, 0.99, and 1.00, and the time constants were identified as 51.8, 25.2, and 29.4 seconds.

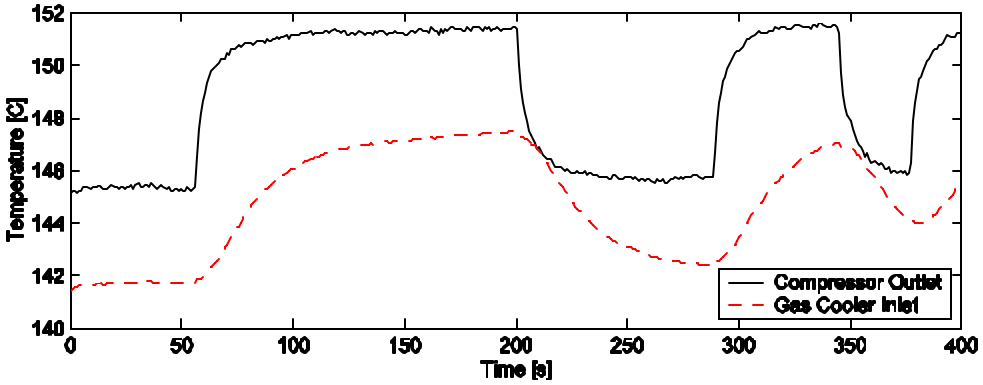

Figure 5.48 System Temperatures for Step Changes in Compressor Speed

This dynamic is not entirely unexpected. The parasitic heat loss through the pipe explains the constant offset. The slowly varying temperature of the pipe mass during a transient response would cause a 1st order filtering effect to the temperature. Note that the gain is approximately unity, and therefore the steady state offset remains virtually constant. The 1st order time constant varies with operating condition, but remains within an order of magnitude. Unfortunately, during the transient tests, the number of temperature measurements was limited, and the necessary information for identifying the dynamics of the other pipe lengths to and from the internal heat exchanger is not available. Although the pipe length between the expansion valve and evaporator is relatively short, the fluid in this section is two-phase, and therefore at a uniform temperature. Undoubtedly, there are also heat transfer losses and possibly dynamics in this section, but these are impossible to identify without the ability to measure fluid quality at each point. Therefore, for all the other pipe lengths, the time constants are assumed to be proportional to the pipe mass. In reality this time constant would also be a function of heat transfer coefficient, heat transfer area, etc. However, as an initial estimate only the mass of the pipe is considered. These values are given in Table 5.8.

Table 5.8 Estimated Time Constants for Inter-Component Pipe Lengths

Inter-Components	Pipe Mass [kg]	Time Constant [s]
Compressor – Gas Cooler	1.36	30.0
Gas Cooler – IHX	0.92	20.2
IHX – EEV	0.18	4.0
EEV – Evaporator	0.32	7.0
Evaporator – IHX	1.25	27.5
IHX – Compressor	0.27	6.0

5.8.1.2 Oil Separator Dynamics

In real systems an oil separator is placed immediately after, or integrated into, the compressor. The experimental system used an oil separator located after the compressor. This device has a chamber that allows most of the oil to be separated from the refrigerant. The oil is then recirculated to the compressor to ensure lubrication. The assumed dynamic effect is two-fold. First, because the oil separator operates intermittently depending on pressure and the amount of oil accumulated, the predicted mass flow rate may be inaccurate depending on the amount of oil being recirculated. When the oil separator is integrated into the system, the semi-empirical compressor

model likely would be calibrated so as to implicitly take into account the mass flow rate of oil being recirculated. However, if the predicted mass flow rate is higher than reality, then the pressure in the gas cooler will build slower than predicted. Second, the chamber of the oil separator will filter the pressure response of the gas cooler due to compressibility effects. Thus the discrepancy between model and data for the gas cooler pressure is attributed to this device. If a detailed model is desired, this component's effect should be considered. However, for this research, the model was deemed sufficient without this addition.

5.8.2 Improved Results

Although an appropriate model for the oil separator was not developed or included in the model, the 1st order delays between components were added to the simulation to evaluate if these dynamics improved the model validation. Figures 5.49 – 5.54 demonstrate that some dynamic effects are improved. The model correctly predicts the 2nd order effect for evaporator pressure, and the gas cooler exit air temperature has a slower response more consistent with the data. However, including these dynamics results in a greater steady state offset for the system pressures. The contribution of these dynamics appears to be minimal. Because the inclusion of these inter-component dynamics would greatly increase the dynamic order while not increasing accuracy significantly, they are deemed nonessential and are not included in the final model used for dynamic analysis or for future control design.

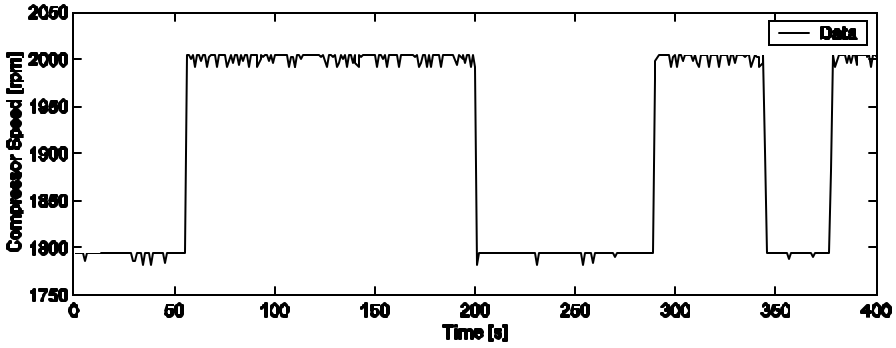

Figure 5.49 Improved Model Validation: Compressor Speed Step Changes

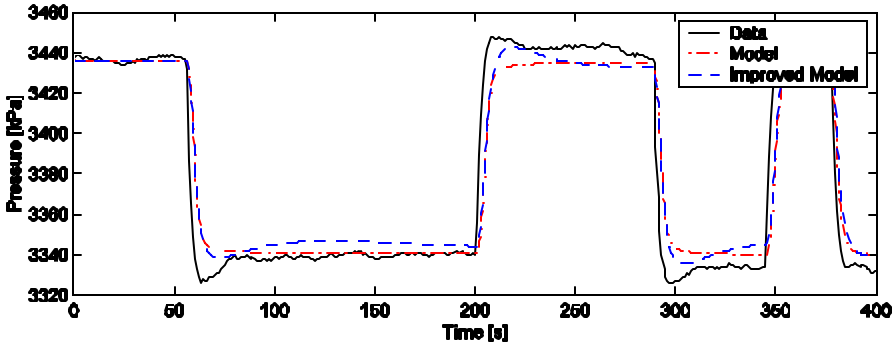

Figure 5.50 Improved Model Validation: Evaporator Pressure for Step Changes in Compressor Speed

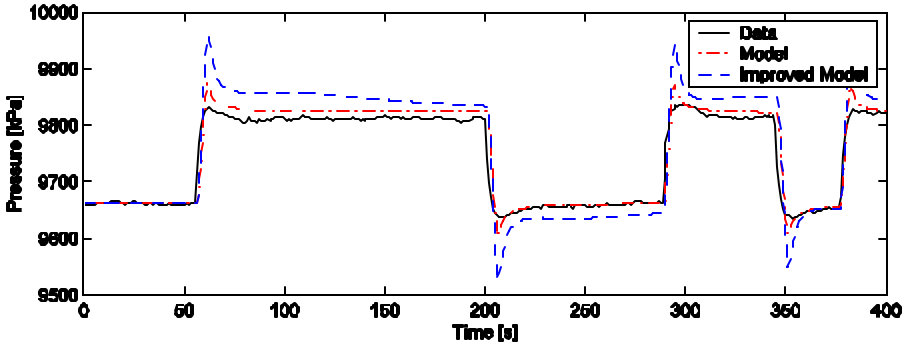

Figure 5.51 Improved Model Validation: Gas Cooler Pressure for Step Changes in Compressor Speed

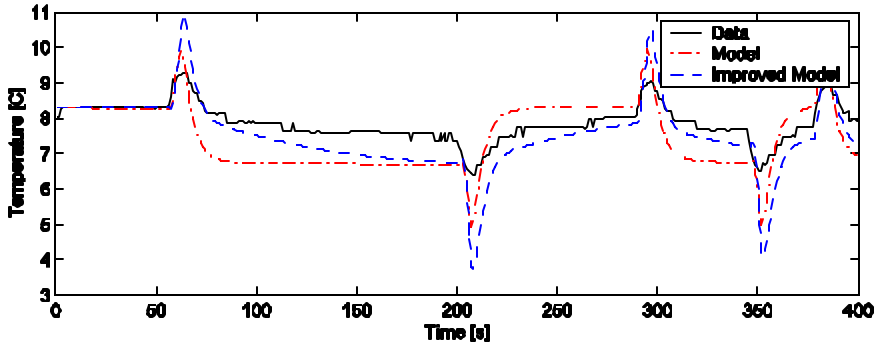

Figure 5.52 Improved Model Validation: Evaporator Superheat for Step Changes in Compressor Speed

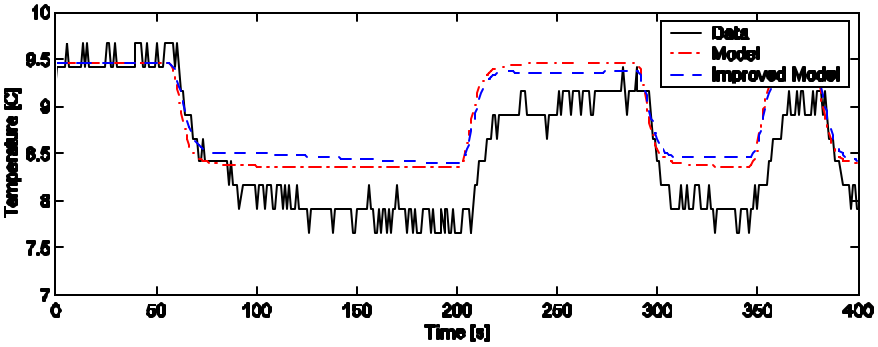

Figure 5.53 Improved Model Validation: Evaporator Exit Air Temperature for Step Changes in Compressor Speed

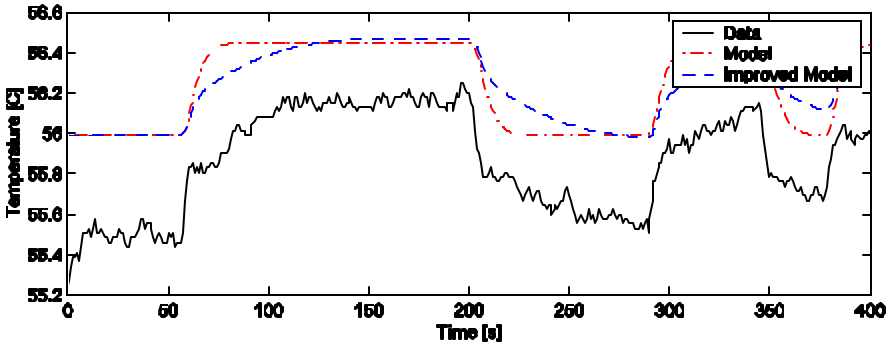

Figure 5.54 Improved Model Validation: Gas Cooler Exit Air Temperature for Step Changes in Compressor Speed

5.9 Summary

Overall the initial model validation demonstrated agreement between model and data. Notable discrepancies can be explained, and in general could be avoided by correcting the experimental setup to perform more like an actual air conditioning system. Some improvements to the model were suggested and evaluated. These improvements did correct minor errors, but were not deemed worth the added complexity and higher dynamic order to use in the final model for analysis or future controller design. The improved model could be used for simulation purposes.

Chapter 6. Model Linearization and Dynamic Analysis

The lumped parameter model developed for two-phase flow heat exchangers in previous sections is highly nonlinear. For analysis and model reduction purposes, a linear model is needed. Furthermore, most classical control design techniques require a linear model. Therefore, in this section we outline the procedure for achieving such a model.

6.10 General Linearization Procedure

This procedure follows a standard linearization procedure, where the partial derivatives of the nonlinear functions with respect to the states and inputs are calculated neglecting the 2nd and higher order terms [20,36]. This is followed for the static components as well as the internal heat exchanger. However, the gas cooler and evaporator models have a unique form. The linearization procedure for these components is as follows.

The heat exchanger models developed previously are of the form of Equation 6.5. Assuming $Z(x,u)$ is full rank for all x and u, this can be rearranged as Equation 6.6. The assumption that $Z(x,u)$ is full rank is true if the original modeling assumptions are true. Specifically, as long as the length of any of the assumed regions is greater than zero, $Z(x,u)$ will be invertible.

$$Z(x,u)\cdot \dot{x} = f(x,u) \tag{6.5}$$

$$\begin{aligned} \dot{x} &= Z(x,u)^{-1} f(x,u) \\ &= g(x,u) \end{aligned} \tag{6.6}$$

Using the assumption $x = x_o + dx$, a local linearization of this, neglecting higher order terms, would be Equation 6.7. Or by making the substitution $dx = x - x_o$, Equation 6.7 becomes 6.8. Because $\dot{x}_o = 0$ this equation simply becomes Equation 6.9.

$$d\dot{x} = \left[\left.\frac{\partial g}{\partial x}\right|_{x_0,u_0}\right]dx + \left[\left.\frac{\partial g}{\partial u}\right|_{x_0,u_0}\right]du \tag{6.7}$$

$$\dot{x} - \dot{x}_o = \left[\left.\frac{\partial g}{\partial x}\right|_{x_0,u_0}\right](x - x_o) + \left[\left.\frac{\partial g}{\partial u}\right|_{x_0,u_0}\right](u - u_o) \tag{6.8}$$

$$\dot{x} = \left[\left.\frac{\partial g}{\partial x}\right|_{x_0,u_0}\right](x - x_o) + \left[\left.\frac{\partial g}{\partial u}\right|_{x_0,u_0}\right](u - u_o) \tag{6.9}$$

Expanding the first term of Equation 6.9 results in Equation 6.10. Likewise, expanding the second term results in Equation 6.11. This is of the familiar form $\dot{x} = Ax + Bu$ (Equation 6.12). This form will be denoted as Equation 6.13, or in the standard form as Equation 6.14 using the substitutions in Equation 6.15.

$$\left[\left.\frac{\partial g}{\partial x}\right|_{x_0,u_0}\right] = \left[\left.Z\right|_{x_0,u_0}\right]^{-1}\left[\left.\frac{\partial f}{\partial x}\right|_{x_0,u_0}\right] - \left[\left.Z\right|_{x_0,u_0}\right]^{-2}\left[\left.\frac{\partial Z}{\partial x}\right|_{x_0,u_0}\right]^{-1}\underbrace{\left[\left.f\right|_{x_0,u_0}\right]}_{0}$$
$$= \left[\left.Z\right|_{x_0,u_0}\right]^{-1}\left[\left.\frac{\partial f}{\partial x}\right|_{x_0,u_0}\right] \tag{6.10}$$

$$\left[\left.\frac{\partial g}{\partial u}\right|_{x_0,u_0}\right] = \left[\left.Z\right|_{x_0,u_0}\right]^{-1}\left[\left.\frac{\partial f}{\partial u}\right|_{x_0,u_0}\right] \tag{6.11}$$

$$\dot{x} = \left[\left.Z\right|_{x_0,u_0}\right]^{-1}\underbrace{\left[\left.\frac{\partial f}{\partial x}\right|_{x_0,u_0}\right]}_{F_x}(x - x_o) + \left[\left.Z\right|_{x_0,u_0}\right]^{-1}\underbrace{\left[\left.\frac{\partial f}{\partial u}\right|_{x_0,u_0}\right]}_{F_u}(u - u_o) \tag{6.12}$$

$$\dot{x} = Z^{-1}F_x dx + Z^{-1}F_u du \tag{6.13}$$

$$\dot{x} = Adx + Bdu \tag{6.14}$$

$$A = Z^{-1}F_x$$
$$B = Z^{-1}F_u \tag{6.15}$$

The nonlinear output equations are denoted as Equation 6.16. The linearized version is then given as Equation 6.17, or in the standard form as Equation 6.18, using the substitutions in Equation 6.19.

$$y = g(x,u) \tag{6.16}$$

$$dy = G_x dx + G_u du \tag{6.17}$$

$$dy = Cdx + Ddu \tag{6.18}$$

$$C = G_x$$
$$D = G_u \tag{6.19}$$

6.11 Derivation

Symbolic results are presented here for each component. Numerical results are included for each component as well as the overall system. These results were achieved evaluating the models at the highway driving condition.

6.11.1 Variable Speed Compressor

Recall that the compressor was modeled with an equation for mass flow (Equation 6.20) and an equation for isentropic efficiency (Equation 6.21) where $r_k = r(P_{in}, h_{in})$, $h_{out,isentropic} = h(P_{out}, s_k)$, and $s_k = s(P_{in}, h_{in})$. The isentropic efficiency is assumed to be a function of pressure ratio (Equation 6.22).

$$\dot{m}_k = w_k V_k r_k \left(1 + C_k - D_k\left(\frac{P_{out}}{P_{in}}\right)^{\frac{1}{n}}\right) \tag{6.20}$$

$$h_{out} = \frac{1}{h_k}\left[h_{out,isentropic} + h_{in}\left(h_k - 1\right)\right] \tag{6.21}$$

$$h_k = A_k\left(\frac{P_{out}}{P_{in}}\right) + B_k \tag{6.22}$$

6.11.1.1 Symbolic Representation

Let the inputs and outputs be defined by Equations 6.23 and 6.24. Thus $y = f(u)$. A local linearization is given as $y = Du$, where D is defined in Equation 6.25, and the matrix elements are listed in Table 6.9, where selected partial derivatives are calculated as $\frac{\partial h_k}{\partial P_{in}} = -A_k\left(\frac{P_{out}}{P_{in}^{\ 2}}\right)$, $\frac{\partial h_k}{\partial P_{out}} = A_k\left(\frac{1}{P_{in}}\right)$,

$\frac{\partial h_{out,s}}{\partial P_{in}} = \left(\left.\frac{\partial h_{out,s}}{\partial s_k}\right|_{P_{out}}\right)\left(\left.\frac{\partial s_k}{\partial P_{in}}\right|_{h_{in}}\right)$, $\frac{\partial h_{out,s}}{\partial P_{out}} = \left(\left.\frac{\partial h_{out,s}}{\partial P_{out}}\right|_{s_k}\right)$, and $\frac{\partial h_{out,s}}{\partial h_{in}} = \left(\left.\frac{\partial h_{out,s}}{\partial s_k}\right|_{P_{out}}\right)\left(\left.\frac{\partial s_k}{\partial h_{in}}\right|_{P_{in}}\right)$.

$$u = \left[w_k \quad P_{in} \quad P_{out} \quad h_{in}\right]^T \tag{6.23}$$

$$y = \left[\dot{m}_k \quad h_{out} \quad T_{out}\right]^T \tag{6.24}$$

$$\frac{\partial f}{\partial u} = D = \begin{bmatrix} d_{11} & d_{12} & d_{13} & d_{14} \\ 0 & d_{22} & d_{23} & d_{24} \\ 0 & d_{32} & d_{33} & d_{34} \end{bmatrix} \tag{6.25}$$

Table 6.9 Matrix Elements for Equation 6.25

d_{11}	$V_k r_k\left(1 + C_k - D_k\left(\frac{P_{out}}{P_{in}}\right)^{\frac{1}{n}}\right)$
d_{12}	$w_k V_k\left(\left.\frac{\partial r_k}{\partial P_{in}}\right\|_{h_{in}}\right)\left(1 + C_k - D_k\left(\frac{P_{out}}{P_{in}}\right)^{\frac{1}{n}}\right) + w_k V_k r_k\left(\frac{1}{n}\right)\left(\frac{D_k}{P_{in}}\right)\left(\frac{P_{out}}{P_{in}}\right)^{\frac{1}{n}}$
d_{13}	$-w_k V_k r_k\left(\frac{1}{n}\right)\left(\frac{D_k}{P_{out}}\right)\left(\frac{P_{out}}{P_{in}}\right)^{\frac{1}{n}}$
d_{14}	$w_k V_k\left(\left.\frac{\partial r_k}{\partial h_{in}}\right\|_{P_{in}}\right)\left(1 + C_k - D_k\left(\frac{P_{out}}{P_{in}}\right)^{\frac{1}{n}}\right)$
d_{22}	$-\left(\frac{1}{h_k^{\ 2}}\right)\left(\frac{\partial h_k}{\partial P_{in}}\right)\left[h_{out,s} + h_{in}\left(h_k - 1\right)\right] + \left(\frac{1}{h_k}\right)\left[\frac{\partial h_{out,s}}{\partial P_{in}} + h_{in}\left(\frac{\partial h_k}{\partial P_{in}}\right)\right]$

Table 6.3 (cont.)

d_{23}	$-\left(\frac{1}{h_k^{\,2}}\right)\left(\frac{\partial h_k}{\partial P_{out}}\right)\left[h_{out,s}+h_{in}\left(h_k-1\right)\right]+\left(\frac{1}{h_k}\right)\left[\frac{\partial h_{out,s}}{\partial P_{out}}+h_{in}\left(\frac{\partial h_k}{\partial P_{out}}\right)\right]$
d_{24}	$\left(\frac{1}{h_k}\right)\left[\frac{\partial h_{out,s}}{\partial h_{in}}+\left(h_k-1\right)\right]$
d_{32}	$\left(\left.\frac{\partial T_{out}}{\partial h_{out}}\right\|_{P_{out}}\right)\left[-\left(\frac{1}{h_k^{\,2}}\right)\left(\frac{\partial h_k}{\partial P_{in}}\right)\left[h_{out,s}+h_{in}\left(h_k-1\right)\right]+\left(\frac{1}{h_k}\right)\left[\frac{\partial h_{out,s}}{\partial P_{in}}+h_{in}\left(\frac{\partial h_k}{\partial P_{in}}\right)\right]\right]$
d_{33}	$\left(\left.\frac{\partial T_{out}}{\partial P_{out}}\right\|_{h_{out}}\right)+\left(\left.\frac{\partial T_{out}}{\partial h_{out}}\right\|_{P_{out}}\right)\left[\begin{array}{l}-\left(\frac{1}{h_k^{\,2}}\right)\left(\frac{\partial h_k}{\partial P_{out}}\right)\left[h_{out,s}+h_{in}\left(h_k-1\right)\right]\\+\left(\frac{1}{h_k}\right)\left[\frac{\partial h_{out,s}}{\partial P_{out}}+h_{in}\left(\frac{\partial h_k}{\partial P_{out}}\right)\right]\end{array}\right]$
d_{34}	$\left(\left.\frac{\partial T_{out}}{\partial h_{out}}\right\|_{P_{out}}\right)\left(\frac{1}{h_k}\right)\left[\frac{\partial h_{out,s}}{\partial h_{in}}+\left(h_k-1\right)\right]$

6.11.1.2 Numerical Representation

The evaluation of these equations at the highway operating condition yields the following matrix (Equation 6.26).

$$D=\begin{bmatrix} 2.4317e-5 & 1.6904e-5 & -1.3667e-6 & -2.1098e-4 \\ 0 & -0.023185 & 0.0081173 & 1.2261 \\ 0 & -0.020016 & 0.016451 & 1.0585 \end{bmatrix} \tag{6.26}$$

6.11.2 Electronic Expansion Valve

Recall that the expansion valve was modeled with an equation for mass flow (Equation 6.27) and assumed isenthalpic expansion (Equation 6.28), where $r_v = r\left(P_{in}, h_{in}\right)$. Recall that the area of the valve is assumed to be a linear function of a given input (Equation 6.29), and that the discharge coefficient is assumed to change with Reynold's number (Equation 6.30). After substitution, the mass flow rate equation is defined by three empirical parameters (Equation 6.31).

$$\dot{m}_v = A_v C_v \left[r_v\left(P_{in}-P_{out}\right)\right]^n \tag{6.27}$$

$$h_{in} = h_{out} \tag{6.28}$$

$$A_v = b_1 + b_2 u_v \tag{6.29}$$

$$\begin{aligned} C_v &= b_3\left(1+\frac{b_4}{\mathrm{Re}_d}\right) \\ &\approx b_3\left(1+\frac{b_5}{\dot{m}_v}\right) \end{aligned} \tag{6.30}$$

$$\dot{m}_v = k_1(1+k_2 u_v)\left(1+\frac{k_3}{\dot{m}_v}\right)\left[r_v(P_{in}-P_{out})\right]^n \tag{6.31}$$

6.11.2.1 Symbolic Representation

Let the inputs and outputs be defined by Equations 6.32 and 6.33. Thus $y = f(u)$. A local linearization is given as $y = Du$, where D is defined in Equation 6.34, and the matrix elements are listed in Table 6.10. For notational simplicity, let $den_v = 1 + k_1(1+k_2 u_v)\left(\frac{k_3}{\dot{m}_v^{\,2}}\right)\left[r_v(P_{in}-P_{out})\right]^n$.

$$u = \begin{bmatrix} u_v & P_{in} & P_{out} & h_{in} \end{bmatrix}^T \tag{6.32}$$

$$y = \begin{bmatrix} \dot{m}_v & h_{out} & T_{out} \end{bmatrix}^T \tag{6.33}$$

$$\frac{\partial f}{\partial u} = D = \begin{bmatrix} d_{11} & d_{12} & d_{13} & d_{14} \\ 0 & 0 & 0 & d_{24} \\ 0 & 0 & d_{33} & d_{34} \end{bmatrix} \tag{6.34}$$

Table 6.10 Matrix Elements for Equation 6.34

d_{11}	$k_1 k_2\left(1+\frac{k_3}{\dot{m}_v}\right)\left[r_v(P_{in}-P_{out})\right]^n\left(\frac{1}{den_v}\right)$
d_{12}	$k_1(1+k_2 u_v)\left(1+\frac{k_3}{\dot{m}_v}\right)n\left[r_v(P_{in}-P_{out})\right]^{n-1}\left[r_v+\left(\frac{\partial r_v}{\partial P_{in}}\Big\|_{h_{in}}\right)(P_{in}-P_{out})\right]\left(\frac{1}{den_v}\right)$
d_{13}	$-k_1(1+k_2 u_v)\left(1+\frac{k_3}{\dot{m}_v}\right)n\left[r_v(P_{in}-P_{out})\right]^{n-1}\left[r_v\right]\left(\frac{1}{den_v}\right)$
d_{14}	$k_1(1+k_2 u_v)\left(1+\frac{k_3}{\dot{m}_v}\right)n\left[r_v(P_{in}-P_{out})\right]^{n-1}\left[\left(\frac{\partial r_v}{\partial h_{in}}\Big\|_{P_{in}}\right)(P_{in}-P_{out})\right]\left(\frac{1}{den_v}\right)$
d_{24}	1
d_{33}	$\left(\frac{\partial T_{out}}{\partial P_{out}}\Big\|_{h_{out}}\right)$
d_{34}	$\left(\frac{\partial T_{out}}{\partial h_{out}}\Big\|_{P_{out}}\right)$

6.11.2.2 Numerical Representation

The evaluation of these equations at the highway operating condition yields the following matrix (Equation 6.35).

$$D = \begin{bmatrix} 0.0019444 & 4.5639e-6 & -3.3549e-6 & -1.5184e-4 \\ 0 & 0 & 0 & 1 \\ 0 & 0 & 0.010952 & 0 \end{bmatrix} \tag{6.35}$$

6.11.3 Gas Cooler

Recall that the gas cooler could be modeled with several different choices of state variables, depending on the derivation approach. Three possible choices of states are given as $x = \begin{bmatrix} P_c & h_c & T_w \end{bmatrix}^T$, $x' = \begin{bmatrix} P_c & m_c & T_w \end{bmatrix}^T$, and $x'' = \begin{bmatrix} U_c & m_c & E_{ww} \end{bmatrix}^T$. The different models are denoted as $Z(x,u)x = f(x,u)$, $Z'(x',u')x' = f(x',u')$, and $x'' = f(x'',u'')$, where the function $f(x,u)$ is defined in Equation 6.36, and the matrices $Z(x,u)$ and $Z'(x',u')$ are defined in Chapter 4. The model outputs are given as nonlinear functions of the states and inputs, $y = g(x,u)$. Let the inputs and outputs for the first representation be defined by Equations 6.37 and 6.38.

$$f(x,u) = \begin{bmatrix} \dot{m}_{in} h_{in} - \dot{m}_{out} h_{out} - a_i A_i (T_r - T_w) \\ \dot{m}_{in} - \dot{m}_{out} \\ a_i A_i (T_r - T_w) - a_o A_o (T_w - T_a) \end{bmatrix} \tag{6.36}$$

$$u = \begin{bmatrix} \dot{m}_{in} & \dot{m}_{out} & h_{in} & T_{a,in} & \dot{m}_a \end{bmatrix}^T \tag{6.37}$$

$$y = \begin{bmatrix} P_c & h_{out} & T_w & T_{a,out} & T_{r,out} & m_c \end{bmatrix}^T \tag{6.38}$$

The assumptions regarding the air temperature T_a are the same for all representations. For heat transfer an average air temperature across the gas cooler is assumed (Equation 6.39). The energy balance for the air given a heat exchanger with n regions is given in Equation 6.40. Solving for T_a (Equation 6.41) and simplifying the expression assuming one region results in Equation 6.42.

$$T_a = \frac{T_{a,in} + T_{a,out}}{2} \tag{6.39}$$

$$\dot{m}_{air} C_{p,air} (T_{a,in} - T_{a,out}) = a_o A_o \left[\sum_{i=1}^{n} \frac{L_i}{L_{Total}} (T_a - T_{w,i}) \right] \tag{6.40}$$

$$T_a = \frac{2 \cdot \dot{m}_{air} C_{p,air} T_{a,in} + a_o A_o \left[\sum_{i=1}^{n} \frac{L_i T_{w,i}}{L_{Total}} \right]}{2 \cdot \dot{m}_{air} C_{p,air} + a_o A_o} \tag{6.41}$$

$$T_a = \frac{2 \cdot \dot{m}_{air} C_{p,air} T_{a,in} + a_o A_o T_w}{2 \cdot \dot{m}_{air} C_{p,air} + a_o A_o} \tag{6.42}$$

For the linearization, the partial derivatives of the average air temperature are required. First recall that the air-side heat transfer coefficient is a function of mass flow rate of air. Specifically, we assume that the heat transfer coefficient scales with Reynold's number (where the prime denotes initial values) as given in Equation 6.43. Thus

the partial derivative of heat transfer coefficient with respect to mass flow rate of air can be written as Equation 6.44. The partial derivatives of air temperature are then given in Equations 6.45, 6.46, and 6.47.

$$\frac{a_o}{a'_o} = \left(\frac{\mathrm{Re}_l}{\mathrm{Re}'_l}\right)^m = \left(\frac{\dot{m}_{air}}{\dot{m}'_{air}}\right)^m \tag{6.43}$$

$$\frac{\partial a_o}{\partial \dot{m}_{air}} = m\left(\frac{\dot{m}_{air}}{\dot{m}'_{air}}\right)^m \left(\frac{a'_o}{\dot{m}_{air}}\right) \tag{6.44}$$

$$\frac{\partial T_a}{\partial T_w} = \frac{a_o A_o}{2 \cdot \dot{m}_{air} C_{p,air} + a_o A_o} \tag{6.45}$$

$$\frac{\partial T_a}{\partial T_{a,in}} = \frac{2 \cdot \dot{m}_{air} C_{p,air}}{2 \cdot \dot{m}_{air} C_{p,air} + a_o A_o} \tag{6.46}$$

$$\frac{\partial T_a}{\partial \dot{m}_{air}} = \frac{2 \cdot C_{p,air} A_o \left(T_{a,in} - T_w\right)\left(a_o - \dot{m}_{air} \dfrac{\partial a_o}{\partial \dot{m}_{air}}\right)}{\left(2 \cdot \dot{m}_{air} C_{p,air} + a_o A_o\right)^2} \tag{6.47}$$

Several assumptions are made to define the output relationships, as well as explicitly relate intermediate variables to states or inputs. These relationships differ for each representation. For the first representation, some of the outputs are states; the other outputs are defined as $h_{out} = 2h_c - h_{in}$, $T_{a,out} = 2T_a - T_{a,in}$, $T_{r,out} = T\left(P_c, h_{out}\right)$, and $m_c = r_c V_c$ where $V_c = A_{cs} L_{total}$. Several intermediate variables are used in the model, and can be related thermodynamically to states or inputs. The average refrigerant temperature is calculated as $T_r = T\left(P_c, h_c\right)$. However, since $h_c = \dfrac{h_{in} + h_{out}}{2}$ then $T_r \approx \dfrac{T(P_c, h_{in}) + T(P_c, h_{out})}{2}$, and for the partial derivatives of T_r the approximations $\dfrac{\partial T_r}{\partial P_c} = \left(\dfrac{\partial T}{\partial P_c}\bigg|_{h_c}\right)$, $\dfrac{\partial T_r}{\partial h_{in}} = \dfrac{1}{2}\left(\dfrac{\partial T}{\partial h_c}\bigg|_{P_c}\right)$, and $\dfrac{\partial T_r}{\partial h_{out}} = \dfrac{1}{2}\left(\dfrac{\partial T}{\partial h_c}\bigg|_{P_c}\right)$ are used.

For the second representation, some of the outputs are again states; the other outputs are defined as $h_{out} = 2h_c - h_{in}$, $T_{a,out} = 2T_a - T_{a,in}$, and $T_{r,out} = T\left(P_c, h_{out}\right)$, where $r_c = \dfrac{m_c}{V_c}$, $h_c = h\left(P_c, r_c\right)$, and $T_r = T\left(P_c, r_c\right)$.

For the third representation, some of the outputs are again states; the other outputs are defined as $h_{out} = 2h_c - h_{in}$, $T_{a,out} = 2T_a - T_{a,in}$, and $T_{r,out} = T\left(P_c, h_{out}\right)$, where $r_c = \dfrac{m_c}{V_c}$, $u_c = \dfrac{U_c}{m_c}$, $P_c = P\left(u_c, r_c\right)$, $h_c = h\left(u_c, r_c\right)$, and $T_r = T\left(u_c, r_c\right)$.

6.11.3.1 Symbolic Representation

For the first representation, the partial derivatives of the functions $f(x,u)$ and $g(x,u)$ with respect to the states and inputs are defined in Equations 6.48 - 6.51, with the matrix elements listed in Table 6.11.

$$\frac{\partial f}{\partial x} = F_x = \begin{bmatrix} f_{x,11} & f_{x,12} & f_{x,13} \\ 0 & 0 & 0 \\ f_{x,31} & f_{x,32} & f_{x,33} \end{bmatrix} \tag{6.48}$$

$$\frac{\partial f}{\partial u} = F_u = \begin{bmatrix} f_{u,11} & f_{u,12} & f_{u,13} & 0 & 0 \\ f_{u,21} & f_{u,22} & 0 & 0 & 0 \\ 0 & 0 & 0 & f_{u,34} & f_{u,35} \end{bmatrix} \tag{6.49}$$

$$\frac{\partial g}{\partial x} = G_x = \begin{bmatrix} 1 & 0 & 0 \\ 0 & g_{x,22} & 0 \\ 0 & 0 & 1 \\ 0 & 0 & g_{x,43} \\ g_{x,51} & g_{x,52} & 0 \\ g_{x,61} & g_{x,62} & 0 \end{bmatrix} \tag{6.50}$$

$$\frac{\partial g}{\partial u} = G_u = \begin{bmatrix} 0 & 0 & 0 & 0 & 0 \\ 0 & 0 & g_{u,23} & 0 & 0 \\ 0 & 0 & 0 & 0 & 0 \\ 0 & 0 & 0 & g_{u,44} & g_{u,45} \\ 0 & 0 & g_{u,53} & 0 & 0 \\ 0 & 0 & 0 & 0 & 0 \end{bmatrix} \tag{6.51}$$

Table 6.11 Matrix Elements of Equations 6.48 - 6.51

$f_{x,11}$	$-a_i A_i \left(\left. \frac{\partial T_r}{\partial P_c} \right\|_{h_c} \right)$
$f_{x,12}$	$-2m_o - a_i A_i \left(\left. \frac{\partial T_r}{\partial h_c} \right\|_{P_c} \right)$
$f_{x,13}$	$a_i A_i$
$f_{x,31}$	$a_i A_i \left(\left. \frac{\partial T_r}{\partial P_c} \right\|_{h_c} \right)$
$f_{x,32}$	$a_i A_i \left(\left. \frac{\partial T_r}{\partial h_c} \right\|_{P_c} \right)$

Table 6.5 (cont.)

$f_{x,33}$	$-a_i A_i - a_o A_o + a_o A_o \left(\frac{\partial T_a}{\partial T_w} \right)$
$f_{u,11}$	h_{in}
$f_{u,12}$	$-h_{out}$
$f_{u,13}$	$m_{in} + m_{out}$
$f_{u,21}$	1
$f_{u,22}$	-1
$f_{u,34}$	$a_o A_o \left(\frac{\partial T_a}{\partial T_{a,in}} \right)$
$f_{u,35}$	$\left(\frac{\partial a_o}{\partial \dot{m}_{air}} \right) A_o \left(T_a - T_w \right) + a_o A_o \left(\frac{\partial T_a}{\partial \dot{m}_{air}} \right)$
$g_{x,22}$	2
$g_{x,43}$	$2\left(\frac{\partial T_a}{\partial T_w} \right)$
$g_{x,51}$	$\left(\frac{\partial T_{r,out}}{\partial P_c}\Big\|_{h_{out}} \right)$
$g_{x,52}$	$2\left(\frac{\partial T_{r,out}}{\partial h_{out}}\Big\|_{P_c} \right)$
$g_{x,61}$	$\left(\frac{\partial r_c}{\partial P_c}\Big\|_{h_c} \right) V_c$
$g_{x,62}$	$\left(\frac{\partial r_c}{\partial h_c}\Big\|_{P_c} \right) V_c$
$g_{u,23}$	-1
$g_{u,44}$	$2\left(\frac{\partial T_a}{\partial T_{a,in}} \right) - 1$
$g_{u,45}$	$2\left(\frac{\partial T_a}{\partial \dot{m}_{air}} \right)$
$g_{u,53}$	$-\left(\frac{\partial T_{r,out}}{\partial h_{out}}\Big\|_{P_c} \right)$

For the second representation, the partial derivatives of the functions $f(x',u')$ and $g(x',u')$ with respect to the states and inputs are defined in Equations 6.52 - 6.55, with the matrix elements listed in Table 6.12.

$$\frac{\partial f}{\partial x'} = F_x' = \begin{bmatrix} f_{x,11}' & f_{x,12}' & f_{x,13}' \\ 0 & 0 & 0 \\ f_{x,31}' & f_{x,32}' & f_{x,33}' \end{bmatrix} \tag{6.52}$$

$$\frac{\partial f}{\partial u'} = F_u' = \begin{bmatrix} f_{u,11}' & f_{u,12}' & f_{u,13}' & 0 & 0 \\ f_{u,21}' & f_{u,22}' & 0 & 0 & 0 \\ 0 & 0 & 0 & f_{u,34}' & f_{u,35}' \end{bmatrix} \tag{6.53}$$

$$\frac{\partial g}{\partial x'} = G_x' = \begin{bmatrix} 1 & 0 & 0 \\ g_{x,21}' & g_{x,22}' & 0 \\ 0 & 0 & 1 \\ 0 & 0 & g_{x,43}' \\ g_{x,51}' & g_{x,52}' & 0 \\ 0 & 1 & 0 \end{bmatrix} \tag{6.54}$$

$$\frac{\partial g}{\partial u'} = G_u' = \begin{bmatrix} 0 & 0 & 0 & 0 & 0 \\ 0 & 0 & g_{u,23}' & 0 & 0 \\ 0 & 0 & 0 & 0 & 0 \\ 0 & 0 & 0 & g_{u,44}' & g_{u,45}' \\ 0 & 0 & g_{u,53}' & 0 & 0 \\ 0 & 0 & 0 & 0 & 0 \end{bmatrix} \tag{6.55}$$

Table 6.12 Matrix Elements of Equations 6.52 - 6.55

$f_{x,11}'$	$-2\dot{m}_{out}\left(\left.\frac{\partial h_c}{\partial P_c}\right\|_{r_c}\right) - a_i A_i \left(\left.\frac{\partial T_r}{\partial P_c}\right\|_{r_c}\right)$
$f_{x,12}'$	$-2\frac{\dot{m}_{out}}{V_c}\left(\left.\frac{\partial h_c}{\partial r_c}\right\|_{P_c}\right) - \frac{a_i A_i}{V_c}\left(\left.\frac{\partial T_r}{\partial r_c}\right\|_{P_c}\right)$
$f_{x,13}'$	$a_i A_i$
$f_{x,31}'$	$a_i A_i \left(\left.\frac{\partial T_r}{\partial P_c}\right\|_{r_c}\right)$
$f_{x,32}'$	$\frac{a_i A_i}{V_c}\left(\left.\frac{\partial T_r}{\partial r_c}\right\|_{P_c}\right)$

Table 6.6 (cont.)

$f'_{x,33}$	$-a_i A_i - a_o A_o + a_o A_o \left(\frac{\partial T_a}{\partial T_w} \right)$
$f'_{u,11}$	h_{in}
$f'_{u,12}$	$-h_{out}$
$f'_{u,13}$	$\dot{m}_{in} + \dot{m}_{out}$
$f'_{u,21}$	1
$f'_{u,22}$	-1
$f'_{u,34}$	$a_o A_o \left(\frac{\partial T_a}{\partial T_{a,in}} \right)$
$f'_{u,35}$	$\left(\frac{\partial a_o}{\partial \dot{m}_{air}} \right) A_o (T_a - T_w) + a_o A_o \left(\frac{\partial T_a}{\partial \dot{m}_{air}} \right)$
$g'_{x,21}$	$2 \left(\frac{\partial h_c}{\partial P_c} \Big\|_{r_c} \right)$
$g'_{x,22}$	$2 \left(\frac{\partial h_c}{\partial r_c} \Big\|_{P_c} \right) \frac{1}{V_c}$
$g'_{x,43}$	$2 \left(\frac{\partial T_a}{\partial T_w} \right)$
$g'_{x,51}$	$\left(\frac{\partial T_{r,out}}{\partial P_c} \Big\|_{h_{out}} \right) + 2 \left(\frac{\partial T_{r,out}}{\partial h_{out}} \Big\|_{P_c} \right) \left(\frac{\partial h_c}{\partial P_c} \Big\|_{r_c} \right)$
$g'_{x,52}$	$2 \left(\frac{\partial T_{r,out}}{\partial h_{out}} \Big\|_{P_c} \right) \left(\frac{\partial h_c}{\partial r_c} \Big\|_{P_c} \right) \frac{1}{V_c}$
$g'_{u,23}$	-1
$g'_{u,44}$	$2 \left(\frac{\partial T_a}{\partial T_{a,in}} \right) - 1$
$g'_{u,45}$	$2 \left(\frac{\partial T_a}{\partial \dot{m}_{air}} \right)$
$g'_{u,53}$	$-\left(\frac{\partial T_{r,out}}{\partial h_{out}} \Big\|_{P_c} \right)$

For the third representation, the partial derivatives of the functions $f(x'',u'')$ and $g(x'',u'')$ with respect to the states and inputs are defined in Equations 6.56 - 6.59, with the matrix elements listed in Table 6.13.

$$\frac{\partial f}{\partial x''} = F_x'' = \begin{bmatrix} f_{x,11}'' & f_{x,12}'' & f_{x,13}'' \\ 0 & 0 & 0 \\ f_{x,31}'' & f_{x,32}'' & f_{x,33}'' \end{bmatrix} \tag{6.56}$$

$$\frac{\partial f}{\partial u''} = F_u'' = \begin{bmatrix} f_{u,11}'' & f_{u,12}'' & f_{u,13}'' & 0 & 0 \\ f_{u,21}'' & f_{u,22}'' & 0 & 0 & 0 \\ 0 & 0 & 0 & f_{u,34}'' & f_{u,35}'' \end{bmatrix} \tag{6.57}$$

$$\frac{\partial g}{\partial x''} = G_x'' = \begin{bmatrix} g_{x,11}'' & g_{x,12}'' & 0 \\ g_{x,21}'' & g_{x,22}'' & 0 \\ 0 & 0 & g_{x,33}'' \\ 0 & 0 & g_{x,43}'' \\ g_{x,51}'' & g_{x,52}'' & 0 \\ 0 & 1 & 0 \end{bmatrix} \tag{6.58}$$

$$\frac{\partial g}{\partial u''} = G_u'' = \begin{bmatrix} 0 & 0 & 0 & 0 & 0 \\ 0 & 0 & g_{u,23}'' & 0 & 0 \\ 0 & 0 & 0 & 0 & 0 \\ 0 & 0 & 0 & g_{u,44}'' & g_{u,45}'' \\ 0 & 0 & g_{u,53}'' & 0 & 0 \\ 0 & 0 & 0 & 0 & 0 \end{bmatrix} \tag{6.59}$$

Table 6.13 Matrix Elements for Equations 6.56 - 6.59

$f_{x,11}''$	$-\frac{2\dot{m}_{out}}{m_c}\left(\left.\frac{\partial h_c}{\partial u_c}\right\|_{r_c}\right)-\frac{a_i A_i}{m_c}\left(\left.\frac{\partial T_r}{\partial u_c}\right\|_{r_c}\right)$
$f_{x,12}''$	$-\frac{2\dot{m}_{out}}{V_c}\left(\left.\frac{\partial h_c}{\partial r_c}\right\|_{u_c}\right)-\frac{a_i A_i}{V_c}\left(\left.\frac{\partial T_r}{\partial r_c}\right\|_{u_c}\right)$
$f_{x,13}''$	$\frac{a_i A_i}{(C_p r V)_w}$
$f_{x,31}''$	$\frac{a_i A_i}{m_c}\left(\left.\frac{\partial T_r}{\partial u_c}\right\|_{r_c}\right)$
$f_{x,32}''$	$\frac{a_i A_i}{V_c}\left(\left.\frac{\partial T_r}{\partial r_c}\right\|_{u_c}\right)$

Table 6.7 (cont.)

$f''_{x,33}$	$-\frac{a_i A_i}{(C_p r V)_w} - \frac{a_o A_o}{(C_p r V)_w}\left[1 - \frac{\partial T_a}{\partial T_w}\right]$
$f''_{u,11}$	h_{in}
$f''_{u,12}$	$-h_{out}$
$f''_{u,13}$	$\dot{m}_{in} + \dot{m}_{out}$
$f''_{u,21}$	1
$f''_{u,22}$	-1
$f''_{u,34}$	$a_o A_o\left(\frac{\partial T_a}{\partial T_{a,in}}\right)$
$f''_{u,35}$	$\left(\frac{\partial a_o}{\partial \dot{m}_{air}}\right)A_o(T_a - T_w) + a_o A_o\left(\frac{\partial T_a}{\partial \dot{m}_{air}}\right)$
$g''_{x,11}$	$\frac{1}{m_c}\left(\left.\frac{\partial P_c}{\partial u_c}\right\|_{r_c}\right)$
$g''_{x,12}$	$\frac{1}{V_c}\left(\left.\frac{\partial P_c}{\partial r_c}\right\|_{u_c}\right)$
$g''_{x,21}$	$\frac{2}{m_c}\left(\left.\frac{\partial h_c}{\partial u_c}\right\|_{r_c}\right)$
$g''_{x,22}$	$\frac{2}{V_c}\left(\left.\frac{\partial h_c}{\partial r_c}\right\|_{u_c}\right)$
$g''_{x,33}$	$\frac{1}{(C_p r V)_w}$
$g''_{x,43}$	$\frac{2}{(C_p r V)_w}\left(\frac{\partial T_a}{\partial T_w}\right)$
$g''_{x,51}$	$\left(\left.\frac{\partial T_{r,out}}{\partial P_c}\right\|_{h_{out}}\right)\left(\left.\frac{\partial P_c}{\partial u_c}\right\|_{r_c}\right)\left(\frac{1}{m_c}\right) + \left(\left.\frac{\partial T_{r,out}}{\partial h_{out}}\right\|_{P_c}\right)\left(\left.\frac{\partial h_c}{\partial u_c}\right\|_{r_c}\right)\left(\frac{2}{m_c}\right)$
$g''_{x,52}$	$\left(\left.\frac{\partial T_{r,out}}{\partial P_c}\right\|_{h_{out}}\right)\left(\left.\frac{\partial P_c}{\partial r_c}\right\|_{u_c}\right)\left(\frac{1}{V_c}\right) + \left(\left.\frac{\partial T_{r,out}}{\partial h_{out}}\right\|_{P_c}\right)\left(\left.\frac{\partial h_c}{\partial r_c}\right\|_{u_c}\right)\left(\frac{2}{V_c}\right)$
$g''_{u,23}$	-1

Table 6.7 (cont.)

$g''_{u,44}$	$2\left(\frac{\partial T_a}{\partial T_{a,in}}\right)-1$
$g''_{u,45}$	$2\left(\frac{\partial T_a}{\partial \dot{m}_{air}}\right)$
$g''_{u,53}$	$-\left(\frac{\partial T_{r,out}}{\partial h_{out}}\bigg\vert_{P_c}\right)$

6.11.3.2 Numerical Representation

The numerical evaluation of these equations can be done using the explicit formulas given in this section. Alternatively, because these representations are simply related by a state transformation, any of the three given representations can be calculated with knowledge of one of the other representations. For example, since $Zx = Z'x'$, the transformation $T' = Z^{-1}Z'$ can be used to substitute $x = \left(Z^{-1}Z'\right)x'$ and solve for $F'_x = F_x\left(Z^{-1}Z'\right)$ and $G'_x = G_x\left(Z^{-1}Z'\right)$. Furthermore, it was shown in Chapter 2 that because $Zx = Z'x' = f(x,u)$, Z' can be solved explicitly from Z. Thus only the first representation needs to be evaluated, and the second representation can then be calculated. Likewise the third representation is related by a transformation matrix $T'' = Z^{-1}$, and can be used to solve for $F''_x = F_x\left(Z^{-1}\right)$ and $G''_x = G_x\left(Z^{-1}\right)$.

Recalling the standard state space form for these equations (Equation 6.60) we can then write the state space matrices $\{A,B,C,D\}$ for all three representations in terms of the matrices $\{Z, F_x, F_u, G_x, G_u\}$ (Equations 6.61 - 6.63).

$$\begin{aligned} \dot{x} &= Adx + Bdu \\ dy &= Cdx + Ddu \end{aligned} \tag{6.60}$$

$$\begin{aligned} A &= Z^{-1}F_x \\ B &= Z^{-1}F_u \\ C &= G_x \\ D &= G_u \end{aligned} \tag{6.61}$$

$$\begin{aligned} A' &= Z'^{-1}F_x Z^{-1}Z' \\ B' &= Z'^{-1}F_u \\ C' &= G_x Z^{-1}Z' \\ D' &= G_u \end{aligned} \tag{6.62}$$

$$
\begin{aligned}
A'' &= F_x Z^{-1} \\
B'' &= F_u \\
C'' &= G_x Z^{-1} \\
D'' &= G_u
\end{aligned}
\tag{6.63}
$$

The evaluation of these equations at the highway operating condition yields the following matrices (Equations 6.64 - 6.73).

$$
A = \begin{bmatrix} -16.202 & -1711.7 & 2706.5 \\ -0.31485 & -33.263 & 52.593 \\ 0.0030427 & 0.2912 & -0.6006 \end{bmatrix} \tag{6.64}
$$

$$
A' = \begin{bmatrix} -49.465 & 8.9885e6 & 2696.7 \\ 0 & 0 & 0 \\ 0.0087329 & -1534.9 & -0.6006 \end{bmatrix} \tag{6.65}
$$

$$
A'' = \begin{bmatrix} -49.465 & -6170.6 & 0.50826 \\ 0 & 0 & 0 \\ 46.335 & 5930.1 & -0.6006 \end{bmatrix} \tag{6.66}
$$

$$
B = \begin{bmatrix} 2.3271e7 & 4.6506e7 & 35937 & 0 & 0 \\ 1.5574e5 & 3.1117e5 & 240.47 & 0 & 0 \\ 0 & 0 & 0 & 0.092348 & -1.8354 \end{bmatrix} \tag{6.67}
$$

$$
B' = \begin{bmatrix} 5.152e5 & -2.0359e5 & 160.49 & 0 & 0 \\ 1 & -1 & 0 & 0 & 0 \\ 0 & 0 & 0 & 0.092348 & -1.8354 \end{bmatrix} \tag{6.68}
$$

$$
B'' = \begin{bmatrix} 56.467 & 112.86 & 0.087208 & 0 & 0 \\ 1 & -1 & 0 & 0 & 0 \\ 0 & 0 & 0 & 0.26625 & -5.2917 \end{bmatrix} \tag{6.69}
$$

$$
C = \begin{bmatrix} 1 & 0 & 0 \\ 0 & 2 & 0 \\ 0 & 0 & 1 \\ 0 & 0 & 0.23025 \\ 0.0061247 & 0.39706 & 0 \\ 3.7011e-6 & -0.00019046 & 0 \end{bmatrix} \tag{6.70}
$$

$$
C' = \begin{bmatrix} 223.92 & -9.2094e7 & 0 \\ 2.9967 & -1.2324e6 & 0 \\ 0 & 0 & 1 \\ 0 & 0 & 0.23025 \\ 1.9664 & -8.0872e5 & 0 \\ 0.00054338 & -223.49 & 0 \end{bmatrix} \tag{6.71}
$$

$$C'' = \begin{bmatrix} 4.1209e5 & 1847 & 0 \\ 5515 & 71.782 & 0 \\ 0 & 0 & 0.34685 \\ 0 & 0 & 0.079861 \\ 3618.8 & 25.563 & 0 \\ 1 & 0 & 0 \end{bmatrix} \tag{6.72}$$

$$D = D' = D'' = \begin{bmatrix} 0 & 0 & 0 & 0 & 0 \\ 0 & 0 & -1 & 0 & 0 \\ 0 & 0 & 0 & 0 & 0 \\ 0 & 0 & 0 & 0.76975 & -0.98402 \\ 0 & 0 & -0.57295 & 0 & 0 \\ 0 & 0 & 0 & 0 & 0 \end{bmatrix} \tag{6.73}$$

6.11.4 Evaporator

Recall that the evaporator could be modeled with several different choices of state variables, depending on the derivation approach. Three possible choices of states are given as $x = [L_1 \quad P_e \quad h_{out} \quad T_{w1} \quad T_{w2}]^T$, $x' = [L_1 \quad P_e \quad m_e \quad T_{w1} \quad T_{w2}]^T$, and $x'' = [\tilde{U}_1 \quad \tilde{U}_2 \quad \tilde{m}_e \quad \tilde{E}_{w1} \quad \tilde{E}_{w2}]^T$. The different models are denoted as $Z(x,u)x = f(x,u)$, $Z'(x',u')x' = f(x',u')$, and $x'' = f(x'',u'')$, where the function $f(x,u)$ is defined in Equation 6.74, and the matrices $Z(x,u)$ and $Z'(x',u')$ are defined in Chapter 4. The model outputs are given as nonlinear functions of the states and inputs, $y = g(x,u)$. Let the inputs and outputs for the first representation be defined by Equations 6.75 and 6.76.

$$f(x,u) = \begin{bmatrix} \dot{m}_{in}(h_{in} - h_g) + a_{i1}A_i\left(\frac{L_1}{L_{Total}}\right)(T_{w1} - T_{r1}) \\ \dot{m}_{out}(h_g - h_{out}) + a_{i2}A_i\left(\frac{L_2}{L_{Total}}\right)(T_{w2} - T_{r2}) \\ \dot{m}_{in} - \dot{m}_{out} \\ a_o A_o(T_a - T_{w1}) - a_{i1}A_i(T_{w1} - T_{r1}) \\ a_o A_o(T_a - T_{w2}) - a_{i2}A_i(T_{w2} - T_{r2}) \end{bmatrix} \tag{6.74}$$

$$u = [\dot{m}_{in} \quad \dot{m}_{out} \quad h_{in} \quad T_{a,in} \quad \dot{m}_a]^T \tag{6.75}$$

$$y = [L_1 \quad P_e \quad h_{out} \quad T_{w1} \quad T_{w2} \quad T_{a,out} \quad T_{r,out} \quad T_{r,sh} \quad m_e]^T \tag{6.76}$$

Several assumptions are made to define the output relationships, as well as explicitly relate intermediate variables to states or inputs. The assumptions regarding the air temperature T_a are the same for all representations. For heat transfer an average air temperature across the evaporator is assumed (Equation 6.77). The energy balance for the air given a heat exchanger with n regions is given in Equation 6.78. Solving for T_a (Equation 6.79) and simplifying the expression assuming two regions results in Equation 6.80.

$$T_a = \frac{T_{a,in} + T_{a,out}}{2} \tag{6.77}$$

$$\dot{m}_{air} C_{p,air} \left(T_{a,in} - T_{a,out}\right) = a_o A_o \left[\sum_{i=1}^{n} \frac{L_i}{L_{Total}} \left(T_a - T_{w,i}\right)\right] \tag{6.78}$$

$$T_a = \frac{2 \cdot \dot{m}_{air} C_{p,air} T_{a,in} + a_o A_o \left[\sum_{i=1}^{n} \frac{L_i T_{w,i}}{L_{Total}}\right]}{2 \cdot \dot{m}_{air} C_{p,air} + a_o A_o} \tag{6.79}$$

$$T_a = \frac{2 \cdot \dot{m}_{air} C_{p,air} T_{a,in} + a_o A_o \left[\frac{L_1 T_{w,1}}{L_{Total}} + \frac{L_2 T_{w,2}}{L_{Total}}\right]}{2 \cdot \dot{m}_{air} C_{p,air} + a_o A_o} \tag{6.80}$$

For the linearization, the partial derivatives of the average air temperature are required. First recall that the air-side heat transfer coefficient is a function of mass flow rate of air. Specifically, we assume that the heat transfer coefficient scales with Reynold's number (where the prime denotes initial values) as given in Equation 6.81. Thus the partial derivative of heat transfer coefficient with respect to mass flow rate of air can be written as Equation 6.82. The partial derivatives of air temperature are then given in Equations 6.83 - 6.87.

$$\frac{a_o}{a'_o} = \left(\frac{\mathrm{Re}_l}{\mathrm{Re}'_l}\right)^m = \left(\frac{\dot{m}_{air}}{\dot{m}'_{air}}\right)^m \tag{6.81}$$

$$\frac{\partial a_o}{\partial \dot{m}_{air}} = m \left(\frac{\dot{m}_{air}}{\dot{m}'_{air}}\right)^m \left(\frac{a'_o}{\dot{m}_{air}}\right) \tag{6.82}$$

$$\frac{\partial T_a}{\partial L_1} = \frac{a_o A_o \left(\frac{T_{w,1} - T_{w,2}}{L_{Total}}\right)}{2 \cdot \dot{m}_{air} C_{p,air} + a_o A_o} \tag{6.83}$$

$$\frac{\partial T_a}{\partial T_{w,1}} = \frac{a_o A_o \left(\frac{L_1}{L_{Total}}\right)}{2 \cdot \dot{m}_{air} C_{p,air} + a_o A_o} \tag{6.84}$$

$$\frac{\partial T_a}{\partial T_{w,2}} = \frac{a_o A_o \left(\frac{L_2}{L_{Total}}\right)}{2 \cdot \dot{m}_{air} C_{p,air} + a_o A_o} \tag{6.85}$$

$$\frac{\partial T_a}{\partial T_{a,in}} = \frac{2 \cdot \dot{m}_{air} C_{p,air}}{2 \cdot \dot{m}_{air} C_{p,air} + a_o A_o} \tag{6.86}$$

$$\frac{\partial T_a}{\partial \dot{m}_{air}} = \frac{2 \cdot C_{p,air} A_o \left(T_{a,in} - \left(\frac{L_1}{L_{Total}} \right) T_{w,1} - \left(\frac{L_2}{L_{Total}} \right) T_{w,2} \right) \left(a_o - \dot{m}_{air} \frac{\partial a_o}{\partial \dot{m}_{air}} \right)}{\left(2 \cdot \dot{m}_{air} C_{p,air} + a_o A_o \right)^2} \tag{6.87}$$

Several assumptions are made to define the output relationships, as well as explicitly relate intermediate variables to states or inputs. These relationships differ for each representation. For the first representation, some of the outputs are states; the other outputs are defined as $T_{a,out} = 2T_a - T_{a,in}$, $T_{r,out} = T(P_e, h_{out})$, $T_{r,sh} = 2(T_{r2} - T_{r1})$, and $m_e = \left[r_f (1-\bar{g}) + r_g (\bar{g}) \right] A_{cs} L_1 + r_2 A_{cs} L_2$. Several intermediate variables are used in the model, and can be related thermodynamically to states or inputs. Because the fluid in the first region is assumed to be a combination of saturated liquid and saturated vapor, the properties for this region, $r_{f,g}$, $h_{f,g}$, and T_{r1}, are only a function of the evaporation pressure, P_e. In the second region the average refrigerant properties are calculated as $T_{r2} = T(P_e, h_2)$ and $r_2 = r(P_e, h_2)$. However, since $h_2 = \frac{h_g + h_{out}}{2}$ then $T_{r2} \approx \frac{T_{sat}(P_e) + T(P_e, h_{out})}{2}$, and for the partial derivatives of T_{r2} the approximations $\frac{\partial T_{r2}}{\partial P_e} = \frac{1}{2}\left(\frac{dT_{sat}}{dP_e} + \left. \frac{\partial T_{r,out}}{\partial P_e} \right|_{h_2} \right)$ and $\frac{\partial T_{r2}}{\partial h_{out}} = \frac{1}{2}\left(\left. \frac{\partial T_{r2}}{\partial h_2} \right|_{P_e} \right)$ are used. Similarly the following partial derivatives of r_2 are used: $\frac{\partial r_2}{\partial P_e} = \left(\left. \frac{\partial r_2}{\partial P_e} \right|_{h_2} \right) + \frac{1}{2}\left(\left. \frac{\partial r_2}{\partial h_2} \right|_{P_e} \right)\left(\frac{dh_g}{dP_e} \right)$ and $\frac{\partial r_2}{\partial h_{out}} = \frac{1}{2}\left(\left. \frac{\partial r_2}{\partial h_2} \right|_{P_e} \right)$. Finally, recall that mean void fraction is a function of the state variables, inputs, and the parameter S (slip ratio): $\bar{g} = f(P_e, h_{out}, h_{in}, S)$.

For the second representation, some of the outputs are again states; the other outputs are defined as $T_{a,out} = 2T_a - T_{a,in}$, $T_{r,out} = T(P_e, h_{out})$, $T_{r,sh} = 2(T_{r2} - T_{r1})$, and $h_{out} = 2h_2 - h_g$, where $h_2 = h(P_e, r_2)$, $r_2 = \frac{m_2}{A_{cs} L_2}$, $m_2 = m_e - m_1$, and $m_1 = \left[r_f (1-\bar{g}) + r_g (\bar{g}) \right] A_{cs} L_1$. Additionally, the following partial derivatives are used: $\frac{\partial r_2}{\partial L_1} = \frac{L_{Total}}{(L_2)^2}\left[\frac{m_e}{A_{cs} L_{Total}} - \left(r_f (1-\bar{g}) + r_g (\bar{g}) \right) \right]$, $\frac{\partial r_2}{\partial P_e} = -\left(\frac{L_1}{L_2} \right)\left[\frac{dr_f}{dP_e}(1-\bar{g}) + \frac{dr_g}{dP_e}(\bar{g}) \right]$, and $\frac{\partial r_2}{\partial m_e} = \left(\frac{1}{A_{cs} L_2} \right)$.

For the third representation, the partial derivatives with respect to the states and inputs are not derived explicitly, but calculated using a matrix transformation (see Section 6.11.4.2). Thus no assumptions about the output relationships or intermediate variables need to be made.

6.11.4.1 Symbolic Representation

For the first representation, the partial derivatives of the functions $f(x,u)$ and $g(x,u)$ with respect to the states and inputs are defined in Equations 6.88 - 6.91, with the matrix elements listed in Table 6.14.

$$\frac{\partial f}{\partial x} = F_x = \begin{bmatrix} f_{x,11} & f_{x,12} & 0 & f_{x,14} & 0 \\ f_{x,21} & f_{x,22} & f_{x,23} & 0 & f_{x,25} \\ 0 & 0 & 0 & 0 & 0 \\ f_{x,41} & f_{x,42} & 0 & f_{x,44} & f_{x,45} \\ f_{x,51} & f_{x,52} & f_{x,53} & f_{x,54} & f_{x,55} \end{bmatrix} \tag{6.88}$$

$$\frac{\partial f}{\partial u} = F_u = \begin{bmatrix} f_{u,11} & 0 & f_{u,13} & 0 & 0 \\ 0 & f_{u,22} & 0 & 0 & 0 \\ f_{u,31} & f_{u,32} & 0 & 0 & 0 \\ 0 & 0 & 0 & f_{u,44} & f_{u,45} \\ 0 & 0 & 0 & f_{u,54} & f_{u,55} \end{bmatrix} \tag{6.89}$$

$$\frac{\partial g}{\partial x} = G_x = \begin{bmatrix} 1 & 0 & 0 & 0 & 0 \\ 0 & 1 & 0 & 0 & 0 \\ 0 & 0 & 1 & 0 & 0 \\ 0 & 0 & 0 & 1 & 0 \\ 0 & 0 & 0 & 0 & 1 \\ g_{x,61} & 0 & 0 & g_{x,64} & g_{x,65} \\ 0 & g_{x,72} & g_{x,73} & 0 & 0 \\ 0 & g_{x,82} & g_{x,83} & 0 & 0 \\ g_{x,91} & g_{x,92} & g_{x,93} & 0 & 0 \end{bmatrix} \tag{6.90}$$

$$\frac{\partial g}{\partial u} = G_u = \begin{bmatrix} 0 & 0 & 0 & 0 & 0 \\ 0 & 0 & 0 & 0 & 0 \\ 0 & 0 & 0 & 0 & 0 \\ 0 & 0 & 0 & 0 & 0 \\ 0 & 0 & 0 & 0 & 0 \\ 0 & 0 & 0 & g_{u,64} & g_{u,65} \\ 0 & 0 & 0 & 0 & 0 \\ 0 & 0 & 0 & 0 & 0 \\ 0 & 0 & g_{u,93} & 0 & 0 \end{bmatrix} \tag{6.91}$$

Table 6.14 Matrix Elements of Equations 6.88 - 6.91

$f_{x,11}$	$\frac{a_{i1}A_i}{L_{Total}}(T_{w1}-T_{r1})$
$f_{x,12}$	$-\dot{m}_{in}\frac{dh_g}{dP_e}-a_{i1}A_i\frac{L_1}{L_{Total}}\left(\frac{dT_{r1}}{dP_e}\right)$
$f_{x,14}$	$a_{i1}A_i\frac{L_1}{L_{Total}}$
$f_{x,21}$	$-\frac{a_{i2}A_i}{L_{Total}}(T_{w2}-T_{r2})$
$f_{x,22}$	$\dot{m}_{out}\frac{dh_g}{dP_e}-a_{i2}A_i\frac{L_2}{L_{Total}}\left(\frac{\partial T_{r2}}{\partial P_e}\right)$
$f_{x,23}$	$-\dot{m}_{out}-a_{i2}A_i\frac{L_2}{L_{Total}}\left(\frac{\partial T_{r2}}{\partial h_{out}}\right)$
$f_{x,25}$	$a_{i2}A_i\frac{L_2}{L_{Total}}$
$f_{x,41}$	$a_oA_o\left(\frac{\partial T_a}{\partial L_1}\right)$
$f_{x,42}$	$a_{i1}A_i\left(\frac{dT_{r1}}{dP_e}\right)$
$f_{x,44}$	$-a_{i1}A_i-a_oA_o+a_oA_o\left(\frac{\partial T_a}{\partial T_{w1}}\right)$
$f_{x,45}$	$a_oA_o\left(\frac{\partial T_a}{\partial T_{w2}}\right)$
$f_{x,51}$	$a_oA_o\left(\frac{\partial T_a}{\partial L_1}\right)$
$f_{x,52}$	$a_{i2}A_i\left(\frac{\partial T_{r2}}{\partial P_e}\right)$
$f_{x,53}$	$a_{i2}A_i\left(\frac{\partial T_{r2}}{\partial h_{out}}\right)$

Table 6.8 (cont.)

$f_{x,54}$	$\alpha_o A_o \left(\frac{\partial T_a}{\partial T_{w1}} \right)$
$f_{x,55}$	$-\alpha_{i2} A_i - \alpha_o A_o + \alpha_o A_o \left(\frac{\partial T_a}{\partial T_{w2}} \right)$
$f_{u,11}$	$h_{in} - h_g$
$f_{u,13}$	$\dot{m}_{in}$
$f_{u,22}$	$h_g - h_{out}$
$f_{u,31}$	1
$f_{u,32}$	-1
$f_{u,44}$	$\alpha_o A_o \left(\frac{\partial T_a}{\partial T_{ai}} \right)$
$f_{u,45}$	$\left(\frac{\partial \alpha_o}{\partial \dot{m}_{air}} \right) A_o \left(T_a - T_{w1} \right) + \alpha_o A_o \left(\frac{\partial T_a}{\partial \dot{m}_{air}} \right)$
$f_{u,54}$	$\alpha_o A_o \left(\frac{\partial T_a}{\partial T_{ai}} \right)$
$f_{u,55}$	$\left(\frac{\partial \alpha_o}{\partial \dot{m}_{air}} \right) A_o \left(T_a - T_{w2} \right) + \alpha_o A_o \left(\frac{\partial T_a}{\partial \dot{m}_{air}} \right)$
$g_{x,61}$	$2\left(\frac{\partial T_a}{\partial L_1} \right)$
$g_{x,64}$	$2\left(\frac{\partial T_a}{\partial T_{w1}} \right)$
$g_{x,65}$	$2\left(\frac{\partial T_a}{\partial T_{w2}} \right)$
$g_{x,72}$	$\left(\frac{\partial T_{r,out}}{\partial P_e} \Big\vert_{h_{out}} \right)$
$g_{x,73}$	$\left(\frac{\partial T_{r,out}}{\partial h_{out}} \Big\vert_{P_e} \right)$

Table 6.8 (cont.)

$g_{x,82}$	$\left(\left.\frac{\partial T_{r,out}}{\partial P_e}\right\|_{h_{out}}\right)-\left(\frac{dT_{r1}}{dP_e}\right)$
$g_{x,83}$	$\left(\left.\frac{\partial T_{r,out}}{\partial h_{out}}\right\|_{P_e}\right)$
$g_{x,91}$	$[[r_f(1-\bar{g})+r_g(\bar{g})]-r_2]A_{cs}$
g_{x92}	$\left[\left[\left(\frac{dr_f}{dP_e}\right)(1-\bar{g})+\left(\frac{dr_g}{dP_e}\right)(\bar{g})\right]+(r_g-r_f)\left(\frac{d\bar{g}}{dP_e}\right)\right]A_{cs}L_1+\left(\left.\frac{\partial r_2}{\partial P_e}\right\|_{h_2}\right)A_{cs}L_2$
$g_{x,93}$	$\frac{1}{2}\left(\left.\frac{\partial r_2}{\partial h_2}\right\|_{P_e}\right)A_{cs}L_2$
$g_{u,65}$	$2\left(\frac{\partial T_a}{\partial T_{ai}}\right)-1$
$g_{u,66}$	$2\left(\frac{\partial T_a}{\partial m_a}\right)$
$g_{u,93}$	$\left[(r_g-r_f)\left(\frac{d\bar{g}}{dh_{in}}\right)\right]A_{cs}L_1$

For the second representation, the partial derivatives of the functions $f(x',u')$ and $g(x',u')$ with respect to the states and inputs are defined in Equations 6.92 - 6.95, with the matrix elements listed in Table 6.15.

$$\frac{\partial f}{\partial x'}=F_x'=\begin{bmatrix} f'_{x,11} & f'_{x,12} & 0 & f'_{x,14} & 0 \\ f'_{x,21} & f'_{x,22} & f'_{x,23} & 0 & f'_{x,25} \\ 0 & 0 & 0 & 0 & 0 \\ f'_{x,41} & f'_{x,42} & 0 & f'_{x,44} & f'_{x,45} \\ f'_{x,51} & f'_{x,52} & f'_{x,53} & f'_{x,54} & f'_{x,55} \end{bmatrix} \tag{6.92}$$

$$\frac{\partial f}{\partial u'}=F_u'=\begin{bmatrix} f'_{u,11} & 0 & f'_{u,13} & 0 & 0 \\ 0 & f'_{u,22} & 0 & 0 & 0 \\ f'_{u,31} & f'_{u,32} & 0 & 0 & 0 \\ 0 & 0 & 0 & f'_{u,44} & f'_{u,45} \\ 0 & 0 & 0 & f'_{u,54} & f'_{u,55} \end{bmatrix} \tag{6.93}$$

$$\frac{\partial g}{\partial x'} = G'_x = \begin{bmatrix} 1 & 0 & 0 & 0 & 0 \\ 0 & 1 & 0 & 0 & 0 \\ g'_{x,31} & g'_{x,32} & g'_{x,33} & 0 & 0 \\ 0 & 0 & 0 & 1 & 0 \\ 0 & 0 & 0 & 0 & 1 \\ g'_{x,61} & 0 & 0 & g'_{x,64} & g'_{x,65} \\ g'_{x,71} & g'_{x,72} & g'_{x,73} & 0 & 0 \\ g'_{x,81} & g'_{x,82} & g'_{x,83} & 0 & 0 \\ 0 & 0 & 1 & 0 & 0 \end{bmatrix} \tag{6.94}$$

$$\frac{\partial g}{\partial u'} = G'_u = \begin{bmatrix} 0 & 0 & 0 & 0 & 0 \\ 0 & 0 & 0 & 0 & 0 \\ 0 & 0 & 0 & 0 & 0 \\ 0 & 0 & 0 & 0 & 0 \\ 0 & 0 & 0 & 0 & 0 \\ 0 & 0 & 0 & g'_{u,64} & g'_{u,65} \\ 0 & 0 & 0 & 0 & 0 \\ 0 & 0 & 0 & 0 & 0 \\ 0 & 0 & 0 & 0 & 0 \end{bmatrix} \tag{6.95}$$

Table 6.15 Matrix Elements of Equations 6.92 - 6.95

$f'_{x,11}$	$\frac{a_{i1}A_i}{L_{Total}}(T_{w1} - T_{r1})$
$f'_{x,12}$	$-\dot{m}_{in}\frac{dh_g}{dP_e} - a_{i1}A_i\frac{L_1}{L_{Total}}\left(\frac{dT_{r1}}{dP_e}\right)$
$f'_{x,14}$	$a_{i1}A_i\frac{L_1}{L_{Total}}$
$f'_{x,21}$	$-2\dot{m}_{out}\left(\left.\frac{\partial h_2}{\partial r_2}\right\|_{P_e}\right)\left(\frac{\partial r_2}{\partial L_1}\right) - \frac{a_{i2}A_i}{L_{Total}}(T_{w2} - T_{r2}) - a_{i2}A_i\frac{L_2}{L_{Total}}\left(\left.\frac{\partial T_{r2}}{\partial r_2}\right\|_{P_e}\right)\left(\frac{\partial r_2}{\partial L_1}\right)$
$f'_{x,22}$	$\dot{m}_{out}\frac{dh_g}{dP_e} - 2\dot{m}_{out}\left(\left(\left.\frac{\partial h_2}{\partial P_e}\right\|_{r_2}\right) + \left(\left.\frac{\partial h_2}{\partial r_2}\right\|_{P_e}\right)\left(\frac{\partial r_2}{\partial P_e}\right)\right)$ $-a_{i2}A_i\frac{L_2}{L_{Total}}\left(\left(\left.\frac{\partial T_{r2}}{\partial P_e}\right\|_{r_2}\right) + \left(\left.\frac{\partial T_{r2}}{\partial r_2}\right\|_{P_e}\right)\left(\frac{\partial r_2}{\partial P_e}\right)\right)$

Table 6.9 (cont.)

$f'_{x,23}$	$-2\dot{m}_{out}\left(\left.\frac{\partial h_2}{\partial r_2}\right\|_{P_e}\right)\left(\frac{\partial r_2}{\partial m_e}\right)-a_{i2}A_i\frac{L_2}{L_{Total}}\left(\left.\frac{\partial T_{r2}}{\partial r_2}\right\|_{P_e}\right)\left(\frac{\partial r_2}{\partial m_e}\right)$
$f'_{x,25}$	$a_{i2}A_i\frac{L_2}{L_{Total}}$
$f'_{x,41}$	$a_oA_o\left(\frac{\partial T_a}{\partial L_1}\right)$
$f'_{x,42}$	$a_{i1}A_i\left(\frac{dT_{r1}}{dP_e}\right)$
$f'_{x,44}$	$-a_{i1}A_i-a_oA_o+a_oA_o\left(\frac{\partial T_a}{\partial T_{w1}}\right)$
$f'_{x,45}$	$a_oA_o\left(\frac{\partial T_a}{\partial T_{w2}}\right)$
$f'_{x,51}$	$a_oA_o\left(\frac{\partial T_a}{\partial L_1}\right)+a_{i2}A_i\left(\left.\frac{\partial T_{r2}}{\partial r_2}\right\|_{P_e}\right)\left(\frac{\partial r_2}{\partial L_1}\right)$
$f'_{x,52}$	$a_{i2}A_i\left(\left(\left.\frac{\partial T_{r2}}{\partial P_e}\right\|_{r_2}\right)+\left(\left.\frac{\partial T_{r2}}{\partial r_2}\right\|_{P_e}\right)\left(\frac{\partial r_2}{\partial P_e}\right)\right)$
$f'_{x,53}$	$a_{i2}A_i\left(\left.\frac{\partial T_{r2}}{\partial r_2}\right\|_{P_e}\right)\left(\frac{\partial r_2}{\partial m_e}\right)$
$f'_{x,54}$	$a_oA_o\left(\frac{\partial T_a}{\partial T_{w1}}\right)$
$f'_{x,55}$	$-a_{i2}A_i-a_oA_o+a_oA_o\left(\frac{\partial T_a}{\partial T_{w2}}\right)$
$f'_{u,11}$	$h_{in}-h_g$
$f'_{u,13}$	$\dot{m}_{in}$
$f'_{u,22}$	h_g-h_{out}
$f'_{u,31}$	1
$f'_{u,32}$	-1
$f'_{u,44}$	$a_oA_o\left(\frac{\partial T_a}{\partial T_{ai}}\right)$

Table 6.9 (cont.)

$f'_{u,45}$	$\left(\frac{\partial a_o}{\partial \dot{m}_{air}}\right)A_o(T_a - T_{w1}) + a_o A_o\left(\frac{\partial T_a}{\partial \dot{m}_{air}}\right)$
$f'_{u,54}$	$a_o A_o\left(\frac{\partial T_a}{\partial T_{ai}}\right)$
$f'_{u,55}$	$\left(\frac{\partial a_o}{\partial \dot{m}_{air}}\right)A_o(T_a - T_{w2}) + a_o A_o\left(\frac{\partial T_a}{\partial \dot{m}_{air}}\right)$
$g'_{x,31}$	$2\left(\left.\frac{\partial h_2}{\partial r_2}\right\|_{P_e}\right)\left(\frac{\partial r_2}{\partial L_1}\right)$
$g'_{x,32}$	$2\left[\left(\left.\frac{\partial h_2}{\partial P_e}\right\|_{r_2}\right) + \left(\left.\frac{\partial h_2}{\partial r_2}\right\|_{P_e}\right)\left(\frac{\partial r_2}{\partial P_e}\right)\right] - \left(\frac{dh_g}{dP_e}\right)$
$g'_{x,33}$	$2\left(\left.\frac{\partial h_2}{\partial r_2}\right\|_{P_e}\right)\left(\frac{\partial r_2}{\partial m_e}\right)$
$g'_{x,61}$	$2\left(\frac{\partial T_a}{\partial L_1}\right)$
$g'_{x,64}$	$2\left(\frac{\partial T_a}{\partial T_{w1}}\right)$
$g'_{x,65}$	$2\left(\frac{\partial T_a}{\partial T_{w2}}\right)$
$g'_{x,71}$	$2\left(\left(\left.\frac{\partial T_{r2}}{\partial r_2}\right\|_{P_e}\right)\right)\left(\frac{\partial r_2}{\partial L_1}\right)$
$g'_{x,72}$	$2\left[\left(\left.\frac{\partial T_{r2}}{\partial P_e}\right\|_{r_2}\right) + \left(\left.\frac{\partial T_{r2}}{\partial r_2}\right\|_{P_e}\right)\left(\frac{\partial r_2}{\partial P_e}\right)\right] - \left(\frac{dT_{r1}}{dP_e}\right)$
$g'_{x,73}$	$2\left(\left.\frac{\partial T_{r2}}{\partial r_2}\right\|_{P_e}\right)\left(\frac{\partial r_2}{\partial m_e}\right)$
$g'_{x,81}$	$2\left(\left.\frac{\partial T_{r2}}{\partial r_2}\right\|_{P_e}\right)\left(\frac{\partial r_2}{\partial L_1}\right)$
$g'_{x,82}$	$2\left[\left(\left.\frac{\partial T_{r2}}{\partial P_e}\right\|_{r_2}\right) + \left(\left.\frac{\partial T_{r2}}{\partial r_2}\right\|_{P_e}\right)\left(\frac{\partial r_2}{\partial P_e}\right) - \left(\frac{dT_{r1}}{dP_e}\right)\right]$

Table 6.9 (cont.)

$g'_{x,83}$	$2\left(\left.\frac{\partial T_{r2}}{\partial r_2}\right\|_{P_e}\right)\left(\frac{\partial r_2}{\partial m_e}\right)$
$g'_{u,64}$	$2\left(\frac{\partial T_a}{\partial T_{ai}}\right)-1$
$g'_{u,65}$	$2\left(\frac{\partial T_a}{\partial m_a}\right)$

For the third representation, the partial derivatives of the functions $f(x'',u'')$ and $g(x'',u'')$ with respect to the states and inputs are calculated by means of a transformation matrix (see Section 6.11.4.2).

6.11.4.2 Numerical Representation

The numerical evaluation of these equations can be done using the explicit formulas given in this section. Alternatively, because these representations are simply related by a state transformation, any of the three given representations can be calculated with knowledge of one of the other representations. For example, since $Zx = Z'x'$, the transformation $T' = Z^{-1}Z'$ can be used to substitute $x = \left(Z^{-1}Z'\right)x'$ and solve for $F'_x = F_x\left(Z^{-1}Z'\right)$ and $G'_x = G_x\left(Z^{-1}Z'\right)$. Furthermore, it was shown in Chapter 2 that because $Zx = Z'x' = f(x,u)$, Z' can be solved explicitly from Z. Thus only the first representation needs to be evaluated, and the second representation can then be calculated. Likewise the third representation is related by a transformation matrix $T'' = Z^{-1}$, and can be used to solve for $F''_x = F_x\left(Z^{-1}\right)$ and $G''_x = G_x\left(Z^{-1}\right)$.

Recalling the standard state space form for these equations (Equation 6.96) we can then write the state space matrices $\{A,B,C,D\}$ for all three representations in terms of the matrices $\{Z,F_x,F_u,G_x,G_u\}$ (Equations 6.97 - 6.99).

$$\begin{aligned} \dot{x} &= Adx + Bdu \\ dy &= Cdx + Ddu \end{aligned} \tag{6.96}$$

$$\begin{aligned} A &= Z^{-1}F_x \\ B &= Z^{-1}F_u \\ C &= G_x \\ D &= G_u \end{aligned} \tag{6.97}$$

$$\begin{aligned} A' &= Z'^{-1}F_x Z^{-1}Z' \\ B' &= Z'^{-1}F_u \\ C' &= G_x Z^{-1}Z' \\ D' &= G_u \end{aligned} \tag{6.98}$$

$$
\begin{aligned}
A'' &= F_x Z^{-1} \\
B'' &= F_u \\
C'' &= G_x Z^{-1} \\
D'' &= G_u
\end{aligned}
\tag{6.99}
$$

The evaluation of these equations at the highway operating condition yields the following matrices (Equations 6.100 - 6.109).

$$
A = \begin{bmatrix}
-1.3172 & 0.019652 & -0.0034846 & -1.8206 & 0.0077459 \\
-95.781 & -13.987 & -80.326 & 1080.3 & 178.56 \\
-556.93 & -1.0525 & -50.097 & -33.407 & 111.36 \\
-0.078365 & 0.016212 & 0 & -1.5469 & 0.0066648 \\
-15.566 & 0.23949 & 0.1724 & -21.378 & -0.7134
\end{bmatrix}
\tag{6.100}
$$

$$
A' = \begin{bmatrix}
-2.6367 & 0.017536 & 221.09 & -1.8206 & 0.0077459 \\
-30512 & -62.765 & 5.0966e6 & 1080.3 & 178.56 \\
0 & 0 & 0 & 0 & 0 \\
-0.078365 & 0.016212 & 0 & -1.5469 & 0.0066648 \\
49.712 & 0.34417 & -10938 & -21.378 & -0.7134
\end{bmatrix}
\tag{6.101}
$$

$$
A' = \begin{bmatrix}
-12.999 & -17.483 & -2988.7 & 1.2049 & 0 \\
-1.2575 & -52.312 & -733.44 & 0 & 0.13311 \\
0 & 0 & 0 & 0 & 0 \\
14.535 & 21.746 & 3717.4 & -1.5469 & 0.0066648 \\
16.045 & 189.24 & 3100.1 & 0.029154 & -0.80448
\end{bmatrix}
\tag{6.102}
$$

$$
B = \begin{bmatrix}
59.205 & -4.9659 & -0.030496 & 0 & 0 \\
73734 & -1.1447e5 & 18.095 & 0 & 0 \\
3744.5 & -7944.2 & -0.55957 & 0 & 0 \\
0 & 0 & 0 & 0.05994 & 9.8119 \\
696.13 & -58.389 & -0.35857 & 0.05994 & 7.5841
\end{bmatrix}
\tag{6.103}
$$

$$
B' = \begin{bmatrix}
59.205 & -4.9659 & -0.030496 & 0 & 0 \\
73734 & -1.1447e5 & 18.095 & 0 & 0 \\
3744.5 & -7944.2 & -0.55957 & 0 & 0 \\
0 & 0 & 0 & 0.05994 & 9.8119 \\
696.13 & -58.389 & -0.35857 & 0.05994 & 7.5841
\end{bmatrix}
\tag{6.104}
$$

$$
B' = \begin{bmatrix}
-78.069 & 0 & 0.043604 & 0 & 0 \\
0 & -13.434 & 0 & 0 & 0 \\
1 & -1 & 0 & 0 & 0 \\
0 & 0 & 0 & 0.12951 & 21.199 \\
0 & 0 & 0 & 0.12951 & 16.386
\end{bmatrix}
\tag{6.105}
$$

$$C = \begin{bmatrix} 1 & 0 & 0 & 0 & 0 \\ 0 & 1 & 0 & 0 & 0 \\ 0 & 0 & 1 & 0 & 0 \\ 0 & 0 & 0 & 1 & 0 \\ 0 & 0 & 0 & 0 & 1 \\ -1.6367 & 0 & 0 & 0.6089 & 0.1392 \\ 0 & 0.012587 & 0.59651 & 0 & 0 \\ 0 & 0.0016356 & 0.59651 & 0 & 0 \\ 0.0059679 & 9.4734e-6 & -1.5761e-5 & 0 & 0 \end{bmatrix} \tag{6.106}$$

$$C' = \begin{bmatrix} 1 & 0 & 0 & 0 & 0 \\ 0 & 1 & 0 & 0 & 0 \\ 378.65 & 0.60725 & -63448 & 0 & 0 \\ 0 & 0 & 0 & 1 & 0 \\ 0 & 0 & 0 & 0 & 1 \\ -1.6367 & 0 & 0 & 0.6089 & 0.1392 \\ 225.87 & 0.37482 & -37848 & 0 & 0 \\ 225.87 & 0.36386 & -37848 & 0 & 0 \\ 0 & 0 & 1 & 0 & 0 \end{bmatrix} \tag{6.107}$$

$$C'' = \begin{bmatrix} -0.69939 & 0.026933 & 4.6041 & 0 & 0 \\ 414.98 & 620.84 & 1.0613.e5 & 0 & 0 \\ -12.833 & 387.2 & 2742.7 & 0 & 0 \\ 0 & 0 & 0 & 0.46284 & 0 \\ -8.2234 & 0.31667 & 54.135 & 0 & 0.46284 \\ 0 & 0 & 0 & 0.28182 & 0.064427 \\ -2.4317 & 238.79 & 2971.9 & 0 & 0 \\ -6.9763 & 231.99 & 1809.6 & 0 & 0 \\ -4.0387e-5 & -6.0422e-5 & 0.98967 & 0 & 0 \end{bmatrix} \tag{6.108}$$

$$D = D' = D'' = \begin{bmatrix} 0 & 0 & 0 & 0 & 0 \\ 0 & 0 & 0 & 0 & 0 \\ 0 & 0 & 0 & 0 & 0 \\ 0 & 0 & 0 & 0 & 0 \\ 0 & 0 & 0 & 0 & 0 \\ 0 & 0 & 0 & 0.2519 & 16.784 \\ 0 & 0 & 0 & 0 & 0 \\ 0 & 0 & 0 & 0 & 0 \\ 0 & 0 & 0 & 0 & 0 \end{bmatrix} \tag{6.109}$$

6.11.5 Internal Heat Exchanger

Recall that the internal heat exchanger was modeled with three differential equations (Equations 6.110 - 6.112), where $T_{h,ave} = \frac{T_{h,in} + T_{h,out}}{2}$ and $T_{c,ave} = \frac{T_{c,in} + T_{c,out}}{2}$. Thus the outlet temperatures are calculated as $T_{h,out} = 2T_{h,ave} - T_{h,in}$ and $T_{c,out} = 2T_{c,ave} - T_{c,in}$. The states are assumed to be $x = \begin{bmatrix} T_{h,ave} & T_{c,ave} & T_{wall} \end{bmatrix}^T$.

$$\dot{m}_h\left(h_{h,in}-h_{h,out}\right)-a_h A_h\left(T_{h,ave}-T_{wall}\right)=\left(rVC_p\right)_h\dot{T}_{h,ave} \tag{6.110}$$

$$\dot{m}_c\left(h_{c,in}-h_{c,out}\right)-a_c A_c\left(T_{c,ave}-T_{wall}\right)=\left(rVC_p\right)_c\dot{T}_{c,ave} \tag{6.111}$$

$$a_c A_c\left(T_{c,ave}-T_{wall}\right)+a_h A_h\left(T_{h,ave}-T_{wall}\right)=\left(rVC_p\right)_{wall}\dot{T}_{wall} \tag{6.112}$$

To simplify the implicit nature of these equations for linearization, the assumptions are made that $h_{h,in}-h_{h,out}\approx C_{p_h}\left(T_{h,in}-T_{h,out}\right)$ and $h_{c,in}-h_{c,out}\approx C_{p_c}\left(T_{c,in}-T_{c,out}\right)$. This assumption of average specific heats will admittedly fail near the critical point. This problem will be addressed in future models of the heat exchanger. After substitution, the differential equations are given in Equations 6.113 - 6.115.

$$2\dot{m}_h C_{p_h}\left(T_{h,in}-T_{h,ave}\right)-a_h A_h\left(T_{h,ave}-T_{wall}\right)=\left(rVC_p\right)_h\dot{T}_{h,ave} \tag{6.113}$$

$$2\dot{m}_c C_{p_c}\left(T_{c,in}-T_{c,ave}\right)-a_c A_c\left(T_{c,ave}-T_{wall}\right)=\left(rVC_p\right)_c\dot{T}_{c,ave} \tag{6.114}$$

$$a_c A_c\left(T_{c,ave}-T_{wall}\right)+a_h A_h\left(T_{h,ave}-T_{wall}\right)=\left(rVC_p\right)_{wall}\dot{T}_{wall} \tag{6.115}$$

6.11.5.1 Symbolic Representation

The inputs and outputs are given in Equation 6.116 and 6.117. The partial derivatives of the differential equations $f(x,u)$ and output equations $g(x,u)$ with respect to the states and inputs are defined in Equations 6.118 - 6.121, with the matrix elements listed in Table 6.16.

$$u=\begin{bmatrix}\dot{m}_h & \dot{m}_c & P_h & P_c & h_{h,in} & h_{c,in}\end{bmatrix}^T \tag{6.116}$$

$$y=\begin{bmatrix}h_{h,out} & h_{c,out} & T_{h,out} & T_{c,out}\end{bmatrix}^T \tag{6.117}$$

$$\frac{\partial f}{\partial x}=F_x=\begin{bmatrix}f_{x,11} & 0 & f_{x,13}\\ 0 & f_{x,22} & f_{x,23}\\ f_{x,31} & f_{x,32} & f_{x,33}\end{bmatrix} \tag{6.118}$$

$$\frac{\partial f}{\partial u}=F_u=\begin{bmatrix}f_{u,11} & 0 & f_{u,13} & 0 & f_{u,15} & 0\\ 0 & f_{u,22} & 0 & f_{u,24} & 0 & f_{u,26}\\ 0 & 0 & 0 & 0 & 0 & 0\end{bmatrix} \tag{6.119}$$

$$\frac{\partial g}{\partial x}=G_x=\begin{bmatrix}g_{x,11} & 0 & 0\\ 0 & g_{x,22} & 0\\ g_{x,31} & 0 & 0\\ 0 & g_{x,42} & 0\end{bmatrix} \tag{6.120}$$

$$\frac{\partial g}{\partial u}=G_u=\begin{bmatrix}0 & 0 & g_{u,13} & 0 & g_{u,15} & 0\\ 0 & 0 & 0 & g_{u,24} & 0 & g_{u,26}\\ 0 & 0 & g_{u,33} & 0 & g_{u,35} & 0\\ 0 & 0 & 0 & g_{u,44} & 0 & g_{u,46}\end{bmatrix} \tag{6.121}$$

Table 6.16 Matrix Elements for Equations 6.118 - 6.121

$f_{x,11}$	$\frac{1}{(rVC_p)_h}\left[\begin{array}{l}-2\dot{m}_h C_{p_h} - a_h A_h + \frac{a_h A_h (T_{h,ave} - T_{wall})}{(C_{p_h})}\left(\frac{\partial C_{p_h}}{\partial T_{h,ave}}\Big\vert_{P_h}\right) \\ + \frac{2\dot{m}_h C_{p_h}(T_{h,ave} - T_{h,in}) + a_h A_h (T_{h,ave} - T_{wall})}{(r_h)}\left(\frac{\partial r_h}{\partial T_{h,ave}}\Big\vert_{P_h}\right)\end{array}\right]$
$f_{x,13}$	$\frac{a_h A_h}{(rVC_p)_h}$
$f_{x,22}$	$\frac{1}{(rVC_p)_c}\left[\begin{array}{l}-2\dot{m}_c C_{p_c} - a_c A_c + \frac{a_c A_c (T_{c,ave} - T_{wall})}{(C_{p_c})}\left(\frac{\partial C_{p_c}}{\partial T_{c,ave}}\Big\vert_{P_c}\right) \\ + \frac{2\dot{m}_c C_{p_c}(T_{c,ave} - T_{c,in}) + a_c A_c (T_{c,ave} - T_{wall})}{(r_c)}\left(\frac{\partial r_c}{\partial T_{c,ave}}\Big\vert_{P_c}\right)\end{array}\right]$
$f_{x,23}$	$\frac{a_c A_c}{(rVC_p)_c}$
$f_{x,31}$	$\frac{a_h A_h}{(rVC_p)_{wall}}$
$f_{x,32}$	$\frac{a_c A_c}{(rVC_p)_{wall}}$
$f_{x,33}$	$\frac{-(a_h A_h + a_c A_c)}{(rVC_p)_{wall}}$
$f_{u,11}$	$\frac{2C_{p_h}(T_{h,in} - T_{h,ave})}{(rVC_p)_h}$
$f_{u,13}$	$\frac{1}{(rVC_p)_h}\left[\begin{array}{l}\frac{a_h A_h (T_{h,ave} - T_{wall})}{(C_{p_h})}\left(\frac{\partial C_{p_h}}{\partial P_h}\Big\vert_{T_{h,ave}}\right) \\ + \frac{2\dot{m}_h C_{p_h}(T_{h,ave} - T_{h,in}) + a_h A_h (T_{h,ave} - T_{wall})}{(r_h)}\left(\frac{\partial r_h}{\partial P_h}\Big\vert_{T_{h,ave}}\right) + 2\dot{m}_h C_{p_h}\left(\frac{\partial T_{h,in}}{\partial P_h}\Big\vert_{h_{h,in}}\right)\end{array}\right]$
$f_{u,15}$	$\frac{2\dot{m}_h C_{p_h}}{(rVC_p)_h}\left(\frac{\partial T_{h,in}}{\partial h_{h,in}}\Big\vert_{P_h}\right)$
$f_{u,22}$	$\frac{2C_{p_c}(T_{c,in} - T_{c,ave})}{(rVC_p)_c}$
$f_{u,24}$	$\frac{1}{(rVC_p)_c}\left[\begin{array}{l}\frac{a_c A_c (T_{c,ave} - T_{wall})}{(C_{p_c})}\left(\frac{\partial C_{p_c}}{\partial P_c}\Big\vert_{T_{c,ave}}\right) \\ + \frac{2\dot{m}_c C_{p_c}(T_{c,ave} - T_{c,in}) + a_c A_c (T_{c,ave} - T_{wall})}{(r_c)}\left(\frac{\partial r_c}{\partial P_c}\Big\vert_{T_{c,ave}}\right) + 2\dot{m}_c C_{p_c}\frac{\partial T_{c,in}}{\partial P_c}\end{array}\right]$

Table 6.10 (cont.)

$f_{u,26}$	$\frac{2\dot{m}_c C_{p_c}}{\left(rVC_p\right)_c}\left(\left.\frac{\partial T_{c,in}}{\partial h_{c,in}}\right\|_{P_c}\right)$
$g_{x,11}$	$2\left(\left.\frac{\partial h_{h,out}}{\partial T_{h,out}}\right\|_{P_h}\right)$
$g_{x,22}$	$2\left(\left.\frac{\partial h_{c,out}}{\partial T_{c,out}}\right\|_{P_c}\right)$
$g_{x,31}$	2
$g_{x,42}$	2
$g_{u,13}$	$-\left(\left.\frac{\partial h_{h,out}}{\partial T_{h,out}}\right\|_{P_h}\right)\left(\left.\frac{\partial T_{h,in}}{\partial P_h}\right\|_{h_{h,in}}\right)+\left(\left.\frac{\partial h_{h,out}}{\partial P_h}\right\|_{T_{h,out}}\right)$
$g_{u,15}$	$-\left(\left.\frac{\partial h_{h,out}}{\partial T_{h,out}}\right\|_{P_h}\right)\left(\left.\frac{\partial T_{h,in}}{\partial h_{h,in}}\right\|_{P_h}\right)$
$g_{u,24}$	$-\left(\left.\frac{\partial h_{c,out}}{\partial T_{c,out}}\right\|_{P_c}\right)\left(\left.\frac{\partial T_{c,in}}{\partial P_c}\right\|_{h_{c,in}}\right)+\left(\left.\frac{\partial h_{c,out}}{\partial P_c}\right\|_{T_{c,out}}\right)$
$g_{u,26}$	$-\left(\left.\frac{\partial h_{c,out}}{\partial T_{c,out}}\right\|_{P_c}\right)\left(\left.\frac{\partial T_{c,in}}{\partial h_{c,in}}\right\|_{P_c}\right)$
$g_{u,33}$	$-\left(\left.\frac{\partial T_{h,in}}{\partial P_h}\right\|_{h_{h,in}}\right)$
$g_{u,35}$	$-\left(\left.\frac{\partial T_{h,in}}{\partial h_{h,in}}\right\|_{P_h}\right)$
$g_{u,44}$	$-\left(\left.\frac{\partial T_{c,in}}{\partial P_c}\right\|_{h_{c,in}}\right)$
$g_{u,46}$	$-\left(\left.\frac{\partial T_{c,in}}{\partial h_{c,in}}\right\|_{P_c}\right)$

6.11.5.2 Numerical Representation

The evaluation of these equations at the highway operating condition yields the following matrices (Equations 6.122 - 6.125).

$$A = \begin{bmatrix} -23.671 & 0 & 4.8072 \\ 0 & -134.21 & 88.852 \\ 0.24584 & 0.24584 & -0.49169 \end{bmatrix} \tag{6.122}$$

$$B = \begin{bmatrix} 1238.6 & 0 & 0.11027 & 0 & 3.3377 & 0 \\ 0 & -21100 & 0 & 0.47957 & 0 & 31.118 \\ 0 & 0 & 0 & 0 & 0 & 0 \end{bmatrix} \tag{6.123}$$

$$C = \begin{bmatrix} 14.819 & 0 & 0 \\ 0 & 2.3046 & 0 \\ 2 & 0 & 0 \\ 0 & 2 & 0 \end{bmatrix} \tag{6.124}$$

$$D = \begin{bmatrix} 0 & 0 & -0.082148 & 0 & -1.4685 & 0 \\ 0 & 0 & 0 & -0.025361 & 0 & -0.68735 \\ 0 & 0 & -0.006122 & 0 & -0.19819 & 0 \\ 0 & 0 & 0 & -0.012587 & 0 & -0.59651 \end{bmatrix} \tag{6.125}$$

6.11.6 System

The model for the overall system is found by appropriately defining the component model inputs in terms of system inputs and component outputs. This procedure can done analytically using selection matrices or numerically by using algorithms available in MATLAB.

6.11.6.1 Symbolic Representation

The complexity of the symbolic representation of the overall system model is obvious given the symbolic representations of the component models. A symbolic representation of the overall system would be too complex to provide useful insight to the system dynamics. Therefore, only the numerical representations are included.

6.11.6.2 Numerical Representation

For simplicity, the numerical entries of the system matrices $\{A, B, C, D\}$ evaluated at the highway driving condition are given in Tables 6.17 - 6.22.

Table 6.17 System 'A' Matrix: Columns 1 - 6

-1.3172	0.02249	0.044662	-1.8206	0.0077459	0.00305
-95.781	-17.332	-105.46	1080.3	178.56	0.0084956
-556.93	-1.1519	-49.853	-33.407	111.36	0.10717
-0.078365	0.016212	0	-1.5469	0.0066648	0
-15.566	0.27286	0.73851	-21.378	-0.7134	0.035862
0	0.96771	-99.131	0	0	-18.701
0	-0.05211	-1.7011	0	0	-0.27629
0	0	0	0	0	0.0030427
0	0.19201	3.0457	0	0	0.10203
0	0.0099758	28.058	0	0	0.028837
0	0	0	0	0	0

Table 6.18 System ‘A’ Matrix: Columns 7 - 11

0.11597	0	-0.58513	-0.16143	0
-20.26	0	102.23	84.283	0
3.3133	0	-16.718	-0.81857	0
0	0	0	0	0
1.3635	0	-6.8799	-1.8981	0
-1802.6	2706.5	458.22	332.37	0
-32.686	52.593	-2.9097	5.7034	0
0.2912	-0.6006	0	0	0
7.2278	0	-26.458	-10.212	4.8702
0	0	0	-123.95	88.852
0	0	0.24584	0.24584	-0.49169

Table 6.19 System ‘B’ Matrix

0.11512	-0.000121	0	0	0	0
143.37	-2.7836	0	0	0	0
7.2809	-0.19318	0	0	0	0
0	0	0.05994	9.8119	0	0
1.3536	-0.00142	0.05994	7.5841	0	0
-395.96	12.557	0	0	0	0
2.5144	0.11633	0	0	0	0
0	0	0	0	0.092348	-1.8354
2.4083	0	0	0	0	0
0	-0.51309	0	0	0	0
0	0	0	0	0	0

Table 6.20 System ‘C’ Matrix: Columns 1 - 6

0	0.0016356	0.59651	0	0	0
0	1	0	0	0	0
0	0	0	0	0	1
-1.6367	0	0	0.6089	0.1392	0
0	0	0	0	0	0

Table 6.21 System ‘C’ Matrix: Columns 7 - 11

0	0	0	0	0
0	0	0	0	0
0	0	0	0	0
0	0	0	0	0
0	0.23025	0	0	0

Table 6.22 System 'D' Matrix

0	0	0	0	0	0
0	0	0	0	0	0
0	0	0	0	0	0
0	0	0.2519	16.784	0	0
0	0	0	0	0.76975	-0.98402

6.12 Simulation

To verify that the linearization procedure does not compromise the model fidelity significantly, the linearized model simulation is added to the model validation plots from the previous chapter and compared (Figures 6.55 - 6.60). Although there are small discrepancies between the nonlinear model and the linearized model, both models adequately predict the transient response of the physical system, as per the discussion in Chapter 5.

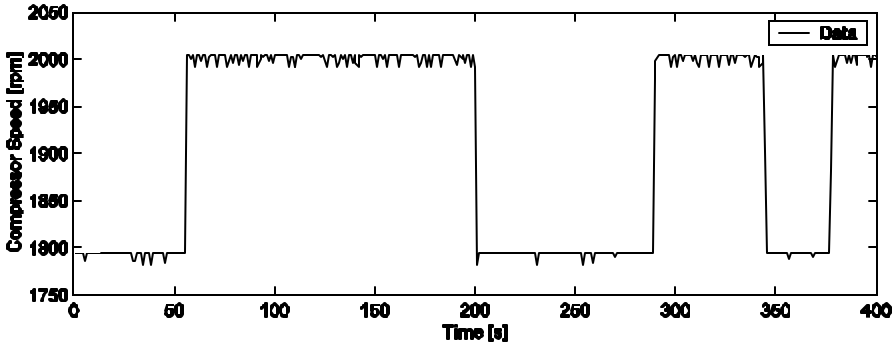

Figure 6.55 Linearized Model Validation: Compressor Speed Step Changes

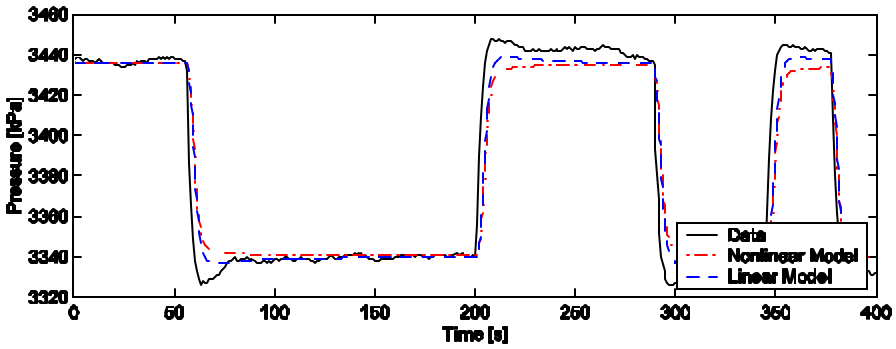

Figure 6.56 Linearized Model Validation: Evaporator Pressure for Step Changes in Compressor Speed

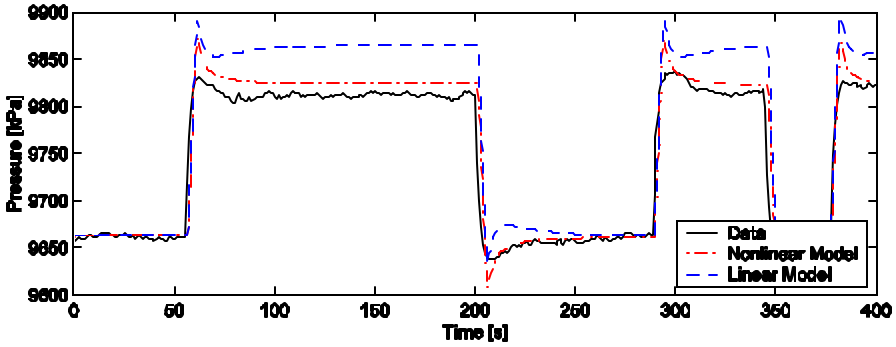

Figure 6.57 Linearized Model Validation: Gas Cooler Pressure for Step Changes in Compressor Speed

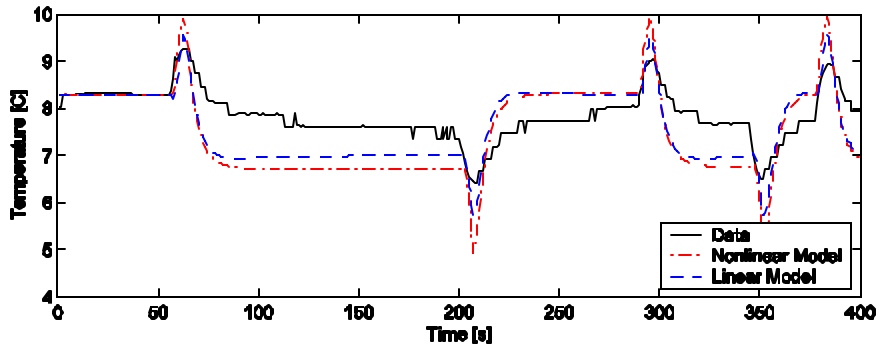

Figure 6.58 Linearized Model Validation: Evaporator Superheat for Step Changes in Compressor Speed

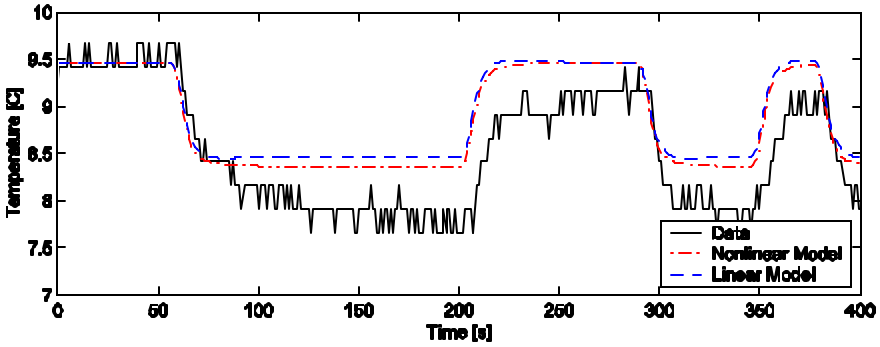

Figure 6.59 Linearized Model Validation: Evaporator Exit Air Temperature for Step Changes in Compressor Speed

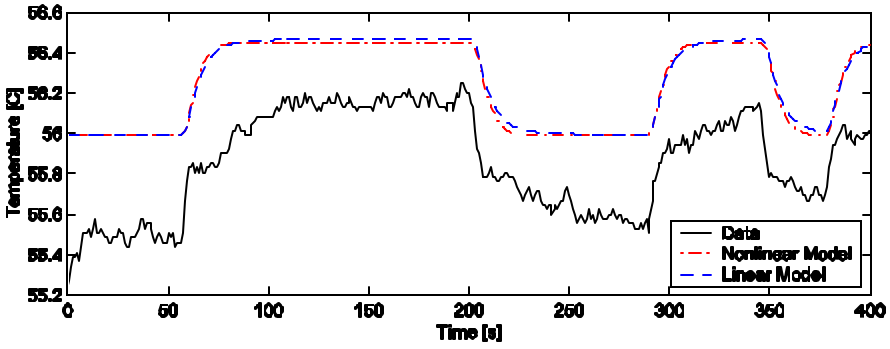

Figure 6.60 Linearized Model Validation: Gas Cooler Exit Air Temperature for Step Changes in Compressor Speed

6.13 Dynamic Analysis

After accepting the linearized models as good approximations of the nonlinear system, the eigenvalues and Hankel singular values can be computed. These numerical measures are helpful for assessing the possibilities for model reduction. The numerical values are given for the highway operating condition.

6.13.1 Eigenvalues

The eigenvalues for the gas cooler, evaporator, internal heat exchanger, and overall system are given in Equations 6.126 - 6.129 respectively. Note the presence of eigenvalues that differ by an order of magnitude. This indicates that the components and system exhibit multiple time scale behavior, and that model reduction is appropriate. Also note the presence of a zero eigenvalue in Equations 6.126 and 6.127 that is a result of the pure integration of mass flow due to the conservation of mass equation in both the gas cooler and evaporator. This exposes the redundant dynamic mode that creates the zero eigenvalue in Equation 6.129. Because there is no change in the total refrigerant mass, both conservation of mass equations are not independent, and only one is truly needed. The most probable choice for a reduced order model-based on the system eigenvalues is a 5^{th} order model (retaining the five slowest eigenvalues).

$$l(A_e) = \begin{bmatrix} -53.374 \\ -13.745 \\ -0.41128 \\ -0.13166 \\ 0 \end{bmatrix} \tag{6.126}$$

$$l(A_c) = \begin{bmatrix} -49.943 \\ -0.12332 \\ 0 \end{bmatrix} \tag{6.127}$$

$$l(A_{hx}) = \begin{bmatrix} -134.37 \\ -23.722 \\ -0.27741 \end{bmatrix} \tag{6.128}$$

$$l\left(A_{sys}\right)=\begin{bmatrix} -124.02 \\ -54.165 \\ -49.608 \\ -28.09 \\ -14.598 \\ -1.9951 \\ -0.47228+0.23312\mathrm{i} \\ -0.47228-0.23312\mathrm{i} \\ -0.17491 \\ -0.06074 \\ 0 \end{bmatrix} \tag{6.129}$$

Comparing these values to the eigenvalues of the identified models is enlightening. The eigenvalues for the MIMO model identified for the idle and city models using subspace methods (direct method) are given in Equations 6.130 and 6.131. Because an identified model was not obtained for the highway condition a direct comparison of eigenvalues cannot be made, but a general comparison of the five slowest eigenvalues of the system model with the eigenvalues of the identified models can be made (Figure 6.61).

$$l\left(A_{idle}\right)=\begin{bmatrix} -0.2386 \\ -0.1073+0.0693i \\ -0.1073-0.0693i \\ -0.0469+0.0038i \\ -0.0469-0.0038i \end{bmatrix} \tag{6.130}$$

$$l\left(A_{city}\right)=\begin{bmatrix} -1.8055 \\ -0.4067 \\ -0.1371 \\ -0.0447+0.0159i \\ -0.0447-0.0159i \\ -0.0130 \end{bmatrix} \tag{6.131}$$

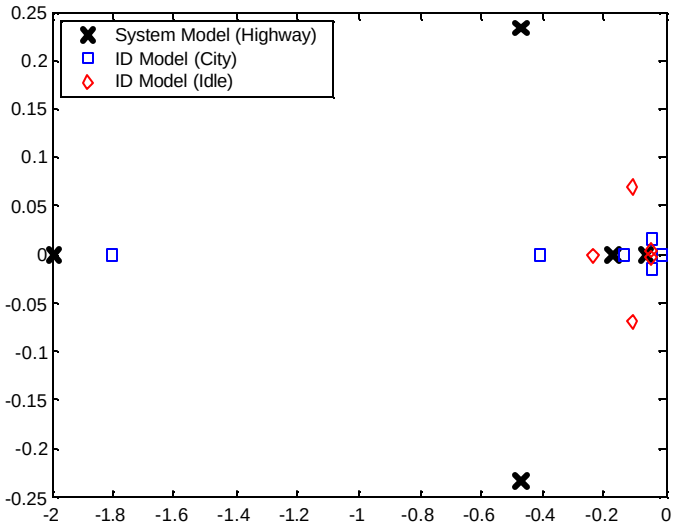

Figure 6.61 Comparison of Eigenvalues: Linearized Model and Identified Models

6.13.2 Hankel Singular Values

The Hankel singular values for the overall system are given in Equation 6.132. Recall that the system has one redundant dynamic mode due to the conservation of mass equations in both the gas cooler and evaporator. This leads to a zero eigenvalue, and an ill-conditioned matrix. Because the calculation of Hankel singular values of a system with an ill-conditioned matrix leads to numerical difficulties, the redundant dynamic mode is removed before calculating these values. Thus only ten Hankel singular values are shown in Equation 6.132 and in Figure 6.62. Note the presence of values that differ by orders of magnitude. This also indicates that model reduction is appropriate. Specifically, logical choices for reduced order models based on the Hankel singular values are 3rd and 6th order models.

$$s_{hsv}(A_{sys}, B_{sys}, C_{sys}) = \begin{bmatrix} 5078.9 \\ 750.69 \\ 333.05 \\ 32.963 \\ 24.088 \\ 15.914 \\ 0.97586 \\ 0.29111 \\ 0.11337 \\ 0.009632 \end{bmatrix} \tag{6.132}$$

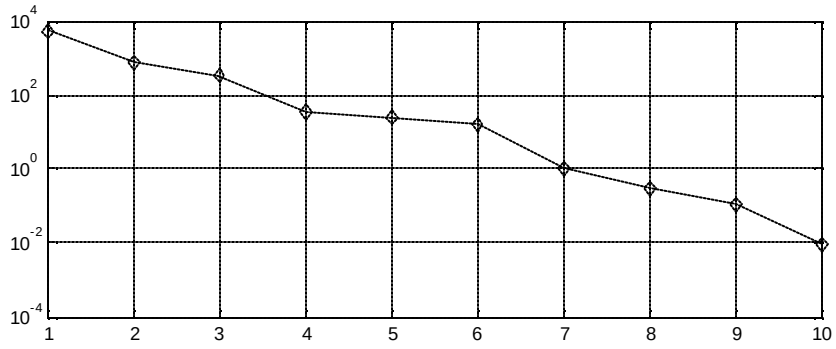

Figure 6.62 Hankel Singular Values

6.13.3 Controllability and Observability

The linearized system model can also be evaluated for controllability and observability. The controllability and observability matrices are calculated using the definitions in Equations 6.133 and 6.134 where n is the number of states [9]. The rank of these matrices is given as $Rank(C) = 5$ and $Rank(O) = 5$.

$$C = \begin{bmatrix} B & AB & A^2B & \dots & A^{n-1}B \end{bmatrix} \tag{6.133}$$

$$O = \begin{bmatrix} C & CA & CA^2 & \dots & CA^{n-1} \end{bmatrix}^T \tag{6.134}$$

6.13.4 Summary

Linearized models for each component were presented. A linearized model of the system was formed by the appropriate combination of the linearized component models. The analysis of the component models revealed multiple-time scale behavior and the presence of a pure integrator in the evaporator and gas cooler models. The linearized system was observed to have five slow eigenvalues, five fast eigenvalues, and one zero eigenvalue resulting from a modeling redundancy. The Hankel Singular Values indicated that a 3rd or 6th order model would be logical choices for a reduced order model. Evaluation of the controllability and observability of the system revealed five observable/controllable modes. All of these results motivate the search for a reduced order model of the system dynamics.

Chapter 7. Model Reduction

"*Modeling for control is parsimonious and implicit. It is parsimonious, because the model should not be more detailed than that required by the specific control task. It is implicit, because the extent of the necessary detail is not known before the control task is accomplished*." P. V. Kokotovic [21]

7.1 Motivation

Using the modeling procedure outlined in Chapter 2, dynamic models for the various components of subcritical and transcritical cycles have been derived and validated with experimental data. Linearized versions of these models have also been developed. While these models are not of excessively high order, simpler and lower order models are always desirable for controller design purposes if they can be achieved without compromising the model's fidelity significantly. Empirical models constructed in Chapter 4 demonstrated that lower order models were sufficient for predicting the dominant dynamic behavior of the system. Furthermore, analysis of the linearized version of the derived models also indicated that the dominant dynamic behavior could be captured with a low order model.

This chapter seeks to answer four questions. First, given several choices of state representations, which will yield the best reduced order model approximation of the full order system? Second, given the chosen representation, which states should be considered fast/slow? Third, does the resulting reduced order model adequately approximate the full order model? Fourth, what is the physical interpretation of the choices of the fast/slow states?

Model reduction for control design is a vast field of study. Many, if not most, of the methods currently available require the model be evaluated numerically so that appropriate balanced realizations or matrix operations can be used. This results in state transformations, in which the physical meaning of the state variables is lost. In contrast, the singular perturbation method allows the symbolic reduction of models based on engineering knowledge of the model parameters. In this thesis, a primary objective of model reduction is the physical insight gained as to which physical phenomenon occur relatively fast, and which can be considered to be the dominant physical dynamics. Thus, although the multitude of numerical model reduction techniques can be performed with the linearized models obtained in Chapter 6, the approaches to be considered in this chapter are restricted to those that preserve the physical meaning of the dynamic states.

7.2 Singular Perturbation Method

In the context of this thesis, a singularly perturbed system is defined by Equation 7.1. The system exhibits multiple time scale behavior. The perturbation parameter, e, is assumed to be small, and x is chosen to represent the slow dynamics and z to represent the fast dynamics of the system. Singularly perturbed systems are observed in many physical systems [26], including fluid dynamics, electrical circuits, aerospace systems, chemical systems, biological systems, and many others. These physical systems often contain small "parasitic" parameters that increase the dynamic order of the model. For control-oriented modeling, these parameters are generally neglected. The singular perturbation approach provides a method for justifying such assumptions, and means for analyzing the implications of these assumptions on the resulting reduced order model.

$$\dot{x} = f(x, z, e, t)$$
$$e\dot{z} = g(x, z, e, t) \tag{7.1}$$

The techniques for applying this model reduction method discussed in this thesis will involve linear time-invariant models of singularly perturbed systems (Equation 7.2). These systems generally involve matrices that are ill-conditioned. The condition number of a matrix is the ratio of the largest singular value to the smallest singular value. A system that exhibits multiple time scale behavior will have eigenvalues that differ by orders of magnitude, and therefore have a large condition number. The perturbation parameter, e, is approximately the ratio of the slow eigenvalues to the fast eigenvalues. Naidu [26] notes that e represents an intrinsic property of the system and does not necessarily have to appear explicitly in the system.

$$\begin{bmatrix} \dot{x} \\ \dot{z} \end{bmatrix} = \begin{bmatrix} A_{11} & A_{12} \\ A_{21} & A_{22} \end{bmatrix} \begin{bmatrix} x \\ z \end{bmatrix} + \begin{bmatrix} B_1 \\ B_2 \end{bmatrix} u$$
$$y = \begin{bmatrix} C_1 & C_2 \end{bmatrix} \begin{bmatrix} x \\ z \end{bmatrix} + [D]u \tag{7.2}$$

7.3 Procedure

As mentioned in the introduction to this chapter, the singular perturbation approach allows the symbolic model reduction of systems, by using the assumption that a certain parameter or ratio of parameters is small. This requires an explicit choice of the perturbation parameter. This may not be possible for complex physical models, where the perturbation parameter may be implicit, or the fast phenomena unknown. The singular perturbation approach can also be applied to a system that is represented numerically. In this case, algorithms are generally used to either approximate the system via residualization, or transform the given representation such that the fast and slow dynamics are completely decoupled. In both approaches, the resulting models are reduced in order, including terms that partially compensate for the effects of the neglected fast dynamics. (Note that references to "neglecting" dynamics does not refer to eliminating these relationships, but merely assuming that fast dynamics can be approximated by instantaneous algebraic relationships). The following sections illustrate both of these approaches in order to properly explain how these approaches need to be adapted to be applied to the models developed in this thesis.

7.3.1 Symbolic Model Reduction

This approach is best illustrated using a common example of a DC motor included in many textbooks about singular perturbation model reduction [20,21]. As described in [21], the model consists of an equation for mechanical torque (Equation 7.3), and an equation for the electrical transient (Equation 7.4), where i, u, R, and L are the armature current, voltage, resistance and inductance respectively, J is the moment of inertia, w is the angular speed, and ki and kw are the torque and back e.m.f. developed with constant excitation flux f. Kokotovic asserts that in all well designed motors L is small, and can be considered to be the perturbation parameter.

$$J\dot{w} = ki \tag{7.3}$$

$$L\dot{i} = -kw - Ri + u \tag{7.4}$$

Assuming that L is zero, Equation 7.4 reduces to an algebraic constraint (Equation 7.5) and after substitution into Equation 7.3 the resulting equation is the commonly used 1st order model of the DC motor (Equation 7.6).

$$i = \frac{u - kw}{R} \tag{7.5}$$

$$J\dot{w} = -\frac{k^2}{R}w + \frac{k}{R}u \tag{7.6}$$

Khalil suggests that it is preferable to choose the perturbation parameter as a dimensionless combination of physical parameters [20]. He extends the above example by first defining several dimensionless variables as $w_r = \frac{w}{\Omega}$, $i_r = \frac{iR}{k\Omega}$, and $u_r = \frac{u}{k\Omega}$, and then rewriting Equations 7.3 and 7.4 as Equations 7.7 and 7.8, where $T_e = L/R$ is the electrical time constant, and $T_m = JR/k^2$ is the mechanical time constant.

$$T_m \frac{dw_r}{dt} = i_r \tag{7.7}$$

$$T_e \frac{di_r}{dt} = -w_r - i_r + u_r \tag{7.8}$$

Assuming that $T_e << T_m$ and defining the dimensionless time variable $t_r = t/T_m$, the state equations can be rewritten as Equations 7.9 and 7.19. The ratio T_e/T_m then becomes the obvious choice for the perturbation parameter.

$$\frac{dw_r}{dt_r} = i_r \tag{7.9}$$

$$\left(\frac{T_e}{T_m}\right)\frac{di_r}{dt_r} = -w_r - i_r + u_r \tag{7.10}$$

To illustrate the relationship between eigenvalues and the perturbation parameter Equations 7.7 and 7.8 are written in state space format (Equation 7.11). The eigenvalues of the full order system can be computed symbolically (Equation 7.12).

$$\begin{bmatrix} \dot{w}_r \\ \dot{i}_r \end{bmatrix} = \underbrace{\begin{bmatrix} 0 & \frac{1}{T_m} \\ -\frac{1}{T_e} & -\frac{1}{T_e} \end{bmatrix}}_{A} \begin{bmatrix} w_r \\ i_r \end{bmatrix} + \underbrace{\begin{bmatrix} 0 \\ \frac{1}{T_e} \end{bmatrix}}_{B} u_r \tag{7.11}$$

$$l(A) = \frac{1}{2}\left[-\frac{1}{T_e} \pm \sqrt{\frac{1}{T_e^{\,2}} - \frac{4}{T_e T_m}} \right] = \frac{1}{2T_e}\left[-1 \pm \sqrt{1-4e} \right] \tag{7.12}$$

The ratio of the eigenvalues is easily computed as well (Equation 7.13). Assuming $\sqrt{1-4e} \approx 1$, the perturbation parameter is found to be the ratio of the eigenvalues (Equation 7.14). This is in agreement with Kokotovic who notes that the perturbation parameter is on the order of the ratio of the slow and fast eigenvalues [21]. This also demonstrates that choosing e as a dimensionless parameter is preferable because the ratio of eigenvalues is always dimensionless.

$$\frac{l_1}{l_2} = \frac{-1+\sqrt{1-4e}}{-1-\sqrt{1-4e}} = \frac{4e}{\left(1+\sqrt{1-4e}\right)^2} \tag{7.13}$$

$$\frac{l_1}{l_2} \approx e \tag{7.14}$$

7.3.2 Numerical Model Reduction

Given the representation in Equation 7.2, different methods for obtaining approximate reduced order models are available. Two methods are discussed here: residualization and a decoupling transformation.

7.3.2.1 Residualization

A common way of approximating the system in Equation 7.2 is to simply set $\dot{z} = 0$. The resulting algebraic equation can be solved for z in terms of x and substituted into the remaining differential equation. This is termed "residualizing" z by Skogestad and Postlethwaite [33]. The resulting formulas for the reduced order state space model are given in Equation 7.15.

$$\begin{aligned} A_r &= A_{11} - A_{12}A_{22}^{-1}A_{21} \\ B_r &= B_1 - A_{12}A_{22}^{-1}B_2 \\ C_r &= C_1 - C_2A_{22}^{-1}A_{21} \\ D_r &= D - C_2A_{22}^{-1}B_2 \end{aligned} \tag{7.15}$$

7.3.2.2 Decoupling Transformation

By applying the transformation in Equation 7.18 to the system in Equation 7.2 it is possible to decouple the fast and slow dynamics, such that the system can be represented as Equation 7.16. Interestingly, no matrix inversion is necessary for calculating T^{-1} (Equation 7.19). The matrices L and M are found as the solution to the Ricatti Equations 7.20 and 7.21. Further explanation of this technique, as well as a proof of its validity can be found in [21] and [26].

$$\begin{bmatrix} \dot{x}_s \\ \dot{z}_f \end{bmatrix} = \begin{bmatrix} A_s & 0 \\ 0 & A_f \end{bmatrix} \begin{bmatrix} x_s \\ z_f \end{bmatrix} + \begin{bmatrix} B_s \\ B_f \end{bmatrix} u \tag{7.16}$$

$$
\begin{aligned}
A_s &= A_{11} - A_{12}L \\
A_f &= A_{22} + LA_{12} \\
B_s &= B_1 - MLB_1 - MB_2 \\
B_f &= B_2 - LB_1
\end{aligned}
\tag{7.17}
$$

$$
T = \begin{bmatrix} I_1 - ML & -M \\ L & I_2 \end{bmatrix}
\tag{7.18}
$$

$$
T^{-1} = \begin{bmatrix} I_1 & M \\ -L & I_2 - LM \end{bmatrix}
\tag{7.19}
$$

$$
LA_{11} + A_{21} - LA_{12}L - A_{22}L = 0
\tag{7.20}
$$

$$
A_s M - MA_f + A_{12} = 0
\tag{7.21}
$$

7.3.3 Application of Singular Perturbation

The application of the singular perturbation method for reducing the models developed in Chapter 2 has some interesting challenges. Specifically, the complexity of the analytical models prevents the explicit identification of a perturbation parameter to reduce the models symbolically. Evaluating the models numerically permits the calculation of eigenvalues and the subsequent observation that the models do exhibit two-time scale behavior. However, the desire to maintain the physical meaning of the dynamic states prevents the application of any type of state transformation, such as a balanced realization. Additionally, for the components modeled, there are several possible choices for state variables, without the knowledge of which state variables are fast and which are slow. A method is needed that identifies the fast and slow states, and provides a means to compare different possible representations as choices for model reduction. This process is separated into four parts: dimensional analysis, comparison, residualization, and evaluation.

7.3.4 Dimensional Analysis

In order to appropriately compare different model representations it is necessary to nondimensionalize the models. The first step is to select the dimensional basis. For each component, we select physical parameters that correspond to the fundamental units of mass, length, temperature, and time. These bases are initially selected independently for each component because the analysis and comparisons made only involve that specific component. If comparisons are to be made of the entire system model, a uniform dimensional basis must be selected for the entire system. For more information regarding the application of dimensional analysis to control systems, see [6].

7.3.5 Comparison

Intuition dictates that the most ideal representation for residualization is a modal form where the states are not coupled and explicitly associated with the eigenvalues. Thus the fast/slow dynamics are explicitly associated with the states and the choice of states to residualize is obvious. Alternatively, a representation that is either upper or lower diagonal is preferable because the off-diagonal terms would not affect the eigenvalues. The off-diagonal terms would, however, affect the conditioning of the matrix and possibly the reduced order model approximation. Thus given several acceptable model representations, the “best” choice for residualization would be the

representation that is diagonally dominant or block diagonally dominant with the fast states decoupled from the slow states. There are several methods available for measuring the relative coupling of the dynamics; these include diagonal dominance, induced matrix norms, and the Relative Gain Array. Block diagonal dominance is much more difficult to measure numerically, and is not discussed. If the system is not diagonal dominant, an alternative means of determining which state should be residualized is finding an appropriate scaling matrix to form a balanced realization.

7.3.5.1 Diagonal Dominance

The mathematical definition of diagonal dominance is given in Equation 7.22. In words, a matrix is diagonally dominant in the sense that the absolute value of the diagonal element of each row is strictly greater than the sum of the absolute values of the off-diagonal elements. To be specific, this is row diagonal dominance. Column diagonal dominance is similarly computed, but not considered here. Note that this comparison is only relevant for dimensionally equivalent representations.

$$|a_{ii}| > \sum_{i \neq j} |a_{ij}| \tag{7.22}$$

7.3.5.2 Matrix Norms

The induced matrix norms also give a measure of diagonal dominance. These are defined in Equations 7.23 - 7.25 as the induced one norm (maximum column sum), the induced infinity norm (maximum row sum), and the induced two norm (maximum singular value). The minimal value of each these norms will occur for a strictly diagonal representation, with the minimal value being equal to the largest eigenvalue (Equation 7.26) (Proof in [33]). Thus these norms can provide a means of comparing the diagonal dominance of different representations. For this thesis, the induced two norm (maximum singular value) is used. Again note that this comparison is only relevant for dimensionally equivalent representations.

$$\|A\|_{i1} = \max_j \left(\sum_i |a_{i,j}| \right) \tag{7.23}$$

$$\|A\|_{i\infty} = \max_i \left(\sum_j |a_{i,j}| \right) \tag{7.24}$$

$$\|A\|_{i2} = s_{\max}(A) = \sqrt{l_{\max}\left(A^T A\right)} \tag{7.25}$$

$$l_{\max}(A) \leq \|A\| \tag{7.26}$$

7.3.5.3 Relative Gain Array

The Relative Gain Array for a square matrix is defined in Equation 7.27, where the $\times$ denotes element-by-element multiplication (Schur product). The RGA will be identity only if the matrix is upper or lower diagonal. Therefore diagonal elements close to unity indicate diagonal dominance.

$$\Lambda(A) = A \times \left(A^{-1}\right)^T \tag{7.27}$$

7.3.5.4 Scaling Matrix

For systems that are not diagonally dominant, but still exhibit multiple time scale behavior, an alternative method for selecting the states to be residualized is by evaluating the scaling matrix necessary to form a balanced

realization. In the context of this thesis, balancing the system matrices is performed by finding a scaling matrix S such that the norm of Equation 7.28 is minimized. When calculating the scaling matrix, the entries of S are generally restricted to integer exponents of 2 so that computation errors are not introduced. By evaluating the diagonal entries of S, appropriate choices of which states should be residualized can be made. This is equivalent to visually inspecting the matrix and determining that the entries of a specific row are an order of magnitude higher than the other rows. This row is assumed to be multiplied by $1/e$. Thus by dividing this row by e places the system of equations in the standard form (Equation 7.1). The elements of the scaling matrix give a numerical measure for which rows have entries that are relatively large. For this method the best representation for model reduction could be chosen as the representation with the lowest condition number (the least ill-conditioned).

$$\begin{bmatrix} S^{-1}AS & S^{-1}B \\ CS & 0 \end{bmatrix} \tag{7.28}$$

7.3.6 Residualization

After determining the best choice of the available representations for model reduction, the states are reordered into the standard form (Equation 7.2). The number of desired states is residualized according to Equation 7.15, and the approximated eigenvalues can be compared to the full order eigenvalues.

7.3.7 Comparison

After the chosen representation has been residualized, the eigenvalues of the reduced order model can be compared to those of the full order model. The approximation error can be calculated and verified to be within acceptable limits. Additionally, many physical insights can be gained by evaluating which physical states are associated with fast dynamics, and which are associated with slow dynamics.

7.4 Results

Using the procedure outlined above, the linearized component models developed can be reduced in order. First, each of the possible representations for the component models is nondimensionalized. The various representations are evaluated to determine the most suitable representation for model reduction, as well as which states should be residualized. Reduced order models are calculated and compared to the full order models. Observations regarding the physical meaning of the negligible dynamics are made. The reduced order models are combined to create a reduced order system model. This model is compared to the full order nonlinear and linearized models through analysis and simulation.

7.4.1 Gas Cooler

Recall the three possible choices of states for the gas cooler were given as $x = [P_c \quad h_c \quad T_w]^T$, $x' = [P_c \quad m_c \quad T_w]^T$, and $x'' = [U_c \quad m_c \quad E_w]^T$. The resulting A matrix for each of these models as presented in Chapter 6 are given in Equations 7.29 - 7.31. These are the numerical results given the chosen dimensions. A nondimensional basis is selected as as: length – length of fluid flow in the gas cooler, mass – refrigerant mass inventory in the gas cooler, temperature – 273 K, and time – refrigerant mass inventory divided by

mass flow rate. These are evaluated for the highway driving condition at steady state. The numerical values for this basis, as well as the resulting numerical values for the nondimensional states are given in Table 7.1.

$$A = \begin{bmatrix} -16.202 & -1711.7 & 2706.5 \\ -0.31485 & -33.263 & 52.593 \\ 0.0030427 & 0.2912 & -0.6006 \end{bmatrix} \tag{7.29}$$

$$A' = \begin{bmatrix} -49.465 & 8.9885e6 & 2696.7 \\ 0 & 0 & 0 \\ 0.0087329 & -1534.9 & -0.6006 \end{bmatrix} \tag{7.30}$$

$$A'' = \begin{bmatrix} -49.465 & -6170.6 & 0.50826 \\ 0 & 0 & 0 \\ 46.335 & 5930.1 & -0.6006 \end{bmatrix} \tag{7.31}$$

Table 7.1 Nondimensional Basis for the Gas Cooler

		Pressure [kPa=kg/m/s^2]	Enthalpy [kJ/kg=m^2/s^2]	Temperature [K]	Mass [kg]	Energy [kJ=m^2*kg/s^2]
Length	2.285	-1	2			2
Mass	0.0423	1			1	1
Time	0.9646	-2	-2			-2
Temperature	273			1		
		1.989E+01	5.612E+03	2.730E+02	4.229E-02	2.373E+02

Using this basis to nondimensionalize the system via a similarity transformation (Equations 7.32 - 7.34) results in the matrices given in Equations 7.35 - 7.37 where the bar denotes the nondimensional representation.

$$T = \begin{bmatrix} 19.8901 & 0 & 0 \\ 0 & 5611.50 & 0 \\ 0 & 0 & 273 \end{bmatrix} \tag{7.32}$$

$$T' = \begin{bmatrix} 19.8901 & 0 & 0 \\ 0 & 0.042288 & 0 \\ 0 & 0 & 273 \end{bmatrix} \tag{7.33}$$

$$T'' = \begin{bmatrix} 237.299 & 0 & 0 \\ 0 & 0.042288 & 0 \\ 0 & 0 & 237.299 \end{bmatrix} \tag{7.34}$$

$$\overline{A} = T^{-1}AT = \begin{bmatrix} -16.202 & -4.8292e5 & 37147 \\ -0.001116 & -33.263 & 2.5587 \\ 0.00022168 & 5.9857 & -0.6006 \end{bmatrix} \tag{7.35}$$

$$\overline{A}' = T'^{-1}A'T' = \begin{bmatrix} -49.465 & 19108 & 37147 \\ 0 & 0 & 0 \\ 0.00063397 & -0.23683 & -0.6006 \end{bmatrix} \tag{7.36}$$

$$\overline{A}'' = T''^{-1}A''T'' = \begin{bmatrix} -49.465 & -1.0996 & 0.50826 \\ 0 & 0 & 0 \\ 46.335 & 1.0568 & -0.6006 \end{bmatrix} \tag{7.37}$$

Evaluating these for diagonal dominance using the measures outlined earlier in this chapter yields no useful information. All the representations given are not diagonally dominant, which can be confirmed by inspection. The best representation is then determined by condition number. The condition number for each of the representations (ignoring the zero singular value) is given as 3465571, 651524, and 729.6 for the A, A', and A'' representations respectively. Based on these values the third representation is chosen for model reduction. The necessary scaling matrix to obtain a balanced realization is calculated, and given as $S = diag([8 \quad 1 \quad 1])$. Thus the obvious choice of the state to be residualized is the first state, or the refrigerant energy.

7.4.1.1 Reduced Order Model

For discussion purposes, reduced order models are calculated for all three representations. These models are not included, but their eigenvalues are calculated and compared to the eigenvalues of the full order model (Tables 7.2 - 7.4). From these tables it is clear that the first representation is a poor choice for model reduction, because the zero eigenvalue dynamic is not explicitly associated with any state. The reduced order models for both the second and third representation yield equivalent eigenvalues. This is due to the fact that the states of the second representation are simply constant multiples of the states of the third representation.

For all representations, it is obvious that residualizing the wall temperature/energy dynamics leads to the removal of the slowest eigenvalue. Thus for the gas cooler the refrigerant energy (equivalent to pressure) dynamic is fast, the wall temperature/energy dynamic is slow, and there is a pure integrator for the conservation of mass. The final reduced order model used is given (in dimensional form) in Equations 7.38 - 7.41. This reduced order model is a 2nd order system with states defined as $x_r'' = [m_c \quad E_w]^T$.

Table 7.2 Gas Cooler Eigenvalue Comparison for Reduced Order Models of A

	Eliminate: Pressure		Eliminate: Enthalpy		Eliminate: Wall Temp.	
Full Order Eigenvalues	**Reduced Order Eigenvalues**	**Percentage Error**	**Reduced Order Eigenvalues**	**Percentage Error**	**Reduced Order Eigenvalues**	**Percentage Error**
-49.943					-10.254	79.5%
-0.123	-0.092	25.1%	-0.140	13.7%		
0	0	0.0%	0	0.0%	0	0.0%

Table 7.3 Gas Cooler Eigenvalue Comparison for Reduced Order Models of A'

	Eliminate: Pressure		Eliminate: Wall Temp.	
Full Order Eigenvalues	**Reduced Order Eigenvalues**	**Percentage Error**	**Reduced Order Eigenvalues**	**Percentage Error**
-49.943			-10.254	79.5%
-0.123	-0.125	1.0%		
0	0	0.0%	0	0.0%

Table 7.4 Gas Cooler Eigenvalue Comparison for Reduced Order Models of A''

	Eliminate: Refrigerant Energy		Eliminate: Wall Energy	
Full Order Eigenvalues	**Reduced Order Eigenvalues**	**Percentage Error**	**Reduced Order Eigenvalues**	**Percentage Error**
-49.943			-10.254	79.5%
-0.123	-0.125	1.0%		
0	0	0.0%	0	0.0%

$$A_r = \begin{bmatrix} 0 & 0 \\ 149.97 & -0.12451 \end{bmatrix} \tag{7.38}$$

$$B_r = \begin{bmatrix} 1 & -1 & 0 & 0 & 0 \\ 52.894 & 105.72 & 0.081689 & 0.26625 & -5.2917 \end{bmatrix} \tag{7.39}$$

$$C_r = \begin{bmatrix} 1.8169e5 & 18.978 \\ -3439.5 & 0.73756 \\ 0 & 0.34685 \\ 0 & 0.079861 \\ 429.94 & 0.26266 \\ 1 & 0 \end{bmatrix} \tag{7.40}$$

$$D_r = \begin{bmatrix} 2108.4 & 4214 & 3.2562 & 0 & 0 \\ 81.943 & 163.78 & -0.87345 & 0 & 0 \\ 0 & 0 & 0 & 0 & 0 \\ 0 & 0 & 0 & 0.76975 & -0.98402 \\ 29.181 & 58.324 & -0.15346 & 0 & 0 \\ 0 & 0 & 0 & 0 & 0 \end{bmatrix} \tag{7.41}$$

7.4.2 Evaporator

Recall the three possible choices of states for the evaporator were given as

$x = \begin{bmatrix} L_1 & P_e & h_o & T_{w1} & T_{w2} \end{bmatrix}^T$, $x' = \begin{bmatrix} L_1 & P_e & m_e & T_{w1} & T_{w2} \end{bmatrix}^T$, and

$x'' = \begin{bmatrix} \tilde{U}_1 & \tilde{U}_2 & \tilde{m}_e & \tilde{E}_{w1} & \tilde{E}_{w2} \end{bmatrix}^T$. The resulting A matrix for each of these models as presented in Chapter 6 are given in Equations 7.42 - 7.44. These are the numerical results given the chosen dimensions. A nondimensional basis is selected as: length – length of fluid flow in the gas evaporator, mass – refrigerant mass inventory in the evaporator, temperature – 273 K, and time – refrigerant mass inventory divided by mass flow rate. These are evaluated for the highway driving condition at steady state. The numerical values for this basis, as well as the resulting numerical values for the nondimensional states are given in Table 7.5.

$$A = \begin{bmatrix} -1.3172 & 0.019652 & -0.0034846 & -1.8206 & 0.0077459 \\ -95.781 & -13.987 & -80.326 & 1080.3 & 178.56 \\ -556.93 & -1.0525 & -50.097 & -33.407 & 111.36 \\ -0.078365 & 0.016212 & 0 & -1.5469 & 0.0066648 \\ -15.566 & 0.23949 & 0.1724 & -21.378 & -0.7134 \end{bmatrix} \tag{7.42}$$

$$A' = \begin{bmatrix} -2.6367 & 0.017536 & 221.09 & -1.8206 & 0.0077459 \\ -30512 & -62.765 & 5.0966e6 & 1080.3 & 178.56 \\ 0 & 0 & 0 & 0 & 0 \\ -0.078365 & 0.016212 & 0 & -1.5469 & 0.0066648 \\ 49.712 & 0.34417 & -10938 & -21.378 & -0.7134 \end{bmatrix} \tag{7.43}$$

$$A'' = \begin{bmatrix} -12.999 & -17.483 & -2988.7 & 1.2049 & 0 \\ -1.2575 & -52.312 & -733.44 & 0 & 0.13311 \\ 0 & 0 & 0 & 0 & 0 \\ 14.535 & 21.746 & 3717.4 & -1.5469 & 0.0066648 \\ 16.045 & 189.24 & 3100.1 & 0.029154 & -0.80448 \end{bmatrix} \tag{7.44}$$

Table 7.5 Nondimensional Basis for the Evaporator

		Length [m]	Pressure [kPa=kg/m/s^2]	Enthalpy [kJ/kg=m^2/s^2]	Temperature [K]	Mass [kg]	Energy [kJ=m^2*kg/s^2]
Length	1.859826	1	-1	2			2
Mass	0.0412		1			1	1
Time	0.9448		-2	-2			-2
Temperature	273				1		
		1.860E+00	2.482E+01	3.875E+03	2.730E+02	4.120E-02	1.596E+02

Using this basis to nondimensionalize the system via a similarity transformation (Equations 7.45 - 7.47) results in the matrices given in Equations 7.48 - 7.50 where the bar denotes the nondimensional representation.

$$T = \begin{bmatrix} 1.85983 & 0 & 0 & 0 & 0 \\ 0 & 24.8150 & 0 & 0 & 0 \\ 0 & 0 & 3874.99 & 0 & 0 \\ 0 & 0 & 0 & 273 & 0 \\ 0 & 0 & 0 & 0 & 273 \end{bmatrix} \tag{7.45}$$

$$T' = \begin{bmatrix} 1.85983 & 0 & 0 & 0 & 0 \\ 0 & 24.8150 & 0 & 0 & 0 \\ 0 & 0 & 0.0411966 & 0 & 0 \\ 0 & 0 & 0 & 273 & 0 \\ 0 & 0 & 0 & 0 & 273 \end{bmatrix} \tag{7.46}$$

$$T'' = \begin{bmatrix} 159.636 & 0 & 0 & 0 & 0 \\ 0 & 159.636 & 0 & 0 & 0 \\ 0 & 0 & 0.0411966 & 0 & 0 \\ 0 & 0 & 0 & 159.636 & 0 \\ 0 & 0 & 0 & 0 & 159.636 \end{bmatrix} \tag{7.47}$$

$$\overline{A} = T^{-1}AT = \begin{bmatrix} -1.30172 & 0.26221 & -7.2603 & -267.25 & 1.137 \\ -7.1785 & -13.987 & -12543 & 11884 & 1964.4 \\ -0.2673 & -0.00674 & -50.097 & -2.3536 & 7.8455 \\ -0.0005339 & 0.0014736 & 0 & -1.5469 & 0.0066648 \\ -0.13605 & 0.021769 & 2.447 & -21.378 & -0.7134 \end{bmatrix} \tag{7.48}$$

$$\overline{A}' = T'^{-1} A' T' = \begin{bmatrix} -2.6367 & 0.23398 & 4.8974 & -267.25 & 1.137 \\ -2286.8 & -62.765 & 8461 & 11884 & 1964.4 \\ 0 & 0 & 0 & 0 & 0 \\ -0.0005339 & 0.0014736 & 0 & -1.5469 & 0.0066648 \\ 0.33866 & 0.031285 & -1.6506 & -21.378 & -0.7134 \end{bmatrix} \tag{7.49}$$

$$\overline{A}'' = T''^{-1} A'' T'' = \begin{bmatrix} -12.999 & -17.483 & -0.77127 & 1.2049 & 0 \\ -1.2575 & -52.312 & -0.18928 & 0 & 0.13311 \\ 0 & 0 & 0 & 0 & 0 \\ 14.535 & 21.746 & 0.95933 & -1.5469 & 0.0066648 \\ 16.045 & 189.24 & 0.80004 & 0.029154 & -0.80448 \end{bmatrix} \tag{7.50}$$

Evaluating these for diagonal dominance using the measures outlined earlier in this chapter yields no useful information. All the representations given are not diagonally dominant, which can be confirmed by inspection. The best representation is then determined by condition number. The condition number for each of the representations (ignoring the zero singular value) is given as 2659305, 2370524, and 6779.1 for the A, A', and A'' representations respectively. Based on these values the third representation is chosen for model reduction. The necessary scaling matrix to obtain a balanced realization is calculated, and given as $S = diag([2 \quad 8 \quad 1 \quad 0.5 \quad 0.25])$. Thus the obvious choice of the states to be residualized is the second state, or the refrigerant energy in the second region, and possibly the first state, or the refrigerant energy in the first region. This is somewhat equivalent to residualizing the pressure and two-phase flow length in the second representation.

7.4.2.2 Reduced Order Model

For discussion purposes, reduced order models are calculated for all three representations. These models are not included, but their eigenvalues are calculated and compared to the eigenvalues of the full order model (Tables 7.6 - 7.8). From these tables it is clear that the first representation is a poor choice for model reduction, because the zero eigenvalue dynamic is not explicitly associated with any state. The reduced order models for both the second and third representation yield similar eigenvalues, but the third representation approximates the slow eigenvalues with the least error. From the gas cooler results, it is obvious that residualizing the wall temperature/energy dynamics leads to the removal of the slowest eigenvalue. Similarly for the evaporator, the refrigerant energy (similar to pressure and two-phase flow length) dynamics are fast, the wall temperature/energy dynamics are slow, and there is a pure integrator for the conservation of mass. The final reduced order models used are shown. The 4th order model is given (in dimensional form) in Equations 7.51 - 7.54. This reduced order model is a 4th order system with states defined as $x''_{r,4} = \begin{bmatrix} \tilde{U}_1 & \tilde{m}_e & \tilde{E}_{w1} & \tilde{E}_{w2} \end{bmatrix}^T$. The 3rd order model is given (in dimensional form) in Equations 7.55 - 7.58. This reduced order model is a 3rd order system with states defined as $x''_{r,3} = \begin{bmatrix} \tilde{m}_e & \tilde{E}_{w1} & \tilde{E}_{w2} \end{bmatrix}^T$.

Table 7.6 Evaporator Eigenvalue Comparison for Reduced Order Models of A

	Eliminate: Pressure		Eliminate: Pressure, Length		Eliminate: Pressure, Enthalpy	
Full Order Eigenvalues	**Reduced Order Eigenvalues**	**Percentage Error**	**Reduced Order Eigenvalues**	**Percentage Error**	**Reduced Order Eigenvalues**	**Percentage Error**
-53.374	-43.033	19.4%				
-13.745						
-0.411	-0.375	8.9%	-0.914	122.3%	-0.336	18.3%
-0.132	-0.048	63.6%	-0.062	52.8%	-0.047	64.6%
0	0	0.0%	0	0.0%	0	0.0%

Table 7.7 Evaporator Eigenvalue Comparison for Reduced Order Models of A'

	Eliminate: Pressure		Eliminate: Pressure, Length	
Full Order Eigenvalues	**Reduced Order Eigenvalues**	**Percentage Error**	**Reduced Order Eigenvalues**	**Percentage Error**
-53.374				
-13.745	-11.622	15.4%		
-0.411	-0.409	0.6%	-0.375	8.8%
-0.132	-0.133	1.2%	-0.151	14.8%
0	0	0.0%	0	0.0%

Table 7.8 Evaporator Eigenvalue Comparison for Reduced Order Models of A''

	Eliminate: Refrig. Energy #2		Eliminate : Refrig. Energy #1, Refrig. Energy #2	
Full Order Eigenvalues	**Reduced Order Eigenvalues**	**Percentage Error**	**Reduced Order Eigenvalues**	**Percentage Error**
-53.374				
-13.745	-13.902	1.1%		
-0.411	-0.414	0.7%	-0.427	3.8%
-0.132	-0.132	0.2%	-0.141	7.4%
0	0	0.0%	0	0.0%

$$A_{r,4} = \begin{bmatrix} -12.579 & -2743.6 & 1.2049 & -0.044488 \\ 0 & 0 & 0 & 0 \\ 14.012 & 3412.5 & -1.5469 & 0.061999 \\ 11.496 & 446.91 & 0.029154 & -0.32294 \end{bmatrix} \tag{7.51}$$

$$B_{r,4} = \begin{bmatrix} -78.069 & 4.4896 & 0.043604 & 0 & 0 \\ 1 & -1 & 0 & 0 & 0 \\ 0 & -5.5843 & 0 & 0.12951 & 21.199 \\ 0 & -48.596 & 0 & 0.12951 & 16.386 \end{bmatrix} \tag{7.52}$$

$$C_{r,4} = \begin{bmatrix} -0.70004 & 4.2265 & 0 & 6.8533e-5 \\ 400.05 & 97427 & 0 & 1.5798 \\ -22.141 & -2686.2 & 0 & 0.98528 \\ 0 & 0 & 0.46284 & 0 \\ -8.231 & 49.695 & 0 & 0.46364 \\ 0 & 0 & 0.28182 & 0.064427 \\ -8.1718 & -375.99 & 0 & 0.60761 \\ -12.553 & -1443 & 0 & 0.59031 \\ -3.8934e-5 & 0.99052 & 0 & -1.5375e-7 \end{bmatrix} \tag{7.53}$$

$$D_{r,4} = \begin{bmatrix} 0 & -0.0069163 & 0 & 0 & 0 \\ 0 & -159.43 & 0 & 0 & 0 \\ 0 & -99.433 & 0 & 0 & 0 \\ 0 & 0 & 0 & 0 & 0 \\ 0 & -0.081322 & 0 & 0 & 0 \\ 0 & 0 & 0 & 0.2519 & 16.784 \\ 0 & -61.32 & 0 & 0 & 0 \\ 0 & -59.574 & 0 & 0 & 0 \\ 0 & 1.5516e-5 & 0 & 0 & 0 \end{bmatrix} \tag{7.54}$$

$$A_{r,3} = \begin{bmatrix} 0 & 0 & 0 \\ 356.23 & -0.20472 & 0.012441 \\ -2060.4 & 1.1303 & -0.3636 \end{bmatrix} \tag{7.55}$$

$$B_{r,3} = \begin{bmatrix} 1 & -1 & 0 & 0 & 0 \\ -86.967 & -0.58294 & 0.048574 & 0.12951 & 21.199 \\ -71.348 & -44.493 & 0.03985 & 0.12951 & 16.386 \end{bmatrix} \tag{7.56}$$

$$C_{r,3} = \begin{bmatrix} 156.91 & -0.67053 & 0.0025444 \\ 10170 & 38.319 & 0.16491 \\ 2143.1 & -2.1208 & 1.0636 \\ 0 & 0.46284 & 0 \\ 1845 & -0.78841 & 0.49276 \\ 0 & 0.28182 & 0.064427 \\ 1406.4 & -0.78274 & 0.63651 \\ 1295 & -1.2024 & 0.63471 \\ 0.99901 & -3.7294e-6 & -1.605e-8 \end{bmatrix} \tag{7.57}$$

$$D_{r,3} = \begin{bmatrix} 4.3448 & -0.25678 & -0.0024297 & 0 & 0 \\ -2482.9 & -16.643 & 1.3868 & 0 & 0 \\ 137.42 & -107.34 & -0.076752 & 0 & 0 \\ 0 & 0 & 0 & 0 & 0 \\ 51.086 & -3.0192 & -0.028533 & 0 & 0 \\ 0 & 0 & 0 & 0.2519 & 16.784 \\ 50.718 & -64.237 & -0.028328 & 0 & 0 \\ 77.91 & -64.054 & -0.43515 & 0 & 0 \\ 0.00024165 & 1.6197e-6 & -1.3497e-7 & 0 & 0 \end{bmatrix} \tag{7.58}$$

7.4.3 Internal Heat Exchanger

Recall the A matrix presented in Chapter 6 for the internal heat exchanger (Equation 7.59). Since multiple representations do not need to be compared, and all the states have the same units, nondimensionalizing the model is not necessary. However, the state(s) to be residualized have yet to be determined. The eigenvalues for A in Equation 7.59 are given in Equation 7.60. Because two of the eigenvalues are two orders of magnitude greater than the third, two states can be residualized.

$$A = \begin{bmatrix} -23.671 & 0 & 4.8072 \\ 0 & -134.21 & 88.852 \\ 0.24584 & 0.24584 & -0.49169 \end{bmatrix} \tag{7.59}$$

$$l(A) = \begin{bmatrix} -134.375 \\ -23.722 \\ -0.277 \end{bmatrix} \tag{7.60}$$

By inspection, the A matrix appears to be diagonally dominant. Using the definition of diagonal dominance, it is confirmed that Equation 7.22 holds. Additionally, using the induced two norm we find that the maximum singular value, 160.98, is the same order of magnitude as the largest eigenvalue, -134.38. Finally, the diagonal elements of the Relative Gain Array are relatively close to unity (Equation 7.61). Accepting the fact that A is diagonally dominant, then the logical choice of states to be residualized are the first and second states (refrigerant temperatures) and to retain the third state (wall temperature). The resulting 1st order model has an eigenvalue of -0.278, which approximates the slow eigenvalue of the full order system with 0.3% error. Again, the conclusion is reached that the refrigerant dynamics are much faster than the heat exchanger wall dynamics. The final reduced order model used is given in Equations 7.62 - 7.65.

$$\Lambda(A) = \begin{bmatrix} 1.182 & 0 & -0.182 \\ 0 & 1.585 & -0.585 \\ -0.182 & -0.585 & 1.766 \end{bmatrix} \tag{7.61}$$

$$A_r = [-0.27835] \tag{7.62}$$

$$B_r = [\,12.864 \quad -38.651 \quad 0.0011452 \quad 0.0008785 \quad 0.034665 \quad 0.057\,] \tag{7.63}$$

$$C_r = \begin{bmatrix} 3.0489 \\ 1.5257 \\ 0.4115 \\ 1.3241 \end{bmatrix} \tag{7.64}$$

$$D_r = \begin{bmatrix} 775.38 & 0 & -0.013118 & 0 & 0.62106 & 0 \\ 0 & -362.32 & 0 & -0.017126 & 0 & -0.15303 \\ 104.65 & 0 & 0.0031947 & 0 & 0.083821 & 0 \\ 0 & -314.44 & 0 & -0.005441 & 0 & -0.1328 \end{bmatrix} \tag{7.65}$$

7.4.4 System

The full order system model was presented in Chapter 6. The reduced order component models derived above are combined to form a reduced order system model. For the system model, only five outputs are considered, $y = [T_{e,sh} \quad P_e \quad P_c \quad T_{e,ao} \quad T_{c,ao}]^T$. If the 4th order model of the evaporator is used, the resulting system model

is 6th order and presented in Equations 7.66 - 7.70. If the 3rd order model of the evaporator is used, the resulting system model is 5th order and presented in Equations 7.71 - 7.74. (Note that the reduced order system has one redundant state from the conservation of energy in both the evaporator and gas cooler, evidenced by the zero eigenvalue. Thus the true reduced order system is found by combining the reduced order component models and removing the redundant state.) The 6th order model approximates the eigenvalues of the full order model within 8%. The eigenvalues of the 5th order system model approximates the eigenvalues of the full order model within 11% error (Table 7.9).

$$A_{r,6} = \begin{bmatrix} -11.974 & -2272.9 & 1.2049 & -0.035315 & 0.001785 & 0.088072 \\ -0.010924 & -4.6201 & 0 & -0.000102 & 9.466e-5 & 0.000126 \\ 13.967 & 3399.3 & -1.5469 & 0.061606 & 0.000162 & 0.001974 \\ 11.1 & 332.19 & 0.029154 & -0.32636 & 0.001411 & 0.017177 \\ -1.2815 & -792.61 & 0 & -0.023462 & -0.10501 & 0.12545 \\ -0.83431 & -129.9 & 0 & 0.061791 & 0.045393 & -0.32448 \end{bmatrix} \tag{7.67}$$

$$B_{r,6} = \begin{bmatrix} -0.076305 & 0.0004555 & 0 & 0 & 0 & 0 \\ 0.001776 & -2.698e-5 & 0 & 0 & 0 & 0 \\ 6.262e-5 & -0.0001459 & 0.12951 & 21.199 & 0 & 0 \\ 0.000545 & -0.0012694 & 0.12951 & 16.386 & 0 & 0 \\ 0.19144 & 0.0004088 & 0 & 0 & 0.26625 & -5.2917 \\ 0.039912 & -0.0007573 & 0 & 0 & 0 & 0 \end{bmatrix} \tag{7.68}$$

$$C_{r,6} = \begin{bmatrix} -13.037 & -4583.6 & 0 & 0.58612 & 0.0017293 & 0.021057 \\ 398.76 & 97050 & 0 & 1.5686 & 0.0046281 & 0.056352 \\ -51.081 & -2.073e5 & 0 & -0.93521 & 19.755 & 5.0006 \\ 0 & 0 & 0.28182 & 0.064427 & 0 & 0 \\ 0 & 0 & 0 & 0 & 0.079861 & 0 \end{bmatrix} \tag{7.69}$$

$$D_{r,6} = \begin{bmatrix} 0.00066801 & -0.0015562 & 0 & 0 & 0 & 0 \\ 0.0017877 & -0.0041646 & 0 & 0 & 0 & 0 \\ 7.6308 & 0.016295 & 0 & 0 & 0 & 0 \\ 0 & 0 & 0.2519 & 16.784 & 0 & 0 \\ 0 & 0 & 0 & 0 & 0.76975 & -0.98402 \end{bmatrix} \tag{7.70}$$

$$A_{r,5} = \begin{bmatrix} -2.5464 & -0.0010992 & -6.995e-5 & 9.303e-5 & 4.5413e-5 \\ 747.96 & -0.14146 & 0.020411 & 0.002244 & 0.10471 \\ -1775 & 1.1462 & -.35911 & 0.0030653 & 0.098827 \\ -549.35 & -0.12895 & -0.019682 & -0.1052 & 0.11603 \\ 28.48 & -0.083953 & 0.064252 & 0.045268 & -0.33062 \end{bmatrix} \tag{7.71}$$

$$B_{r,5} = \begin{bmatrix} 0.001846 & -2.739e-5 & 0 & 0 & 0 & 0 \\ -0.088945 & 0.0003855 & 0.12951 & 21.199 & 0 & 0 \\ -0.070196 & -0.0008471 & 0.12951 & 16.386 & 0 & 0 \\ 0.1996 & 0.0003601 & 0 & 0 & 0.26625 & -5.2917 \\ 0.045229 & -0.0007891 & 0 & 0 & 0 & 0 \end{bmatrix} \tag{7.72}$$

$$C_{r,5} = \begin{bmatrix} 891.31 & -1.3119 & 0.62457 & -0.00021397 & -0.074841 \\ 21354 & 40.125 & 0.39245 & 0.064065 & 2.9894 \\ -1.9761e5 & -5.1401 & -0.78455 & 19.747 & 4.6249 \\ 0 & 0.28182 & 0.064427 & 0 & 0 \\ 0 & 0 & 0 & 0.079861 & 0 \end{bmatrix} \tag{7.73}$$

$$D_{r,5} = \begin{bmatrix} 0.083753 & -0.002052 & 0 & 0 & 0 & 0 \\ -2.5394 & 0.011005 & 0 & 0 & 0 & 0 \\ 7.9563 & 0.014352 & 0 & 0 & 0 & 0 \\ 0 & 0 & 0.2159 & 16.784 & 0 & 0 \\ 0 & 0 & 0 & 0 & 0.76975 & -0.98402 \end{bmatrix} \tag{7.74}$$

Table 7.9 Comparison of System Eigenvalues: Full Order and Reduced Order Models

Full Order Eigenvalues	-124.02	-54.165	-49.608	-28.09	-14.598	-1.995	-0.472±0.233i	-0.175	-0.0607	0
Reduced Order Eigenvalues	Eliminated	Eliminated	Eliminated	Eliminated	-15.648	-2.060	-0.475±0.232i	-0.177	-0.0613	0
Percentage Error					7.2%	3.3%	0.4%	1.4%	0.9%	0.0%
Reduced Order Eigenvalues	Eliminated	Eliminated	Eliminated	Eliminated	Eliminated	-2.202	-0.518±0.238i	-0.182	-0.0628	0
Percentage Error						10.4%	8.3%	3.9%	3.4%	0.0%

To verify that the reduced order model approximations are sufficient, simulation results for both the 5th and 6th order system models are compared to the original nonlinear and linearized models, as well as data. Figures 7.1 - 7.6 show that residualizing the fast states has negligible impact on the transient response of the system. In fact the simulation results from both reduced order models are indistinguishable from the full order linearized model (11th order).

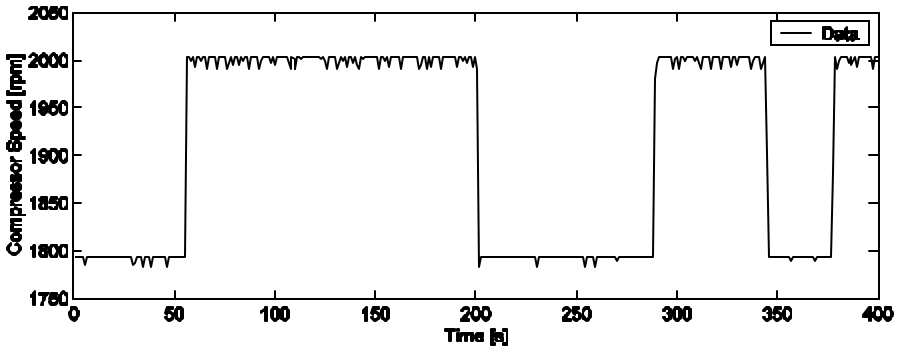

Figure 7.1 Reduced Order Model Validation: Compressor Speed Step Changes

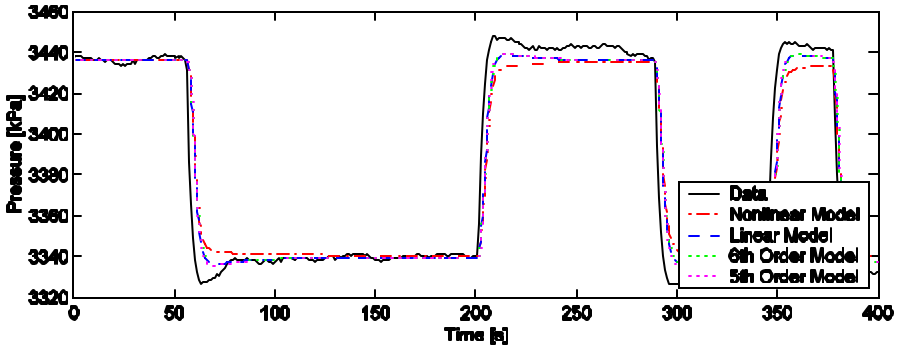

Figure 7.2 Reduced Order Model Validation: Evaporator Pressure for Step Changes in Compressor Speed

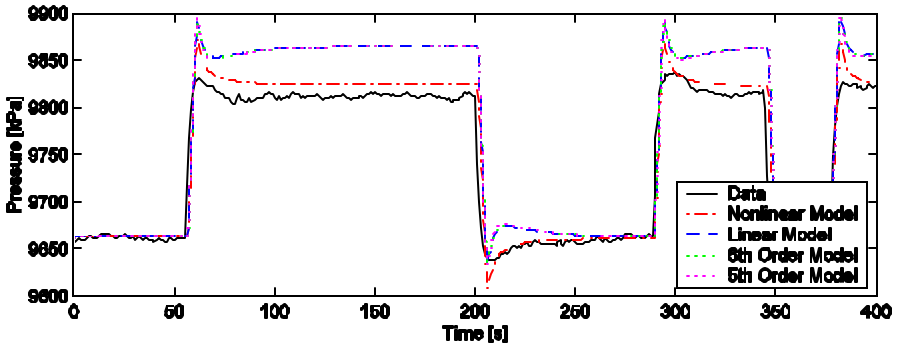

Figure 7.3 Reduced Order Model Validation: Gas Cooler Pressure for Step Changes in Compressor Speed

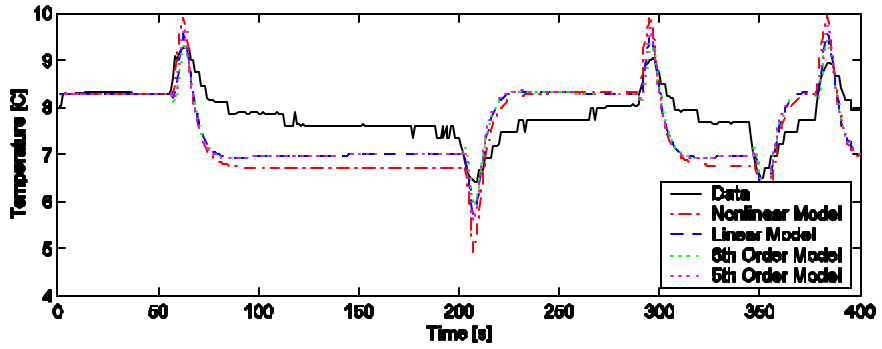

Figure 7.4 Reduced Order Model Validation: Evaporator Superheat for Step Changes in Compressor Speed

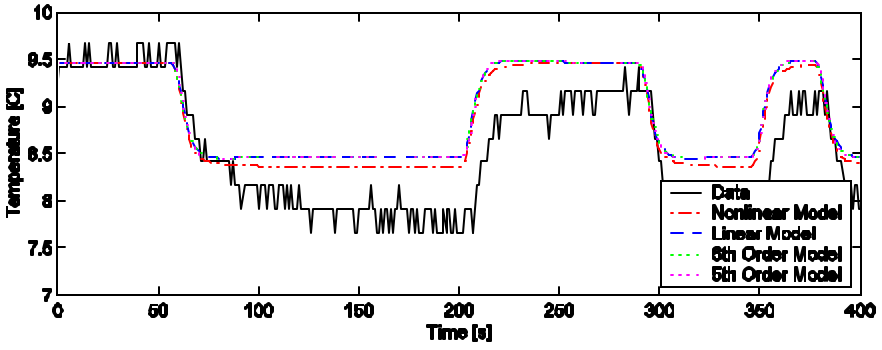

Figure 7.5 Reduced Order Model Validation: Evaporator Exit Air Temperature for Step Changes in Compressor Speed

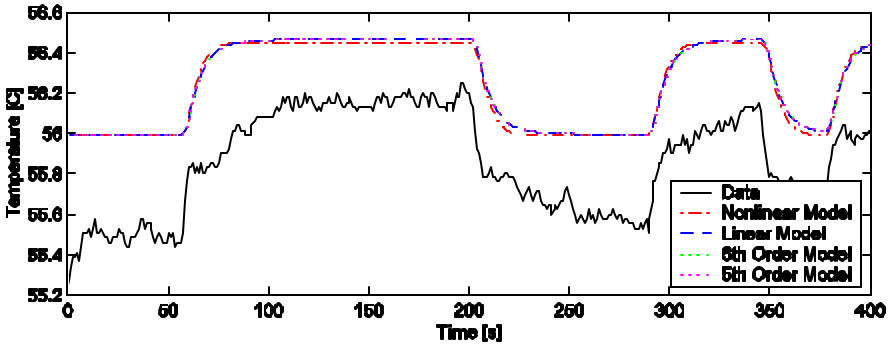

Figure 7.6 Reduced Order Model Validation: Gas Cooler Exit Air Temperature for Step Changes in Compressor Speed

7.5 Other Model Reduction Possibilities

While attempting to discover the dominant dynamics of the system, several alternative model reduction attempts were made with mixed success. These attempts are included here to inform the reader of methods to avoid, as well as possibilities for model reduction under certain conditions.

7.5.1 Lumped Evaporator Wall Temperature

The wall temperature/energy dynamics have been shown to be the dominant dynamics of the system, along with the location of refrigerant mass. A logical step for reducing the system order further is to simplify the wall temperature assumptions by considering a single uniform wall temperature rather than separate wall temperatures for each region. The principle difficulty with this approach is the calculated initial conditions. As explained in Chapter 5, given measured data and component parameters, the initial conditions for the dynamic state variables can be calculated. This includes the lumped wall temperatures and the effective length of two-phase flow. When a uniform wall temperature is assumed, the resulting initial condition can be drastically different from that calculated assuming separate wall temperatures. This difference can affect the transient response noticeably. While this assumption is not implausible, more research as to the implications needs to be made before a conclusion can be drawn.

7.5.2 Negligible Gas Cooler Outlet Air Temperature

Experience has shown that residualizing the wall temperature state in the gas cooler model leads to gross errors in the prediction of gas cooler exit air temperature. However, the effects on the other system outputs appear to be limited. Thus if gas cooler air temperature is not a variable of concern, a possibility exists of reducing the order of the system model further. Again, more research is needed before a recommendation can be made.

7.6 Summary

In this chapter, an 11^{th} order dynamic model for a transcritical air conditioning system has been reduced to a 5^{th} order dynamic model without considerable loss in model accuracy. Experience has shown that further reduction may be possible. The common model resulting from the PDE derivation was shown to be less desirable for model reduction. The dominant dynamics of the system were identified to be the wall temperature/energy dynamics and the location of refrigerant mass. The refrigerant energy dynamics were shown to be faster than the

dominant dynamics by an order of magnitude, and could thus be residualized without notable loss of model accuracy.

Chapter 8. Conclusions and Future Work

8.1 Summary of Results

This thesis makes several key contributions to the study of vapor compression system dynamics. First, an existing modeling approach is applied to a unique type of vapor compression cycle, namely the transcritical cycle. Second, a different modeling approach is presented and shown to be equivalent to the more common approach of simplifying the governing PDEs to achieve the desired ODEs. This energy based approach is more straightforward to derive and simpler conceptually. This approach also exposes some freedom in choosing the system states. Third, the resulting models are validated using experimental data and recommendations are made for improving the model validation. Fourth, both the analysis of the linearized models, as well as the empirical models constructed using system identification techniques indicate that a reduced order model of the system dynamics is adequate for predicting the dominant system dynamics. Finally, variations of the singular perturbation technique are used to find reduced order component models. The more commonly derived models are shown to be inappropriate for model reduction, while the reduced order models using the alternatively derived models result in good approximations of the full order system, as well as expose a redundant dynamic mode. A reduced order system model is constructed using the reduced order component models and validated against experimental data.

8.2 Future Work

This research has many aspects that have yet to be explored. A few of these are mentioned here, including improvements in model validation, model reduction, controller design, and modeling of complex systems.

8.2.1 Model Validation

In Chapter 4 many observations were made regarding problems with the experimental data. Specifically: 1) maldistribution of refrigerant in the prototype evaporator, 2) oil recirculation altering the temperature measurement of fluid entering the compressor, 3) lack of necessary temperature measurements to explore the inter-component dynamics, and 4) need for unfiltered mass flow measurements. Correcting the problem with evaporator maldistribution is necessary for system efficiency, and therefore should not be a problem in a commercially manufactured system. Also, most commercial compressors have oil recirculation built into the compressor chamber, and skewed temperature readings should not be a problem with non-prototype compressors. In the future, additional temperature measurements will be included to verify component dynamics, and venturi meters to measure transient mass flow will be used.

At the time of writing of this thesis, experimental data for validation of a transcritical system with low-side receiver was not available. However, all practical transcritical systems operate with this component. Therefore the predictive ability of this approach should be compared to data collected on such a system.

Additionally, the modeling approach presented has been validated principally on an automotive transcritical air conditioning system. To truly test the validity of this approach, it should be extended to include subcritical air conditioning cycles, and could be experimentally verified on automotive, residential or industrial systems. This obviously requires a large amount of additional work, but is necessary to provide exhaustive validation of the modeling approach.

8.2.2 Model Reduction

The justification for the reduced order models is obviously dependent on the experimental system. All results presented in this thesis are for an automotive transcritical cycle. A logical part of future work is to validate the modeling approach and explore possibilities for model reduction on other types of systems. Preliminary investigations into residential or commercial systems indicate that long pipe lengths between components would necessitate the inclusion of inter-component dynamics. However, the principal conclusion that the dominant dynamics are the storage of energy in the heat exchanger walls should hold for these other systems where the heat exchangers are more massive.

8.2.3 Controller Design

This thesis has repeatedly discussed the objective of developing control-oriented models. Therefore, this research is only partially complete until the models have been used for controller design and verified with experimental implementation.

8.2.4 Complex Systems

Finally, a largely unexplored area of research is the control of more complex multi-component air conditioning systems. These systems have the potential to benefit the most from more advanced control strategies whose design would require a control-oriented model. The approach presented in this thesis of component level modeling and model reduction makes the transition to more complex systems easy and straightforward, by simply appropriately defining the component input-output relationships to form the overall system model.

List of References

[1] "Energy Information Administration: A Look at Residential Energy Consumption in 1997," http://www.eia.doe.gov/emeu/recs/contents.html, 2002.

[2] Anderson, B. D. O., "Controller Design: Moving From Theory to Practice," *IEEE Control Systems Magazine*, vol. 13, no. 4, pp. 16-25, Aug, 1993.

[3] Astrom, K. J. and Bell, R. D., "Drum-Boiler Dynamics," *Automatica*, vol. 36, no. 3, pp. 363-78, Mar, 2000.

[4] Beck, B. T. and Wedekind, G. L., "A Generalization of the System Mean Void Fraction Model for Transient Two-Phase Evaporating Flows," *Journal of Heat Transfer-Transactions of the ASME*, vol. 103, no. 1, pp. 81-85, Feb, 1981.

[5] Bendapudi, S. and Braun, J. E., "A Review of Literature on Dynamic Models of Vapor Compression Equipment," ASHRAE Report #4036-5, May 2002.

[6] Brennan, S., On Size and Control, Thesis, University of Illinois at Urbana-Champaign, 2002.

[7] Broersen, P. M. T. and van der Jagt, M. F. G., "Hunting of Evaporators Controlled by a Thermostatic Expansion Valve," *Journal of Dynamic Systems Measurement & Control-Transactions of the ASME*, vol. 102, no. 2, pp. 130-135, Jun, 1980.

[8] Y.A. Cengel and M.A. Boles. Thermodynamics: An Engineering Approach, Boston, MA: WCB McGraw-Hill, 1998.

[9] C.-T. Chen. Linear System Theory and Design, New York: Oxford University Press, 1999.

[10] Chi, J. and Didion, D., "A Simulation Model of the Transient Performance of a Heat Pump," *International Journal of Refrigeration*, vol. 5, no. 3, pp. 176-184, May, 1982.

[11] Dhar, M. and Soedel, W., "Transient Analysis of a Vapor Compression Refrigeration System," *XVth International Congress of Refrigeration*, Venice, pp. 1031-1067.

[12] Giannavola, M. S., Experimental Study of System Performance Improvements in Transcritical R744 Systems for Mobile Air conditioning and Heat Pumping, Thesis, University of Illinois at Urbana-Champaign, 2002.

[13] Grald, E. W. and MacArthur, J. W., "A Moving boundary Formulation for Modeling Time-Dependent Two-Phase Flows," *International Journal of Heat & Fluid Flow*, vol. 13, no. 3, pp. 266-272, Sep, 1992.

[14] Gruhle, W. D. and Isermann, R., "Modeling and Control of a Refrigerant Evaporator," *Journal of Dynamic Systems Measurement & Control-Transactions of the ASME*, vol. 107, no. 4, pp. 235-240, Dec, 1985.

[15] He, X.-D., Dynamic Modeling and Multivariable Control of Vapor Compression Cycles in Air Conditioning Systems, Thesis, Massachusetts Institute of Technology, 1996.

[16] He, X.-D., Asada, H. H., Liu, S., and Itoh, H., "Multivariable Control of Vapor Compression Systems," *HVAC&R Research*, vol. 4, no. 3, pp. 205-230, Jul, 1998.

[17] He, X.-D., Liu, S., and Asada, H. H., "Modeling of Vapor Compression Cycles for Multivariable Feedback Control of HVAC Systems," *Journal of Dynamic Systems Measurement & Control-Transactions of the ASME*, vol. 119, no. 2, pp. 183-191, Jun, 1997.

[18] F.P. Incropera and D.P. DeWitt. Fundamentals of Heat and Mass Transfer, New York: John Wiley & Sons, 1996.

[19] Jensen, J. M. a. H. T., "Moving Boundary Models for Dynamic Simulations of Two-Phase Flows," *Modelica 2002 Conference Proceedings*, 2002.

[20] H.K. Khalil. Nonlinear Systems, Upper Saddle River, New Jersey: Prentice-Hall Inc., 1996.

[21] P.V. Kokotovic. Singular Perturbation Methods in Control: Analysis and Design, Orlando, Florida: Academic Press Inc., 1986.

[22] Lebrun, J. and Bourdouxhe, J.-P., "Reference Guide for Dynamic Models of HVAC Equipment," ASHRAE Project 738-TRP, 1996.

[23] L. Ljung. System Identification: Theory for the User, Upper Saddle River, New Jersey: Prentice Hall PTR, 1999.

[24] MacArthur, J. W. , "Transient Heat Pump Behaviour: a Theoretical Investigation," *International Journal of Refrigeration-Revue Internationale du Froid*, vol. 7, no. 2, pp. 123-132, Mar, 1984.

[25] MacArthur, J. W. and Grald, E. W., "Unsteady Compressible Two-Phase Flow Model for Predicting Cyclic Heat Pump Performance and a Comparison With Experimental Data," *International Journal of Refrigeration-Revue Internationale du Froid*, vol. 12, no. 1, pp. 29-41, Jan, 1989.

[26] D. Naidu. Singular Perturbation Methodology in Control Systems , London, United Kingdom: Peter Peregrinus, 1988.

[27] Najork, H., "Investigations on the Dynamical Behavior of Evaporators with Thermostatic Expansion Valve," *Proceedings of the 13th International Congress of Refrigeration*, Washington, pp. 759-769.

[28] Pettersen, J., Rieberer, R., and Munkejord, S. T., "Heat Transfer and Pressure Drop for Flow of Supercritical and Subcritical CO2 in Microchannel Tubes," Sintef Energy Research TR A5127, Feb 2000.

[29] Pettit, N. B. O. L., Willatzen, M., and Ploug-Sorensen, L., "General Dynamic Simulation Model for Evaporators and Condensers in Refrigeration. Part Ii: Simulation and Control of an Evaporator," *International Journal of Refrigeration*, vol. 21, no. 5, pp. 404-414, Aug, 1998.

[30] Pfafferott, T. and Schmitz, G., "Numeric Simulation of an Integrated CO2 Cooling System," *Modelica Workship 2000 Proceedings*, Lund, Sweden, pp. 89-92.

[31] Rasmussen, B. P. "Thermosys Toolbox User's Manual," http://mr-roboto.me.uiuc.edu/VC3, 2002.

[32] Rice, C. K., "Effect of Void Fraction Correlation and Heat Flux Assumption on Refrigerant Charge Inventory Predictions," *ASHRAE Transactions*, vol. 93, no. 1, pp. 341-367,

[33] S. Skogestad and I. Postlethwaite. Multivariable Feedback Control: Analysis and Design, New York: John Wiley & Sons, 1996.

[34] Span, R. and Wagner, W., "A New Equation of State for Carbon Dioxide Covering the Fluid Region From the Triple-Point Temperature to 1100 K at Pressures up to 800 Mpa," *Journal of Physical & Chemical Reference Data*, vol. 25, no. 6, pp. 1509-1596, Nov, 1996.

[35] Stoecker, W. F., "Stability of an Evaporator-Expansion Valve Control Loop," *ASHRAE Transactions*, vol. 72, no. 2007, 1966.

[36] S.H. Strogatz. Nonlinear Dynamics and Chaos, Reading, Massachusetts: Perseus Books Publishing, L.L.C., 1994.

[37] Wedekind, G. L., Bhatt, B. L., and Beck, B. T., "A System Mean Void Fraction Model for Predicting Various Transient Phenomena Associated With Two-Phase Evaporating and Condensing Flows," *International Journal of Multiphase Flow*, vol. 4, no. 1, pp. 97-114, Mar, 1978.

[38] Wedekind, G. L. Stoecker W. F. "Transient Response of the Mixture-Vapor Transition Point in Horizontal Evaporating Flow," *ASHRAE Transactions*, vol. 72, no. 1. 1966.

[39] F.M. White. Fluid Mechanics , New York: McGraw-Hill, Inc., 1994.

[40] Willatzen, M., Pettit, N. B O L, and Ploug-Sorensen, L., "General Dynamic Simulation Model for Evaporators and Condensers in Refrigeration. Part I: Moving boundary Formulation of Two-Phase Flows With Heat Exchange," *International Journal of Refrigeration*, vol. 21, no. 5, pp. 398-403, Aug, 1998.

[41] Wilson, M. J., Newell, T. A., and Chato, J. C., "Experimental Investigation of Void Fraction During Horizontal Flow in Larger Diameter Refrigeration Applications," Air Conditioning and Refrigeration Center, University of Illinois at Urbana Champaign, ACRC TR-140, Jul 1998.

[42] Zahn, W. R., A Visual Study of Two-Phase Flow While Evaporating in Horizontal Tubes ASME Paper No. 63-WA-166, 1963.